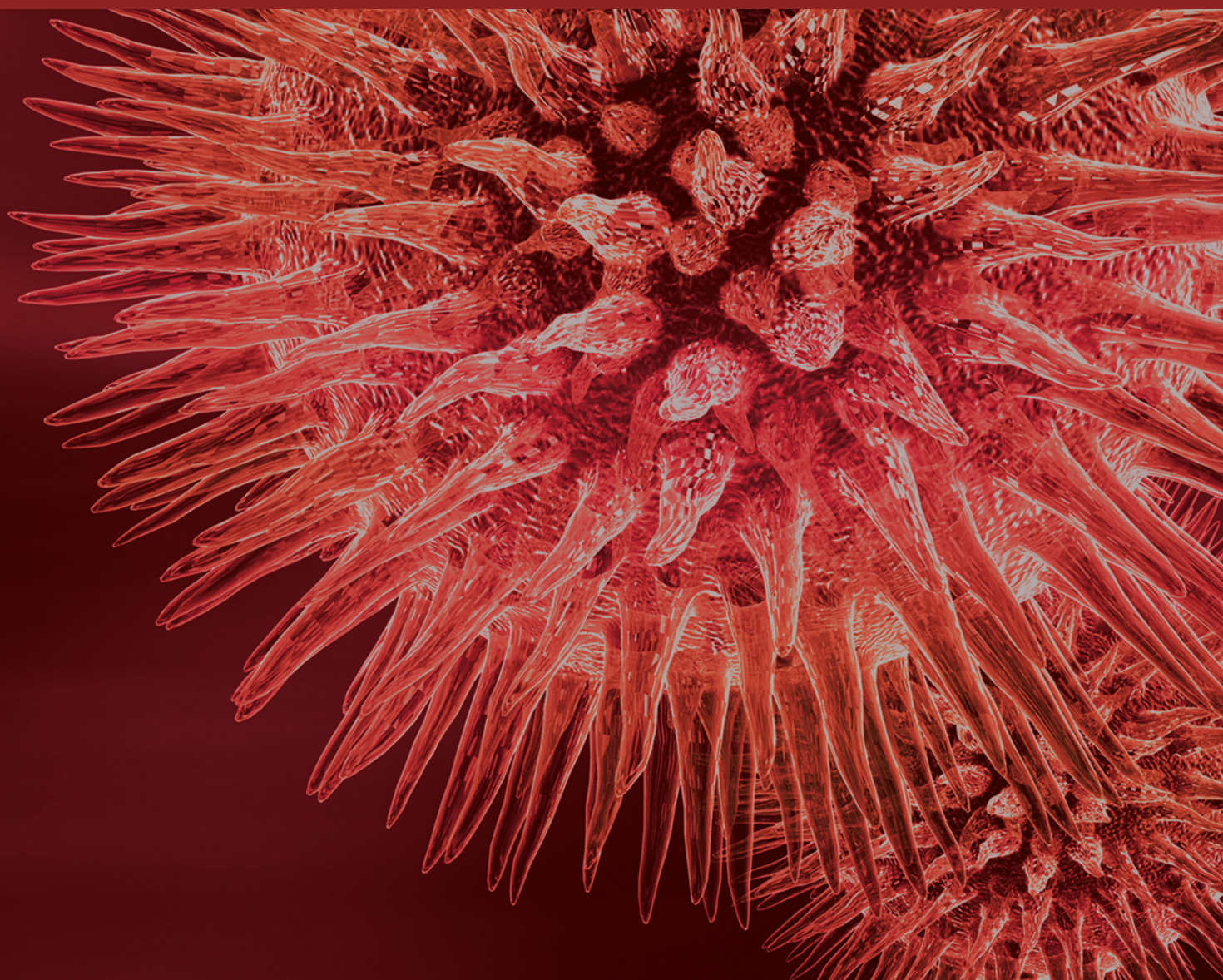


New Biomaterials and Regenerative Medicine Strategies in Periodontology, Oral Surgery, and Esthetic and Implant Dentistry

Guest Editors: David M. Dohan Ehrenfest, Hom-Lay Wang, Jean-Pierre Bernard, and Gilberto Sammartino





New Biomaterials and Regenerative Medicine Strategies in Periodontology, Oral Surgery, Esthetic and Implant Dentistry

BioMed Research International

New Biomaterials and Regenerative Medicine Strategies in Periodontology, Oral Surgery, Esthetic and Implant Dentistry

Guest Editors: David M. Dohan Ehrenfest, Hom-Lay Wang,
Jean-Pierre Bernard, and Gilberto Sammartino



Copyright © 2015 Hindawi Publishing Corporation. All rights reserved.

This is a special issue published in “BioMed Research International.” All articles are open access articles distributed under the Creative Commons Attribution License, which permits unrestricted use, distribution, and reproduction in any medium, provided the original work is properly cited.

Contents

New Biomaterials and Regenerative Medicine Strategies in Periodontology, Oral Surgery, Esthetic and Implant Dentistry, David M. Dohan Ehrenfest, Hom-Lay Wang, Jean-Pierre Bernard, and Gilberto Sammartino

Volume 2015, Article ID 210792, 3 pages

Histological and Histomorphometric Human Results of HA-Beta-TCP 30/70 Compared to Three Different Biomaterials in Maxillary Sinus Augmentation at 6 Months: A Preliminary Report,

Susanna Annibali, Giovanna Iezzi, Gian Luca Sfasciotti, Maria Paola Cristalli, Iole Vozza, Carlo Mangano, Gerardo La Monaca, and Antonella Polimeni

Volume 2015, Article ID 156850, 7 pages

Oral Streptococci Biofilm Formation on Different Implant Surface Topographies,

Pedro Paulo Cardoso Pita, José Augusto Rodrigues, Claudia Ota-Tsuzuki, Tatiane Ferreira Miato, Elton G. Zenobio, Gabriela Giro, Luciene C. Figueiredo, Cristiane Gonçalves, Sergio A. Gehrke, Alessandra Cassoni, and Jamil Awad Shibli

Volume 2015, Article ID 159625, 6 pages

Influence of Leukocyte- and Platelet-Rich Fibrin (L-PRF) in the Healing of Simple Postextraction

Sockets: A Split-Mouth Study, Gaetano Marenzi, Francesco Riccitiello, Mariano Tia, Alessandro di Lauro, and Gilberto Sammartino

Volume 2015, Article ID 369273, 6 pages

Clinical Evaluation of the Regenerative Potential of EMD and NanoHA in Periodontal Infrabony

Defects: A 2-Year Follow-Up, Andrea Pilloni, Matteo Saccucci, Gabriele Di Carlo, Blerina Zeza, Marco Ambrosca, Michele Paolantonio, Gilberto Sammartino, Claudio Mongardini, and Antonella Polimeni

Volume 2014, Article ID 492725, 9 pages

Adhesion and Proliferation of Human Periodontal Ligament Cells on Poly(2-methoxyethyl acrylate),

Erika Kitakami, Makiko Aoki, Chikako Sato, Hiroshi Ishihata, and Masaru Tanaka

Volume 2014, Article ID 102648, 14 pages

Physicochemical Characteristics of Bone Substitutes Used in Oral Surgery in Comparison to

Autogenous Bone, Antoine Berberi, Antoine Samarani, Nabih Nader, Ziad Noujeim, Maroun Dagher, Wasfi Kanj, Rita Mearawi, Ziad Saleme, and Bassam Badran

Volume 2014, Article ID 320790, 9 pages

Biological Width around One- and Two-Piece Implants Retrieved from Human Jaws, Ricardo Judgar,

Gabriela Giro, Elton Zenobio, Paulo G. Coelho, Magda Feres, Jose A. Rodrigues, Carlo Mangano, Giovanna Iezzi, Adriano Piattelli, and Jamil Awad Shibli

Volume 2014, Article ID 850120, 5 pages

Effect of Low-Level Laser on Bone Defects Treated with Bovine or Autogenous Bone Grafts: *In Vivo*


Study in Rat Calvaria, Mércia J. S. Cunha, Luis A. Esper, Michyele C. Sbrana, Paula G. F. P. de Oliveira, Accácio L. do Valle, and Ana Lúcia P. F. de Almeida

Volume 2014, Article ID 104230, 9 pages

Osteoconductive Potential of Barrier NanoSiO₂ PLGA Membranes Functionalized by Plasma Enhanced Chemical Vapour Deposition, Antonia Terriza, Jose I. Vilches-Pérez, Emilio de la Orden, Francisco Yubero,

Juan L. Gonzalez-Caballero, Agustin R. González-Elipé, José Vilches, and Mercedes Salido

Volume 2014, Article ID 253590, 10 pages



Vertical Ridge Augmentation of the Atrophic Posterior Mandible with Sandwich Technique: Bone Block from the Chin Area versus Corticocancellous Bone Block Allograft—Clinical and Histological Prospective Randomized Controlled Study, Luigi Laino, Giovanna Iezzi, Adriano Piattelli, Lorenzo Lo Muzio, and Marco Ciccù
Volume 2014, Article ID 982104, 7 pages

Surface Characteristics and Bioactivity of a Novel Natural HA/Zircon Nanocomposite Coated on Dental Implants, Ebrahim Karamian, Amirsalar Khandan, Mahmood Reza Kalantar Motamedi, and Hesam Mirmohammadi
Volume 2014, Article ID 410627, 10 pages

Solubility of Two Resin Composites in Different Mouthrinses, Sezin Ozer, Emine Sen Tunc, Nuray Tuloglu, and Sule Bayrak
Volume 2014, Article ID 580675, 4 pages

Editorial

New Biomaterials and Regenerative Medicine Strategies in Periodontology, Oral Surgery, Esthetic and Implant Dentistry

**David M. Dohan Ehrenfest,^{1,2} Hom-Lay Wang,¹
Jean-Pierre Bernard,³ and Gilberto Sammartino⁴**

¹Department of Periodontics and Oral Medicine, University of Michigan School of Dentistry, Ann Arbor, MI 48109-1078, USA

²LoB5 Research Unit, School of Dentistry & Research Center for Biomineralization Disorders, Chonnam National University, Gwangju 500-757, Republic of Korea

³Department of Stomatology, Implantology and Dental and Maxillofacial Radiology, School of Dental Medicine, University of Geneva, 1205 Geneva, Switzerland

⁴Department of Oral Surgery, Faculty of Medicine, University of Naples Federico II, 80131 Naples, Italy

Correspondence should be addressed to David M. Dohan Ehrenfest; lob5@mac.com

Received 1 March 2015; Accepted 1 March 2015

Copyright © 2015 David M. Dohan Ehrenfest et al. This is an open access article distributed under the Creative Commons Attribution License, which permits unrestricted use, distribution, and reproduction in any medium, provided the original work is properly cited.

Periodontology, Oral Surgery, Esthetic and Implant Dentistry (the POSEID disciplines) are strongly interconnected clinical and research fields, even if they are taught as separate disciplines in most academic environments. Depending on the professional organization of each country, dental implants are often placed by periodontists or oral surgeons (and even sometimes prosthodontists), even if implant dentistry is today one of the most active independent fields of education and research by itself. Esthetic dentistry is also a general term that concerns in fact most of the Dental Arts: per definition, all dental treatments are expected to lead to an esthetic result nowadays. The separation between these dental disciplines appears sometimes quite artificial, even if each discipline has clearly its own themes and specificities. Behind this question of terminology and limits between the disciplines the question of transdisciplinarity in dental therapeutics and the need for a global conception of the dental rehabilitations rises. However, when it is related to the development of new technologies, the borders between these disciplines vanish in front of the paradigm of translational transversal research.

These POSEID dental disciplines are currently very active and are the source of development of many new techniques and technologies. It is in their domains that the highest number of innovation and publications can be

found in dentistry nowadays. Implantable biomaterials were particularly investigated and have significantly evolved in the recent years: new dental implant design and surfaces [1], new bone biomaterials [2], new surgical adjuvants such as platelet concentrates [3], and so forth. The objectives of all these biomaterials and technologies are not only to replace missing or damaged tissues but also now to promote tissue regeneration [4]. This regenerative medicine approach and the many recent technological evolutions are associated with the development of new therapeutic strategies that still require to be duly evaluated and validated. We can cite, among the main current research biomaterial themes in the POSEID disciplines, the development of new biomaterials and techniques of bone grafting or bone regeneration and for periodontal and peri-implant soft tissue management [4], the development of new bone substitutes and healing membranes for periodontal and implant reconstructions [5], the development of new technologies and strategies in oral regenerative medicine and bioengineering (e.g., the use of growth factors or fibrin-based healing surgical adjuvants) [3], the development of new pharmacological technologies and strategies during periodontal treatments and oral surgery (e.g., mouthwash and oral gel), or new dental implant surfaces and design for the improvement of osseointegration [1].

All these themes are very transdisciplinary/transversal, both in their clinical impact (it concerns almost all aspects of periodontology, oral surgery, implantology, and even dentistry in general) and in their research methods (it concerns physics/biophysics, pharmacology, biology, and material sciences).

These themes are also very transversal, as they are concerning many clinical disciplines outside of dentistry, such as orthopedics/sports medicine or plastic surgery. For example, regenerative medicine strategies with platelets (Platelet-Rich Plasma (PRP) and Platelet-Rich Fibrin (PRF)) or advanced cell therapies (with various forms of stem cells) are a frequent theme in the POSEID field [4], but they are also widely developed in medical research [6]. If Leukocyte- and Platelet-Rich Fibrin (L-PRF) is sometimes perceived as a dental biomaterial (due to historical reasons and its frequent use in oral surgery and implant dentistry) [4], it is also very promising in orthopedics, sports medicine [7, 8], and regenerative strategies of the chronic ulcer wounds [9]. Transdisciplinarity is very strong in most POSEID research themes.

These research fields are also the most active translational research topics in orofacial sciences, as any research about new biomaterials or techniques requires basic sciences research, in vitro and in vivo. For example, the development of new healing growth factors based materials (such as Leukocyte- and Platelet-Rich Fibrin (L-PRF)) requires pharmacologic, biological, and tissue engineering concepts to be tested, validated, optimized, and finally redeveloped for extended applications in other fields [6, 9, 10]. On the other hand the development of new mouthwash solutions or healing gels implies biological and biophysical research (e.g., with microencapsulated bioactive molecules) for the production of new technologies and their final validation. Finally, the implantable materials are ideal examples of translational research (e.g., titanium implants or bone substitute materials) [1, 2] as they require very accurate engineering of the chemical and morphological characteristics of the materials (using physical instruments from surface and material science) [1, 11], its correlation and validation with biological behaviors and concepts [1, 12], its validation in vivo and in humans, and finally the understanding of its long-term clinical outcomes and eventual pathologies (such as associated peri-implantitis mechanisms). In this case, many parameters are integrated (surface, macrodesign, and biomechanics) [13] and have a strong impact in several domains (orthopedics particularly). It is a good example of translational transversal research.

The quantity of new biomaterials and biotechnologies with direct clinical applications in the interconnected POSEID fields is considerable and reflects very strongly this need for transdisciplinarity and translational culture [4]. However, the borders between these disciplines are often artificially maintained and the conception of these themes is still frequently lacking this global approach. For example, it can be often observed in the dental literature that teams working on implant materials (e.g., surfaces) are neglecting the material science expertise of other specialties (e.g., surface engineers) [1, 12, 14], leading sometimes to a very dental simplification of some topics and to serious approximations and flaws in the literature [1]. The same could

be described in all transversal fields, such as regenerative medicine [9], platelet concentrates for surgical use [3], or bone materials [2]. The specialty-centered culture is often a big limitation for the development of these sciences and a better integration of this transdisciplinarity has to be promoted.

Finally, it is also important to notice that many review articles can be found in these fields about various aspects of these biomaterials and their clinical impact, but we are lacking specific review articles making the synthesis of new approaches in these fields and leading to international consensus. In many review articles, the conclusions are too often that data are missing. Concrete perspectives with new approaches are often lacking, while many data from other fields could allow drawing more perspectives and feeding the debates and discussions. This need for multidisciplinary debates and consensus is very strong [1, 3], but works promoting this transcollaborative culture are still scarce, even if officially promoted by most academic institutions.

As a conclusion, it is a real need nowadays to consider the research about biomaterials and biotechnologies in the interconnected fields of periodontology, oral surgery, and esthetic and implant dentistry as a whole. It is the essence of the POSEIDO Academic Consortium (Periodontology, Oral Surgery, Esthetic & Implant Dentistry Organization) to promote this transdisciplinary philosophy [15]. First, these disciplines are so tightly interconnected that research in this domain deserves often to be regrouped under such an acronym (POSEID disciplines). Second, this transdisciplinarity has to be extended to all related medical, biological, and engineering disciplines able to collaborate on these topics. Finally, the culture of translational sciences is really needed to promote development in this domain. It is expected that this POSEIDO philosophy will continue to develop and become a standard in this field.

Acknowledgments

This work and special issue about new biomaterials and regenerative medicine strategies in the POSEID disciplines were supported by the POSEIDO Academic Consortium (Periodontology, Oral Surgery, Esthetic & Implant Dentistry Organization), by a Grant from the National Research Foundation of Korea (NRF) funded by the Korean Government (MEST) (no. 2011-0030121) and by the LoB5 Foundation for Research, France. The authors also want to thank Ms. Lidia M. Wisniewska, from the Department of Didactics and School Organization, Faculty of Education Sciences, University of Granada, Granada, Spain, and Department of International Relations, Paris Sorbonne University, Paris, France, for her help and contribution in the management of this special issue.

*David M. Dohan Ehrenfest
Hom-Lay Wang
Jean-Pierre Bernard
Gilberto Sammartino*

References

- [1] D. M. Dohan Ehrenfest, P. G. Coelho, B. S. Kang, Y. T. Sul, and T. Albrektsson, "Classification of osseointegrated implant surfaces: materials, chemistry and topography," *Trends in Biotechnology*, vol. 28, no. 4, pp. 198–206, 2010.
- [2] H. Browaeys, P. Bouvry, and H. de Bruyn, "A literature review on biomaterials in sinus augmentation procedures," *Clinical Implant Dentistry and Related Research*, vol. 9, no. 3, pp. 166–177, 2007.
- [3] D. M. Dohan Ehrenfest, L. Rasmusson, and T. Albrektsson, "Classification of platelet concentrates: from pure platelet-rich plasma (P-PRP) to leucocyte- and platelet-rich fibrin (L-PRF)," *Trends in Biotechnology*, vol. 27, no. 3, pp. 158–167, 2009.
- [4] M. Del Corso, A. Vervelle, A. Simonpieri et al., "Current knowledge and perspectives for the use of platelet-rich plasma (PRP) and platelet-rich fibrin (PRF) in oral and maxillofacial surgery part 1: periodontal and dentoalveolar surgery," *Current Pharmaceutical Biotechnology*, vol. 13, no. 7, pp. 1207–1230, 2012.
- [5] A. Simonpieri, M. Del Corso, A. Vervelle et al., "Current knowledge and perspectives for the use of platelet-rich plasma (PRP) and platelet-rich fibrin (PRF) in oral and maxillofacial surgery part 2: bone graft, implant and reconstructive surgery," *Current Pharmaceutical Biotechnology*, vol. 13, no. 7, pp. 1231–1256, 2012.
- [6] P. A. Everts, M. M. Hoogbergen, T. A. Weber, R. J. Devilee, G. van Monfort, and I. H. de Hingh, "Is the use of autologous platelet-rich plasma gels in gynecologic, cardiac, and general, reconstructive surgery beneficial?" *Current Pharmaceutical Biotechnology*, vol. 13, no. 7, pp. 1163–1172, 2012.
- [7] A. Mishra, K. Harmon, J. Woodall, and A. Vieira, "Sports medicine applications of platelet rich plasma," *Current Pharmaceutical Biotechnology*, vol. 13, no. 7, pp. 1185–1195, 2012.
- [8] M. A. Zumstein, S. Berger, M. Schober et al., "Leukocyte- and platelet-rich fibrin (L-PRF) for long-term delivery of growth factor in rotator cuff repair: review, preliminary results and future directions," *Current Pharmaceutical Biotechnology*, vol. 13, no. 7, pp. 1196–1206, 2012.
- [9] A. Cieslik-Bielecka, J. Choukroun, G. Odin, and D. M. Dohan Ehrenfest, "L-PRP/L-PRF in esthetic plastic surgery, regenerative medicine of the skin and chronic wounds," *Current Pharmaceutical Biotechnology*, vol. 13, no. 7, pp. 1266–1277, 2012.
- [10] T. M. Bielecki, T. S. Gazdzik, J. Arendt, T. Szczepanski, W. Krol, and T. Wielkoszynski, "Antibacterial effect of autologous platelet gel enriched with growth factors and other active substances: an in vitro study," *The Journal of Bone and Joint Surgery: British Volume*, vol. 89, no. 3, pp. 417–420, 2007.
- [11] D. M. Dohan Ehrenfest, M. Del Corso, and B.-S. Kang, "Identification card and codification of the chemical and morphological characteristics of 62 dental implant surfaces. Part 1: description of the Implant Surface Identification Standard (ISIS) codification system," *POSEIDO*, vol. 2, no. 1, pp. 7–22, 2014.
- [12] Y. T. Sul, B. S. Kang, C. Johansson, H. S. Um, C. J. Park, and T. Albrektsson, "The roles of surface chemistry and topography in the strength and rate of osseointegration of titanium implants in bone," *Journal of Biomedical Materials Research: Part A*, vol. 89, no. 4, pp. 942–950, 2009.
- [13] M. M. Al-Nsour, H. L. Chan, and H. L. Wang, "Effect of the platform-switching technique on preservation of peri-implant marginal bone: a systematic review," *The International Journal of Oral & Maxillofacial Implants*, vol. 27, no. 1, pp. 138–145, 2012.
- [14] B. S. Kang, Y. T. Sul, S. J. Oh, H. J. Lee, and T. Albrektsson, "XPS, AES and SEM analysis of recent dental implants," *Acta Biomaterialia*, vol. 5, no. 6, pp. 2222–2229, 2009.
- [15] D. M. Dohan Ehrenfest, G. Sammartino, and J. P. Bernard, "The periodontology, oral surgery, esthetic and implant dentistry organization (POSEIDO) and open journal: an international academic and scientific community for a new approach of open-access publishing," *POSEIDO*, vol. 1, no. 1, pp. 1–5, 2013.

Clinical Study

Histological and Histomorphometric Human Results of HA-Beta-TCP 30/70 Compared to Three Different Biomaterials in Maxillary Sinus Augmentation at 6 Months: A Preliminary Report

Susanna Annibali,¹ Giovanna Iezzi,² Gian Luca Sfasciotti,¹ Maria Paola Cristalli,³ Iole Vozza,¹ Carlo Mangano,⁴ Gerardo La Monaca,¹ and Antonella Polimeni¹

¹Department of Oral and Maxillofacial Sciences, Oral Surgery Unit, School of Dentistry, Sapienza University of Rome, Via Caserta 6, 00161 Rome, Italy

²Department of Medical, Oral and Biotechnological Sciences, University of Chieti-Pescara, Chieti, Italy

³Department of Biotechnologies and Medical Surgical Sciences, Sapienza University of Rome, Rome, Italy

⁴Department of Surgical and Morphological Sciences, University of Insubria, Varese, Italy

Correspondence should be addressed to Susanna Annibali; susanna.annibali@uniroma1.it

Received 19 September 2014; Accepted 13 December 2014

Academic Editor: David M. Dohan Ehrenfest

Copyright © 2015 Susanna Annibali et al. This is an open access article distributed under the Creative Commons Attribution License, which permits unrestricted use, distribution, and reproduction in any medium, provided the original work is properly cited.

Objective. The aim of this investigation was to examine the bone regenerative potential of newly biphasic calcium phosphate ceramics (HA- β -TCP 30/70), by assessing histological and histomorphometric results of human specimens retrieved from sinuses augmented with HA- β -TCP 30/70, and comparing them to anorganic bovine bone (ABB), mineralized solvent-dehydrated bone allograft (MSDBA), and equine bone (EB), after a healing period of 6 months. **Materials and Methods.** Four consecutive patients with edentulous atrophic posterior maxilla were included in this report. A two-stage procedure was carried out for sinus augmentation with HA- β -TCP 30/70, ABB, MSDBA, and EB. After 6 months, specimens were retrieved at the time of implant placement and processed for histological and histomorphometric analyses. **Results.** At histological examination, all biomaterials were in close contact with the newly formed bone and showed the same pattern of bone formation; the grafted granules were surrounded by a bridge-like network of newly formed bone. A limited number of ABB particles were partially covered by connective tissue. The histomorphometric analysis revealed 30.2% newly formed bone for HA- β -TCP 30/70, 20.1% for ABB, 16.4% for MSDBA, and 21.9% for EB. **Conclusions.** Within the limitations of the present investigation, these results support the successful use of HA- β -TCP 30/70 for sinus augmentation.

1. Introduction

Deficiencies in the volume and quality of available bone can complicate implant placement in the resorbed maxillary jaw. Sinus grafting in the maxillary posterior region is a highly predictable procedure to increase the vertical volume of sinus floor bone to accommodate dental implants [1, 2].

Autologous bone is considered the gold standard for bone regeneration [3, 4], even if different bone substitutes have been proposed to overcome the limits related to its use, specifically, donor site morbidity, increased operating time, need of a second surgical site to obtain the transplant, and

potential intraoperative and postoperative complications [5–7]. After implant placement, a resorption with up to 49.5% marked volume loss has been reported in the literature after 6 months from sinus grafting [8, 9]. A number of graft materials with different origin and mechanism of bone regeneration have been used alone or in combination with autografts in sinus floor augmentations [10–20]. Therefore the current issue is the definition of the best filling material for the sinus cavity. The presence or absence of autogenous bone in a graft did not affect implant survival [21, 22] and different studies have suggested that some alternative augmentation materials

may not adversely influence clinical outcomes and implant survival [23, 24].

Among the graft materials used in maxillary sinus augmentation procedures, biphasic calcium phosphate ceramics, reached by mixing hydroxyapatite (HA) and tricalcium phosphate (TCP), are considered biocompatible, osteoconductive, and suitable to obtain bone formation [24]-[25]. The HA, undergoing slow resorption, works as a scaffold to maintain space, while the TCP that underwent quick dissolution leads to more interparticle space and releases calcium and phosphorus ions that could stimulate new bone formation, promoting osteogenic activity [26]. Currently several bio-ceramic materials are used and differences in HA/TCP ratio, phase composition, formulation, sizes, and shapes affect their biological and mechanical properties [10, 18], [24], [27-29].

The newly biphasic calcium phosphate ceramics (HA- β -TCP 30/70) with reticular structure, tested in the present investigation, seem to have a better resorption and an increased bone formation [18].

Anorganic bovine bone (ABB) is a deproteinized sterilized bovine bone, constituted by a calcium-deficient carbonate apatite, with 75% porosity and a crystal size of about 10 nm in the form of granules. Due to its natural structure, it is chemically and physically comparable to human bone and its porous nature, greatly increasing the surface area of the material, promotes angiogenesis and immigration of osteogenic cells [19]. The usage of ABB is widely documented and shows that it can well integrate in host bone tissue in different clinical and histological results [30-32].

MSDBA is a solvent-dehydrated, limited-dose, gamma-irradiated portions of human iliac crest bone wedge. The allograft mixture contains 50% cortical and 50% cancellous microchips with a particle size of 1-2 mm. MSDBA showed significant histological results in terms of new bone formation after sinus augmentation procedures [10, 11, 33].

Equine-derived bone (EB) is an equine-derived bone tissue deantigenated by a proteolytic low-temperature process that eliminates the organic components but leaves the mineral structure of the hydroxyapatite unaltered, saving the resorption potential [12]. Recent investigations showed that also the equine-derived bone (EB) is able to induce bone formation in maxillary sinus augmentations [12, 13, 34, 35].

Although the number of newly formed bones in the augmented sinus is not directly related to the survival rate of the implants, histological and histomorphometric analysis of specimens, retrieved at the time of implant placement (after a healing period of 6 months), represents a reliable indicator to assess and compare the performance of the graft materials [19].

The aim of this investigation was to examine the bone regenerative potential of a newly biphasic calcium phosphate ceramics (HA- β -TCP 30/70), by assessing histological and histomorphometric results of human specimens retrieved from sinuses augmented with HA- β -TCP 30/70, and comparing them to anorganic bovine bone (ABB), mineralized solvent-dehydrated bone allograft (MSDBA), and equine bone (EB), after a healing period of 6 months.

2. Materials and Methods

2.1. Patient Selection. Four healthy patients (3 males, 1 females, all nonsmokers, mean age 52 years, range 36-70 years), scheduled for sinus augmentation in the atrophic posterior maxilla to receive fixed restorations, were recruited for this study. Inclusion criteria were maxillary partial edentulism in the premolar/molar areas and subsinus residual bone height, measured on computerized tomography (CT) scan, ranging from 2 to 4 mm and bone thickness 3-5 mm. Exclusion criteria were smoking, patients with systemic diseases and maxillary sinus pathology. The clinical procedures were performed in accordance with the Declaration of Helsinki and the Good Clinical Practice Guidelines. All patients signed a written informed consent form. After reviewing medical history and making a preliminary clinical examination, digital panoramic radiography and CT scan were performed. A two-stage procedure was carried out for sinus floor augmentation with HA- β -TCP 30/70, ABB, MCBA, and EB. These materials were allocated to the participant's sinus under randomized conditions. After a healing period of 6 months, specimens were retrieved at the time of implant placement and processed for histological and histomorphometric analyses.

2.2. Surgical Procedure. Surgery was performed under sterile conditions and local anaesthesia with mepivacaine 2% with epinephrine 1:100.000 (Carbocaine, AstraZeneca, Italy). On the day of surgery, each patient was administered 2g amoxicillin + clavulanic acid (Augmentin, GlaxoSmithKline, London, UK) 1 hour prior to surgery and rinsed with a chlorhexidine digluconate solution 0.2% (Corsodyl, GlaxoSmithKline, Belgium) for 2 min immediately prior to the intervention. Sinus floor elevation was performed utilizing a lateral window technique. A slightly palatal crestal incision was made and supplemented by buccal releasing incisions mesially and distally. Full thickness flaps were elevated to expose the alveolar crest and the lateral sinus wall. An oval-shaped osteotomy, with the inferior border about 5 mm superior to the alveolar bone margin, was made on the lateral aspect of the sinus wall using a round bur under cold sterile saline irrigation. The center of the bony window was gently in-fractured with care to ensure that its most superior portion was left intact. The sinus membrane was carefully elevated and rotated, together with the osteotomy window, inward and upward. The exposed sinus cavity was augmented with HA- β -TCP 30/70 ABB, MCBA, or EB. The graft was placed and carefully packed into the area between the elevated Schneiderian membrane and sinus floor without excessive pressure. A resorbable membrane was placed over the lateral wall of the sinus and the mucoperiosteal flap was replaced and stabilized with monofilament, nonresorbable, expanded polytetrafluoroethylene (e-PTFE) (Gore-Tex Suture, W. L. Gore, Flagstaff, AZ, USA) sutures. No Schneiderian membranes were perforated during any of the sinus augmentation procedures. For the postoperative phase, the patients were protected from infection by administration of prophylactic antibiotics (Augmentin, GlaxoSmithKline, London, UK) 1g, 2 times daily for 1 week; an analgesic and antiphlogistic

medication (Ibifen, 200 mg -IBI-Lorenzini, Aprilia, Italy) was prescribed 3 times daily. The patient was instructed to avoid use of a removable prosthesis, not to blow the nose, and to rinse twice daily for a period of 2 weeks with 0.2% chlorhexidine gluconate. Following a healing period of 2 weeks, sutures were removed. Six months after the augmentation procedure, clinical and radiographic examination were undertaken and each patient was reappointed for biopsy at the time of implant placement in the same location. Under local anesthesia, a vertical incision was made buccally and continued horizontally and distally at the palatal side of the alveolar crest. A full thickness flap was raised and mobilized for tension-free closure. During this surgery, a total of 4 bone samples were retrieved with a 3.5 trephine bur under sterile saline solution irrigation, one from each augmented site. From 1 to 6 implants were placed into each patient's augmented sinus according to the manufacturer's directions.

2.3. Histological Procedure. The bone cores were retrieved and were immediately stored in 10% buffered formalin and processed to obtain thin ground sections. The specimens were processed using the Precise 1 Automated System (Assing, Rome, Italy) [36]. The specimens were dehydrated in a graded series of ethanol rinses and embedded in a glycolmethacrylate resin (Technovit 7200 VLC, Kulzer, Wehrheim, Germany). After polymerization, the specimens were sectioned, along their longitudinal axis, with a high precision diamond disk at about 150 μm and ground down to about 30 μm with a specially designed grinding machine Precise 1 Automated System (Assing, Rome, Italy). Three slides were obtained from each specimen. These slides were stained with acid fuchsin and toluidine blue and examined with transmitted light Leitz Laborlux microscope (Leitz, Wetzlar, Germany). Histomorphometry of the percentages of newly formed bone, residual grafted material, and marrow spaces was carried out using a light microscope (Laborlux S, Leitz, Wetzlar, Germany) connected to a high-resolution video camera (3CCD, JVC KY-F55B, JVC, Yokohama, Japan) and interfaced with a monitor and PC (Intel Pentium III 1200 MMX, Intel, Santa Clara, CA, USA). This optical system was associated with a digitizing pad (Matrix Vision GmbH, Oppenweiler, Germany) and a histometry software package with image capturing capabilities (Image-Pro Plus 4.5, Media Cybernetics Inc., Immagini & Computer Snc, Milano, Italy).

3. Results

3.1. Clinical Results. In all cases, no perforations of the Schneiderian membrane were present, primary stability of the implants was achieved, regardless of the bone graft substitute used, and postoperative complications were absent. The healing process after sinus augmentation procedure was uneventful and no clinical signs of sinus pathology were observed. Six months after augmentation, the radiographic examination showed in all patients the presence of dense bone in the maxillary sinuses where the biomaterials were inserted.

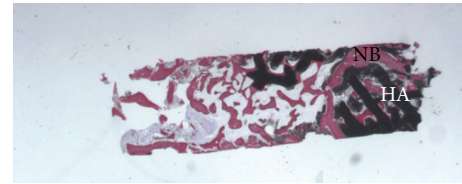


FIGURE 1: Grafted HA- β -TCP 30/70 (HA) particles, almost completely surrounded by newly formed bone (NB) (acid fuchsin-toluidine blue; original magnification 12x).

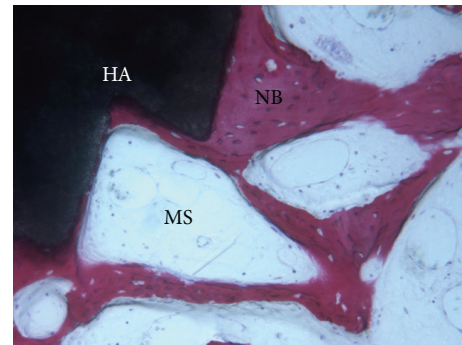


FIGURE 2: Marrow stromal cells (MS) and blood vessels were found in the vicinity of newly formed bone (NB) surrounding HA- β -TCP 30/70 particles (HA) (acid fuchsin-toluidine blue; original magnification 100x).

3.2. Histological and Histomorphometric Results

3.2.1. Biphasic Calcium Phosphate Ceramics (HA- β -TCP 30/70). At low magnification, a large number of grafted biomaterials, completely surrounded by newly formed bone, were observed (Figure 1). In some fields osteoblasts were detected in the process of apposing bone directly on the particle surface. No gaps were present at the bone-particles interface, and the bone was always in close contact with the particles. Marrow stromal cells and blood vessels were found inside the marrow spaces. A vascular growth was also observed next to the newly formed bone (Figure 2). No inflammatory cells or foreign body reaction was noted around the grafted particles. Histomorphometry showed that newly formed bone represented 30.2%, marrow spaces 40.7%, and the residual graft material 29.1%.

3.2.2. Anorganic Bovine Bone (ABB). At low magnification, trabecular bone with large marrow spaces was observed (Figure 3). Some of the particles appeared to be cemented by this newly formed bone. At higher magnification, the bone presented wide osteocyte lacunae (Figure 4). A limited number of anorganic bovine bone particles were partially covered by connective tissue. No inflammatory cell infiltrate was present around the particles or at the interface with bone. Histomorphometry showed that newly formed bone represented 20.1%, marrow spaces 60.8%, and the residual graft material 19.1%.

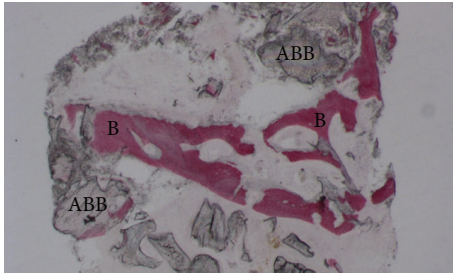


FIGURE 3: Trabecular bone (B) with large marrow spaces and residual ABB (ABB) particles can be observed (acid fuchsin-toluidine blue; original magnification 30x).

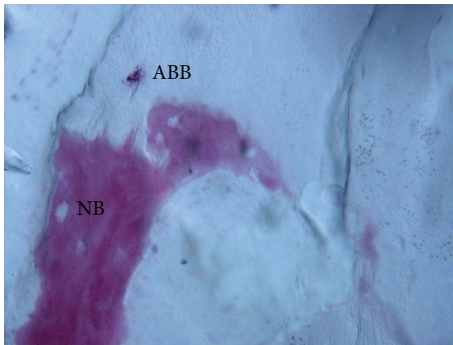


FIGURE 4: Newly formed trabecular bone (NB) is in close contact with ABB (ABB) particle, with no gaps at the bone-particle interface (acid fuchsin-toluidine blue; original magnification 400x).

3.2.3. Mineralized Solvent-Dehydrated Bone Allograft (MSDBA). At low magnification, trabecular bone with large marrow spaces was observed (Figure 5). Few particles presented irregularly shaped margins, probably due to a resorption process. There were no gaps at the bone-particle interface and the new bone was in strict contact with the granules. In some fields, osteoblasts were observed in the process of apposing bone directly on the particle surface (Figure 6). Newly formed bone was characterized by large osteocyte lacunae and bridged up most part of the biomaterial particles. Histomorphometry showed that newly formed bone represented 16.4%, marrow spaces 65.1%, and the residual graft material 18.5%.

3.2.4. Equine Bone (EB). At low magnification, trabecular bone with large marrow spaces was observed. In a portion of the specimen, preexisting bone with areas of remodeling was present (Figure 7). Some of the particles appeared to be cemented by the newly formed bone. At higher magnification, the bone showed wide osteocyte lacunae (Figure 8). Some trabeculae of the grafted material were bridged by newly formed bone. No inflammatory cells or multinucleated cells were observed around the particles or at newly formed bone-biomaterial interface in the marrow spaces. Histomorphometry showed that newly formed bone represented 21.9%, marrow spaces 54.9%, and the residual graft material 23.2%.

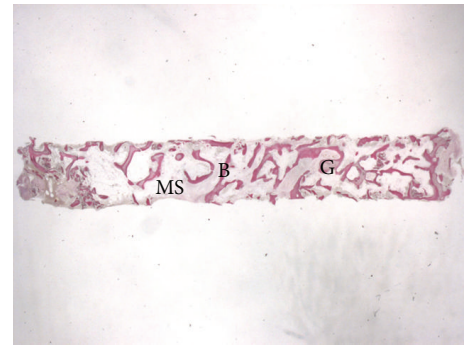


FIGURE 5: Trabecular bone (B) with large marrow spaces (MS) and residual MSDBA (G) particles can be observed (acid fuchsin-toluidine blue; original magnification 10x).

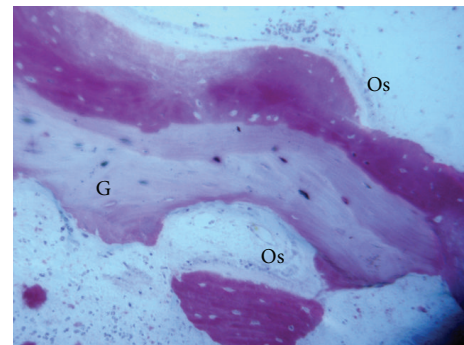


FIGURE 6: In some fields, osteoblasts (Os) were observed in the process of apposing bone directly on the MSDBA (G) particles' surface (acid fuchsin-toluidine blue; original magnification 200x).

4. Discussion

In sinus augmentation procedures, the choice of bone substitutes plays a key role, because their different properties affect medium and long-term success of implant rehabilitation. However, clinical and histological outcomes about bone substitute materials and management and timing of implant placement and their follow-up still remain open questions, because there are no clear guidelines for the use of autogenous bone or bone substitutes [24]. Numerous studies have compared grafting materials after sinus augmentation, reporting small numbers of histology samples as our investigation [11, 19, 21, 22, 26, 27, 30]. Therefore, it is very important to histologically evaluate the healing process of bone substitute materials, after two-stage sinus augmentation, in order to increase the knowledge about their biological behavior in humans [37].

In the present preliminary investigation, to examine the bone regenerative potential of a newly biphasic calcium phosphate ceramic, the histologic process of healing and bone formation of HA- β -TCP (30/70) was compared to those of the most frequently used and well documented biomaterials after six months from sinus augmentation [10–13, 17–20]. The present scaffold was developed by the direct rapid prototyping technique dispense-plotting, as previously

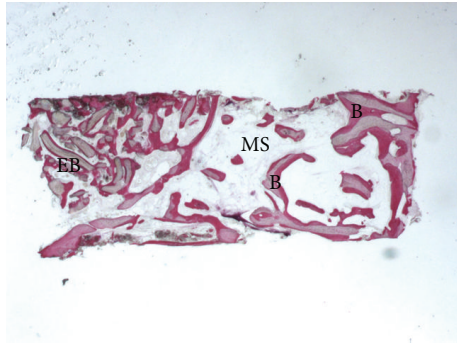


FIGURE 7: Trabecular bone (B) with large marrow spaces (MS) and residual EB (EB) particles were present (acid fuchsin-toluidine blue; original magnification 12x).

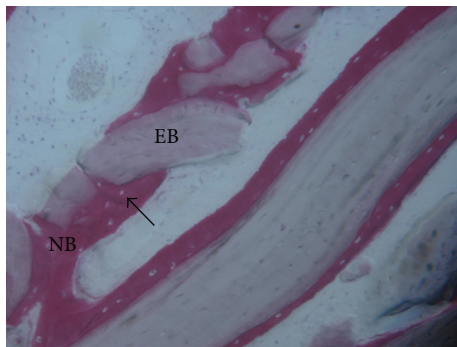


FIGURE 8: Newly formed bone (NB) with wide osteocyte lacunae (black arrow) in tight contact with EB (EB) particles (acid fuchsin-toluidine blue; original magnification 200x).

described by Deisinger et al. [38] and Mangano et al. [18]. This method enables tuning the HA/ β -TCP ratio, surface, structure, and micro- and macroporosity which in turn influence the regenerative potential. Indeed, the pattern of resorption and the healing process would be influenced by the variation of the ratio between the component at slow resorption (HA) and those at more fast resorption (β -TCP), even if no statistical significant difference was found by Schopper et al. [39], comparing two different ratios (30/70 versus 50/50) of HA/TCP in a sheep model, although a better integration into the host bone was observed in the 30/70 composition. On the contrary in a comparative study of biphasic calcium phosphates with different HA/TCP ratios in mandibular bone defects of minipig, the BCP (20/80), unlike BCP (60/40) and BCP (80/20), showed results similar to those of autogenous bone grafts, indicating that the ratio of HA/TCP (60/40) might not be optimal for bone healing [40]. The three-dimensional network with an interconnecting pore structure promotes the vascularization that is essential for the proliferation and differentiation of osteoblasts and therefore for the ingrowth of new bone into the graft [41].

At the histologic examination, the HA- β -TCP (30/70) scaffold showed a pattern of bone formation similar to the other biomaterials tested, with a large number of grafts,

completely surrounded by newly formed bone, that was always in close contact, without gaps, with the particles. Furthermore, osteoblasts, in some fields, were detected in the apposing bone directly on the particle surface, the marrow stromal cells and blood vessels were found inside the marrow spaces and the vascular growth was observed next to the newly formed bone. These histological data, in agreement with those reported in a similar study about evaluation of HA- β -TCP (40/60) in sinus elevation after a healing period of 6 months [42], demonstrated that the HA- β -TCP is an osteoconductive and resorbable material. The absence of inflammatory cells or foreign body reaction around the grafted particles testifies safety and biocompatibility.

For the ABB sample a limited number of grafted particles were found partially covered by connective tissue while some of the particles appeared to be cemented by this newly formed bone. The ABB sample was smaller than the others and this was due to the fracture of the bone biopsy retrieved from the ABB augmented site during the removal from the trephine bur. ABB is a nonresorbable bone substitute and has osteoconductive properties. Its structure could represent a type of protection against bone resorption, guaranteeing long-term stability of the augmented maxillary sinus [10]. The MSDBA sample confirmed the biocompatibility, ease of use, and ability to form and maintain new bone in the maxillary sinus as reported by previous studies [11, 26]. No signs of acute inflammation were present, and the percentage of newly formed bone and residual graft material were comparable to those reported for other biomaterials [43]. The EB sample showed some trabeculae bridged by newly formed bone. Our results are comparable to other investigations [12, 13]. It is evident resorption phenomena, and its ability to achieve a more rapid and intense vascularization is very important also in influencing long-term integration and predictability of implant-prosthetic rehabilitation in regenerated sites. Its higher resorption ability could probably be due to a deantigenation process this grafting material undergoes [13]. The results of the present investigation revealed that HA- β -TCP (30/70) could provide a better result in sinus augmentation procedures compared to the other biomaterials. No histological signs of adverse reactions were observed. Results from this preliminary investigation have shown that HA- β -TCP (30/70) has good biocompatibility, with no histological signs of adverse reactions, and osteoconductivity, with bone formation directly on the biomaterial surface. Nevertheless the presence of a high quantity of the biomaterial particles after 6 months will require long-term histological studies to better understand the times and the modalities of the resorption of this graft.

In conclusion, within the limitations of the present report the histological and histomorphometric observations support the fact that Ha-TCP (30/70) can be suitable for successful augmentation procedures of the maxillary sinus and represents a very interesting option.

Conflict of Interests

The authors declare that they have no conflict of interests.

Acknowledgment

The work was partially supported by the Ministry of Education, University and Research (MIUR), Rome, Italy (PRIN 2010ZLNJ5), without any influence or interference.

References

- [1] M. Chiapasco, P. Casentini, and M. Zaniboni, "Bone augmentation procedures in implant dentistry," *The International Journal of Oral & Maxillofacial Implants*, vol. 24, supplement, pp. 237–259, 2009.
- [2] T. L. Aghaloo and P. K. Moy, "Which hard tissue augmentation techniques are the most successful in furnishing bony support for implant placement?" *International Journal of Oral and Maxillofacial Implants*, vol. 22, pp. 49–70, 2007.
- [3] M. Hallman and A. Thor, "Bone substitutes and growth factors as an alternative/complement to autogenous bone for grafting in implant dentistry," *Periodontology 2000*, vol. 47, no. 1, pp. 172–192, 2008.
- [4] R. J. Klijn, G. J. Meijer, E. M. Bronkhorst, and J. A. Jansen, "A meta-analysis of histomorphometric results and graft healing time of various biomaterials compared to autologous bone used as sinus floor augmentation material in humans," *Tissue Engineering—Part B: Reviews*, vol. 16, no. 5, pp. 493–507, 2010.
- [5] C. M. Misch, "Autogenous bone: is it still the gold standard?" *Implant Dentistry*, vol. 19, no. 5, p. 361, 2010.
- [6] D. Rickert, J. J. R. H. Slater, H. J. A. Meijer, A. Vissink, and G. M. Raghoobar, "Maxillary sinus lift with solely autogenous bone compared to a combination of autogenous bone and growth factors or (solely) bone substitutes. A systematic review," *International Journal of Oral & Maxillofacial Surgery*, vol. 41, no. 2, pp. 160–167, 2012.
- [7] G. D. Rabelo, P. M. de Paula, F. S. Rocha, C. Jordão Silva, and D. Zanetta-Barbosa, "Retrospective study of bone grafting procedures before implant placement," *Implant Dentistry*, vol. 19, no. 4, pp. 342–350, 2010.
- [8] P. Galindo-Moreno, I. Moreno-Riestra, G. Ávila et al., "Histomorphometric comparison of maxillary pristine bone and composite bone graft biopsies obtained after sinus augmentation," *Clinical Oral Implants Research*, vol. 21, no. 1, pp. 122–128, 2010.
- [9] R. J. Klijn, J. J. P. van den Beucken, E. M. Bronkhorst, S. J. Berge, G. J. Meijer, and J. A. Jansen, "Predictive value of ridge dimensions on autologous bone graft resorption in staged maxillary sinus augmentation surgery using Cone-Beam CT," *Clinical Oral Implants Research*, vol. 23, no. 4, pp. 409–415, 2012.
- [10] C. M. Schmitt, H. Doering, T. Schmidt, R. Lutz, F. W. Neukam, and K. A. Schlegel, "Histological results after maxillary sinus augmentation with Straumann BoneCeramic, Bio-Oss, Puros, and autologous bone. A randomized controlled clinical trial," *Clinical Oral Implants Research*, vol. 24, no. 5, pp. 576–585, 2013.
- [11] S. Annibaldi, M. P. Cristalli, G. La Monaca et al., "Human maxillary sinuses augmented with mineralized, solvent-dehydrated bone allograft: a longitudinal case series," *Implant Dentistry*, vol. 20, no. 6, pp. 445–454, 2011.
- [12] M. Nevins, F. Heinemann, U. W. Janke et al., "Equine-derived bone mineral matrix for maxillary sinus floor augmentation: a clinical, radiographic, histologic, and histomorphometric case series," *The International Journal of Periodontics and Restorative Dentistry*, vol. 33, no. 4, pp. 483–489, 2013.
- [13] S. Tetè, R. Vinci, V. L. Zizzari et al., "Maxillary sinus augmentation procedures through equine-derived biomaterial or calvaria autologous bone: immunohistochemical evaluation of OPG/RANKL in humans," *European Journal of Histochemistry*, vol. 57, no. 1, p. e10, 2013.
- [14] J. Bassil, N. Naaman, R. Lattouf et al., "Clinical, histological, and histomorphometrical analysis of maxillary sinus augmentation using inorganic bovine in humans: preliminary results," *Journal of Oral Implantology*, vol. 39, no. 1, pp. 73–80, 2013.
- [15] C. Mangano, B. Barboni, L. Valbonetti et al., "In vivo behavior of a custom-made 3D synthetic bone substitute in sinus augmentation procedure in sheep," *Journal of Oral Implantology*. In press.
- [16] B. Barboni, C. Mangano, L. Valbonetti et al., "Synthetic bone substitute engineered with amniotic epithelial cells enhances bone regeneration after maxillary sinus augmentation," *PLoS ONE*, vol. 8, no. 5, Article ID e63256, 2013.
- [17] A. Mordenfeld, M. Hallman, C. B. Johansson, and T. Albrektsson, "Histological and histomorphometrical analyses of biopsies harvested 11 years after maxillary sinus floor augmentation with deproteinized bovine and autogenous bone," *Clinical Oral Implants Research*, vol. 21, no. 9, pp. 961–970, 2010.
- [18] C. Mangano, B. Sinjari, J. A. Shibli et al., "A human clinical, histological, histomorphometrical, and radiographical study on biphasic ha-beta-tcp 30/70 in maxillary sinus augmentation," *Clinical Implant Dentistry and Related Research*, 2013.
- [19] G. Iezzi, M. Degidi, A. Piattelli et al., "Comparative histological results of different biomaterials used in sinus augmentation procedures: a human study at 6 months," *Clinical Oral Implants Research*, vol. 23, no. 12, pp. 1369–1376, 2012.
- [20] Y.-K. Kim, J. Lee, J.-Y. Yun, P.-Y. Yun, and I.-W. Um, "Comparison of autogenous tooth bone graft and synthetic bone graft materials used for bone resorption around implants after crestal approach sinus lifting: a retrospective study," *Journal of Periodontal & Implant Science*, vol. 44, no. 5, pp. 216–221, 2014.
- [21] S. S. Wallace and S. J. Froum, "Effect of maxillary sinus augmentation on the survival of endosseous dental implants. A systematic review," *Annals of periodontology*, vol. 8, no. 1, pp. 328–343, 2003.
- [22] M. Chiapasco, P. Casentini, and M. Zaniboni, "Bone augmentation procedures in implant dentistry," *The International Journal of oral & Maxillofacial implants*, vol. 24, pp. 237–259, 2009.
- [23] E. Nkenke and F. Stelzle, "Clinical outcomes of sinus floor augmentation for implant placement using autogenous bone or bone substitutes: a systematic review," *Clinical Oral Implants Research*, vol. 20, no. 4, pp. 124–133, 2009.
- [24] S. S. Jensen, N. Brogini, E. Hjørtting-Hansen, R. Schenk, and D. Buser, "Bone healing and graft resorption of autograft, anorganic bovine bone and β -tricalcium phosphate. A histologic and histomorphometric study in the mandibles of minipigs," *Clinical Oral Implants Research*, vol. 17, no. 3, pp. 237–243, 2006.
- [25] S. V. Dorozhkin, "Self-setting calcium orthophosphate formulations," *Journal of Functional Biomaterials*, vol. 4, no. 4, pp. 209–311, 2013.
- [26] S. V. Dorozhkin, "Calcium orthophosphates in dentistry," *Journal of Materials Science: Materials in Medicine*, vol. 24, no. 6, pp. 1335–1363, 2013.
- [27] S. V. Dorozhkin, "Biomaterials and hybrid biomaterials based on calcium orthophosphates," *Biomaterials*, vol. 1, no. 1, pp. 3–56, 2011.
- [28] C. Mangano, V. Perrotti, J. A. Shibli et al., "Maxillary sinus grafting with biphasic calcium phosphate ceramics: clinical and histologic evaluation in man," *The International Journal of Oral & Maxillofacial Implants*, vol. 28, no. 1, pp. 51–56, 2013.

- [29] C. Lindgren, A. Mordenfeld, and M. Hallman, "A prospective 1-year clinical and radiographic study of implants placed after maxillary sinus floor augmentation with synthetic biphasic calcium phosphate or deproteinized bovine bone," *Clinical Implant Dentistry and Related Research*, vol. 14, no. 1, pp. 41–50, 2012.
- [30] S. J. Froum, S. S. Wallace, S.-O. Cho, N. Elian, and D. P. Tarnow, "Histomorphometric comparison of a biphasic bone ceramic to anorganic bovine bone for sinus augmentation: 6- to 8-month postsurgical assessment of vital bone formation. A Pilot Study," *International Journal of Periodontics and Restorative Dentistry*, vol. 28, no. 3, pp. 273–281, 2008.
- [31] C. M. Schmitt, T. Moest, R. Lutz, F. W. Neukam, and K. A. Schlegel, "Anorganic bovine bone (ABB) vs. autologous bone (AB) plus ABB in maxillary sinus grafting. A prospective non-randomized clinical and histomorphometrical trial," *Clinical Oral Implants Research*, 2014.
- [32] G. Iezzi, A. Scarano, C. Mangano, B. Cirotti, and A. Piattelli, "Histologic results from a human implant retrieved due to fracture 5 years after insertion in a sinus augmented with anorganic bovine bone," *Journal of Periodontology*, vol. 79, no. 1, pp. 192–198, 2008.
- [33] S. J. Froum, S. S. Wallace, N. Elian, S. C. Cho, and D. P. Tarnow, "Comparison of mineralized cancellous bone allograft (Puros) and anorganic bovine bone matrix (Bio-Oss) for sinus augmentation: histomorphometry at 26 to 32 weeks after grafting," *International Journal of Periodontics and Restorative Dentistry*, vol. 26, no. 6, pp. 543–551, 2006.
- [34] S. Tetè, V. L. Zizzari, R. Vinci et al., "Equine and porcine bone substitutes in maxillary sinus augmentation: a histological and immunohistochemical analysis of VEGF expression," *Journal of Craniofacial Surgery*, vol. 25, no. 3, pp. 835–839, 2014.
- [35] L. Artese, A. Piattelli, D. A. Di Stefano et al., "Sinus lift with autologous bone alone or in addition to equine bone: an immunohistochemical study in man," *Implant Dentistry*, vol. 20, no. 5, pp. 383–388, 2011.
- [36] A. Piattelli, A. Scarano, and M. Quaranta, "High-precision, cost-effective cutting system for producing thin sections of oral tissues containing dental implants," *Biomaterials*, vol. 18, no. 7, pp. 577–579, 1997.
- [37] Y. K. Kim, P. Y. Yun, S. G. Kim, and S. C. Lim, "Analysis of the healing process in sinus bone grafting using various grafting materials," *Oral Surgery, Oral Medicine, Oral Pathology, Oral Radiology and Endodontology*, vol. 107, no. 2, pp. 204–211, 2009.
- [38] U. Deisinger, S. Hamisch, M. Schumacher, F. Uhl, R. Detsch, and G. Ziegler, "Fabrication of tailored hydroxyapatite scaffolds: comparison between a direct and an indirect rapid prototyping technique," *Key Engineering Materials*, vol. 361–363, pp. 915–918, 2008.
- [39] C. Schopper, F. Ziya-Ghazvini, W. Goriwoda et al., "HA/TCP compounding of a porous CaP biomaterial improves bone formation and scaffold degradation. A long-term histological study," *Journal of Biomedical Materials Research Part: B Applied Biomaterials*, vol. 74, no. 1, pp. 458–467, 2005.
- [40] S. S. Jensen, M. M. Bornstein, M. Dard, D. D. Bosshardt, and D. Buser, "Comparative study of biphasic calcium phosphates with different HA/TCP ratios in mandibular bone defects. A long term histomorphometric study in minipigs," *Journal of Biomedical Materials Research B*, vol. 90, pp. 171–181, 2009.
- [41] C. R. Campion, C. Chander, T. Buckland, and K. Hing, "Increasing strut porosity in silicate-substituted calcium-phosphate bone graft substitutes enhances osteogenesis," *Journal of Biomedical Materials Research. Part B Applied Biomaterials*, vol. 97, no. 2, pp. 245–254, 2011.
- [42] J. W. F. H. Frenken, W. F. Bouwman, N. Bravenboer, S. A. Zijdeveld, E. A. J. M. Schulten, and C. M. ten Bruggenkate, "The use of Straumann Bone Ceramic in a maxillary sinus floor elevation procedure: a clinical, radiological, histological and histomorphometric evaluation with a 6-month healing period," *Clinical Oral Implants Research*, vol. 21, no. 2, pp. 201–208, 2010.
- [43] A. Scarano, M. Degidi, G. Iezzi et al., "Maxillary sinus augmentation with different biomaterials: a comparative histologic and histomorphometric study in man," *Implant Dentistry*, vol. 15, no. 2, pp. 197–207, 2006.

Research Article

Oral Streptococci Biofilm Formation on Different Implant Surface Topographies

Pedro Paulo Cardoso Pita,¹ José Augusto Rodrigues,^{1,2} Claudia Ota-Tsuzuki,¹ Tatiane Ferreira Miato,¹ Elton G. Zenobio,³ Gabriela Giro,¹ Luciene C. Figueiredo,¹ Cristiane Gonçalves,¹ Sergio A. Gehrke,⁴ Alessandra Cassoni,¹ and Jamil Awad Shibli¹

¹ Department of Periodontology and Oral Implantology, Dental Research Division, Guarulhos University, Praça Tereza Cristina 229, 07023-070 Guarulhos, SP, Brazil

² Department of Operative Dentistry, Dental Research Division, Guarulhos University, Praça Tereza Cristina 229, 07023-070 Guarulhos, SP, Brazil

³ Department of Oral Implantology, PUC Minas, Avenida Dom Cabral 500, Prédio 46, Coração Eucarístico, 30535-901 Belo Horizonte, MG, Brazil

⁴ Biotecnos-Tecnologia e Ciência Ltda, Rua Dr. Bozano, 571 Centro, 97015-001 Santa Maria, RS, Brazil

Correspondence should be addressed to José Augusto Rodrigues; gutojar@yahoo.com

Received 7 September 2014; Revised 4 November 2014; Accepted 4 November 2014

Academic Editor: David M. Dohan Ehrenfest

Copyright © 2015 Pedro Paulo Cardoso Pita et al. This is an open access article distributed under the Creative Commons Attribution License, which permits unrestricted use, distribution, and reproduction in any medium, provided the original work is properly cited.

The establishment of the subgingival microbiota is dependent on successive colonization of the implant surface by bacterial species. Different implant surface topographies could influence the bacterial adsorption and therefore jeopardize the implant survival. This study evaluated the biofilm formation capacity of five oral streptococci species on two titanium surface topographies. *In vitro* biofilm formation was induced on 30 titanium discs divided in two groups: sandblasted acid-etched (SAE- $n = 15$) and as-machined (M- $n = 15$) surface. The specimens were immersed in sterilized whole human unstimulated saliva and then in fresh bacterial culture with five oral streptococci species: *Streptococcus sanguinis*, *Streptococcus salivarius*, *Streptococcus mutans*, *Streptococcus sobrinus*, and *Streptococcus cricetus*. The specimens were fixed and stained and the adsorbed dye was measured. Surface characterization was performed by atomic force and scanning electron microscopy. Surface and microbiologic data were analyzed by Student's *t*-test and two-way ANOVA, respectively ($P < 0.05$). *S. cricetus*, *S. mutans*, and *S. sobrinus* exhibited higher biofilm formation and no differences were observed between surfaces analyzed within each species ($P > 0.05$). *S. sanguinis* exhibited similar behavior to form biofilm on both implant surface topographies, while *S. salivarius* showed the lowest ability to form biofilm. It was concluded that biofilm formation on titanium surfaces depends on surface topography and species involved.

1. Introduction

Establishment of the dental subgingival microbiota is dependent on successive colonization of the tooth surface by several bacterial species [1]. Each of these bacterial species appears to facilitate enamel surface colonization by the next wave of bacterial settlers, resulting in the establishment of an anaerobic Gram-negative microbiota [2]. So far, it is believed that a similar pattern of the same colonization process may occur on the titanium implant surfaces [3–5].

However, the different implant surface topographies could influence the bacterial adsorption [6–8]. Physical and chemical factors may affect the attachment of biofilms to hard surfaces. The surface roughness at micrometer level can increase the surface area and hence increase the bacterial colonization. Roughness also provides protection from shear forces and increases the difficulty of cleaning methods. Furthermore, Kolenbrander et al. [2] have shown that supragingival plaque formation, after initial bacterial colonization, was faster on a rough surface. The roughness

of different dental implant surfaces can work like grooves for initial periodontal pathogen adhesion [6, 9, 10].

The oral streptococci are members of the indigenous microbiota mainly in the supragingival environment [11] and species of mutans group such as *Streptococcus mutans*, *Streptococcus sobrinus*, and *Streptococcus cricetus* were related to individuals with teeth because they are able to adhere to nonshedding surfaces, with *S. mutans* being the most prevalent species in humans [12]. Other species such as *Streptococcus sanguinis* and *Streptococcus salivarius* are commonly found in healthy periodontal individuals and the latter is related to mucosal surfaces; besides it can contribute to the coaggregation of pathogenic bacteria, such as *Porphyromonas gingivalis*. Thus the oral streptococci are considered the pioneer colonizers and might participate in the process, which can lead to implant failure on the long term [6].

Therefore, the aim of this *in vitro* study was to verify the ability of five oral streptococci species to form biofilm on two different titanium surface topographies.

2. Material and Methods

2.1. Implant Surface Topography. Thirty discs (5 mm diameter and 3 mm thickness) made of grade-4 titanium (Implacil De Bortoli, Sao Paulo, SP, Brazil) were prepared with 2 surface topographies: as-machined (M) and sandblasted acid-etched (SAE) surfaces. The titanium discs with sandblasted acid-etched surface were blasted with 50–100 μm TiO_2 particles. After sandblasting, the specimens were ultrasonically cleaned with an alkaline solution, washed in distilled water, and pickled with maleic acid.

2.2. Implant Surface Characteristics. The samples were first checked for chemical composition with XPS/ESCA (X-ray photoelectron spectroscopy/electron spectroscopy for chemical analysis), and no significant pollution was detected [13]. The topographies at the microscale were then visualized using routine scanning electron microscopy (SEM) control. At the nanoscale, the SEM confirmed that both surface types were nanosmooth, following the current definition [13, 14]. The sole difference between these 2 tested implant types was therefore the specific surface microtopography.

Atomic force microscopy (AFM, PicoSPM I plus 2100 PicoScan Controller, in contact mode) was used for the surface topography analysis, in contact mode. The AFM scanned areas of 60 $\mu\text{m} \times 60 \mu\text{m}$ of each specimen. The measured parameters, such as the arithmetic average of all profile point absolute values (Ra), the root-mean-square of all point values (Rq), and the average absolute height values of the five highest peaks and the depths of the five deepest valleys (Rz), were measured for each group. Representative images of the surfaces of each group of specimens were also taken by scanning electronic microscopy.

2.3. Strains. *Streptococcus sanguinis* (ATCC 10556), *Streptococcus salivarius* (ATCC 7073), *Streptococcus mutans* (ATCC 25175) and *Streptococcus sobrinus* (ATCC 33478), and

Streptococcus cricetus (ATCC 19642) were used in this study in biofilm formation.

2.4. Saliva Coating of the Specimens. Unstimulated saliva from 6 healthy nonsmoker and systemic healthy donors was collected for one hour per day, for seven days. Then the saliva samples were sterilized and frozen at -20°C until a total of 500 mL was collected per donor. All donors signed the informed consent. Subsequently, the saliva samples were pooled and centrifuged (30 min; 4°C ; 27,000 $\times g$). The supernatant was pasteurized (60°C , 30 min) to inactivate endogenous enzymes, recentrifuged (30 min, 4°C ; 27,000 $\times g$) in sterile bottles, and stored at -20°C . The pasteurization efficacy was evaluated by plating 100 μL of saliva onto brain heart infusion (BHI) agar and by observing the absence of bacterial growth after 72 hours. The sterile disks were placed in a sterile 24-well polystyrene cell culture plate containing 500 μL of saliva for 4 hours to allow salivary pellicle formation.

2.5. Biofilm Formation Assay. After coating period, saliva was aspirated from each well and replaced with 500 μL of BHI broth (double concentrated) and 500 μL of saliva. Inocula were prepared by harvesting each standard reference strain cell from BHI agar plates previously inoculated and incubated under microaerophilic conditions for 24 hours (candle jar, 37°C). The bacterial cells were suspended in sterile saline solution, adjusting the turbidity to OD_{630} 0.15 ($\sim 10^6$ UFC/mL). Each well was inoculated with 100 μL of this inoculum suspension. Plates were then incubated for 16 hours under microaerophilic conditions. Afterwards, the specimens were gently washed in sterile saline solution three times in order to remove unattached cells.

The specimens with remaining attached bacteria were fixed using 0.25 mL of 2.5% glutaraldehyde per well for 15 min and, subsequently, air-dried. The specimens were transferred to clean well plates and were stained with 0.25 mL of crystal violet for 5 min. Excess stain was rinsed off by placing the microplate under running tap water, and after this it was air-dried. The specimens were transferred to clean tubes, and, in order to resolubilize the dye bound to the adherent cells on specimen surfaces, 0.3 mL of ethanol was added per well. The supernatant was transferred to a clean 96-well microplate, and the absorbance was measured at 570 nm using an automated 96-well microplate reader.

2.6. Statistical Analysis. The surface characterization was tested using Student's *t*-test. Two-way analysis of variance (ANOVA) was used in order to compare the groups of species within the same group of implant surface topography and to verify possible differences among specimen surfaces within the same species ($\alpha = 0.05$).

3. Results

3.1. Surface Characterization of Implants Surfaces Substrata. Scanning electronic microscopy showed that M group exhibited only the grid of machining (Figure 1(a)). On the other

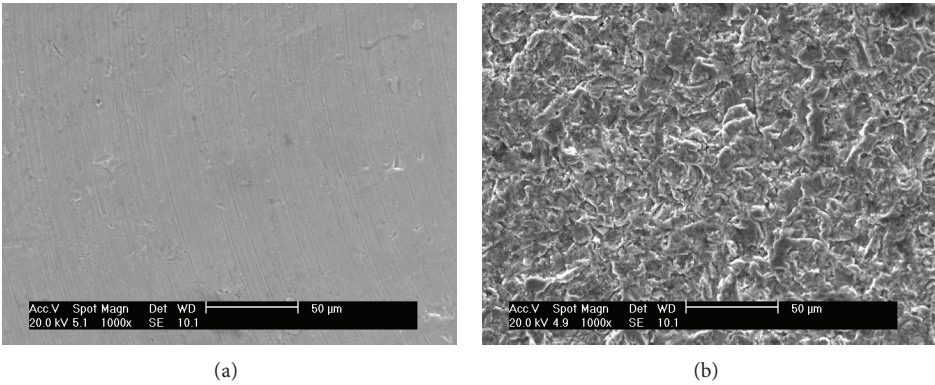


FIGURE 1: Scanning electron microphotograph of the implant surface topography: (a) as-machined implant surface and (b) sandblasted acid-etched surface.

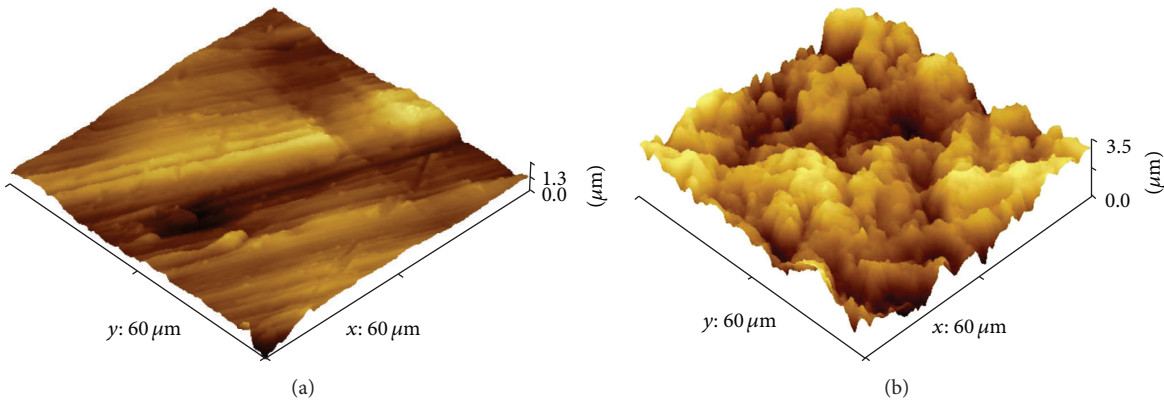


FIGURE 2: Atomic force microscopy (AFM) of the implant surface topography: (a) as-machined implant surface and (b) sandblasted acid-etched surface.

hand, the SAE exhibited peaks and valleys with diverse irregularities (Figure 1(b)).

The surfaces were characterized by atomic force microscopy, which revealed differences between the surfaces ($P < 0.0001$). M showed only the machining grids with peaks of $1.3\text{ }\mu\text{m}$ and some regions that were almost flat (Figure 2(a)). The SAE exhibited irregular surfaces with peaks of about $6.5\text{ }\mu\text{m}$ (Figure 2(b)). The roughness values are shown in Table 1.

3.2. In Vitro Determination of Microbial Adhesion. The bio-film forming ability was evaluated and the means of readings are shown in Figure 3. The group mutans streptococci (*S. cricetus*, *S. mutans*, and *S. sobrinus*) exhibited higher levels of biofilm formation and no differences were observed between surfaces analyzed within each species ($P > 0.05$). It was observed that although *S. cricetus* exhibited the highest ability to form biofilm on SAE, among all species, within this species this difference was not significant ($P > 0.05$) between the surfaces analyzed.

S. sanguinis exhibited a similar behavior to form biofilm on both implant surface topographies (Figure 4), and their ability to do so was lower than that of the group mutans streptococci species. The lowest ability was observed for *S. salivarius*.

TABLE 1: Mean \pm standard deviation of the as-machined (MS) and titanium discs blasted with titanium oxide particles and washed with maleic acid solution (SAE) profilometry.

Implant surface topography*	Ra (μm)	Rq (μm)	Rz (μm)
As-machined (M)	0.14 ± 0.02	0.16 ± 0.01	1.61 ± 0.10
Sandblasted acid-etched surface (SAE)	0.87 ± 0.14	1.12 ± 0.18	5.14 ± 0.69

* Statistically significant between the implant surface topographies (Student's t -test $P = 0.0001$), $M < \text{SAE}$; Ra: arithmetic average of the absolute values of all profile points; Rq: the root-mean-square of the values of all points; Rz: the average value of the absolute heights of the five highest peaks and the depths of the five deepest valleys.

4. Discussion

Titanium has been widely used as a component of dental implants since the 1970s. More than the improvements in biomechanical performance, these modifications on implant surfaces lead to other biological responses, such as differences in the protein adsorption profiles [15, 16], attachment, cell proliferation and differentiation, and fibrin adhesion [17]. The present study presented the biofilm forming ability of 5 oral streptococci species on two different types of surfaces.

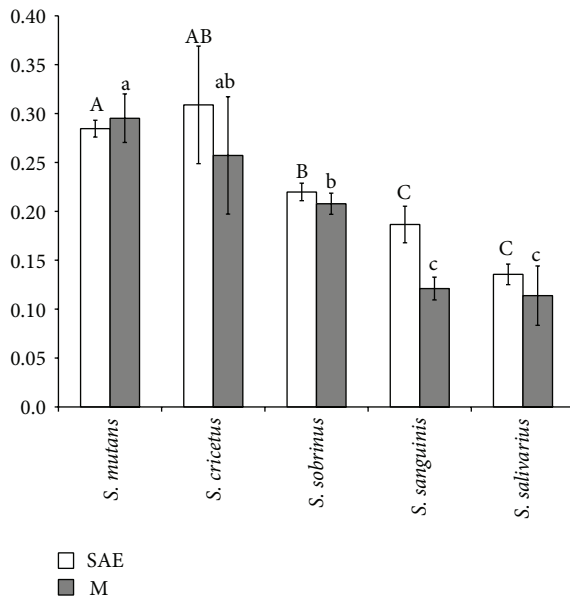


FIGURE 3: Mean \pm standard deviation of the amount of adsorbed dye released after the assay ($P > 0.05$; two-way ANOVA). Letters: differences among biofilm accumulated by each species ($P < 0.05$; two-way ANOVA/Tukey test). Different letters indicate groups with distinct characteristics. Capital letters compare SAE surfaces, while lower case letters compare M surfaces.

The blasting process with titanium oxide particle (50–100 μm) and maleic acid solution etching modified substantially the surface, which was indeed confirmed by SEM and AFM. AFM revealed higher density of irregularities on R surface as well higher peaks. An earlier study [17] detected different profiles of plasma adsorption depending on surface treatment (acid etching only and blasting plus acid etching processes) and attributed this difference mainly to the changes in physical properties, since minor alterations in chemical composition were detected. On the other hand, Li et al. [18] found differences on titanium surfaces after application of different treatments, including chemical changes such as an oxide layer and surface contamination, and these might exert some influence on biocompatibility issues. Recently, it has been shown that nanosurfaces could impair bacterial adsorption, suggesting that further studies must be done to evaluate the role of implant surface topography on bacterial colonization [19].

However, there is an unclear debate about the link between bacterial contamination and peri-implantitis [20, 21]. These papers suggested that peri-implantitis is pathology of bone-to-implant interface and that bacterial contamination is only the associated consequence, not the triggering factor. However, we must point out that, until now, there are now clear and consistent evidences to follow this idea.

In addition, these surface changes might also influence biofilm formation, since the earlier steps of this process are related to contact surface extension, surface free energy, topography, wettability, hydrophobicity, and other surface traits [17, 18, 22–26].

The results of the present study revealed differences as regards the biofilm forming ability among *S. salivarius*,

S. cricetus, *S. mutans*, *S. sobrinus*, and *S. sanguinis*. Among them, *S. salivarius* and *S. sanguinis* exhibited the lowest capacity to form biofilm. Two aspects of biofilm forming ability must be pointed out: the specific traits of each species and surface topographies.

Differences on adhesion to glass surface among mutans streptococci group were already observed [27]. The authors found that *S. rattus* adhered less than the other species (*S. sobrinus*, *S. mutans*, and *S. cricetus*) and attributed these results to different properties of the *S. rattus* surface like negative zeta-potentials. In the present study, three species of mutans streptococci group (*S. mutans*, *S. cricetus*, and *S. sobrinus*) were evaluated and although the raw values showed a high capacity of *S. mutans* to accumulate biofilm on titanium surface followed by *S. cricetus* and *S. sobrinus*, statistical differences were observed only between *S. mutans* and *S. sobrinus* ($P < 0.05$).

Although roughness seems to promote an increase in the amount of plaque, the biofilm composition did not show substantial changes and the establishment of irreversible attachment in the surface irregularities, where microorganisms are protected against mechanical shear [10]. Despite this, the results of our study demonstrated that biofilm formation does not increase markedly on rougher surfaces.

Oral strains, most of them having high surface free energy, might adhere better to hydrophilic substrata [28]. Differences with regard to surface hydrophobicity could be attributed to the acid etching, which could introduce ^-OH groups on the surface, thus modifying its chemical properties [29]. According to this hypothesis, these treatments can originate different surfaces, and, consequently, new patterns of adsorbed substances will be originated, which may offer different profiles of receptors for bacterial colonization.

Another issue concerns virulence traits of each species like tooth colonization mechanisms; *S. mutans* apparently attach by adhesin and glucan mediated mechanisms, whereas *S. sobrinus* utilize primarily the latter process [30].

5. Conclusions

In conclusion, within the limitations of the study, the present findings showed the following: (a) biofilm formation by oral streptococci might vary according to the species; (b) *S. salivarius* and *S. sanguinis* showed the lowest ability to accumulate biofilm; (c) group mutans streptococci accumulated higher amounts of biofilm; (d) the substratum roughness is not the only issue to be considered with regard to bacterial biofilm formation.

Conflict of Interests

The authors declare that there is no conflict of interests regarding the publication of this paper.

Authors' Contribution

Jamil Awad Shibli, Claudia Ota-Tsuzuki, and José Augusto Rodrigues were in charge of the elaboration of the study proposal and the financial support of the study, and they

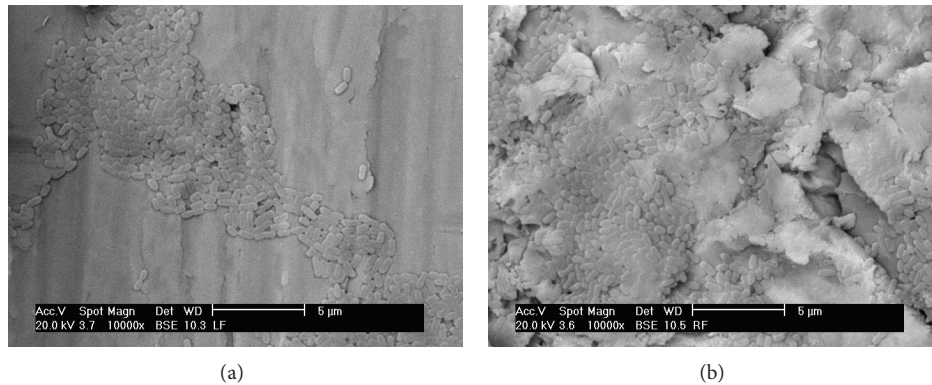


FIGURE 4: Representative scanning electron microscopy ($\times 10,000$) in a back scattering mode (BSE) of the *Streptococcus sanguinis* in (a) as-machined (M) and (b) sandblasted acid-etched (SAE) surface. Note proliferation of the *S. sanguinis* in the pitches and notches of the SAE surface.

participated in the elaboration of the paper. Luciene C. Figueiredo and Elton G. Zenobio were in charge of the statistical analysis, the implant surface characterization, and the financial support for the study. Pedro Paulo Cardoso Pita, Tatiane Ferreira Miato, Sergio A. Gehrke, Gabriela Giro, and Cristiane Gonçalves were in charge of the saliva collection, laboratory processing, and oral biofilm maintenance and they participated in the elaboration of the paper. Claudia Ota-Tsuzuki and Alessandra Cassoni were in charge of the laboratory processing of the samples and participated in the data analyses and elaboration of the paper.

Acknowledgments

Dr. Miato received grant from the University of Guarulhos (fellowship PIBIC-UnG). Implacil De Bortoli, Sao Paulo, Brazil, provided the titanium discs.

References

- [1] S. S. Socransky and A. D. Haffajee, "Periodontal microbial ecology," *Periodontology* 2000, vol. 38, pp. 135–187, 2005.
- [2] P. E. Kolenbrander, R. J. Palmer Jr., A. H. Rickard, N. S. Jakubovics, N. I. Chalmers, and P. I. Diaz, "Bacterial interactions and successions during plaque development," *Periodontology* 2000, vol. 42, no. 1, pp. 47–79, 2006.
- [3] J. A. Shibli, L. Melo, D. S. Ferrari, L. C. Figueiredo, M. Faveri, and M. Feres, "Composition of supra- and subgingival biofilm of subjects with healthy and diseased implants," *Clinical Oral Implants Research*, vol. 19, no. 10, pp. 975–982, 2008.
- [4] J. A. Shibli, M. C. Martins, R. F. M. Lotufo, and E. Marcantonio Jr., "Microbiologic and radiographic analysis of ligature-induced peri-implantitis with different dental implant surfaces," *The International Journal of Oral & Maxillofacial Implants*, vol. 18, no. 3, pp. 383–390, 2003.
- [5] J. A. Shibli, T. R. C. Vitussi, R. V. Garcia et al., "Implant surface analysis and microbiologic evaluation of failed implants retrieved from smokers," *The Journal of Oral Implantology*, vol. 33, no. 4, pp. 232–238, 2007.
- [6] G. Nakazato, H. Tsuchiya, M. Sato, and M. Yamauchi, "In vivo plaque formation on implant materials," *The International Journal of Oral and Maxillofacial Implants*, vol. 4, no. 4, pp. 321–326, 1989.
- [7] S. Sardin, J.-J. Morrier, G. Benay, and O. Barsotti, "In vitro streptococcal adherence on prosthetic and implant materials. Interactions with physicochemical surface properties," *Journal of Oral Rehabilitation*, vol. 31, no. 2, pp. 140–148, 2004.
- [8] J. A. Shibli, M. C. Martins, L. H. Theodoro, R. F. M. Lotufo, V. G. Garcia, and E. J. Marcantonio, "Lethal photosensitization in microbiological treatment of ligature-induced peri-implantitis: a preliminary study in dogs," *Journal of Oral Science*, vol. 45, no. 1, pp. 17–23, 2003.
- [9] B. Gröbner-Schreiber, M. Griepentrog, I. Haustein et al., "Plaque formation on surface modified dental implants—an in vitro study," *Clinical Oral Implants Research*, vol. 12, no. 6, pp. 543–551, 2001.
- [10] M. Quirynen, H. C. van der Mei, C. M. Bollen et al., "An in vivo study of the influence of the surface roughness of implants on the microbiology of supra- and subgingival plaque," *Journal of Dental Research*, vol. 72, no. 9, pp. 1304–1309, 1993.
- [11] M. Quirynen, H. C. van der Mei, C. M. Bollen et al., "The influence of surface-free energy on supra- and subgingival plaque microbiology. An in vivo study on implants," *Journal of Periodontology*, vol. 65, no. 2, pp. 162–167, 1994.
- [12] H. K. Kuramitsu, X. He, R. Lux, M. H. Anderson, and W. Shi, "Interspecies interactions within oral microbial communities," *Microbiology and Molecular Biology Reviews*, vol. 71, no. 4, pp. 653–670, 2007.
- [13] A. L. Coykendall, "Classification and identification of the viridans streptococci," *Clinical Microbiology Reviews*, vol. 2, no. 3, pp. 315–328, 1989.
- [14] D. M. D. Ehrenfest, B. S. Kang, G. Sammartino et al., "Guidelines for the publication of articles related to implant surfaces and design from the POSEIDO: a standard for surface characterization," *POSEIDO*, vol. 1, no. 1, pp. 7–15, 2013.
- [15] A. Shibli and D. M. Dohan Ehrenfest, "In dental implant surfaces, NanoWar has begun... but NanoQuest is still at stake!," *POSEIDO*, vol. 1, no. 3, pp. 131–140, 2013.
- [16] J. P. Davidas, "Looking for a new international standard for characterization, classification and identification of surfaces in implantable materials: the long march for the evaluation of dental implant surfaces has just begun," *POSEIDO*, vol. 2, no. 1, pp. 1–5, 2014.

- [17] M. N. Sela, L. Badihi, G. Rosen, D. Steinberg, and D. Kohavi, "Adsorption of human plasma proteins to modified titanium surfaces," *Clinical Oral Implants Research*, vol. 18, no. 5, pp. 630–638, 2007.
- [18] D. Li, S. J. Ferguson, T. Beutler et al., "Biomechanical comparison of the sandblasted and acid-etched and the machined and acid-etched titanium surface for dental implants," *Journal of Biomedical Materials Research*, vol. 60, no. 2, pp. 325–332, 2002.
- [19] E. Elizabeth, G. Baranwal, A. G. Krishnan, D. Menon, and M. Nair, "ZnO nanoparticle incorporated nanostructured metallic titanium for increased mesenchymal stem cell response and antibacterial activity," *Nanotechnology*, vol. 25, no. 11, Article ID 115101, 2014.
- [20] R. Trindade, T. Albrektsson, P. Tengvall, and A. Wennerberg, "Foreign body reaction to biomaterials: on mechanisms for buildup and breakdown of osseointegration," *Clinical Implant Dentistry and Related Research*, 2014.
- [21] T. Albrektsson, C. Dahlin, T. Jemt, L. Sennerby, A. Turri, and A. Wennerberg, "Is marginal bone loss around oral implants the result of a provoked foreign body reaction?" *Clinical Implant Dentistry and Related Research*, vol. 16, no. 2, pp. 155–165, 2014.
- [22] E. M. C. X. Lima, H. Koo, A. M. Vacca Smith, P. L. Rosalen, and A. A. Del Bel Cury, "Adsorption of salivary and serum proteins, and bacterial adherence on titanium and zirconia ceramic surfaces," *Clinical Oral Implants Research*, vol. 19, no. 8, pp. 780–785, 2008.
- [23] K. Mustafa, A. Wennerberg, J. Wroblewski, K. Hultenby, B. S. Lopez, and K. Arvidson, "Determining optimal surface roughness of TiO₂ blasted titanium implant material for attachment, proliferation and differentiation of cells derived from human mandibular alveolar bone," *Clinical Oral Implants Research*, vol. 12, no. 5, pp. 515–525, 2001.
- [24] L. le Guéhennec, A. Soueidan, P. Layrolle, and Y. Amouriq, "Surface treatments of titanium dental implants for rapid osseointegration," *Dental Materials*, vol. 23, no. 7, pp. 844–854, 2007.
- [25] W. Teughels, N. Van Assche, I. Sliepen, and M. Quirynen, "Effect of material characteristics and/or surface topography on biofilm development," *Clinical Oral Implants Research*, vol. 17, no. 2, pp. 68–81, 2006.
- [26] A. Leonhardt, J. Olsson, and G. Dahlén, "Bacterial colonization on titanium, hydroxyapatite, and amalgam surfaces in vivo," *Journal of Dental Research*, vol. 74, no. 9, pp. 1607–1612, 1995.
- [27] H. J. Busscher and H. C. van der Mei, "Physico-chemical interactions in initial microbial adhesion and relevance for biofilm formation," *Advances in Dental Research*, vol. 11, no. 1, pp. 24–32, 1997.
- [28] M. M. Fürst, G. E. Salvi, N. P. Lang, and G. R. Persson, "Bacterial colonization immediately after installation on oral titanium implants," *Clinical Oral Implants Research*, vol. 18, no. 4, pp. 501–508, 2007.
- [29] A. H. Weerkamp, H. M. Uyen, and H. J. Busscher, "Effect of zeta potential and surface energy on bacterial adhesion to uncoated and saliva-coated human enamel and dentin," *Journal of Dental Research*, vol. 67, no. 12, pp. 1483–1487, 1988.
- [30] H. M. W. Uyen, J. M. Schakenraad, J. Sjollem et al., "Amount and surface structure of albumin adsorbed to solid substrata with different wettabilities in a parallel plate flow cell," *Journal of Biomedical Materials Research*, vol. 24, no. 12, pp. 1599–1614, 1990.

Clinical Study

Influence of Leukocyte- and Platelet-Rich Fibrin (L-PRF) in the Healing of Simple Postextraction Sockets: A Split-Mouth Study

Gaetano Marenzi,¹ Francesco Riccitiello,² Mariano Tia,³
Alessandro di Lauro,¹ and Gilberto Sammartino¹

¹Division of Oral Surgery and Implantology, Department of Neurosciences, Reproductive and Odontostomatological Sciences, University of Naples "Federico II", Via Pansini 5, 80131 Naples, Italy

²Department of Neurosciences, Reproductive and Odontostomatological Sciences, University of Naples "Federico II", Via Pansini 5, 80131 Naples, Italy

³Private Practice, Via Austria 6, Sant'Antimo, Naples, Italy

Correspondence should be addressed to Gaetano Marenzi; gaetano.marenzi@tiscali.it

Received 12 August 2014; Revised 11 November 2014; Accepted 11 November 2014

Academic Editor: David M. Dohan Ehrenfest

Copyright © 2015 Gaetano Marenzi et al. This is an open access article distributed under the Creative Commons Attribution License, which permits unrestricted use, distribution, and reproduction in any medium, provided the original work is properly cited.

The aim of this study was to evaluate the effects of leukocyte- and platelet-rich fibrin (L-PRF) on the pain and soft tissue healing after tooth extractions. Twenty-six patients (9 males and 17 females) were treated with multiple extractions (2 to 8), with a total of 108 extractions. This was an exploratory single blinded randomized clinical trial with a split-mouth design. The pain after the surgery was assessed in each patient by the VAS scale (1 to 10) at intervals of 24-48-72-96 hours. The soft tissue healing was clinically evaluated at 3, 7, 14, and 21 days after surgery by the same examiner surgeon, using the modified Healing Index (4 to 12). The mean value of postextraction pain was 3.2 ± 0.3 in the experimental sides and 4.1 ± 0.1 in the control sides. After 7 days from the extractions, the values of modified Healing Index in the experimental and control groups were, respectively, 4.8 ± 0.6 and 5.1 ± 0.9 . The use of L-PRF in postextraction sockets filling can be proposed as a useful procedure in order to manage the postoperative pain and to promote the soft tissue healing process, reducing the early adverse effects of the inflammation.

1. Introduction

Many studies revealed that platelet concentrates for surgical use can be used as efficient adjuvants for tissue repair [1–5]. The growth factors (particularly platelet-derived growth factors (PDGF), transforming growth factors (TGF- β), and vascular endothelial growth factors (VEGF)) and the other molecules (fibrinogen, fibronectin, and vitronectin) contained in platelets (α -granules) give to these products the ability to modulate many phases of the healing process like the hemostasis and the neoangiogenesis [6]. The clinical results of these products are interesting but remain quite mixed and controversial in the literature, depending on the kind of preparation [7–10]. Platelet concentrates are classified into 4 main families depending on their leukocyte and fibrin content: pure platelet-rich plasma (P-PRP), leukocyte- and

platelet-rich plasma (L-PRP), pure platelet-rich fibrin (P-PRF), and leukocyte- and platelet-rich fibrin (L-PRF) [11]. Each family of products has different aspect, biological content, and potential application [12].

The PRPs were already tested in many oral surgery applications, with mixed results depending on the kind of preparations [13–16]. Numerous protocols have attempted to optimize the preparation of the autologous factors, using various performances standards and centrifugation parameters [17, 18]. Several authors demonstrated the effectiveness of some PRP types during tooth extractions to stimulate soft tissue healing and wound control [19, 20] and in prevention of postoperative bleeding in anticoagulated patients undergoing oral surgery. However, these PRP techniques remain quite complex and expensive on a daily use basis, and their use may not be justified for daily oral surgery applications [13, 14].

On the other hand, L-PRF represents a more recent generation of platelet concentrates. The development of L-PRF is very significant in oral and maxillofacial surgery, with many validated applications in periodontal surgery [13, 21] and implant dentistry [14–22]. L-PRF is easy and inexpensive to prepare for frequent use in private practice, and it exists in the form of L-PRF clots or membranes (after compression). The membrane releases a significant quantity of autologous growth factors (particularly PDGF-AB, TGF β , and VEGF) [23], cytokines, and healing proteins (fibronectin, etc.) during more than 7 days in vitro [24], while other platelet gels dissolve in vitro in 3 days [12]. In another study, when compared with a procedure for platelet-rich plasma (PRP), L-PRF released more than 15-fold VEGF and more than 2-fold TGF β 1 [25]. According to the literature, L-PRF was a useful tool in postextraction hemostasis control [26] and in prevention of hemorrhagic complications in cardiopathic patients [27].

The aim of this study is to evaluate the effectiveness of L-PRF to improve the soft tissues healing and to reduce pain after tooth extractions.

2. Materials and Methods

2.1. Study Population. From January 2012 to July 2013 at the Unit of Oral Surgery and Implantology of the University of Naples “Federico II,” 26 healthy patients were selected, including 9 males and 17 females with a mean age of 53 ± 4 years. The selected patients were nonsmokers or light smokers (<5 /day); they did not have systemic diseases that could interfere with the healing process (such as diabetes, liver disease, heart disease, or immune-disorders) or diseases of the oral mucosa. The study was designed as a prospective split-mouth trial on patients who needed bilateral paired dental extractions; on the side chosen to be the study side, the sockets were filled with L-PRF, whereas on the other side (control), they were allowed to undergo natural healing. Test and control sites were chosen with coin toss randomization. This cross-sectional split-mouth research study was conducted in accordance with the requirements of Helsinki Declaration of 1975 as revised in 2008. Patients were verbally informed about the sample to be taken and gave their written consent. The patients who did not sign the agreement and also the patients with poor oral hygiene, patients with local infections of the soft tissues, patients undergoing bisphosphonates therapy, patients irradiated to the jaws in the past, and patients with psychiatric illness or pregnant patients were excluded from the study.

2.2. Surgical Procedure. An alveolar nerve block infiltration was administrated with local or regional anesthesia, depending on the dental arch, using 2% mepivacaine. Mepivacaine does not contain epinephrine, so it was used to prevent restriction of the blood supply. To prevent interference with the healing process, no intraligamentous or intrapapillary infiltration was made. The teeth were extracted in a nontraumatic manner without elevation of full-thickness flaps and preserving the buccal and lingual walls of the alveolar sockets in order to minimize the possible trauma



FIGURE 1: Presurgery clinical occlusal view. For orthodontic motive, this patient needed the bilateral extraction of the upper first premolars.



FIGURE 2: The postextraction sockets.

and to give adequate support to the L-PRF filling (Figures 1 and 2). All extraction sites were simple with alveolar walls preserved. All alveolar sockets were sutured with a 3/0 Vicryl (Ethicon/Johnson & Johnson, Somerville, NJ, USA). Each patient also served as the control (split-mouth design): a socket was treated with L-PRF application (study socket) whereas the other (control socket) had to undergo natural healing by clot formation without socket filling (Figure 3). The number of paired extractions per patient ranged from 2 to 4 for a total of 108 extractions. Indication for tooth extraction included root or crown fractures, residual roots, no restorable caries, periapical granuloma, and orthodontic reasons. Patients showing anatomic and pathologic conditions not comparable between the study and control sites were excluded as study subject. Antibiotic prophylaxis was undertaken (amoxicillin 875 mg and clavulanic acid 125 mg) starting 2 days before surgery up to 3 days after it.

2.3. L-PRF Preparation Protocol. The L-PRF was prepared through a single centrifugation of blood according to the protocol of Dohan Ehrenfest et al. (now marketed as Intra-Spin L-PRF kit, Intra-Lock, Boca-Raton, FL, USA) for a period of 12 minutes at 2700 rpm. Blood was taken in 9 mL tubes, 30 minutes before the surgery, immediately centrifuged, and used for the filling of the experimental sites. The total amount of blood collected (from 18 mL to 54 mL) was related to the number of tooth extractions, in order to obtain the complete filling of the sockets with the L-PRF. After centrifugation, each L-PRF clot was separated from the portion of red blood

TABLE 1

Number of patients	Number of paired extractions per patient	Tooth extracted
10	1	Premolar
7	2	Canine/premolar/molar
6	3	Canine/premolar/molar
3	4	Canine/premolar/molar



FIGURE 3: The upper right socket (study site) was filled with L-PRF, while the upper left socket (control site) had to follow natural healing. Both sites were sutured.

cells (red thrombus), obtaining a fibrin clot with a red small portion in order to include the “buffy” coat richer in large leucocytes [24]. The L-PRF clot was condensed and modeled on a sterile surgical plate before the application in the sockets [24].

L-PRF was used within 60 minutes after the preparation. It was accurately positioned in the extraction sites and stabilized with a resorbable suture. In the control sites, the same suture was used (Figure 3). All patients were advised to follow soft and liquid diet, avoiding hot food in the following hours. In all cases, the sutures were removed after one week. Table 1 reports the number and the type of paired extractions per patient.

2.4. Study Variables and Statistical Methods. The predictor variable was the treatment group status: L-PRF versus control socket. The outcome variables of interest were as follows: pain, postsurgical complications to soft and hard tissues, and the Healing Index modified.

A 10-point visual analog scale (VAS) with a score of 0 that equals “no pain” and a score of 10 that equals “very severe pain” was used by the same patient to assess the postoperative pain at 24, 48, and 72 hours. Between groups comparisons for VAS outcomes were carried out by means of univariate analysis of variance, considering the group (i.e., PRF versus CTR) and the recording time point as factors and VAS score as dependent variable.

The quality of the socket soft tissue healing was clinically evaluated at 3, 7, 14, and 21 days after surgery by an examiner surgeon, using the Healing Index modified [28] which involved 3 scoring levels for each of the four parameters considered: bleeding, suppuration, tissue color, and consistency of the healing tissue. The scoring scale ranged from 4, corresponding to excellent healing, to 12, indicating

TABLE 2

Healing Index	3 days	7 days	14 days	21 days
L-PRF	4.8 ± 0.6	4.5 ± 0.5	4.2 ± 0.2	4.1 ± 0.1
CTRL	5.1 ± 0.9	4.9 ± 0.3	4.3 ± 0.3	4.2 ± 0.2
<i>P</i>	0.197	0.05	0.01	0.0002

L-PRF = study site; CTRL = control site.



FIGURE 4: Clinical occlusal view 3 days after surgery. In the study site, the epithelialization process was more advanced than in the control site. In the study site, the inflammatory reaction was reduced.

severely impaired healing. The Wilcoxon signed-rank test for comparison of 2 correlated samples matched pairs with the level of significance predetermined at 0.05 was used.

3. Results

All patients completed the study. No cases of bleeding, infection, alveolar osteitis, or other surgical complications were reported.

Regarding the postextraction pain, patients enrolled in the study reported a mean value of the study sites of 3.2 ± 0.3 , which is lower ($P < 0.0001$) than the mean value of the control sites (4.5 ± 0.7), with a statistical difference average of 0.9 ± 0.3 . The VAS score was nearly equal for the 2 sides after 4 days (decreasing to 0).

Results concerning the healing of the socket are reported in Table 2. Comparisons between values relative to the study and control sides showed better healing and faster socket closure for the side treated with L-PRF, with differences statistically significant at days 3 and 7 (Figures 4 and 5).

4. Discussion

This study was designed to test the efficacy of L-PRF in fostering socket healing after tooth extractions. The 26 split-mouth case control extractions that constituted our study were statistically enough to prove the ability of L-PRF to improve the early healing phases (hemostasis and epithelial closure), reducing the inflammatory process and the risk of infection. The reported results of the experimental sites showed, in the first 7 days after the tooth extractions, a fast evolution of the healing and a positive effect on pain. After a week, minor differences between the two groups are reported (Figures 6 and 7). These effects could be related to the biochemical and structural features of the L-PRF [29], which collects a large quantity of leukocytes (about 60% of the initial blood



FIGURE 5: Clinical occlusal views 7 days after surgery. The sutures were removed. Both postextraction socket cavities presented a decreased volume and appeared epithelialized.



FIGURE 6: Clinical follow-up at 14 days after surgery. Both postextraction sockets were completely closed with the soft tissues.

harvest) and platelets embedded in a fibrin matrix [30, 31]. The fibrin architecture of L-PRF, constituted by connected trimolecular junctions (or equatorial), due to a slow polymerization of the platelet concentrate and due to the absence of heterologous thrombin, induces a flexible fibrin network, able to promote the gradual release of growth factors and leukocytes migration. The fibrin membrane promotes the mechanical protection of the surgical site and, biologically, it interacts with the physiological mechanisms of healing favoring the angiogenesis [13, 14]. The fibrin induces the expression of $\alpha v\text{-}\beta 3$ integrin by endothelial cells, allowing the links with structural proteins, such as fibronectin and vitronectin, supporting the process of formation of capillaries [12]. In relation to the previous properties, the fibrin also allows the association of some growth factors, such as FGFb (fibroblast growth factor basic) and PDGF (platelet-derived growth factor) involved in the angiogenic process and useful as chemotactic factors, favoring diapedesis of white blood cells [12]. The immunological properties of the L-PRF, resulting from its content in leukocytes, could be useful to prevent the surgical site infections, such as postextraction alveolitis, with a consequent reduction of the inflammation symptoms. The presence of leukocytes is a very important parameter to stimulate healing and wound control [32].

The main limitation of this exploratory study was that the extraction sites were voluntarily very simple, with all alveolar walls preserved. It allowed standardizing the study easily to

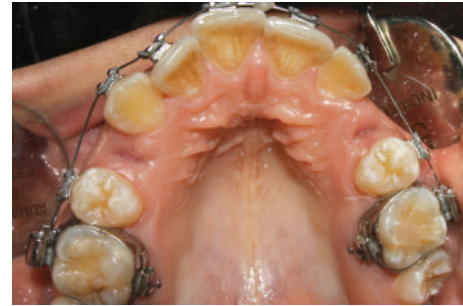


FIGURE 7: At 21 days after surgery, both postextraction healing sites were completely closed with the soft tissues.

reach a very clean result, but it does not reflect the real strength and advantages of L-PRF. This material is particularly useful and efficient in complex situations, when some walls are destroyed and the bone regeneration is difficult, but an accurate split-mouth study with this kind of cases is virtually impossible to standardize. It is however the needed next step of evaluation and validation of the use of L-PRF during tooth extractions.

5. Conclusion

Even if the selected samples are limited, the reported results suggested that the use of L-PRF in postextraction sockets filling is an efficient and useful procedure in order to manage the postoperative pain and to enhance the alveolar soft tissue healing process, especially in the first days after the extractions, reducing the early adverse effects of the inflammation. This study represents a preliminary clinical trial, which could be used as baseline for further histologic studies.

Conflict of Interests

The authors have no conflict of interests to declare regarding the devices used for this study. The current research was not influenced by any secondary interests, such as financial gain.

References

- [1] T. Bielecki and D. M. Dohan Ehrenfest, "Leukocyte- and platelet-rich Plasma (L-PRP)/fibrin (L-PRF) in medicine—past, present, future," *Current Pharmaceutical Biotechnology*, vol. 13, no. 7, pp. 1–2, 2012.
- [2] R. Gruber, F. Varga, M. B. Fisher, and G. Watzek, "Platelet stimulate proliferation of bone cells: involvement of platelet-derived growth factor, microparticles and membranes," *Clinical Oral Implants Research*, vol. 13, pp. 529–535, 2002.
- [3] N. E. Carlson and J. R. B. Roach, "Platelet-rich plasma: clinical application in dentistry," *The Journal of the American Dental Association*, vol. 133, pp. 1383–1386, 2002.
- [4] A. R. Sanchez, P. J. Sheridan, and L. I. Kupp, "Is platelet-rich plasma the perfect enhancement factor? A current review," *The International Journal of Oral & Maxillofacial Implants*, vol. 18, pp. 93–103, 2003.

- [5] E. Anitua, I. Andia, B. Ardanza et al., "Autologous platelets as a source of proteins for healing and tissue regeneration," *Thrombosis and Haemostasis*, vol. 91, pp. 4–15, 2004.
- [6] R. E. Marx, E. R. Carlson, R. M. Eichstaedt, S. R. Schimmele, J. E. Strauss, and K. R. Georgeff, "Platelet-rich plasma: growth factor enhancement for bone grafts," *Oral Surgery, Oral Medicine, Oral Pathology, Oral Radiology, and Endodontics*, vol. 85, no. 6, pp. 638–646, 1998.
- [7] P. A. M. Everts, M. M. Hoogbergen, T. A. Weber, R. J. J. Devilee, G. van Monfort, and I. H. J. T. de Hingh, "Is the use of autologous platelet-rich plasma gels in gynecologic, cardiac, and general, reconstructive surgery beneficial?" *Current Pharmaceutical Biotechnology*, vol. 13, no. 7, pp. 1163–1172, 2012.
- [8] T. Yuan, S.-C. Guo, P. Han, C. Q. Zhang, and B. F. Zeng, "Applications of leukocyte- and platelet-rich plasma (L-PRP) in trauma surgery," *Current Pharmaceutical Biotechnology*, vol. 13, no. 7, pp. 1173–1184, 2012.
- [9] M. del Fabbro, M. Bortolin, and S. Tascheri, "Is autologous platelet concentrate beneficial for post-extraction socket healing? A systematic review," *International Journal of Oral and Maxillofacial Surgery*, vol. 40, pp. 891–900, 2011.
- [10] M. Esposito, M. G. Grusovin, J. Rees et al., "Effectiveness of sinus lift procedures for dental implant rehabilitation: a Cochrane systematic review," *European Journal of Oral Implantology*, vol. 3, pp. 7–26, 2010.
- [11] D. M. Dohan Ehrenfest, G. Sammartino, J. A. Shibli, H. L. Wang, D. R. Zou, and J. P. Bernard, "Guidelines for the publication of articles related to platelet concentrates (Platelet-Rich Plasma—PRP, or Platelet-Rich Fibrin—PRF): the international classification of the POSEIDO," *POSEIDO*, vol. 1, no. 1, pp. 17–27, 2013.
- [12] D. M. Dohan Ehrenfest, T. Bielecki, R. Jimbo et al., "Do the fibrin architecture and leukocyte content influence the growth factor release of platelet concentrates? An evidence-based answer comparing a pure platelet-rich plasma (P-PRP) gel and a leukocyte- and platelet-rich fibrin (L-PRF)," *Current Pharmaceutical Biotechnology*, vol. 13, no. 7, pp. 1145–1152, 2012.
- [13] M. del Corso, A. Vervelle, A. Simonpieri et al., "Current knowledge and perspectives for the use of platelet-rich plasma (PRP) and platelet-rich fibrin (PRF) in oral and maxillofacial surgery part I: periodontal and dentoalveolar surgery," *Current Pharmaceutical Biotechnology*, vol. 13, no. 7, pp. 1207–1230, 2012.
- [14] A. Simonpieri, M. del Corso, A. Vervelle et al., "Current knowledge and perspectives for the use of platelet-rich plasma (PRP) and platelet-rich fibrin (PRF) in oral and maxillofacial surgery. Part 2. Bone graft, implant and reconstructive surgery," *Current Pharmaceutical Biotechnology*, vol. 13, no. 7, pp. 1231–1256, 2012.
- [15] N. Geurs, A. Ntounis, P. Vassilopoulos, U. van der Velden, B. G. Loos, and M. Reddy, "Using growth factors in human extraction sockets: a histologic and histomorphometric evaluation of short-term healing," *The International Journal of Oral & Maxillofacial Implants*, vol. 29, no. 2, pp. 485–496, 2014.
- [16] P. Kaur and A. Maria, "Efficacy of platelet rich plasma and hydroxyapatite crystals in bone regeneration after surgical removal of mandibular third molars," *Journal of Maxillofacial and Oral Surgery*, vol. 12, no. 1, pp. 51–59, 2013.
- [17] G. Weibrich, W. K. G. Kleis, and G. Hafner, "Growth factor levels in the platelet-rich plasma produced by 2 different methods: curasan-type PRP kit versus PCCS PRP system," *International Journal of Oral & Maxillofacial Implants*, vol. 17, no. 2, pp. 184–190, 2002.
- [18] P. Borzini, V. Balbo, and L. Mazzucco, "Platelet concentrates for topical use: bedside device and blood transfusion technology. Quality and versatility," *Current Pharmaceutical Biotechnology*, vol. 13, no. 7, pp. 1138–1144, 2012.
- [19] C. Rivera, F. Monsalve, J. Salas, A. Morán, and I. Suazo, "Platelet-rich plasma, plasma rich in growth factors and simvastatin in the regeneration and repair of alveolar bone," *Experimental and Therapeutic Medicine*, vol. 6, no. 6, pp. 1543–1549, 2013.
- [20] G. Sammartino, M. Tia, T. Bucci, and H. L. Wang, "Prevention of mandibular third molar extraction-associated periodontal defects: a comparative study," *Journal of Periodontology*, vol. 80, no. 3, pp. 389–396, 2009.
- [21] Y. C. Chang and J. H. Zhao, "Effect of platelet-rich fibrin on human periodontal ligament fibroblasts and application for periodontal infrabony defects," *Australian Dental Journal*, vol. 56, pp. 365–371, 2011.
- [22] R. Toeroek and D. M. Dohan Ehrenfest, "The concept of Screw-Guided Bone Regeneration (S-GBR). Part 3: fast screw-guided bone regeneration (FS-GBR) in the severely resorbed preimplant posterior mandible using allograft and leukocyte- and platelet-rich fibrin (L-PRF): a 4-year follow-up," *POSEIDO*, vol. 1, no. 2, pp. 93–100, 2013.
- [23] M. A. Zumstein, S. Berger, M. Schober et al., "Leukocyte- and platelet-rich fibrin (L-PRF) for long-term delivery of growth factor in rotator cuff repair: review, preliminary results and future directions," *Current Pharmaceutical Biotechnology*, vol. 13, no. 7, pp. 1196–1206, 2012.
- [24] D. M. Dohan Ehrenfest, G. M. de Peppo, P. Doglioli, and G. Sammartino, "Slow release of growth factors and thrombospondin-1 in Choukroun's platelet-rich fibrin (PRF): a gold standard to achieve for all surgical platelet concentrates technologies," *Growth Factors*, vol. 27, no. 1, pp. 63–69, 2009.
- [25] F. Passaretti, M. Tia, V. Desposito et al., "Growth-promoting action and growth factor release by different platelet derivatives," *Platelets*, vol. 25, no. 4, pp. 252–256, 2014.
- [26] D. M. Dohan Ehrenfest and L. Vazquez, "Pulling out, extraction or avulsion?" *Implant Dentistry*, vol. 17, no. 1, p. 4, 2008.
- [27] G. Sammartino, D. M. Dohan Ehrenfest, F. Carile, M. Tia, and P. Bucci, "Prevention of hemorrhagic complications after dental extractions into open heart surgery patients under anticoagulant therapy: the use of leukocyte- and platelet-rich fibrin," *The Journal of Oral Implantology*, vol. 37, no. 6, pp. 681–690, 2011.
- [28] M. Mozzati, G. Galesio, S. di Romana, L. Bergamasco, and R. Pol, "Efficacy of plasma-rich growth factor in the healing of postextraction sockets in patients affected by insulin-dependent diabetes mellitus," *Journal of Oral and Maxillofacial Surgery*, vol. 72, no. 3, pp. 456–462, 2014.
- [29] D. M. Dohan Ehrenfest, M. del Corso, F. Inchingolo, and J. B. Charrier, "Selecting a relevant in vitro cell model for testing and comparing the effects of a Choukroun's platelet-rich fibrin (PRF) membrane and a platelet-rich plasma (PRP) gel: tricks and traps," *Oral Surgery, Oral Medicine, Oral Pathology, Oral Radiology and Endodontology*, vol. 110, no. 4, pp. 409–413, 2010.
- [30] J. Choukroun, A. Diss, A. Simonpieri et al., "Platelet-rich fibrin (PRF): a second-generation platelet concentrate. Part IV: clinical effects on tissue healing," *Oral Surgery, Oral Medicine, Oral Pathology, Oral Radiology, and Endodontics*, vol. 101, pp. 56–60, 2006.
- [31] Y.-H. Kang, S. H. Jeon, and J.-Y. Park, "Platelet-rich fibrin is a bioscaffold and reservoir of growth factors for tissue

regeneration,” *Tissue Engineering Part A*, vol. 17, pp. 349–359, 2011.

- [32] T. Bielecki, D. M. Dohan Ehrenfest, P. A. Everts, and A. Wiczowski, “The role of leukocytes from L-PRP/L-PRF in wound healing and immune defense: new perspectives,” *Current Pharmaceutical Biotechnology*, vol. 13, no. 7, pp. 1153–1162, 2012.

Clinical Study

Clinical Evaluation of the Regenerative Potential of EMD and NanoHA in Periodontal Infrabony Defects: A 2-Year Follow-Up

Andrea Pilloni,¹ Matteo Saccucci,¹ Gabriele Di Carlo,¹
Blerina Zeza,¹ Marco Ambrosca,¹ Michele Paolantonio,² Gilberto Sammartino,³
Claudio Mongardini,¹ and Antonella Polimeni¹

¹ Department of Oral and Maxillofacial Science, Sapienza University of Rome, Via Caserta 6, 00161 Rome, Italy

² Department of Medical, Oral and Biotechnological Sciences, University "G. d'Annunzio", Chieti, Italy

³ Department of Oral Surgery, Faculty of Medicine, University Federico II, Naples, Italy

Correspondence should be addressed to Matteo Saccucci; matteo.saccucci@uniroma1.it

Received 4 July 2014; Revised 24 July 2014; Accepted 14 August 2014; Published 8 September 2014

Academic Editor: David M. Dohan Ehrenfest

Copyright © 2014 Andrea Pilloni et al. This is an open access article distributed under the Creative Commons Attribution License, which permits unrestricted use, distribution, and reproduction in any medium, provided the original work is properly cited.

Introduction. The aim of this retrospective study was to compare the clinical efficacy of four different surgical techniques in promoting periodontal regeneration in patients with infrabony defects: open flap debridement, application of enamel matrix derivatives (EMD), nanohydroxyapatite (nanoHA) application, and combined nanoHA and EMD application. Probing attachment level (PAL), pocket depth (PD), and position of gingival margin at completion of therapy (REC) were measured. **Materials and Methods.** Data were collected from 64 healthy patients (34 women and 30 men, mean age 37,7 years). Clinical indices were measured by a calibrated examiner at baseline and at 12, 18, and 24 months. The values obtained for each treatment were compared using nonparametric tests. **Results.** All treatments resulted in a tendency toward PD reduction over time, with improvements in REC and PAL. The differences in PD, REC, and PAL values at baseline compared with values after 12, 18, and 24 months were statistically significant for all treatments. Statistically significant differences in PAL and PD were detected between nanoHA and nanoHA + EMD at 12, 18, and 24 months. **Conclusion.** In this study, EMD and nanoHA used together in patients with infrabony periodontal lesions had better clinical efficacy than nanoHA alone, EMD alone, or open flap debridement.

1. Introduction

In the past three decades periodontal regenerative treatment has received increasing attention as an alternative to tooth extraction in patients with periodontal disease. Implant insertion, although highly predictable, has been shown to be less predictable than saving a periodontally compromised tooth with regenerative therapy [1]. Given the proper conditions for optimal wound healing (wound stability, adequate space, and healing by primary intention), the periodontal tissues are capable of significant regeneration [2]. Unfortunately, systemic and local factors can interfere with these conditions, making periodontal regeneration difficult without the use of grafting biomaterials, biologics, and devices for periodontal regeneration [2]. Biomaterials in periodontal regeneration, as for bone reconstruction around implants, are of different

sources [3, 4]. The ideal material for periodontal wound healing and regeneration would combine biologics with an easy-to-use, moldable, space-providing, biocompatible, bioadhesive, porous, and biodegradable matrix for local applications [2]. The simultaneous use of enamel matrix derivative (EMD) and nanohydroxyapatite (nanoHA) seems to fulfill the aforementioned criteria for an ideal combination. The *in vitro* combination has shown promising results, with each material stimulating periodontal fibroblasts differently, enhancing the potential of each [5]. Amelogenins, present in EMD, are extracellular matrix proteins that induce the formation of acellular cementum when absorbed on the root surface [6] and that stimulate the proliferation and differentiation of periodontal fibroblasts and osteoblasts [7, 8]. The role of amelogenins in periodontal regeneration is primarily related to regeneration of the periodontal ligament

and cementum. In contrast, nanoHA is an alloplastic material chemically similar to the inorganic component of bone matrix and is known for its osteoinductive and osteoconductive properties in alveolar bone regeneration [9]. The clinical relevance of EMD is supported by its long-term outcome stability in studies with 10–15 years of follow-up [10]. In contrast, the literature on nanoHA remains scarce and contradictory. In 2008, Kasaj et al. [11] reported significant clinical improvement in patients treated with nanoHA compared with open debridement. However, in 2013, Horváth et al. [12] could not confirm those findings. In 2014, Al Machot et al. [13] reported that EMD and nanoHA powder performed similarly and resulted in significant bone filling and clinical improvement. The aim of the present study was to compare the clinical efficacy of EMD and nanoHA applied individually and in combination, using open flap debridement (OFD) as a control.

2. Materials and Methods

2.1. Study Design and Population. This retrospective study was conducted in the Department of Oral and Maxillofacial Science, Sapienza University of Rome, Italy. Data were collected between 2009 and 2012. Sixty-four generally healthy patients (34 women and 30 men; mean age 37,7 years) were screened for inclusion. Study inclusion criteria were as follows:

- (i) age over 18 years;
- (ii) systemic health: lack of acute or chronic condition that would contraindicate oral surgery;
- (iii) bone defect characteristics: a single 1-, 2-, or 3-wall infrabony defect more than 3 mm deep on radiographs, with pocket depth (PD) ≥ 5 mm;
- (iv) tooth condition: periodontally, endodontically, and prosthetically healthy tooth.

Patients were excluded for the following reasons:

- (i) pregnancy or lactation;
- (ii) taking medications that could interfere with the healing of periodontal tissues;
- (iii) furcation involvement;
- (iv) overhanging restorations;
- (v) teeth with grade 2 or higher mobility;
- (vi) teeth with endodontic lesions.

Baseline measurements of probing attachment level (PAL), position of gingival margin at completion of therapy (REC), and PD, according to gender and age, are shown in Figures 1, 2, 3, 4, 5, and 6. Chronic periodontitis was diagnosed in all patients, because the location of defects and number of teeth affected did not meet the criteria of aggressive periodontitis, even in those younger than 30 years of age. Each patient participating in this study signed a consent form approved by the Ethical Committee of the Faculty of Medicine, G. D'Annunzio University, Chieti, Italy. The study protocol was performed in accordance with the Declaration of Helsinki of 1975, revised in Tokyo in 2004.

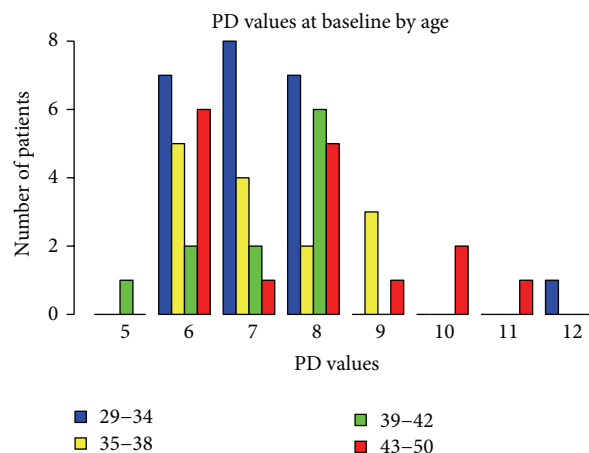


FIGURE 1

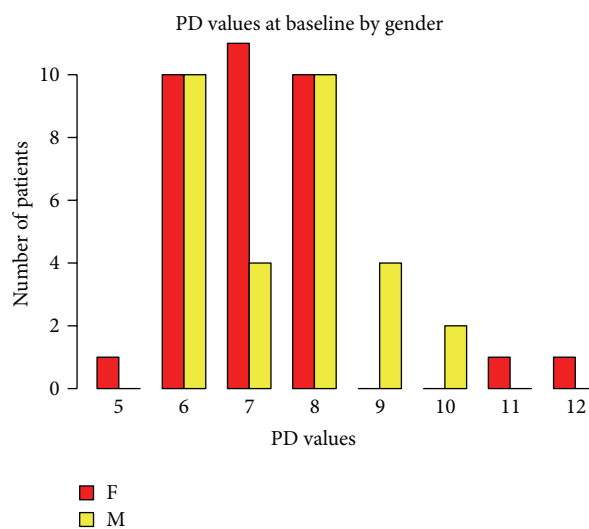


FIGURE 2

2.2. Treatments. Patients were randomly allocated to one of the following surgical treatment groups:

- (i) open flap debridement;
- (ii) EMD application (Emdogain Straumann, Basel, Switzerland);
- (iii) nanoHA (NeoActive Ghimas, Casalecchio di Reno, Italy);
- (iv) Sandwich technique combining nanoHA and EMD.

All patients underwent the same presurgical and surgical procedure, differing only in the material used for bone regeneration.

2.3. Presurgical Treatment. All patients underwent phase I therapy with reevaluation within 3 months. If the full-mouth plaque score and full-mouth bleeding score were under 15% at recheck, the patient entered the surgical protocol. Otherwise, an additional motivation and professional cleaning phase was performed.

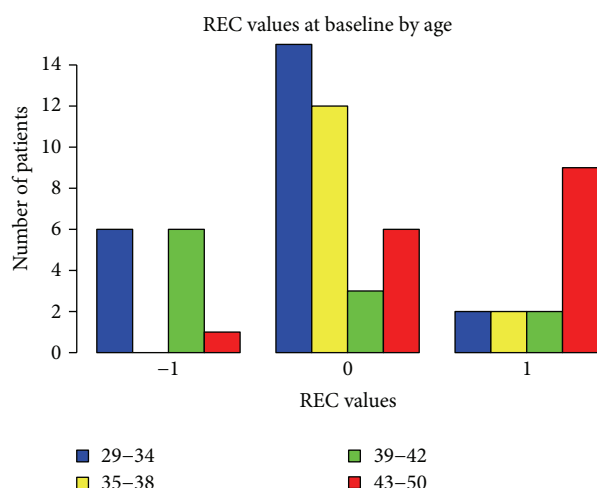


FIGURE 3

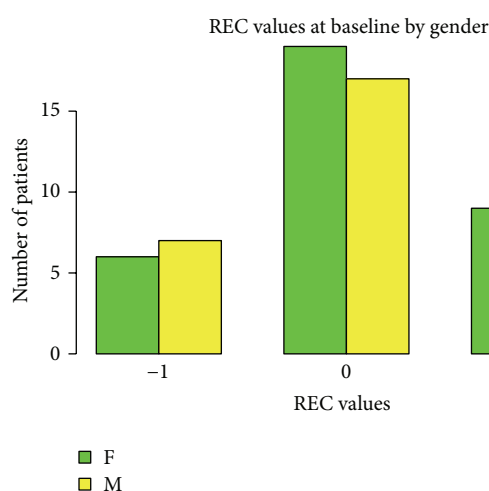


FIGURE 4

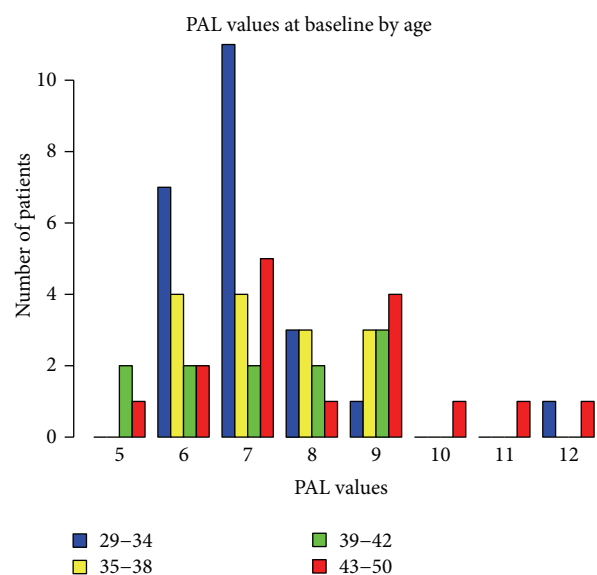


FIGURE 5

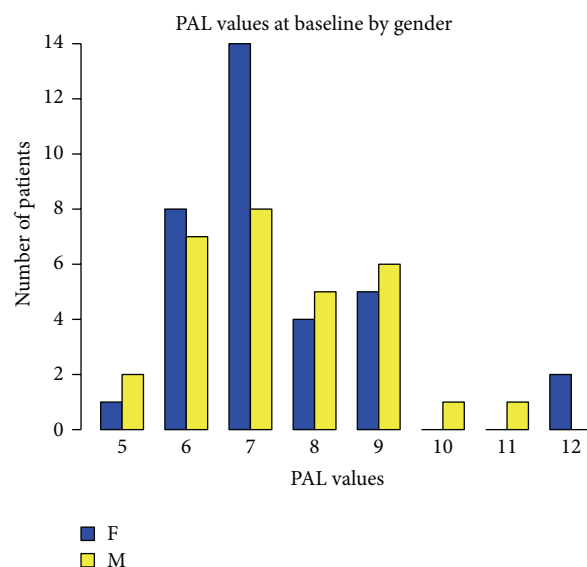


FIGURE 6

2.4. Periodontal Surgery. After local anesthesia, intrasulcular incisions were made, in conjunction with vertical releasing incisions if needed for bone defect exposure. A full-thickness flap was then prepared, the bone defect exposed, and granulation tissue removed with manual and ultrasonic root planing instruments. The area of the infrabony defect was rinsed with saline, dried, and treated according to treatment group allocation:

- chemical root conditioning (EDTA, 24%) before application of EMD to the root surface;
- application of adequate nanoHA powder to fill the defect and maintain root surface area sufficient for its biological width to be reestablished;
- chemical root conditioning (EDTA, 24%), EMD application, bone defect filling with nanoHA, and layer of EMD over of the bone substitute, using the sandwich technique;
- open flap debridement.

Gingival flaps were closed with 5-0 nylon suture in a simple interrupted pattern (Figures 7, 8, 9(a), 9(b), 10(a), 10(b), 11(a), and 10(b)).

2.5. Postsurgical Treatment. Patients received a prescription for amoxicillin, 1g every 12 h for 5 days, and for ibuprofen, 600 mg every 12 h for 3 days. The use of synthetic ice in 5-minute intervals for the first 30 minutes was prescribed immediately after completion of surgery. All patients used 0.12% chlorhexidine rinse for 1 min twice daily, not within 1 hour of tooth brushing. Patients were examined each week for the first month and each month during the first year. Frequency of rechecks after the first year was customized based on the patient's plaque control and level of compliance. During recheck appointments patients underwent professional oral hygiene treatment.



FIGURE 7: Probing at baseline showing PAL = 7 mm on the mesial aspect of tooth number 9.

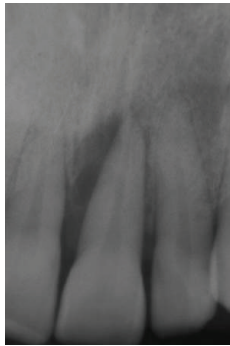


FIGURE 8: Periapical X-ray at baseline.

2.6. Examiner and Surgeon. One individual was selected to make clinical measurements and a second to perform surgical treatments. Surgical treatments were performed by a highly experienced surgeon (AP).

2.7. Clinical Parameters. Patients were evaluated at baseline and at 12, 18, and 24 months after regenerative therapy by the above-mentioned calibrated dental hygienist. Clinical parameters measured at each time point included PD, REC, and PAL. All measurements were recorded using a standard periodontal probe (PCP-15, UNC) at six sites per tooth: mesiobuccal, midbuccal, distobuccal, mesiolingual, midlingual, and distolingual. The highest value obtained for PD and PAL and the lowest for REC were considered for statistical analysis. As suggested by Kasaj et al. [11], the cemento-enamel junction or restoration margin was used as the fixed reference point.

2.8. Statistical Analysis. Statistical analyses were performed with R software, version 3.1.0. Clinical parameters were described as minimum, 1st quartile, median, 3rd quartile, maximum, mean, and standard deviation and were calculated by treatment (OFD, nanoHA, EMD, and nanoHA + EMD), time (baseline, 12 months, 18 months, and 24 months), site (mesiovestibular, distovestibular), and position (anterior, posterior). First, we evaluated differences in PAL, REC, and PD among patients assigned to each treatment. We accepted the hypothesis of equal location parameters at 5%. To test the

efficacy of each treatment after 12, 18, and 24 months, the null hypothesis was that the mean of PD, REC, and PAL in each treatment group was the same at baseline and after 12, 18, and 24 months. The normal distribution of data within each group was confirmed with the Shapiro-Wilks test (SW test) [14]. If the hypothesis of normal distribution of the data was confirmed, comparisons among groups were made with a *t*-test or analysis of variance. If the hypothesis of normal distribution was rejected, then comparisons among groups were performed with Wilcoxon's test for paired data (W test) [15]. Values of $P < 0.05$ were considered significant. Median and mean differences in the location parameters for PD, REC, and PAL among the four treatment groups at 12, 18, and 24 months were tested for statistical significance. If the hypothesis of normality in the data was rejected according to the SW test, the nonparametric Kruskal-Wallis test (KW test) was performed in place of analysis of variance. If the null hypothesis where the median and mean location parameters were the same in each group was rejected, Siegel and Castellan's post hoc multiple comparison was performed at 5% significance level.

3. Results

The group that received EMD+HA showed greater mean reduction in PD (5.75 mm) and improvement in gingival recession compared with the EMD-only group. The group that received nanoHA alone had the poorest clinical results, although they did improve from baseline. All treatments resulted in PD reduction over time, with improvements in REC and PAL.

3.1. Differences between Baseline and Follow-Ups

3.1.1. PD Index. According to the SW test, the hypothesis of normality could be confirmed only for baseline data in the nanoHA + EMD group ($P = 0.26$). In the other groups the hypothesis was rejected, because P values were near 5% or much lower. The differences between PD levels at baseline and after 12, 18, and 24 months were statistically significant (W test, $P < 0.01$) for all treatments. The reductions in median and mean PD levels shown in Figures 12, 13, 14, and 15 are significant.

3.1.2. REC Index. According to the SW test, the hypothesis of normality could be accepted at 5% significance level only for nanoHA at 12 months and for EMD at 18 and 24 months. In the other groups the hypothesis was rejected, because P values were lower or much lower than 5%. The differences in REC levels at baseline compared with levels after 12, 18, and 24 months were statistically significant (W test, $P < 0.01$) for all treatments. The reductions in median and mean REC levels shown in Figures 16, 17, 18, and 19 can be considered significant.

3.1.3. PAL Index. According to the SW test, the hypothesis of normality could be accepted at 5% significance level only in the EMD treatment group, so both the *t*-test and W test

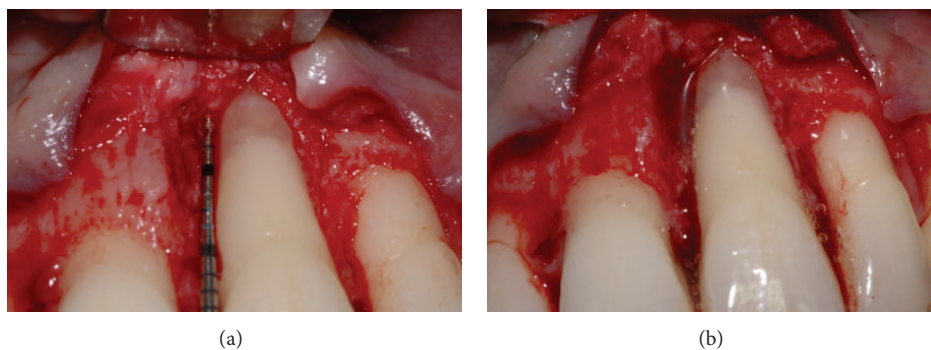


FIGURE 9: (a) Root surface appearance after flap reflection and degranulation. (b) EMD applied on root surface.

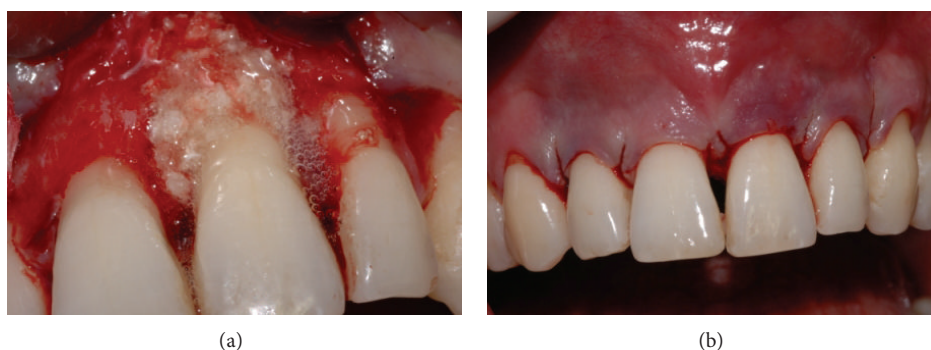


FIGURE 10: (a) NanoHA + EMD application on root surface using sandwich technique. (b) Sutured flap.

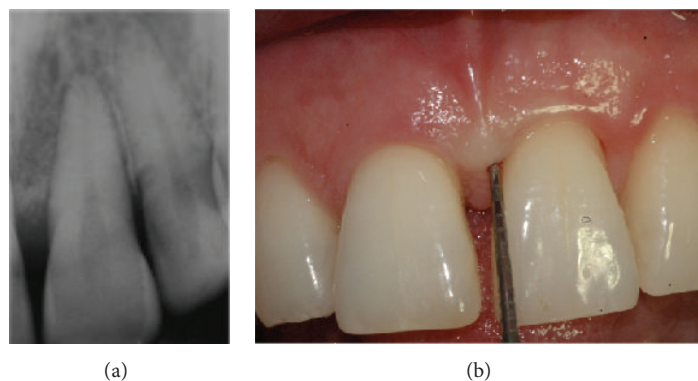


FIGURE 11: (a) X-ray at 24 months. (b) Clinical aspect showing attachment gain.

were performed. In the other treatment groups the hypothesis of normality was rejected (P values lower than 5%). The differences in REC levels at baseline compared with levels after 12, 18, and 24 months were statistically significant at 10% for defects treated with nanoHA after 18 and 24 months and at 5% for the other treatments. The median and mean reductions in PAL levels shown in Figures 20, 21, 22, and 23 were significant.

3.2. Differences among Treatments after 12 Months. The null hypothesis where location parameters were the same among treatments was rejected for PD, REC, and PAL ($P < 0.03$). For PD, post hoc multiple comparison at 5% showed statistically

significant differences between nanoHA and nanoHA + EMD (observed difference (obs diff) = 33.01, critical difference (crit diff) = 21.12) and between nanoHA + EMD and OFD (obs diff = 24.29, crit diff = 21.12). For REC, post hoc multiple comparison at 5% showed statistically significant differences between EMD and nanoHA (obs diff = 22.05, crit diff = 21.12). Post hoc multiple comparison for PAL at 5% showed statistically significant differences between nanoHA and nanoHA + EMD (obs diff = 24.33, crit diff = 21.12) in favor of nanoHA + EMD.

3.3. Differences among Treatments after 18 Months. The null hypothesis where location parameters were the same among

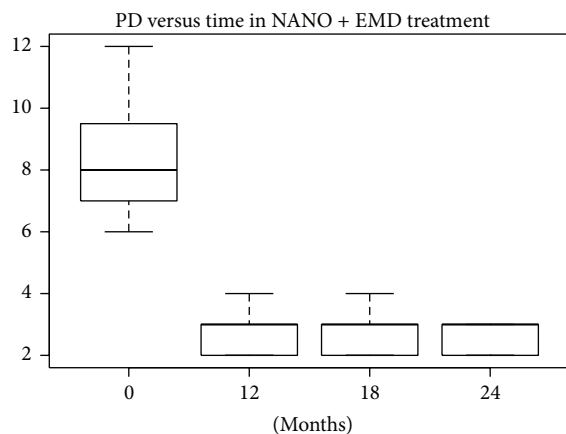


FIGURE 12

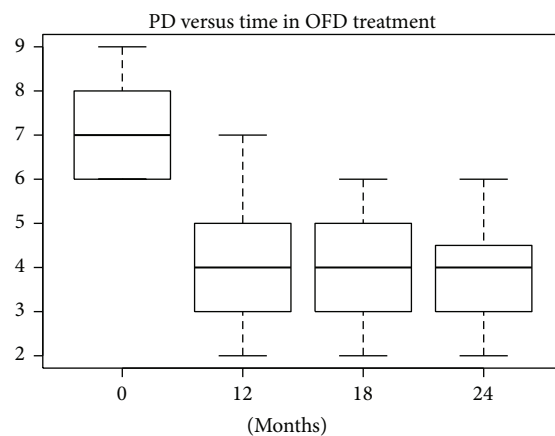


FIGURE 15

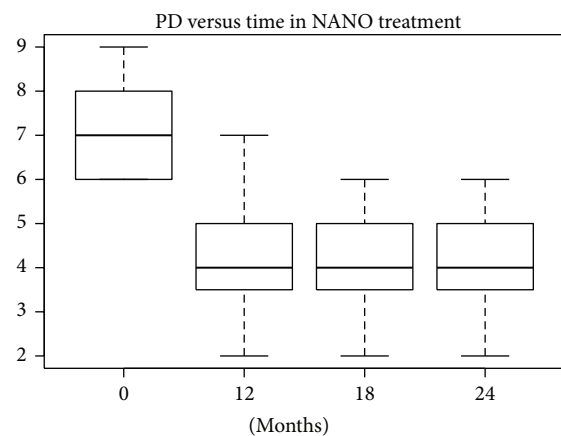


FIGURE 13

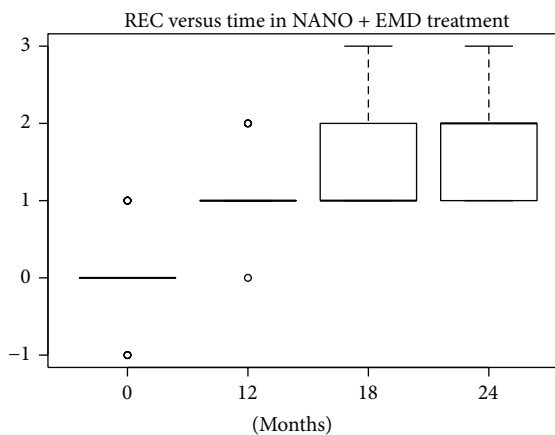


FIGURE 16

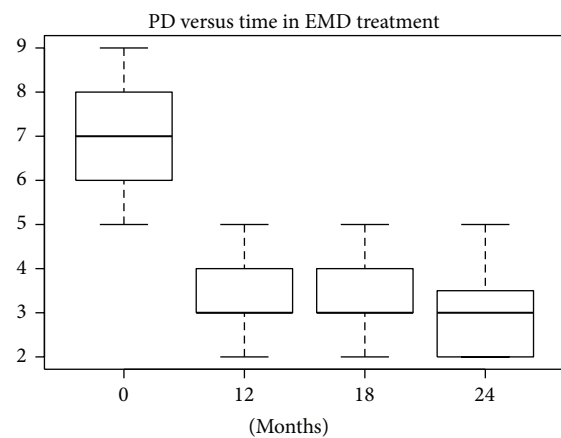


FIGURE 14

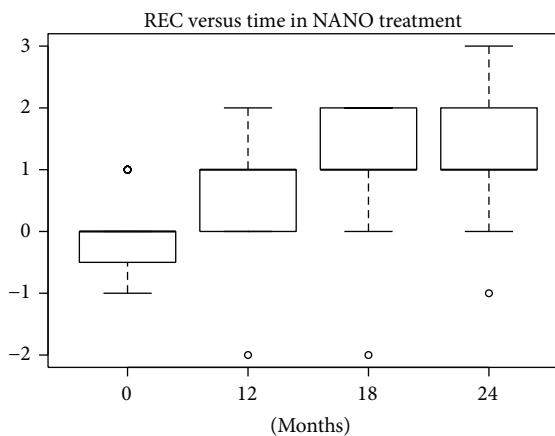


FIGURE 17

treatments was accepted for REC ($P = 0.53$) and rejected for PD and PAL ($P < 0.01$). Median and mean location parameters for REC were not statistically different among treatments; parameters were significantly different for PD and PAL ($P < 0.03$).

For PD, post hoc multiple comparison at 5% showed statistically significant differences between nanoHA and nanoHA + EMD (obs diff = 31.38, crit diff = 21.12) and between nanoHA + EMD and OFD (obs diff = 24.13, crit diff = 21.12). These were the same results as at the 12-month evaluation. For PAL, post hoc multiple comparison at 5%

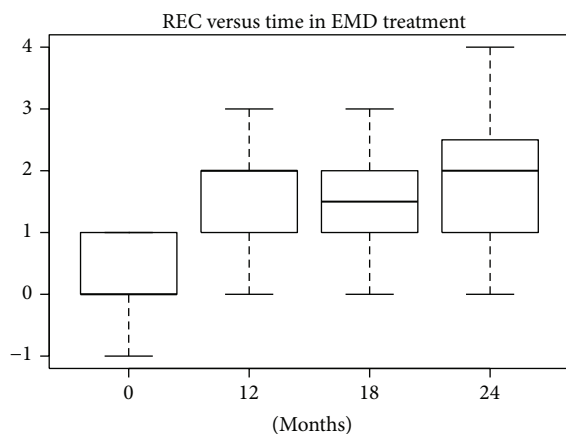


FIGURE 18

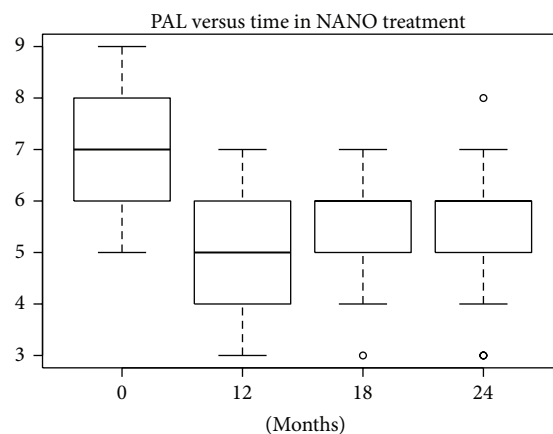


FIGURE 21

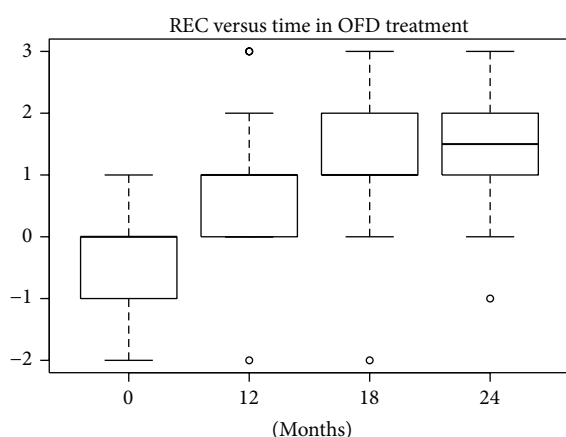


FIGURE 19

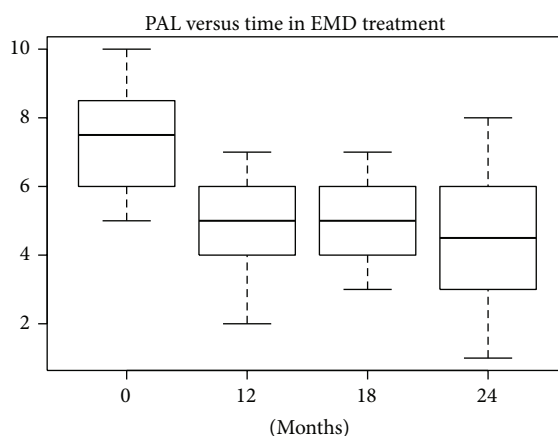


FIGURE 22

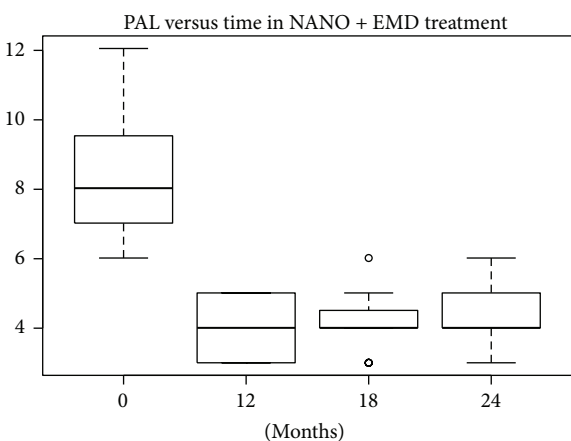


FIGURE 20

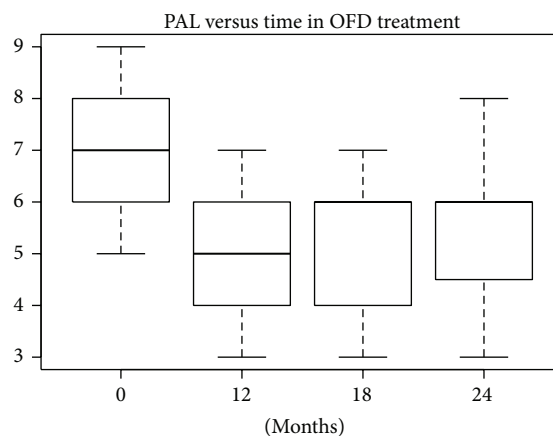


FIGURE 23

showed statistically significant differences between nanoHA and nanoHA + EMD (obs diff = 26.75, crit diff = 21.12) and between nanoHA + EMD and OFD (obs diff = 26.25, crit diff = 21.12).

3.4. Differences among Treatments after 24 Months. The null hypothesis that location parameters were the same among

treatments was accepted for REC ($P = 0.28$) and rejected for PD and PAL ($P < 0.02$). Median and mean location parameters were not statistically different among treatments for REC, but they were different for PD and PAL. The same results were obtained as for the 18-month evaluation ($P < 0.03$).

For PD, post hoc multiple comparison at 5% showed statistically significant differences between EMD and nanoHA (obs diff = 22.27, crit diff = 21.12), between nanoHA and nanoHA + EMD (obs diff = 33.58, crit diff = 21.12), and between nanoHA + EMD and OFD (obs diff = 25.26, crit diff = 21.12). For PAL, post hoc multiple comparison at 5% showed statistically significant differences between nanoHA and nanoHA + EMD (obs diff = 21.55, crit diff = 21.12).

4. Discussion

All four methods employed in this study fulfilled the main purposes of periodontal surgery: controlling periodontal infection and providing periodontal maintainable sites. Thus, reduction of PD was found in all four treatment groups. However, periodontal regeneration requires more than control of infection and gingival recession. Calculation of the clinical attachment level reflects the degree of regeneration obtained. In this study, gingival recession showed an improving trend over time in all treatment groups. Regeneration without significant gingival recession was statistically important for OFD, EMD, and nanoHA + EMD but not for nanoHA alone. NanoHA alone showed less beneficial clinical effect than removal of granulation tissue without use of defect-filling material. This was an unexpected result, because biomaterials, especially osteoconductive materials such as nanoHA, are supposed to provide support for soft tissues and to prevent their prolapse. However, the clinical observations in the present study are in accordance with the histological results of Horváth et al., showing the limited potential of nanoHA in promoting periodontal regeneration over a 7-month period [12]. This finding could be explained by the rationale of Susin and Wikesjö [2], who reported that most biomaterials interfere with rather than support periodontal regeneration because of their sequestration within connective tissues. Susin and Wikesjö [2] and Trombelli et al. [16] evaluated a minimally invasive surgical protocol as a stand-alone approach or in combination with membranes and hydroxyapatite-based biomaterials. No significant differences were observed between experimental groups; sites treated with a minimally invasive technique exhibited clinical attachment gain averaging 4.7 ± 2.5 mm, probing depth reduction of 5.3 ± 2.4 mm, and gingival recession of 0.4 ± 1.4 mm. Similarly, Cortellini and Tonetti [17] evaluated a minimally invasive surgical technique, alone and in conjunction with an EMD and a bovine bone-based biomaterial. No significant differences between treatments were observed; the minimally invasive surgical approach without additions achieved substantial clinical attachment gain of 4.1 ± 1.2 mm and radiographic bone fill of $77 \pm 19\%$. In contrast, our results suggest a significant difference between nanoHA and nanoHA + EMD in terms of changes in PD and PAL indices, measured at each follow-up interval. Our results suggest that EMD plays a prominent role in promoting better results when used in conjunction with nanoHA, compared with nanoHA alone. This clinical outcome is supported by a 12-month follow-up study conducted by Kasaj et al. [11], who reported that EMD had advantages over nanoHA in patient comfort and adverse effects. Kasaj et al. [5] reported that

EMD acts as a chemoattractant, while nanoHA paste is a synthetic extracellular matrix component in its coated form. Al Machot et al. [13] hypothesized a potential synergic effect of combining the materials with resulting possible beneficial effects on wound healing.

Avoiding the Hawthorne effect is supposed to provide a more realistic picture of how a treatment functions in everyday practice. However, retrospective treatment evaluations have limitations that could bias the results. However, this bias can be reduced by using multiple control groups as in the present study, which compared four treatment groups, and by the triple blinding of the operator, the patient, and the analyst. Moreover, restricting patient selection criteria reduced confounding factors. One important tool in analyzing clinical outcome from the patient's perspective is the visual analog scale, which can confirm or cast doubt on the effects of biomaterials and techniques as regenerative strategies [18]. Such evaluation could have been useful in our study; postoperative data, including patient perception, could have been matched to clinical outcome, in both short- and long-term evaluation. One limit of the present study is that clinical parameters alone were used to evaluate the regeneration process. Previous studies have associated these parameters with radiographic measurements to reduce possible biases. However, clinical and radiographic parameters cannot fully replace histological analysis to confirm the true regeneration of all periodontal tissues. Therefore, even using both sources of information could be considered insufficient. Because the purpose of treatment is controlling infection by eliminating periodontal pockets and at the same time preventing soft tissue collapse, clinical data can be considered a primary outcome in everyday clinical practice. The combined use of nanoHA and EMD seems to fulfill such clinical criteria.

5. Conclusions

In summary, within the limitations of this study, we found that EMD and nanoHA played a synergic role in promoting restoration of the tooth-supporting apparatus.

Conflict of Interests

The authors declare that there is no conflict of interests regarding the publication of this paper.

References

- [1] N. Donos, L. Laurell, and N. Mardas, "Hierarchical decisions on teeth vs. implants in the periodontitis-susceptible patient: the modern dilemma," *Periodontology* 2000, vol. 59, no. 1, pp. 89–110, 2012.
- [2] C. Susin and U. M. E. Wikesjö, "Regenerative periodontal therapy: 30 years of lessons learned and unlearned," *Periodontology* 2000, vol. 62, no. 1, pp. 232–242, 2013.
- [3] Y.-K. Tu, A. Woolston, and C. M. Faggion Jr., "Do bone grafts or barrier membranes provide additional treatment effects for infrabony lesions treated with enamel matrix derivatives? A network meta-analysis of randomized-controlled trials," *Journal of Clinical Periodontology*, vol. 37, no. 1, pp. 59–79, 2010.

- [4] I. Bouchlariotou, J. P. Bernard, J. P. Carrel, and L. Vazquez, "Long-term stability of osseointegrated implants in bone regenerated with a collagen membrane in combination with a deproteinized bovine bone graft: 5-year follow-up of 20 implants," *POSEIDO Journal*, vol. 1, no. 1, pp. 1–64, 2013.
- [5] A. Kasaj, B. Willershausen, R. Junker, S.-I. Stratul, and M. Schmidt, "Human periodontal ligament fibroblasts stimulated by nanocrystalline hydroxyapatite paste or enamel matrix derivative. An in vitro assessment of PDL attachment, migration, and proliferation," *Clinical Oral Investigations*, vol. 16, no. 3, pp. 745–754, 2012.
- [6] S. Gestrelus, C. Andersson, A. C. Johansson et al., "Formulation of enamel matrix derivative for surface coating kinetics and cell colonization," *Journal of Clinical Periodontology*, vol. 24, no. 9, pp. 678–684, 1997.
- [7] D. B. Palioto, R. D. Coletta, E. Graner, J. C. Joly, and A. F. Martorelli de Lima, "The influence of enamel matrix derivative associated with insulin-like growth factor-I on periodontal ligament fibroblasts," *Journal of Periodontology*, vol. 75, no. 4, pp. 498–504, 2004.
- [8] J. He, J. Jiang, K. E. Safavi, L. S. W. Spångberg, and Q. Zhu, "Emdogain promotes osteoblast proliferation and differentiation and stimulates osteoprotegerin expression," *Oral Surgery, Oral Medicine, Oral Pathology, Oral Radiology, and Endodontics*, vol. 97, no. 2, pp. 239–245, 2004.
- [9] A. Pilloni, G. Pompa, M. Saccucci et al., "Analysis of human alveolar osteoblast behavior on a nano-hydroxyapatite substrate: an in vitro study," *BMC Oral Health*, vol. 20, no. 1, pp. 14–22, 2014.
- [10] M. Silvestri, G. Rasperini, and S. Milani, "120 Infrabony defects treated with regenerative therapy: long-term results," *Journal of Periodontology*, vol. 82, no. 5, pp. 668–675, 2011.
- [11] A. Kasaj, B. Röhrig, G.-G. Zafiroopoulos, and B. Willershausen, "Clinical evaluation of nanocrystalline hydroxyapatite paste in the treatment of human periodontal bony defects: a randomized controlled clinical trial: 6-month results," *Journal of Periodontology*, vol. 79, no. 3, pp. 394–400, 2008.
- [12] A. Horváth, A. Stavropoulos, P. Windisch, L. Lukács, I. Gera, and A. Sculean, "Histological evaluation of human intrabony periodontal defects treated with an unsintered nanocrystalline hydroxyapatite paste," *Clinical Oral Investigations*, vol. 17, no. 2, pp. 423–430, 2013.
- [13] E. Al Machot, T. Hoffmann, K. Lorenz, I. Khalili, and B. Noack, "Clinical outcomes after treatment of periodontal intrabony defects with nanocrystalline hydroxyapatite (Ostim) or enamel matrix derivatives (Emdogain): a randomized controlled clinical trial," *BioMed Research International*, vol. 2014, Article ID 786353, 9 pages, 2014.
- [14] S. S. Shapiro and M. B. Wilk, "An analysis of variance test for normality: complete samples," *Biometrika*, vol. 52, pp. 591–611, 1965.
- [15] M. Hollander and D. A. Wolfe, "Nonparametric statistical methods," *Wiley Series in Probability and Statistics*, vol. 17, no. 8, pp. 526–1975, 2007.
- [16] L. Trombelli, A. Simonelli, M. Pramstraller, U. M. E. Wikesjö, and R. Farina, "Single flap approach with and without guided tissue regeneration and a hydroxyapatite biomaterial in the management of intraosseous periodontal defects," *Journal of Periodontology*, vol. 81, no. 9, pp. 1256–1263, 2010.
- [17] P. Cortellini and M. S. Tonetti, "Clinical and radiographic outcomes of the modified minimally invasive surgical technique with and without regenerative materials: a randomized-controlled trial in intra-bony defects," *Journal of Clinical Periodontology*, vol. 38, no. 4, pp. 365–373, 2011.
- [18] J. L. Wennström and J. Lindhe, "Some effects of enamel matrix proteins on wound healing in the dento-gingival region," *Journal of Clinical Periodontology*, vol. 29, no. 1, pp. 9–14, 2002.

Research Article

Adhesion and Proliferation of Human Periodontal Ligament Cells on Poly(2-methoxyethyl acrylate)

Erika Kitakami,¹ Makiko Aoki,¹ Chikako Sato,¹ Hiroshi Ishihata,² and Masaru Tanaka¹

¹ Graduate School of Science and Engineering, Yamagata University, Jonan 4-3-16, Yonezawa, Yamagata 992-8510, Japan

² Graduate School of Dentistry, Division of Periodontology and Endodontology, Tohoku University, Seiryō-machi 4-1, Sendai, Miyagi 980-8575, Japan

Correspondence should be addressed to Masaru Tanaka; tanaka@yz.yamagata-u.ac.jp

Received 15 May 2014; Accepted 29 June 2014; Published 6 August 2014

Academic Editor: David M. Dohan Ehrenfest

Copyright © 2014 Erika Kitakami et al. This is an open access article distributed under the Creative Commons Attribution License, which permits unrestricted use, distribution, and reproduction in any medium, provided the original work is properly cited.

Human periodontal ligament (PDL) cells obtained from extracted teeth are a potential cell source for tissue engineering. We previously reported that poly(2-methoxyethyl acrylate) (PMEA) is highly biocompatible with human blood cells. In this study, we investigated the adhesion, morphology, and proliferation of PDL cells on PMEA and other types of polymers to design an appropriate scaffold for tissue engineering. PDL cells adhered and proliferated on all investigated polymer surfaces except for poly(2-hydroxyethyl methacrylate) and poly[(2-methacryloyloxyethyl phosphorylcholine)-*co*-(*n*-butyl methacrylate)]. The initial adhesion of the PDL cells on PMEA was comparable with that on polyethylene terephthalate (PET). In addition, the PDL cells on PMEA spread well and exhibited proliferation behavior similar to that observed on PET. In contrast, platelets hardly adhered to PMEA. PMEA is therefore expected to be an excellent scaffold for tissue engineering and for culturing tissue-derived cells in a blood-rich environment.

1. Introduction

Periodontal diseases, caused by the bacterial biofilm, can affect up to 90% of adults worldwide [1]. Severe periodontitis leads to losing connective tissue and bone support and finally losing teeth [1]. Therefore, much research is being conducted on periodontal tissue regeneration for restoring the alveolar support of the teeth. The periodontal ligament (PDL) is an important structure that is composed of periodontal tissue, in which PDL cells generate connective tissue fibers that span the gap between the cementum and the alveolar bone [2] to suspend the tooth. This complex structure of PDL tissue comprises several different cell populations [3], including PDL cells, which are predominantly fibroblasts and play crucial roles in maintaining and regenerating periodontal tissue [2, 3].

Human PDL cells obtained from extracted teeth are a promising cell source for periodontal tissue regeneration, regenerative medicine, and tissue engineering [3–6], because they include stem cells that have a high capacity for proliferation, self-renewal, and multilineage differentiation and also

have the ability to form cementum/periodontal ligament-like tissue *in vivo* [3, 4]. Human PDL stem cells, similar to bone marrow mesenchymal stem cells, are able to suppress immune responses and inflammatory reactions, which suggests that PDL stem cells may be used in allogeneic stem cell-based therapies [5]. In the first clinical application of human autologous PDL-derived cells, including PDL stem cells, the transplanted cells were used to reconstruct periodontal intrabony defects in 3 patients, and a significant improvement of periodontal disease was achieved, which suggests that PDL stem cell transplantation may be an efficacious and safe alternative for the treatment of human periodontitis [6].

Furthermore, human induced pluripotent stem cells (iPS cells) have been generated from adult human periodontal ligament fibroblasts [7]. Nomura et al. reported that the reprogramming efficiency of human PDL fibroblasts was 0.025%, which is not lower than the reprogramming efficiency of dental stem cells, even though the stem cells already express a number of ES cell-associated genes; therefore, human PDL fibroblasts may be an optimal cell source for generating iPS cells [7]. Additionally, the use of PDL cells

is advantageous because it efficiently utilizes extracted teeth. However, for periodontal tissue regeneration, it is necessary to culture PDL cells on a biocompatible scaffold to deliver the cells to the wound site and also to provide space for the formation of the new periodontal tissue. Biomaterial scaffolds designed for tissue-engineered constructs must accommodate cell viability, growth, and function [8]. There is increasing interest in designing new biomaterials for scaffolds with minimal or no immune response that encourage stable implant/tissue interaction [9]. In addition, the surface characterization of biomaterials is important to design new implantable materials [10–14].

We previously reported that poly(2-methoxyethyl acrylate) (PMEA) shows excellent biocompatibility with human blood coagulation and complement systems and does not activate leukocytes, erythrocytes, and platelets *in vitro* and *ex vivo* relative to other polymer surfaces during the early stages of immune reactions [15–19]. On the basis of our results, superior biocompatible catheters and oxygenators coated with PMEA were approved by the Food and Drug Administration (FDA) and made available to the global market [16–19]. We further determined why PMEA has excellent biocompatibility [15, 20–22]. In particular, the low extent of platelet adhesion and spreading observed was closely related to a low degree of denaturation and high dissociation rate for proteins adsorbed onto PMEA [15].

The objective of this study was to examine the hypothesis that PMEA is a biocompatible polymer for tissue engineering that can facilitate adhesion and proliferation of PDL cells with low platelet adhesion. Cell-material interactions determine many cellular processes such as adhesion, spreading, and proliferation and are thus essential for tissue engineering [23–27]. However, the influence of the chemical components of synthesized polymers on the biology of PDL cells remains unclear. To investigate PDL cell-material interactions, we characterized the localization of focal adhesions, which are multifunctional organelles that mediate cell-material adhesion, force transmission, and cytoskeletal regulation and signaling [28]. To analyze the formation of focal adhesions, we evaluated the localization of vinculin, which is a membrane-cytoskeletal protein present in focal adhesions that is involved in the linkage of integrin adhesion molecules to the actin cytoskeleton [29].

2. Material and Methods

2.1. Preparation of Polymer Surfaces. PMEA was prepared by free-radical polymerization using 2,2'-azobisisobutyronitrile (Kanto Chemical Co., Inc., Japan) as the initiator and 2-methoxyethyl acrylate (MEA) as the monomer. The MEA was obtained from Wako Pure Chemical Industries, Ltd. (Osaka, Japan), poly(2-hydroxyethyl methacrylate) (HEMA) was obtained from Scientific Polymer Products, Inc. (Ontario, NY), and poly[(2-methacryloyloxyethyl phosphorylcholine)-co-(*n*-butyl methacrylate)] (PMPC) was obtained from NOF corporation (Tokyo, Japan). The molecular weight of each polymer was estimated by gel permeation chromatography using polystyrene standards. The molecular weight (*M_w*) of PMEA, PHEMA, and PMPC was 85,000,

300,000, and 600,000, respectively. The chemical structure of each polymer PMEA, PHEMA, and PMPC is shown in Figure 1 in Supplementary Material available online at <http://dx.doi.org/10.1155/2014/102648>, and the polymers were prepared on polyethylene terephthalate (PET film: T100E125; Mitsubishi Plastics, Tokyo, Japan; 14 mm diameter and 125 μ m thickness) using a spin coater (MS-A100; Mikasa, Tokyo, Japan). Exactly 40 μ L of a 0.2 wt% solution of each polymer was cast twice onto the PET films. Analytical grade methanol (Kanto Chemical Co., Inc) was used as the solvent for each solution. The surfaces of the polymer films were analyzed by X-ray photoelectron spectroscopy (XPS) (ESCA-1000; Shimadzu, Kyoto, Japan) to confirm the coverage of the coated polymer. The take-off angle was 45°.

For cell culture, the films were sterilized by UV exposure for 2 h. Subsequently, the films were soaked in medium composed of Minimum Essential Medium (MEM-Alpha; Life Technologies) containing 10% heat-inactivated fetal bovine serum (Equitech-Bio, Inc., Kerrville, TX) and antibiotic solution (100 U/mL penicillin G sodium, 100 μ g/mL streptomycin sulfate, and 0.25 μ g/mL amphotericin B; Life Technologies) (culture medium) for one hour (preconditioning).

2.2. Characterization of Polymer Films. We analyzed each polymer film by atomic force microscopy (AFM; Agilent Technologies 5550 Scanning Probe Microscope, Agilent Technologies, Inc., Santa Clara, CA). The maximum scan range was approximately 10 μ m \times 10 μ m using a cantilever with a force constant of 21–78 N/m, resonance frequency of 250–390 kHz, and tip height of 10–15 μ m (NCH-10, Nano World, Zurich, Switzerland). AFM was performed in air acoustic AC mode. AFM image analysis was performed using Pico Image Software (Agilent Technologies).

The wettability of the polymer surfaces was characterized by contact angle measurement [15]. The static contact angle on each polymer surface was measured using the sessile drop method at room temperature. For the sessile drop method, 2 μ L of deionized water was dropped on a dried polymer film using a microsyringe. The static contact angle was observed 30 s later under a microscope (G-I-1000; ERMA Inc., Tokyo, Japan). After at least five readings which were obtained for different areas of the polymer, the measurements were averaged to arrive at a final contact angle ($n = 6$).

2.3. Cell Preparation and Culture. Primary PDL cells were obtained as previously reported [30]. Fibroblast-like PDL cells were derived from the periodontal ligament of human third molars extracted from healthy individuals aged 17–21 years who had no clinical signs of chronic periodontal disease. Informed consent was obtained prior to each extraction. The cells were obtained from the Dental Faculty of Tohoku University. Periodontal ligament tissues were dissected into small pieces from the midportion of the root with a sharp blade. The pieces were then cultivated in tissue culture dishes (Asahi Glass Co., LTD, Tokyo, Japan) until the formation of a confluent cell monolayer using culture medium. After confluence was achieved, the cells were washed with phosphate-buffered saline (PBS; Takara Bio Inc., Shiga, Japan) and resuspended with 0.075 g/L protease and 0.1 g/L EDTA to

enable passage. These experiments were approved by the Ethics Committee of the Dental Faculty of Tohoku University and the Graduate School of Science and Engineering of Yamagata University, Japan.

We used PDL cells at passages six and eight for adhesion and proliferation assays. PET, PMEA, PHEMA and PMPC films were put in 24-well polystyrene plates (Asahi Glass Co., LTD). After preconditioning of these films, PDL cells were seeded at 1×10^4 cells/cm² onto the tested films, and grown for up to 1 hour (1 h), 1 day, 3 days, and 7 days using culture medium. During culturing, the cells were maintained at 37°C in 5% CO₂ and 95% air, and the medium was changed every three days. The progression of the cultures was examined by using phase contrast microscopy (CKX41; Olympus, Tokyo, Japan).

2.4. Immunofluorescence Staining. The adhesion, proliferation, and focal adhesion formation of the cultured PDL cells were observed by confocal laser scanning microscopy (CLSM; FV-1000; Olympus). To visualize cell adhesion, spreading, proliferation, and focal adhesion formation on the polymers, staining of vinculin, actin fibers, and cell nuclei was performed. After culture for the indicated period, the cells were washed with PBS twice. After washing, the cells were fixed with PBS containing 4% paraformaldehyde obtained from Wako Pure Chemical Industries, Ltd. (Osaka, Japan) for 10 min at 37°C and washed again three times with PBS. Subsequently, the cells were permeated three times with 1% Triton-X-100 (MP Biomedicals, LLC, Solon, OH) in PBS for 10 min at room temperature and then immersed in 0.02% Tween-PBS (MP Biomedicals, LLC) three times for 10 min each. To assess PDL cell-material interactions, PDL cells on polymers were stained for vinculin, which is localized at focal adhesions, using a mouse antivinculin monoclonal antibody (Millipore, Temecula, CA) as a primary antibody for 1 h, followed by treatment with Alexa Fluor 546 goat anti-mouse IgG (Life Technologies) as a secondary antibody for 1 h. For actin staining, the samples were incubated with Alexa Fluor 488 phalloidin (Life Technologies) for 1 h. For detection of Ki-67 antigen as a cell proliferation marker, the samples were treated with rabbit anti-Ki-67 antigen monoclonal antibody (Life Technologies) for 2 h. The samples were then incubated with Alexa Fluor 488 goat anti-rabbit antibody (Life Technologies) for 1 h ($n = 9$). The stained cells were rinsed three times with PBS and subsequently immersed in PBS for 10 min. All specimens were placed on glass slides, mounted by using ProLong Gold antifade reagent with DAPI (Life Technologies), and covered with glass cover slips.

The specimens were imaged by CLSM, and cell morphology parameters were quantified by Olympus Fluoview software. The total number of adherent cells on polymer films was counted in five randomly selected CLSM images ($n = 3$).

2.5. Scanning Electron Microscopy. To assess the morphology of adherent PDL cells cultured on each polymer for 1 h, the cells were observed by field emission scanning electron microscopy (SEM; SU-8000, Hitachi, Ltd., Tokyo, Japan). Cultured cells were fixed with 2.5% glutaraldehyde (Polysciences, Inc., Warrington, PA) in PBS and incubated

overnight at 4°C. They were next washed three times with PBS and then with pure water and subsequently air-dried. The dried samples were coated with carbon using an ion sputter coater (HPC-1SW; Vacuum Device Inc., Ibaraki, Japan).

2.6. Platelet Adhesion Test. To investigate the number of platelets adhering to the polymers, blood was drawn from 3 healthy volunteers (nonsmokers; age 22 male, age 33 female, and age 42 male) and mixed with a 1/9 volume of 3.2% sodium citrate. Platelet-rich plasma (PRP) and platelet-poor plasma (PPP) were obtained by centrifugation of citrated blood at 1,500 rpm for 5 min and 4,000 rpm for 10 min, respectively. Plasma containing $3-4 \times 10^7$ cells/cm² was prepared by mixing PRP with PPP. Then, 200 μ L of the platelet suspension was placed on each polymer surface and incubated for 1 h at 37°C. After the films were washed three times with PBS, they were immersed in 1% glutaraldehyde in PBS for 120 min at 4°C to fix the adhered platelets. The samples were dried and sputter-coated in platinum-palladium using an ion sputter coater prior to SEM (JSM-7600FA, JEOL Ltd., Tokyo, Japan). The number of adherent platelets on the polymer films was counted in five randomly selected SEM images ($n = 6$).

2.7. Data Analyses. The results were analyzed using Student's *t*-test. $P < 0.05$ was used as the threshold for statistical significance between groups.

3. Results and Discussion

3.1. Characterization of Polymer Films. The surface roughness of each polymer film was analyzed by AFM (Table 1). The AFM topographical values (root mean squared; RMS) for PET, PMEA, PHEMA, and PMPC were 10, 6.7, 5.8, and 6.5 nm, respectively. The polymer-coated films were smoother than the PET film.

Figure 1(a) shows the XPS spectrum of the PET film coated nitrogen-modified PET film (Figures 1(a)–1(c), line A). C 1s and O 1s peaks derived from PMEA were observed, whereas an N 1s peak for the nitrogen-modified PET film was not observed (Figure 1(a), line B). The XPS spectrum of the coated PHEMA also showed the same result (Figure 1(b)). The XPS spectra of coated PMPC also did not show an N 1s peak but showed a P 2s peak (Figure 1(c), line B). These results indicate that the PET film surface was completely covered with each polymer.

The static contact angle (θ) on each polymer surface was measured by the sessile drop method as shown in Table 2. The θ values determined by the sessile drop method for deionized water were $69^\circ \pm 2.6^\circ$, $45^\circ \pm 2.2^\circ$, $36^\circ \pm 2.7^\circ$, and $105^\circ \pm 3.3^\circ$ on PET, PMEA, PHEMA, and PMPC, respectively. These data indicate that the hydrophilicity of PMEA is between that of PET and PHEMA. The static contact angle of each polymer was consistent with values in the literature [31, 32].

3.2. Morphology of PDL Cells on Polymer Surfaces. Cell morphology and proliferation behavior observed by CLSM demonstrated that PDL cells adhered to PMEA and other polymer surfaces, except PMPC, with a round shape within 1 h (Figure 2). After 1 day, PDL cells had spread across the

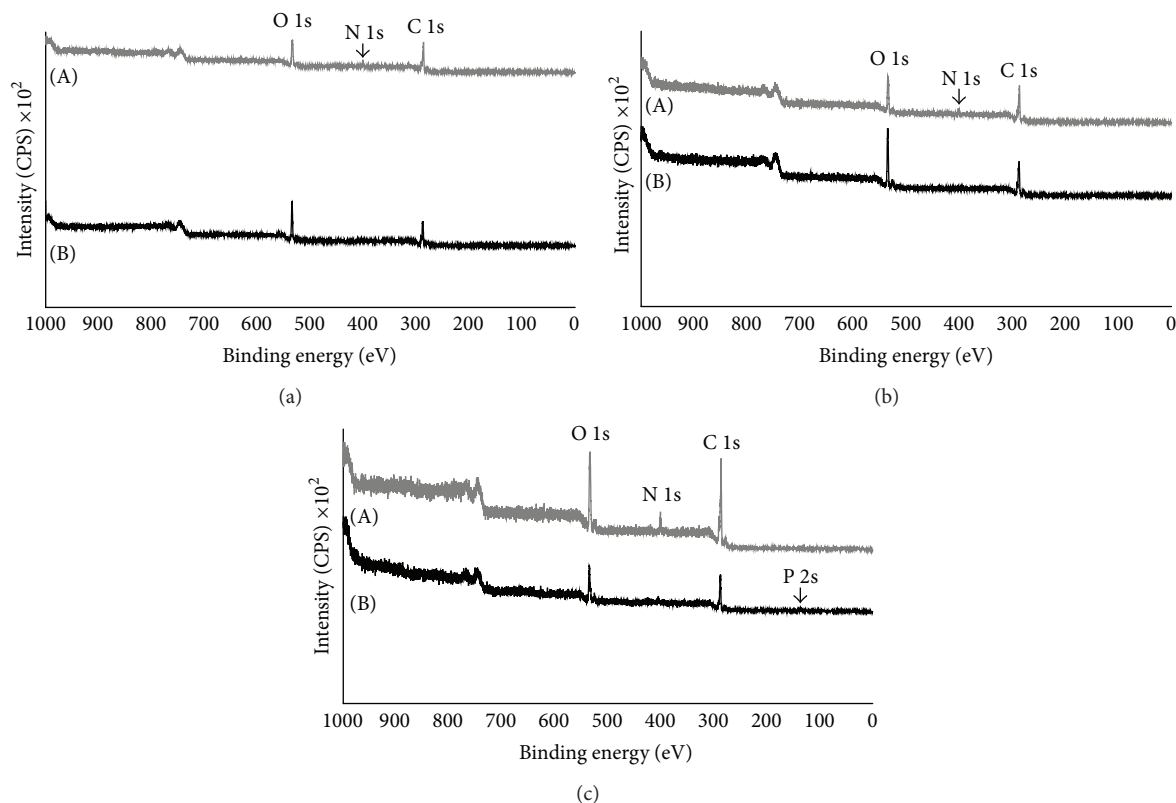


FIGURE 1: XPS spectrum of the PET film surface coated with PMEA (a), PHEMA (b), and PMPC (c). (A) indicates the XPS spectrum of the PET film surface. (B) indicates the XPS spectrum of the coated film. The atomic compositions determined from the XPS spectra match the expected composition based on the structure of each polymer.

TABLE 1: AFM topographical data. RMS: root mean squared roughness. Scan size $10 \times 10 \mu\text{m}^2$.

Polymer	RMS (nm)
PET	10
PMEA	6.7
PHEMA	5.8
PMPC	6.5

polymers. After 3 days, PDL cells had spread further and showed proliferation behavior on all polymers. After 7 days, PDL cells on PET and PMEA were confluent, and developed actin fibers were observed. PDL cells on PHEMA were not confluent but had aggregated. PDL cells did not adhere and proliferate on PMPC throughout the experiment.

3.3. Initial Adhesion of PDL Cells. The nuclei of adherent PDL cells on each polymer surface were counted under CLSM. PDL cells adhered to PMEA and the other polymer surfaces, except for PMPC, upon incubation for 1 h (Figure 3(a)). The number of adherent PDL cells on PMEA was almost identical to that on PET and was 5 times higher than that on PHEMA.

The cell morphology observed by SEM showed differences for each polymer after 1 h (Figure 3(b)). PDL cells

TABLE 2: Static contact angles of polymer surfaces.

Polymer	Sessile drop (degrees), (\pm SD)
PET	69.2 (\pm 2.6)
PMEA	45.0 (\pm 2.2)
PHEMA	36.0 (\pm 2.7)
PMPC	105.2 (\pm 3.3)

on PET contained some pseudopodia (white circle) and spikes (white arrow). PDL cells on PMEA contained some pseudopodia (white circle) and many spikes (white arrows). PDL cells on PHEMA contained lamellipodia. The surfaces of adherent PDL cells adherent to PET and PMEA were rougher than those on PHEMA.

3.4. Quantification of Projected Area, Perimeter, and Long Axis of PDL Cells. The morphology of the adherent PDL cells was quantified using CLSM images (Figure 4(a)). Figure 4(b) shows the projected cell area on each polymer. After 1 h, the projected cell areas were $270 \pm 100 \mu\text{m}^2$, $230 \pm 90 \mu\text{m}^2$, and $270 \pm 110 \mu\text{m}^2$ on PET, PMEA, and PHEMA, respectively. After 1 day, the projected cell areas were $1390 \pm 660 \mu\text{m}^2$, $1770 \pm 610 \mu\text{m}^2$, and $690 \pm 360 \mu\text{m}^2$ on PET, PMEA, and PHEMA, respectively. The projected cell areas increased

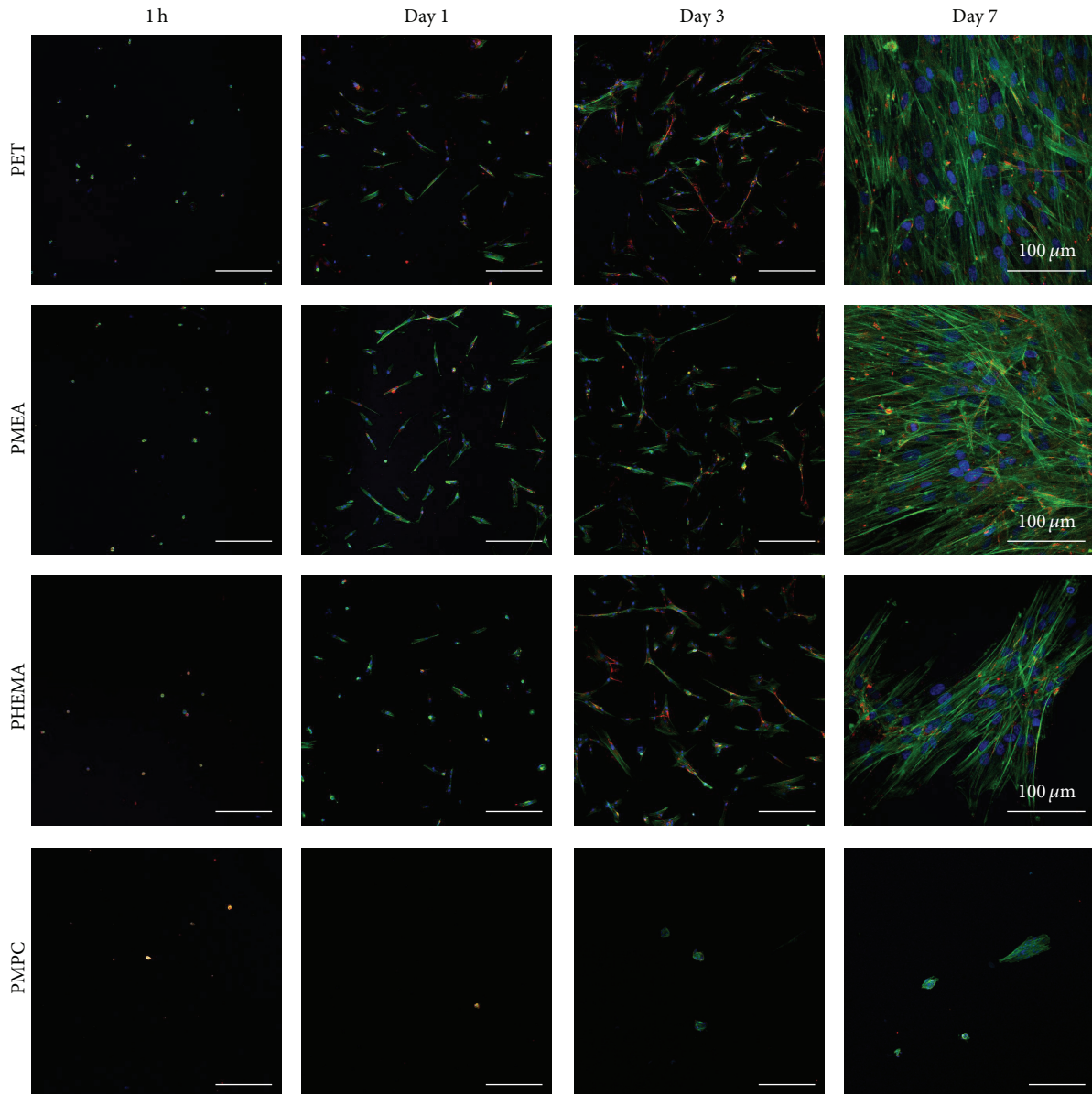


FIGURE 2: CLSM images of PDL cells cultured on polymer surfaces. Scale bars: 300 μm . Blue: nucleus, green: actin, and red: vinculin. Time points are 1 h, 1 day, 3 days, and 7 days. Polymers: PET, PMEA, PHEMA, and PMPC.

by 5.1-, 7.7-, and 2.6-fold on PET, PMEA, and PHEMA, respectively, from 1 h up to 1 day.

Figure 4(c) shows the perimeter of adherent PDL cells on each polymer. After 1 h, the perimeters were $75 \pm 15 \mu\text{m}$, $80 \pm 17 \mu\text{m}$, and $82 \pm 27 \mu\text{m}$ on PET, PMEA, and PHEMA, respectively. After 1 day, the perimeters were $300 \pm 85 \mu\text{m}$, $380 \pm 130 \mu\text{m}$, and $180 \pm 80 \mu\text{m}$ on PET, PMEA, and PHEMA, respectively. The perimeter of the adherent cells increased by 4.0-, 4.8-, and 2.2-fold on PET, PMEA, and PHEMA, respectively, from 1 h up to 1 day.

Figure 4(d) shows each axis of the adherent PDL cells on each polymer. After 1 h, the long axes (i.e., length) were $22 \pm 5 \mu\text{m}$, $22 \pm 7 \mu\text{m}$, and $22 \pm 8 \mu\text{m}$ on PET, PMEA, and

PHEMA, respectively. After 1 day, the lengths were $85 \pm 37 \mu\text{m}$, $110 \pm 44 \mu\text{m}$, and $50 \pm 33 \mu\text{m}$ on PET, PMEA, and PHEMA, respectively. The length of adherent cells increased by 3.9-, 5.0-, and 2.3-fold on PET, PMEA, and PHEMA, respectively, from 1 h up to 1 day. After 1 h, the short axes (i.e., width) were $14 \pm 5 \mu\text{m}$, $9 \pm 2 \mu\text{m}$, and $13 \pm 2 \mu\text{m}$ on PET, PMEA, and PHEMA, respectively. After 1 day, the widths were $21 \pm 10 \mu\text{m}$, $24 \pm 9 \mu\text{m}$, and $18 \pm 6 \mu\text{m}$ on PET, PMEA, and PHEMA, respectively. The width of adherent cells increased by 1.5-, 2.7-, and 1.4-fold on PET, PMEA, and PHEMA, respectively, from 1 h up to 1 day. Figures 4(a)–4(d) show that PDL cells on PMEA were more spread than cells on any other polymer surface.

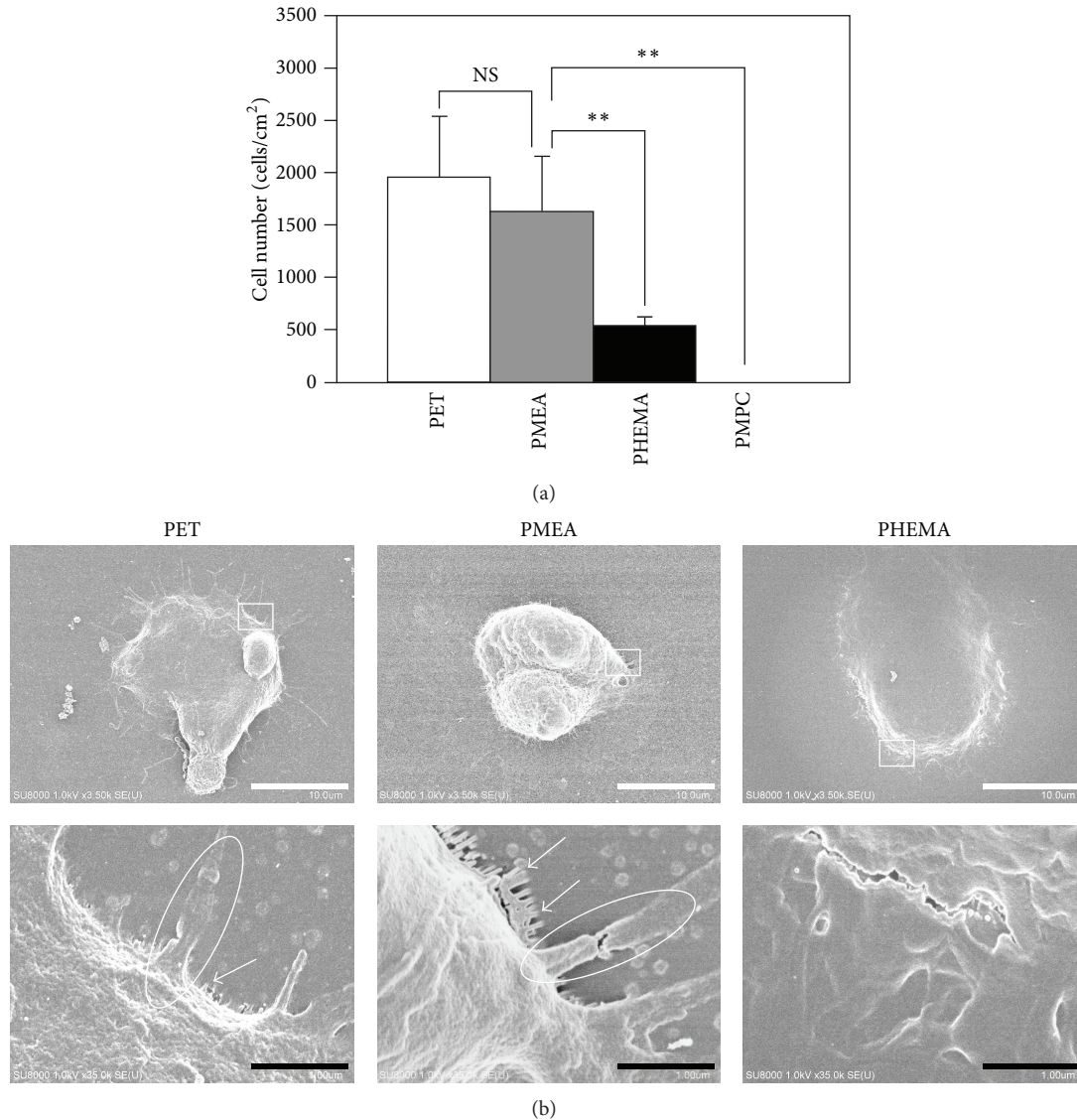


FIGURE 3: Initial adhesion of PDL cells on polymer surfaces after 1 h. (a) The number of adherent PDL cells on polymer surfaces. Polymers: PET, PMEA, PHEMA, and PMPC. $**P < 0.01$ versus PMEA, mean \pm standard deviation, $n = 3$. (b) SEM images of PDL cells on polymer surfaces. Top scale bars: 10 μm , bottom scale bars: 1.0 μm . Polymers: PET, PMEA, and PHEMA. White circles indicate pseudopodia formation. White arrows indicate spike formation.

3.5. Proliferation of PDL Cells. PDL cells adhered and proliferated on all polymer surfaces, except for PMPC, during the culture period (Figure 5). After 1 day and 3 days, the number of adherent PDL cells was almost identical on all of the polymer surfaces. After 7 days, the number of PDL cells on PMEA was almost the same as that on PET. The number of PDL cells on PHEMA was lower than that on PET and PMEA.

Figures 6(a)–6(c) show the percentage of Ki-67-positive cells during the culture period. Ki-67-positive cells (proliferating cells; Figures 6(d)–6(e)) were categorized into types I and II. Type I showed stronger staining, while type II showed weaker staining. Ki-67-negative cells (quiescent or resting cells) were categorized as type III (Figures 6(d)–6(e)). PDL cells did not show a statistically significant difference between 1 day (Figure 6(a)) and 7 days (Figure 6(c)). After

3 days, only type II adherent PDL cells on PMEA showed a statistically significant difference relative to cells on PHEMA (Figure 6(b)), which indicates that the number of proliferating PDL cells on PMEA was higher than that on PHEMA.

3.6. Localization of Vinculin in Two- and Three-Dimensional Observation. Figures 7(a)–7(c) show a top view and cross sections of adherent cells. We classified the localization of vinculin into 4 types: (i) focal adhesions (FAs) and (ii) nonfocal adhesions (non-FAs), where FAs were localized at basal cell surfaces, and non-FAs were localized at apical cell surfaces; (iii) vinculin rods that were composed of a complex of FAs and non-FAs and that were connected vertically and penetrated the cells; and (iv) vinculin fibers that were mainly oriented along the long axis of the cells.

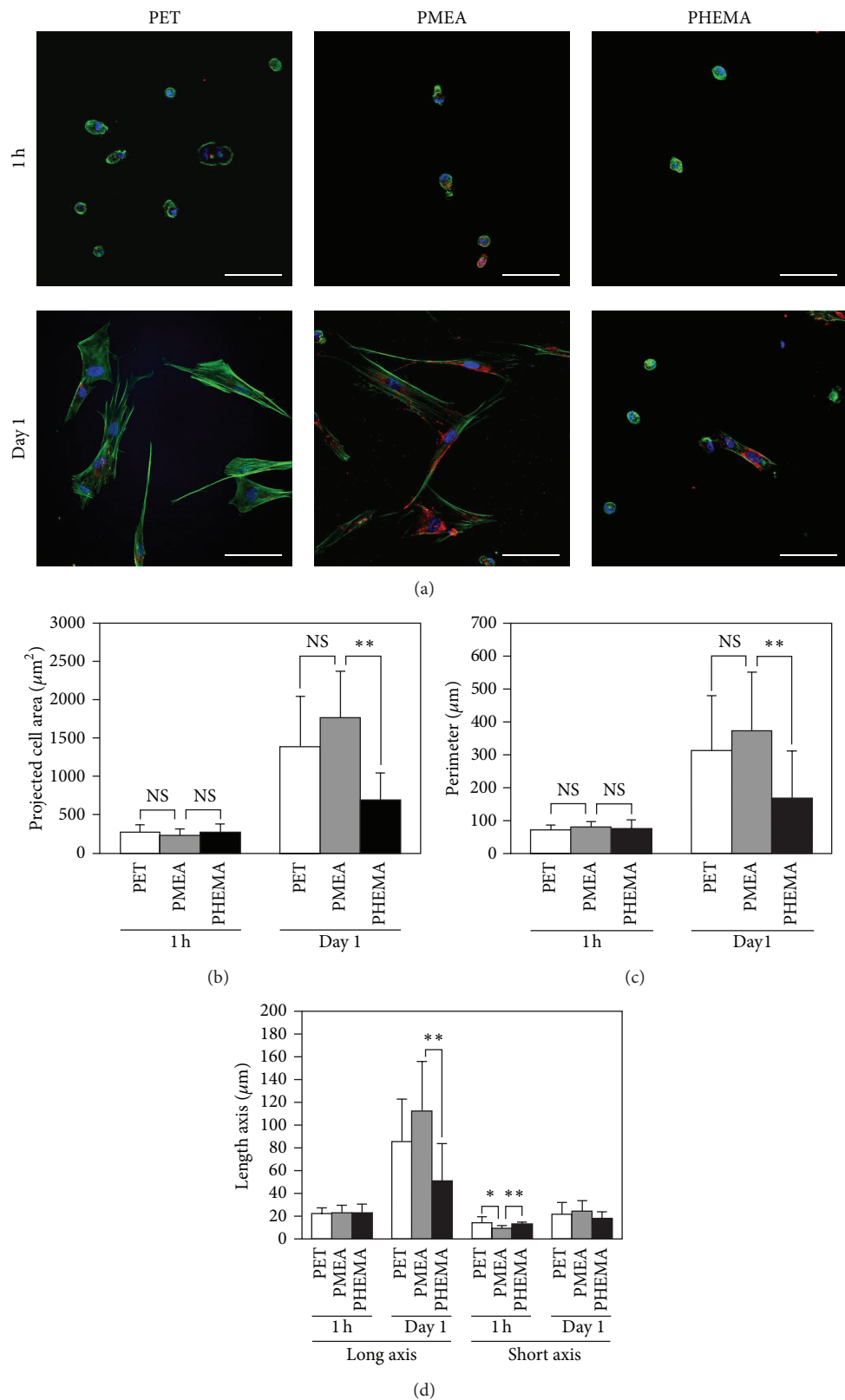


FIGURE 4: Quantification of adherent PDL cell morphologies for 1 h and 1 day. (a) CLSM images for the quantification of adherent PDL cell morphology on polymer surfaces. Scale bars: 100 μm . Blue: nucleus, green: actin, and red: vinculin. Polymers: PET, PMEA, and PHEMA. (b) Projected cell area. (c) Perimeter of adherent PDL cells. (d) Long and short axes of adherent PDL cells. Polymers: PET, PMEA, and PHEMA. $**P < 0.01$ and $*P < 0.05$ versus PMEA, mean \pm standard deviation, $n = 10$.

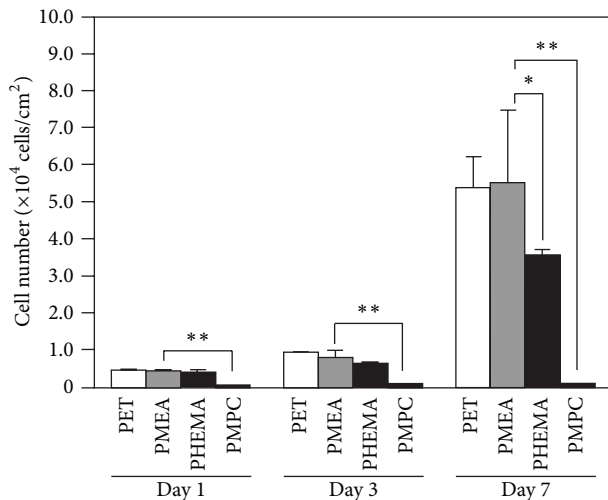


FIGURE 5: The number of PDL cells on polymer surfaces. Time points are 1 day, 3 days, and 7 days. Polymers: PET, PMEA, PHEMA, and PMPC. ** $P < 0.01$ and * $P < 0.05$ versus PMEA, mean \pm standard deviation, $n = 3$.

Figure 7(a) shows PDL cells cultured on PET. After 1 h, adherent PDL cells were shaped similarly to gourds (Figure 7(a)). The cells were spherical with a thickness of approximately $15\ \mu\text{m}$, and their actin and vinculin were undeveloped. After 4 h, the cells had spread to form disc-like shapes and FAs. Large spots of actin and vinculin were localized at the apical cell surfaces. The thickness of the adherent PDL cells was approximately $10\ \mu\text{m}$. Vinculin was mainly localized at basal cell surfaces in FAs and apical cell surfaces in non-FAs. After 1 day, the cells were spread out thinly. Large vinculin spots were localized at apical cell surfaces in non-FAs, and FAs were also observed in addition to vinculin rods. After 3 days, the cells were spread out more thinly. Many vinculin rods were observed. FAs, non-FAs, and vinculin fibers were also observed.

Figure 7(b) shows PDL cells cultured on PMEA. After 1 h, the adherent PDL cells were shaped similarly to gourds. The cells were spherical with a thickness of approximately $11\ \mu\text{m}$. Their actin and vinculin were undeveloped. After 4 h, PDL cells had spread to form disc-like shapes and FAs. Large actin spots and small vinculin spots were localized at the apical cell surfaces in non-FA. The thickness of the cells was approximately $10\ \mu\text{m}$. Vinculin was mainly localized at basal cell surfaces in FAs and apical cell surfaces in non-FAs. After 1 day, the cells were spread out and spindle shaped. Large vinculin spots were localized at apical cell surfaces in non-FAs, and FAs were also observed in addition to vinculin fibers. After 3 days, the cells were spread out more thinly. FAs and non-FAs were observed, and vinculin fibers were also observed.

Figure 7(c) shows PDL cells cultured on PHEMA. After 1 h, the adherent cells were spherical with a thickness of approximately $15\ \mu\text{m}$. Their actin and vinculin were undeveloped. After 4 h, the cells were slightly spread out, and they possessed FAs. After 1 day, the cells had a round shape relative

to the shape of cells on the other polymers (Figures 7(a) and 7(b)). Large vinculin spots were localized at apical cell surfaces in non-FAs. FAs and vinculin rods were also observed. After 3 days, the PDL cells had spread out. Vinculin rods were also observed. FAs and non-FAs were observed in addition to vinculin fibers. The vinculin fiber-formation process is summarized in Figure 7(d). PDL cells on PMEA contained few vinculin rods, whereas PDL cells on PET and PHEMA contained many vinculin rods.

3.6.1. Relationship between Cell Proliferation and Ki-67 Protein Production. As shown in Figures 2, 3(a)–3(b), 4(a)–4(d), and 5, PDL cells on PMEA showed similar adhesion and proliferation behavior to cells on PET at all-time points. The low proliferation on PHEMA was consistent with the results of Peluso et al., who found that human embryonic lung fibroblasts did not proliferate on PHEMA [33]. Based on this finding, we focused on differences in the cell cycle and quantified the percentage of Ki-67-positive cells on the polymers to identify differences in cell proliferation. As shown in Figure 6(b), the percentage of Ki-67-positive cells on PMEA at 3 days was higher than that on PHEMA. These data suggest that the higher proliferation of PDL cells on PMEA was related to the higher percentage of Ki-67-positive cells at 3 days (Figures 5 and 6(b)).

3.6.2. Relationship between Vinculin Localization and Cell Proliferation. Next, we analyzed the localization of vinculin in 2 and 3 dimensions to investigate the cause of difference in the proportion of Ki-67-positive cells and to analyze cell-material interactions. Our results suggest that PDL cells on PMEA have stronger PDL cell-material interactions than cells on PHEMA because cells on PMEA exhibited high vinculin localization and Ki-67 protein production. In our next study, we will attempt to elucidate the influence of the chemical structure of the synthetic polymer on cell behavior by altering the composition of the main chain and/or the terminal functional group of the side chain.

As shown in Figures 7(a)–7(d), we observed some unique vinculin localization in non-FAs, vinculin rods, and vinculin fibers. Kanchanawong et al. reported that focal adhesions link the extracellular matrix to the actin cytoskeleton, and vinculin localized in focal adhesions probably links integrin to actin directly, as the distribution of vinculin is consistent with its binding to sites along the talin rod domain and actin, which may serve to buttress the integrin-talin-actin linkage [29]. Therefore, vinculin localization was expected to occur at basal cell surfaces contacting the materials; however, we observed that vinculin localized in non-FAs at apical cell surfaces and in vinculin rods that were composed of a complex of FAs and non-FAs that were connected vertically and penetrated the cells (Figures 7(a)–7(d)). In addition, we observed that vinculin fibers appeared to be similar to the supermaturation of focal adhesions reported by Dugina et al., who showed that increased extracellular matrix A fibronectin expression induced by transforming growth factor β (TGF β) was accompanied by α -smooth muscle actin expression and focal adhesion supermaturation in fibroblasts [34]. The non-FAs probably link extracellular matrix proteins such as fibronectin

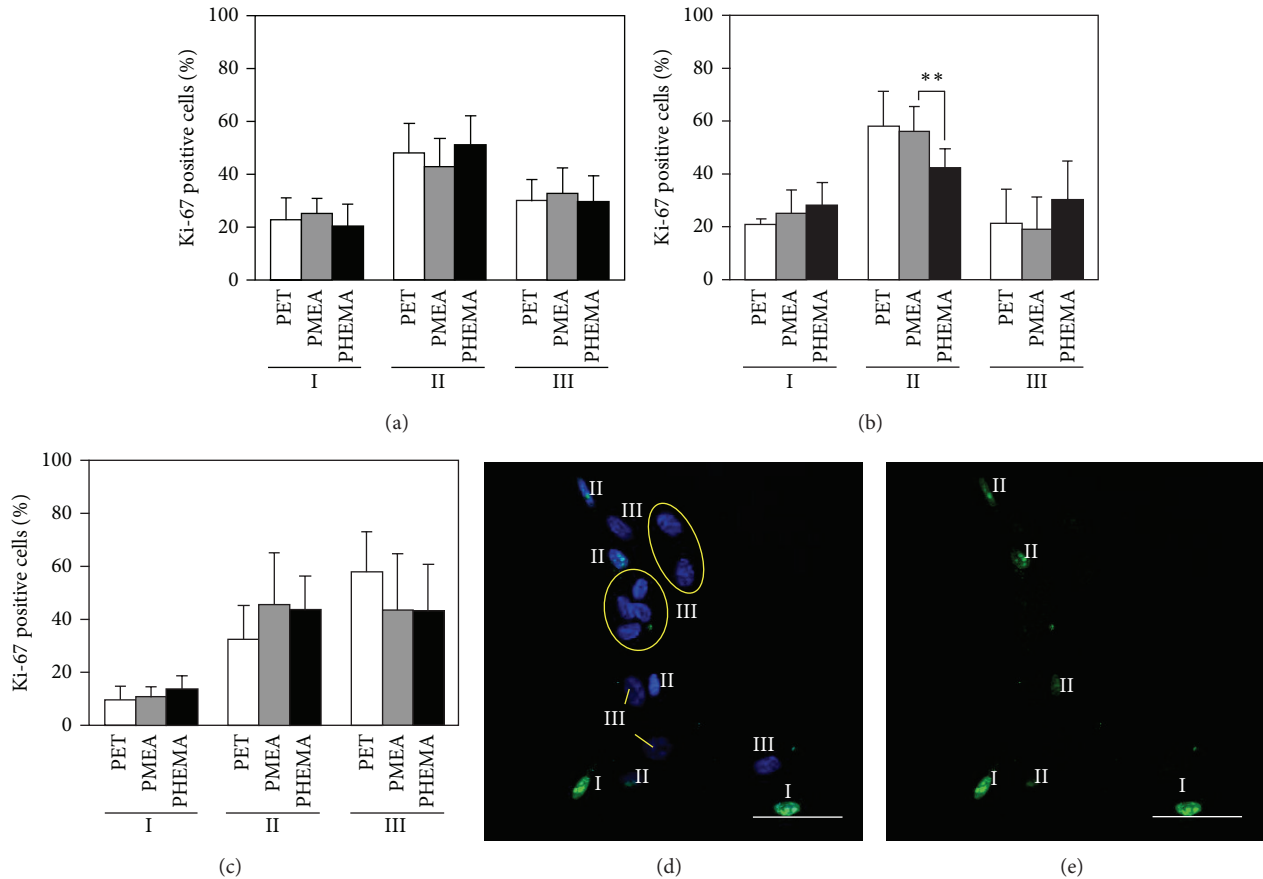


FIGURE 6: Percentage of Ki-67-positive cells on polymer surfaces: (a) 1 day, (b) 3 days, and (c) 7 days. Polymers: PET, PMEA, and PHEMA. ** $P < 0.01$ and * $P < 0.05$ versus PMEA, mean \pm standard deviation, $n = 9$. (d)-(e) Classification of Ki-67 staining. The images show Ki-67 staining of PDL cells on PHEMA after 3 days. Scale bars: 100 μ m. Blue: nucleus, green: Ki-67-positive cells. (d) CLSM images of PDL cells showing the nucleus and Ki-67 staining. (e) CLSM images of PDL cells showing Ki-67 staining. Types I and II: the Ki-67 antigen is present in the nucleus during the G1, S, and G2 phases of cell division and during mitosis. Type III: quiescent or resting cells in the G0 phase do not express the Ki-67 antigen.

with the apical cell surface. In future studies, we will evaluate the role of the unique vinculin localization in non-FAs, vinculin rods, and vinculin fibers with regard to cell behavior.

3.7. Comparison of Platelet and PDL Cell Adhesion on PMEA and PMPC. Figure 8(a) shows the adherent platelets on each polymer as determined by SEM. Figure 8(b) shows the number of adherent platelets and PDL cells on each polymer relative to that on PET. Platelet adhesion on PMEA and PMPC was low, and the number of platelets on PMEA was not significantly different from that on PMPC. Many adherent PDL cells were observed on PMEA and PET, whereas relatively few adherent PDL cells were observed on PHEMA and PMPC. PDL cells adhered to PMEA, whereas platelets hardly adhered to PMEA. In contrast, both platelets and PDL cells did not adhere to PMPC.

3.7.1. Relationship between Biocompatibility and Cell Adhesions. Conventional synthetic biocompatible polymers such as PMPC, poly(sulfobetaine methacrylate), poly(carboxybetaine methacrylate), and poly(ethylene glycol) (PEG) are known to demonstrate low protein adsorption and/or no

platelet adhesion [35–39]. PDL cells hardly adhered and proliferated on PMPC, which was consistent with the findings of a previous study by Iwasaki et al., who reported that adhesion of human promyelocytic leukemia cells and human uterine cervical cancer cells was completely suppressed on PMPC [36]. We previously reported that, we previously reported that PMEA has excellent biocompatibility with human blood cells [15]. As shown in Figures 8(a)–8(b), the number of platelets on PMEA was not significantly different from the number of platelets on PMPC. In contrast, PDL cells adhered to PMEA, and the number of PDL cells on PMEA was higher than that on PHEMA and PMPC (Figure 8(b)). These findings raise the question of why PDL cells adhere to biocompatible PMEA but platelets do not, especially when both platelets and PDL cells do not adhere to PMPC in a limited manner. Although we have no clear evidence to answer this question or to explain why PDL cells demonstrate higher growth rates on PMEA, we can offer the following speculations in terms of the 3 steps required for cell adhesion on polymer surfaces.

3.7.2. Relationship between Adsorbed Proteins and Cell Adhesion. Initially, when a polymer surface comes in contact with

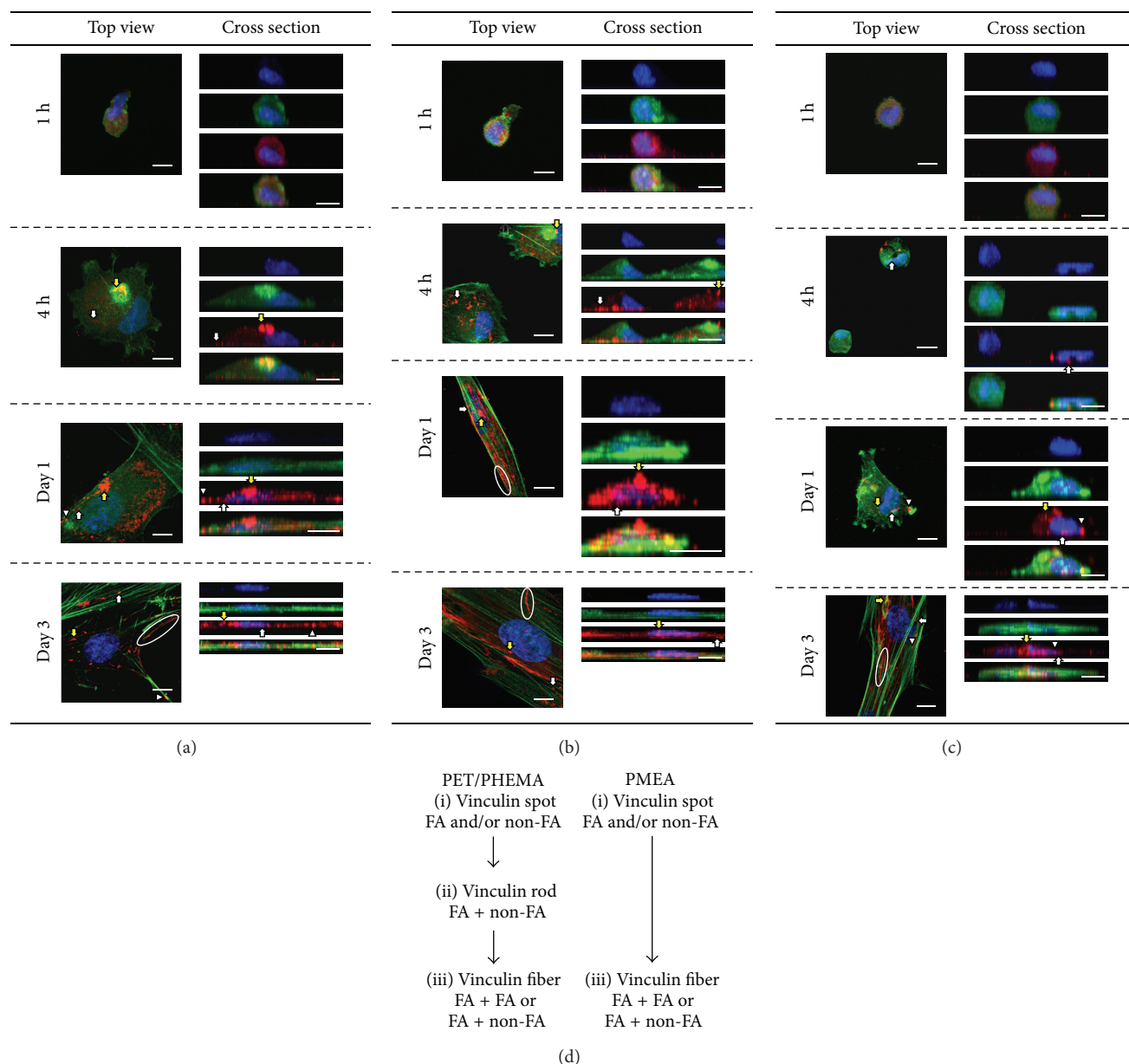


FIGURE 7: Localization of nucleus, actin, and vinculin in adherent PDL cells on polymer surfaces. Scale bars: 10 μm . In the cross-section images, the top panel shows the nucleus (blue), the second panel shows the nucleus and actin (green), the third panel shows the nucleus and vinculin (red), and the bottom panel shows a merged image. The time points are 1 h, 4 h, 1 day, and 3 days. (a) PDL cells on PET. (b) PDL cells on PMEA. (c) PDL cells on PHEMA. White arrows indicate focal adhesions that were localized at the basal cell surface. Yellow arrows indicate nonfocal adhesions (non-FA) localized at the apical cell surface. White arrowheads indicate vinculin rods that were connected vertically and penetrated the adherent cell. White circles indicate vinculin fibers that were mainly oriented along the long axis of the adherent cells. (d) Schematic representation of vinculin fiber formation.

cell culture medium, it absorbs water, and a specific water structure is formed on the polymer surface [21]. On PET or PHEMA, the absorbed water creates a nonfreezing water layer and a free water layer. We have also reported that PMEA and PMPC form another layer called the intermediate water layer [20, 23, 40].

Proteins in the cell culture medium then adsorb to the water layer. When proteins adsorb to the nonfreezing water layer on polymer surfaces such as PET and PHEMA, a strong

conformational change of the adsorbed proteins occurs, and many cell-binding sites are exposed. Intermediate water in PMEA does not induce a conformational change in the adsorbed proteins (bovine serum albumin and fibrinogen), and, thus, potential platelet-binding sites are minimally exposed [15, 20].

Finally, platelets and PDL cells adhere to the cell-binding sites of the adsorbed proteins. We recently found that adsorption-induced deformation of fibrinogen (platelet

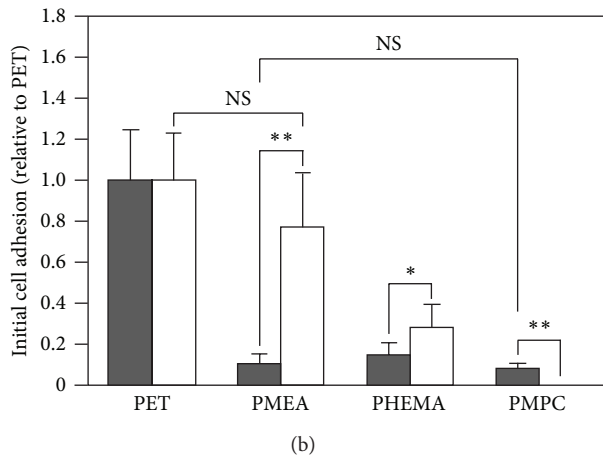
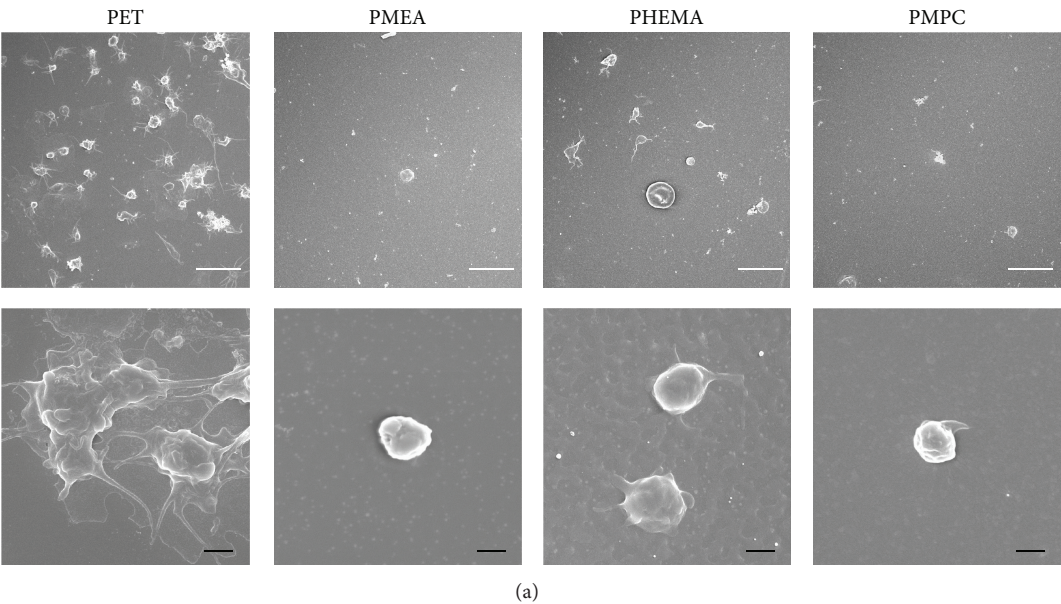


FIGURE 8: Comparison of platelet and PDL cell adhesion after 1 h. (a) SEM images of adherent platelets on polymer surfaces. Top scale bars: 10 μm , bottom scale bars: 1.0 μm . Polymers: PET, PMEA, PHEMA, and PMPC. (b) Comparison of platelet and PDL cell adhesion after 1 h. Gray bar indicates platelet adhesion and white bar indicates PDL cell adhesion, respectively, relative to PET. Polymers: PET, PMEA, PHEMA, and PMPC. ** $P < 0.01$ and * $P < 0.05$ versus PET, mean \pm standard deviation, platelets: $n = 6$, PDL cells: $n = 9$.

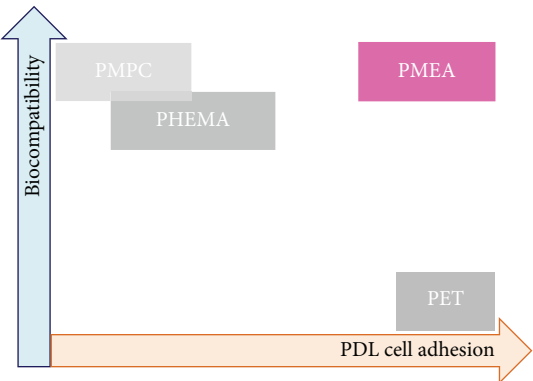


FIGURE 9: Relationship between PDL cell adhesion and biocompatibility on PET, PMEA, PHEMA, and PMPC.

adhesion ligand), which is required for the adhesion of platelets, does not occur on PMEA [41]. In contrast, fibronectin (PDL cell adhesion ligand) was deformed on PMEA [41]. Therefore, we concluded that PDL cells and not platelets are capable of adhering to PMEA based on this protein deformation difference between polymer films. We suppose that the existence of an intermediate water layer alters the amount of exposed cell-binding sites, which results in differing cell adhesion on each polymer.

3.7.3. Relationship between Biocompatibility and Intermediate Water. In addition, we have reported that hydrated PMPC and PEG, as well as various proteins and polysaccharides that are well-known biocompatible polymers, contain intermediate water [20, 23, 42, 43]. In contrast, poorly biocompatible

polymers do not contain intermediate water [31]. Free water has high mobility and is unable to shield the polymer surface or the nonfreezing water layer on the polymer surface [23]. Because intermediate water is weakly bound to the polymer molecules or to nonfreezing water, it forms a more stable structure than free water [23]. Based on these findings, we hypothesized that intermediate water, which prevents proteins and platelets from directly contacting the polymer surface or nonfreezing water on the polymer surface, plays an important role in biocompatibility and cell adhesion [23], and the amount of intermediate water affects protein adsorption and cell adhesion [20, 44, 45].

3.7.4. Relationship between Intermediate Water Content and Cell Adhesion. Intermediate water content in hydrated PMEA (4.5 wt%) [31] prevented platelet adhesion but did not prevent PDL cell adhesion. In contrast, higher intermediate water content in hydrated PMPC (28.5 wt%) [40] prevented the adhesion of both platelets and PDL cells. The value of the intermediate water content in hydrated PMPC reflects the value for the MPC homopolymer because Kitano et al. confirmed that the MPC-rich domain is directed toward the surface in water [32]. We assume that the higher intermediate water content in hydrated PMPC relative to PMEA prevented cell adhesion because the thick intermediate water layer may have shielded the polymer surface or nonfreezing water layer. In contrast, the thin intermediate water layer in hydrated PMEA likely prevented platelet adhesion but did not prevent PDL cell adhesion.

3.7.5. Relationship between Cell Properties and Cell Adhesion. We also consider the possibility that cell characteristics affected cell adhesion. Platelets are floating cells and mainly adhere to surfaces via glycoprotein IIb/IIIa [46]. PDL cells are anchorage-dependent and mainly adhere to surfaces via integrin $\alpha_5\beta_1$ [47]. Furthermore, differences of cell size and weight are present, as PDL cells are larger (10–15 μm) and heavier than platelets (2–4 μm); therefore, PDL cells may demonstrate increased adhesion simply because of their weight. In our next study, we will attempt to clarify the molecular mechanisms underlying cell adhesion on PMEA with regard to the intermediate water content and cell adhesion.

3.8. PMEA: Applications for Tissue Engineering Scaffolds in a Blood-Rich Environment. As shown in Figures 2, 3(a), 5, and 8(b), PDL cells adhered to and proliferated on PET, whereas PET was not biocompatible for human platelets. PDL cells on PHEMA proliferated but had aggregated (Figures 2 and 5), and PHEMA was thus also found to be nonbiocompatible for tissue engineering using PDL cells. As shown in Figures 2, 3(a), 5, and 8(b), PDL cells adhered and proliferated on biocompatible PMEA without platelet adhesion; however, PDL cells did not adhere and proliferate on biocompatible PMPC. PMEA and PMPC have been previously identified as blood-compatible (nonplatelet-adhesive) polymers. However, recent advances in medicine require the use of blood-compatible polymers that do not exhibit blood cell attachment to isolate stem cells from blood. Our results

challenge the widely accepted notion that biocompatible (blood-compatible) polymers (such as PMPC) do not permit cell adhesion as shown in Figure 9. We observed PDL cell adhesion on the biocompatible (blood-compatible) polymer PMEA in the absence of incorporated, substrate-bound, cell-adhesive ligands and antibodies. We therefore consider that PMEA could be used in smart biomaterials. Different cell types may thus be selected by PMEA based on differences in cell adhesion strength. It should be noted that PMEA has been approved by the FDA and can be used in a blood-rich environment. Therefore, biocompatible PMEA may provide an excellent scaffold for tissue engineering using PDL cells in humans as well as for culturing tissue-derived cells in a blood-rich environment.

4. Conclusion

We found that PDL cells, but not platelets, adhered to biocompatible PMEA. We also observed unique vinculin localization in non-FAs, vinculin rods, and vinculin fibers. In addition, PDL cells on PMEA proliferated better than those on PHEMA. Therefore, PMEA may provide an excellent scaffold material for tissue engineering using PDL cells in humans and also for culturing tissue-derived cells in a blood-rich environment.

Conflict of Interests

The authors declare that there is no conflict of interests regarding the publication of this paper.

Acknowledgments

The authors thank Ayano Sasaki for introduction to AFM measurements. This work is supported by Grants-in-Aid and Special Coordination Funds for Promoting Science and Technology of the Ministry of Education, Culture, Sports, Science and Technology of Japan. This work is also part of the financial support from Funding Program for Next Generation World-Leading Researchers (NEXT Program, Japan). Erika Kitakami is also supported in part by a Grant-in-Aid for Japan Society of the Promotion of Science (JSPS) Fellows, Grant no. 248746, Japan.

References

- [1] B. L. Pihlstrom, B. S. Michalowicz, and N. W. Johnson, "Periodontal diseases," *The Lancet*, vol. 366, no. 9499, pp. 1809–1820, 2005.
- [2] H. Choi, W. Noh, J. Park, J. Lee, and J. Suh, "Analysis of gene expression during mineralization of cultured human periodontal ligament cells," *Journal of Periodontal and Implant Science*, vol. 41, no. 1, pp. 30–43, 2011.
- [3] B. M. Seo, M. Miura, S. Gronthos et al., "Investigation of multipotent postnatal stem cells from human periodontal ligament," *The Lancet*, vol. 364, no. 9429, pp. 149–155, 2004.
- [4] I. C. Gay, S. Chen, and M. MacDougall, "Isolation and characterization of multipotent human periodontal ligament stem

- cells," *Orthodontics & Craniofacial Research*, vol. 10, no. 3, pp. 149–160, 2007.
- [5] N. Wada, D. Menicanin, S. Shi, P. M. Bartold, and S. Gronthos, "Immunomodulatory properties of human periodontal ligament stem cells," *Journal of Cellular Physiology*, vol. 219, no. 3, pp. 667–676, 2009.
 - [6] F. Feng, K. Akiyama, Y. Liu et al., "Utility of PDL progenitors for in vivo tissue regeneration: a report of 3 cases," *Oral Diseases*, vol. 16, no. 1, pp. 20–28, 2010.
 - [7] Y. Nomura, M. Ishikawa, Y. Yashiro et al., "Human periodontal ligament fibroblasts are the optimal cell source for induced pluripotent stem cells," *Histochemistry and Cell Biology*, vol. 137, no. 6, pp. 719–732, 2012.
 - [8] L. Petrovic, A. K. Schlegel, S. Schultze-Mosgau, and J. Wiltfang, "Different substitute biomaterials as potential scaffolds in tissue engineering," *International Journal of Oral and Maxillofacial Implants*, vol. 21, no. 2, pp. 225–231, 2006.
 - [9] R. Schmelzeisen, R. Shimming, and M. Sitter, "Making bone: implant insertion into tissue-engineered bone for maxillary sinus floor augmentation—a preliminary report," *Journal of Cranio-Maxillofacial Surgery*, vol. 31, no. 1, pp. 34–39, 2003.
 - [10] J. P. Davidas, "Looking for a new international standard for characterization, classification and identification of surfaces in implantable materials: the long march for the evaluation of dental implant surfaces has just begun," *Poseido*, vol. 2, no. 1, pp. 1–5, 2014.
 - [11] D. M. Dohan Ehrenfest, B. S. Kang, G. Sammartino et al., "Guidelines for the publication of articles related to implant surfaces and design from the POSEIDO: a standard for surface characterization," *Poseido*, vol. 1, no. 1, pp. 7–15, 2013.
 - [12] N. Metoki, L. Liu, E. Beilis, N. Eliaz, and D. Mandler, "Preparation and characterization of alkylphosphonic acid self-assembled monolayers on titanium alloy by chemisorptions and electrochemical deposition," *Langmuir*, vol. 30, no. 23, pp. 6791–6799, 2014.
 - [13] R. França, T. D. Samani, G. Bayade, L. Yahia, and E. Sacher, "Nanoscale surface characterization of biphasic calcium phosphate, with comparisons to calcium hydroxyapatite and β -tricalcium phosphate bioceramics," *Journal of Colloid and Interface Science*, vol. 420, pp. 182–188, 2014.
 - [14] M. Catauro, F. Bollino, and F. Papale, "Preparation, characterization, and biological properties of organic-inorganic nanocomposite coatings on titanium substrates prepared by sol-gel," *Journal of Biomedical Materials Research A*, vol. 102, no. 2, pp. 392–399, 2014.
 - [15] M. Tanaka, T. Motomura, M. Kawada et al., "Blood compatible aspects of poly(2-methoxyethylacrylate) (PMEA)-relationship between protein adsorption and platelet adhesion on PMEA surface," *Biomaterials*, vol. 21, no. 14, pp. 1471–1481, 2000.
 - [16] X. M. Mueller, D. Jegger, M. Augstburger, J. Horisberger, and L. K. von Segesser, "Poly(2-methoxyethylacrylate) (PMEA) coated oxygenator: An ex vivo study," *The International Journal of Artificial Organs*, vol. 25, no. 3, pp. 223–229, 2002.
 - [17] B. L. Greenfield, K. R. Brinkman, K. L. Koziol et al., "The effect of surface modification and aprotinin on cellular injury during simulated cardiopulmonary bypass," *The Journal of Extra-Corporeal Technology*, vol. 34, no. 4, pp. 267–270, 2002.
 - [18] F. D. Rubens, "Cardiopulmonary bypass technology transfer: musings of a cardiac surgeon," *Journal of Biomaterials Science, Polymer Edition*, vol. 13, no. 4, pp. 485–499, 2002.
 - [19] H. Suhara, Y. Sawa, M. Nishimura et al., "Efficacy of a new coating material, PMEA, for cardiopulmonary bypass circuits in a porcine model," *Annals of Thoracic Surgery*, vol. 71, no. 5, pp. 1603–1608, 2001.
 - [20] M. Tanaka, T. Hayashi, and S. Morita, "The roles of water molecules at the biointerface of medical polymers," *Polymer Journal*, vol. 45, no. 7, pp. 701–710, 2013.
 - [21] M. Tanaka, A. Mochizuki, T. Motomura, K. Shimura, M. Onishi, and Y. Okahata, "In situ studies on protein adsorption onto a poly(2-methoxyethylacrylate) surface by a quartz crystal microbalance," *Colloids and Surfaces A: Physicochemical and Engineering Aspects*, vol. 193, no. 1–3, pp. 145–152, 2001.
 - [22] M. Tanaka, A. Mochizuki, T. Shiroya et al., "Study on kinetics of early stage protein adsorption on poly(2-methoxyethylacrylate) (PMEA) surface," *Colloids and Surfaces A: Physicochemical and Engineering Aspects*, vol. 203, no. 1–3, pp. 195–204, 2002.
 - [23] M. Tanaka, "Design of novel 2D and 3D biointerfaces using self-organization to control cell behavior," *Biochimica et Biophysica Acta*, vol. 1810, no. 3, pp. 251–258, 2011.
 - [24] M. J. Dalby, N. Gadegaard, R. Tare et al., "The control of human mesenchymal cell differentiation using nanoscale symmetry and disorder," *Nature Materials*, vol. 6, no. 12, pp. 997–1003, 2007.
 - [25] M. Tanaka, K. Nishikawa, H. Okubo et al., "Control of hepatocyte adhesion and function on self-organized honeycomb-patterned polymer film," *Colloids and Surfaces A: Physicochemical and Engineering Aspects*, vol. 284–285, pp. 464–469, 2006.
 - [26] A. Saminathan, K. J. Vinodh, H. H. Low, T. Cao, and M. C. Meikle, "Engineering three-dimensional constructs of the periodontal ligament in hyaluronan-gelatin hydrogel films and a mechanically active environment," *Journal of Periodontal Research*, vol. 48, no. 6, pp. 790–801, 2013.
 - [27] M. Nune, P. Kumaraswamy, U. M. Krishnan, and S. Sethuraman, "Self-assembling peptide nanofibrous scaffolds for tissue engineering: novel approaches and strategies for effective functional regeneration," *Current Protein and Peptide Science*, vol. 14, no. 1, pp. 70–84, 2013.
 - [28] B. Geiger, A. Bershadsky, R. Pankov, and K. M. Yamada, "Transmembrane extracellular matrix-cytoskeleton crosstalk," *Nature Reviews Molecular Cell Biology*, vol. 2, no. 11, pp. 793–805, 2001.
 - [29] P. Kanchanawong, G. Shtengel, A. M. Pasapera et al., "Nanoscale architecture of integrin-based cell adhesions," *Nature*, vol. 468, no. 7323, pp. 580–584, 2010.
 - [30] H. Ishihata, M. Tanaka, N. Iwama et al., "Proliferation of periodontal ligament cells on biodegradable honeycomb film scaffold with unified micropore organization," *Journal of Biomechanical Science and Engineering*, vol. 5, no. 3, pp. 252–261, 2010.
 - [31] M. Tanaka and A. Mochizuki, "Effect of water structure on blood compatibility-thermal analysis of water in poly(meth)acrylate," *Journal of Biomedical Materials Research A*, vol. 68, no. 4, pp. 684–695, 2004.
 - [32] H. Kitano, M. Imai, T. Mori, M. Gemmei-Ide, Y. Yokoyama, and K. Ishihara, "Structure of water in the vicinity of phospholipid analogue copolymers as studied by vibrational spectroscopy," *Langmuir*, vol. 19, no. 24, pp. 10260–10266, 2003.
 - [33] G. Peluso, O. Petillo, J. M. Anderson et al., "The differential effects of poly(2-hydroxyethyl methacrylate) and poly(2-hydroxyethyl methacrylate)/poly(caprolactone) polymers on cell proliferation and collagen synthesis by human lung fibroblasts," *Journal of Biomedical Materials Research*, vol. 34, no. 3, pp. 327–336, 1997.

- [34] V. Dugina, L. Fontao, C. Chaponnier, J. Vasiliev, and G. Gabbiani, "Focal adhesion features during myofibroblastic differentiation are controlled by intracellular and extracellular factors," *Journal of Cell Science*, vol. 114, no. 18, pp. 3285–3296, 2001.
- [35] K. Ishihara, H. Nomura, T. Mihara, K. Kurita, Y. Iwasaki, and N. Nakabayashi, "Why do phospholipid polymers reduce protein adsorption?" *Journal of Biomedical Materials*, vol. 39, no. 2, pp. 323–330, 1998.
- [36] Y. Iwasaki, E. Tabata, K. Kurita, and K. Akiyoshi, "Selective cell attachment to a biomimetic polymer surface through the recognition of cell-surface tags," *Bioconjugate Chemistry*, vol. 16, no. 3, pp. 567–575, 2005.
- [37] F. Zhang, G. Li, P. Yang, W. Qin, C. Li, and N. Huang, "Fabrication of biomolecule-PEG micropattern on titanium surface and its effects on platelet adhesion," *Colloids and Surfaces B: Biointerfaces*, vol. 102, pp. 457–465, 2013.
- [38] Y. Inoue and K. Ishihara, "Reduction of protein adsorption on well-characterized polymer brush layers with varying chemical structures," *Colloids and Surfaces B: Biointerfaces*, vol. 81, no. 1, pp. 350–357, 2010.
- [39] T. Kondo, K. Nomura, M. Gemmei-Ide et al., "Structure of water at zwitterionic copolymer film-liquid water interfaces as examined by the sum frequency generation method," *Colloids and Surfaces B: Biointerfaces*, vol. 113, pp. 361–367, 2014.
- [40] T. Hatakeyama, M. Tanaka, and H. Hatakeyama, "Studies on bound water restrained by poly(2-methacryloyloxyethyl phosphorylcholine): comparison with polysaccharide-water systems," *Acta Biomaterialia*, vol. 6, no. 6, pp. 2077–2082, 2010.
- [41] T. Hoshiba, M. Nikaido, and M. Tanaka, "Characterization of the attachment mechanisms of tissue-derived cell lines to blood-compatible polymers," *Advanced Healthcare Materials*, vol. 3, no. 5, pp. 775–784, 2014.
- [42] T. Hatakeyama, H. Kasuga, M. Tanaka, and H. Hatakeyama, "Cold crystallization of poly(ethylene glycol)-water systems," *Thermochimica Acta*, vol. 465, no. 1-2, pp. 59–66, 2007.
- [43] M. Tanaka and A. Mochizuki, "Clarification of blood compatibility mechanism by controlling water structure," *Journal of Biomaterials Science Polymer Edition*, vol. 21, no. 14, pp. 1849–1863, 2010.
- [44] M. Tanaka, E. Kitakami, S. Yagi et al., "Biocompatible polymers with intermediate water," Patent 256467, Japan, 2010.
- [45] T. Hayashi, Y. Tanaka, Y. Koide, M. Tanaka, and M. Hara, "Mechanism underlying bioinertness of self-assembled monolayers of oligo(ethyleneglycol)-terminated alkanethiols on gold: protein adsorption, platelet adhesion, and surface forces," *Physical Chemistry Chemical Physics*, vol. 14, no. 29, pp. 10196–10206, 2012.
- [46] S. J. Shattil, H. Kashiwagi, and N. Pampori, "Integrin signaling: the platelet paradigm," *Blood*, vol. 91, no. 8, pp. 2645–2657, 1998.
- [47] S. Ivanovski, M. Komaki, P. M. Bartold, and A. S. Narayanan, "Periodontal-derived cells attach to cementum attachment protein via $\alpha 5 \beta 1$ integrin," *Journal of Periodontal Research*, vol. 34, no. 3, pp. 154–159, 1999.

Research Article

Physicochemical Characteristics of Bone Substitutes Used in Oral Surgery in Comparison to Autogenous Bone

**Antoine Berberi,¹ Antoine Samarani,² Nabih Nader,¹ Ziad Noujeim,¹
Maroun Dagher,³ Wasfi Kanj,¹ Rita Mearawi,¹ Ziad Saleme,¹ and Bassam Badran²**

¹ School of Dentistry, Lebanese University, P.O. Box 4, Hadath, Lebanon

² Ecole Doctorale, PRASE, Lebanese University, P.O. Box 4, Hadath, Lebanon

³ Faculty of Dental Medicine, Saint Joseph University, P.O. Box 17-5208, Beirut, Lebanon

Correspondence should be addressed to Antoine Berberi; anberberi@gmail.com

Received 11 May 2014; Accepted 8 June 2014; Published 8 July 2014

Academic Editor: David M. Dohan Ehrenfest

Copyright © 2014 Antoine Berberi et al. This is an open access article distributed under the Creative Commons Attribution License, which permits unrestricted use, distribution, and reproduction in any medium, provided the original work is properly cited.

Bone substitutes used in oral surgery include allografts, xenografts, and synthetic materials that are frequently used to compensate bone loss or to reinforce repaired bone, but little is currently known about their physicochemical characteristics. The aim of this study was to evaluate a number of physical and chemical properties in a variety of granulated mineral-based biomaterials used in dentistry and to compare them with those of autogenous bone. Autogenous bone and eight commercial biomaterials of human, bovine, and synthetic origins were studied by high-resolution X-ray diffraction, atomic absorption spectrometry, and laser diffraction to determine their chemical composition, calcium release concentration, crystallinity, and granulation size. The highest calcium release concentration was 24.94 mg/g for Puros and the lowest one was 2.83 mg/g for Ingenios β -TCP compared to 20.15 mg/g for natural bone. The range of particles sizes, in terms of median size D50, varied between 1.32 μ m for BioOss and 902.41 μ m for OsteoSponge, compared to 282.1 μ m for natural bone. All samples displayed a similar hexagonal shape as bone, except Ingenios β -TCP, Macrobone, and OsteoSponge, which showed rhomboid and triclinic shapes, respectively. Commercial bone substitutes significantly differ in terms of calcium concentration, particle size, and crystallinity, which may affect their *in vivo* performance.

1. Introduction

Bone is a living tissue that serves for structural support and calcium metabolism. Bone matrix is organic and consists of a network of collagen protein fibers impregnated with mineral salts (85% of calcium phosphate, 10% of calcium carbonate, and 5% of calcium fluoride and magnesium fluoride). The mineral compartment of bone is predominantly present in the form of calcium hydroxyapatites ($\text{Ca}_{10}[\text{PO}_4]_6[\text{OH}]_2$). Bone tissue also contains negligible quantities of noncollagen proteins, including the family of bone morphogenetic proteins (BMPs) [1].

Calcium (Ca) plays an important role in osteoconductivity and may enhance bone tissue integration by entrapping and concentrating circulating bone growth factors (BMPs) and osteoprogenitor cells, thus imparting osteoinductive properties to calcium-based bone graft materials [2, 3].

Autogenous bone is osteogenic (cells within a donor graft synthesize new bone at implantation sites), osteoinductive (new bone is formed by active recruitment of host mesenchymal stem cells from surrounding tissue, which differentiate into bone-forming osteoblasts), osteoconductive (vascularization and new bone formation into the transplant), and highly biocompatible [3, 4]. These characteristics should be present in an ideal substitute and all bone grafting materials can be classified according to these characteristics [5].

Bone substitutes (BS) are frequently used in oral and maxillofacial surgery, periodontics, and orthopedics. They include inorganic or organic, natural or synthetic materials to compensate for bone loss or to reinforce new bone ingrowth into defect sites [6–17]. This second option is, in fact, the role played by calcium phosphate and constitutes materials that show the closest similarity to the mineral component of bone

[14]. The greatest success in bone grafting has been achieved with autogenous bone (gold standard), which fulfills all essential physicochemical and biological properties needed in a bone graft material, despite its inherent limitations in availability and postoperative pain at donor sites [6, 8, 10, 11, 13, 18–20].

Numerous BS biomaterials have been successfully used, such as allografts (human), xenografts (porcine, equine, or bovine, and synthetic calcium-based materials (calcium phosphates [β -tricalcium phosphate/ β -TCP, hydroxyapatite/HA], bioactive glasses), calcium sulfate, calcium hydroxide), and a combination of these with or without the use of membrane and screws [6–23].

Allografts do not have the drawbacks of autografts but are less successful in clinical practice. They also display several other disadvantages: risk of disease transmission or infection, difficulties in obtaining and processing, possible rapid resorption, [8–10, 24], and partial loss of mechanical strength after sterilization [25, 26]. Xenogenic bone substitutes of porcine, bovine, or, more recently, equine origin are used because of their chemical and structural composition similarity when compared to human bone [27]. They represent an unlimited supply of available material and may reduce morbidity by eliminating the donor site [5, 10, 22, 23]. Heat or other treatments are used to deproteinate bone particles and eliminate immunogenicity risks [25, 28]. Synthetic calcium phosphate ceramics with their excellent biocompatibility are common alternatives to autogenous bone [15].

Ideally, a BS should have specific biological and clinical particularities. Biologically, it should mediate recruitment of mesenchymal cells derived from host site and have bioactive effects on ossification (osteinduction). Furthermore, it must be osteoconductive, providing three-dimensional scaffolds for the ingrowth of vessels and osteoprogenitor cells. Finally, it should be resorbable. Clinically, a BS should be easy to use, cost effective, and with adequate density to allow easy radiographic recognition during the entire healing process [27, 29]. This feature is particularly important to radiographically follow the rate of resorption/substitution [30, 31].

Regarding material structure, particle size affects not only contact area but also the packing characteristics of the materials, which ultimately determines the macroporosity of a particulate graft [32, 33]. It is also known that pore size exerts a major influence over the interaction of osteogenic cells with the biomaterial surface [34, 35]. Biological integration requires pores that are greater than 100–150 μ m in diameter to provide a blood supply to the tissues [27]. A BS should gradually degrade with time until it is completely replaced with vital new bone tissue. Moreover, a material's resorption rate should match the formation rate of the new bone tissue [29]. Biomaterial degradation that occurs too rapidly can exert a negative effect on bone regeneration processes, [24] and the presence of residual BS graft particles after bone healing may lead to composite tissue repair rather than to bone tissue regeneration [27].

The aim of this study was to evaluate some of physical and chemical properties in a variety of commercially available granulated mineral-based biomaterials that are frequently

used for dental applications as bone substitutes and to compare them with autogenous bone.

2. Materials and Methods

This study evaluated the physicochemical characteristics of the eight commercially available bone substitutes of human, bovine, and synthetic origins. Each material was used in its lowest available particle size range, and all samples were obtained directly from their manufacturers in sealed vials and evaluated without alteration.

- (i) DynaBlast (Keystone Dental, Inc., Burlington, MA) is a combination of mineralized and demineralized allogenic bone that is mixed with a proprietary poloxamer reverse-phase resorbable medium and processed into a paste or puttylike form [28, 36].
- (ii) Puros bone allograft (Zimmer Dental, Inc., Carlsbad, CA) is an allogenic graft material treated by a proprietary process (Tutoplast, RTI Biologics, Inc., Alachua, FL) designed to inactivate pathogens and remove fat, cells, and antigens, while preserving the minerals and collagen matrix of the native bone tissue. After processing, the material is preserved by solvent dehydration, which can also help to ensure pathogen inactivation [13]. It is available in cortical, cancellous, and a cortical-cancellous mix in particle sizes ranging from 0.25 to 2 mm [26, 37].
- (iii) OsteoSponge allograft (Bacterin International, Inc., Belgrade, MT) consists of 100% of demineralized human cancellous bone, with no additional carrier materials. It is prepared using undisclosed methods that reportedly preserve native growth factors [25]. The granule size varies from 1 to 4 mm.
- (iv) BioOss (Geistlich Pharma AG, Wolhusen, Switzerland) xenogenic spongiosa granules are reported to be a natural bone mineral derived from bovine bone which contain carbonate apatite. Granules are rendered nonorganic through a proprietary extraction process that involves treatment with strong alkalis and organic solvents under high-temperature processing up to 300°C, which allegedly renders the substrate antigenic and protein-free [37]. The material was used in granules of 0.25–1 mm.
- (v) Cerabone (AAP Biomaterials GmbH, Berlin, Germany) xenogenic granulate is a bovine bone material sintered at high temperature (>1200°C), which retains the inorganic part of bone (hydroxyapatite) [38]. The material used was granulate of 0.5–1.0 mm in size.
- (vi) Macrobone (Euroteknika Groupe, Sallanches, France) is a high-porosity (90%), synthetic bone substitute made of pure β -TCP that is completely and rapidly resorbable [39]. Particle size varies between 0.15 mm and 2 mm.
- (vii) IngeniOs β -TCP (Zimmer Dental, Inc.) is a bioactive material made of silicated β -TCP of non-biologic origin. The structure is a porous biocompatible synthetic

scaffold of ceramic material [40]. The size of the particles is 0.25–1 mm.

- (viii) IngeniOs HA (Zimmer Dental Inc.) is a synthetic spongy bone substitute. The structure is a porous scaffold that resembles cancellous bone. Particles are biocompatible and made of 100% hydroxyapatite ceramic with a putty phase of $\geq 95\%$, and granules range 1–2 mm in size [41].
- (ix) Autogenous bone samples were collected during mandibular third-molar surgery, rinsed with ethanol, dried in vacuum at room temperature, ground in an agate mortar, and sterilized by gamma irradiation [42, 43].

Atomic Absorption Spectroscopy (AAS) (WFX-210, Ray-Leigh, BRAIC, China) was used to determine the concentration of calcium ions in the bone substitutes by quantifying the release of calcium and phosphorous from the graft material in demineralized water. For this aim, standards for calcium and phosphorous within the range between 0.5 and 10 $\mu\text{g/L}$ were prepared, and 0.4 mg of each biomaterial (all nine samples) was immersed in 100 mL of 0.9% NaCl and the pH was adjusted at 7 by using hydrochloric acid (0.1N). The variation of Ca concentration was determined at D_0 (day 0), D_2 (day two), and each week after, until the sixth week. The concentration was calculated based on the Beer-Lambert law [44].

LASER Diffraction (LD) was used to determine particle size by evaluating the distribution of the granules using a laser scattering particle size analyzer (Patric LA-950 V2 Horiba Instruments, Japan). The measurement method relied on the Mie scattering theory [45]. Using an ultrasonic probe with measuring time of 20 s at a frequency of 20 kHz, the unit's measuring range varied between 0.01 and 3.00 μm . The device was equipped with an optical system of two light sources, a laser diode of approximately 1.6 mW with $\lambda = 650 \text{ nm}$, and a 405 nm light emitting diode of approximately 0.3 mW. Large particles scatter light at small angles relative to the laser beam and small particles scatter light at large angles. The particle size is reported as a volume equivalent sphere diameter [43, 46]. Samples were well mixed and homogenized in their powder state prior to their analysis. Average particle size and distribution were calculated for all nine biomaterials and autogenous bone.

X-ray Diffraction (XRD) (D8 Advance, Bruker Corporation, Billerica, MA) was used to identify phase and composition features and qualitatively evaluate the crystallinity of all study materials. Homogenized powder samples (1–2 g) were compressed in polyvinyl chloride lenses (diameter 2.5 cm, thickness 2 mm) and measured using a diffract meter (copper anticathode $\lambda K\alpha = 0.154060 \text{ nm}$). A range of 2θ between x° and y° was chosen to obtain maximum information about crystal phases. Collected diffractograms were analyzed by software EVA (EVA, Bruker Corporation) based on powder diffraction files provided by the International Center for Diffraction Data (Newtown Square, PA). Crystallite size analysis was calculated using the peak broadening of XRD reflection that is used to estimate the crystallite size in an

orthogonal direction to the crystal plane according to the following formula:

$$X_s = \frac{0.9\lambda}{(\text{FWHM} \times \cos \theta)}, \quad (1)$$

where X_s is the crystallite size in nanometer, λ is the wavelength of X-ray beam in nanometer ($\lambda = 0.15406 \text{ nm}$ in our case), and FWHM is the full width at half maximum for the diffraction angle at $2\theta = 25.9^\circ$ that was selected according to (002) Miller's plane family [47].

3. Results

AAS results of calcium concentration over the observation period are summarized in Table 1. Cerabone showed less calcium release than BioOss. In the synthetic xenograft category, Macrobone displayed a high calcium release concentration (17.30 mg/g), compared to IngeniOs HA (2.92 mg/g) and IngeniOs β -TCP (2.83 mg/g). In the allograft group, OsteoSponge revealed the lowest calcium release concentration (4.05 mg/g). The calcium concentration of Puros (24.94 mg/g) was comparable to autogenous bone (20.15 mg/g).

The particles median size D_{50} (in volume percentages), the particle size range expressed by the 10% and 90% percentiles (D_{10} and D_{90}), and the particles size ranges reported by the manufacturers as determined by the LD measurements are all presented in Table 2.

Results showed that BioOss had the lowest median particle size (1.32 μm) followed by IngeniOs β -TCP (6.72 μm), while OsteoSponge had the highest one (902.41 μm).

The median size of Macrobone (262.37 μm) was close to autogenous bone (282.1 μm). The narrowest size distribution was observed with BioOss (0.26–8.92 μm), followed by IngeniOs β -TCP (3.90–15.18 μm). The widest size distribution was observed with OsteoSponge (174.62–2301.84 μm) followed by DynaBlast (39.24–1754.62 μm).

X-ray diffractograms for all bone substitutes are shown in Figure 1. They represent the intensity of X-ray (cps) as a function of the diffraction angles (2θ , θ).

Results of the XRD experiments that are indicative for the chemical composition of the BS are shown in Table 3 except for DynaBlast, as the puttylike material was not granular in form. All study materials showed small amounts of impurities. These materials diffract more and less the X-ray, which means diverse degrees of crystallinity, as indicated in the different peaks widths.

The common crystal phase was calcium phosphate silicate hydroxide ($\text{Ca}_5(\text{PO}_4)_{2.85}(\text{SiO}_4)_{0.15}(\text{OH})$) in BioOss, IngeniOs HA, Puros, OsteoSponge, and autogenous bone. Macrobone was composed from calcium phosphate ($\text{Ca}_3(\text{PO}_4)_2$). Cerabone and IngeniOs β -TCP were composed, respectively, of calcium gadolinium oxide phosphate ($\text{Ca}_8\text{Gd}_2(\text{PO}_4)_6\text{O}_2$) and sodium calcium iron phosphate ($\text{Na}_2\text{Ca}_{19}\text{Fe}_{0.667}(\text{PO}_4)_{14}$) as the main crystal phases. Except for IngeniOs β -TCP, Macrobone, and Osteosponge, all samples were crystallized at different levels of crystallinity in hexagonal systems.

TABLE 1: The calcium concentration as derived from AAS experiments by brand names and time period.

Ca (mg/g)	BioOss	Cerabone	Macrobone	Ingenios B-TCP	Ingenios HA	Puros	OsteoSponge	Dyna Blast	Autogenous bone
Day 0	1.977	0.98	1.4485	0.892	0.7485	2.104	1.521	2.768	3.77
Day 2	2.643	1.061	3.0735	1.276	2.3862	3.613	1.723	3.7132	4.2
Week 1	7.849	2.605	10.9865	1.663	2.5515	6.99	1.859	4.871	6.73
Week 3	8.79	3.308	15.301	2.306	2.7427	15.1535	2.018	5.6507	16.4
Week 4	9.451	3.445	16.081	2.682	2.7502	18.879	2.18	5.8985	17.96
Week 5	10.205	4.023	16.11	2.834	2.8282	23.11	2.493	6.0485	19.64
Week 6	11.8	4.194	17.308	2.835	2.9275	24.942	4.051	6.2	20.15

TABLE 2: Particle size parameters in volume percentage of the samples.

Sample	Median size (D_{50} μm)	Size range (D_{10} – D_{90} μm)	Size range reported By producers (μm)
Bio-Oss	1.32	0.26–8.92	250–1000
Cerabone	663.31	174.62–1337.48	500–1000
Macrobone	262.37	22.79–517.2	150–500
Ingenios B-TCP	6.72	3.90–15.18	250–1000
Ingenios HA	592.39	8.82–1337.48	1000–2000
Puros	630.47	174.62–1167.72	250–2000
OsteoSponge	902.41	152.45–2301.84	1000–4000
Dyna Blast	777.14	39.24–1754.62	Nonindicated
Autogenous bone	282.1	90.5–465.15	

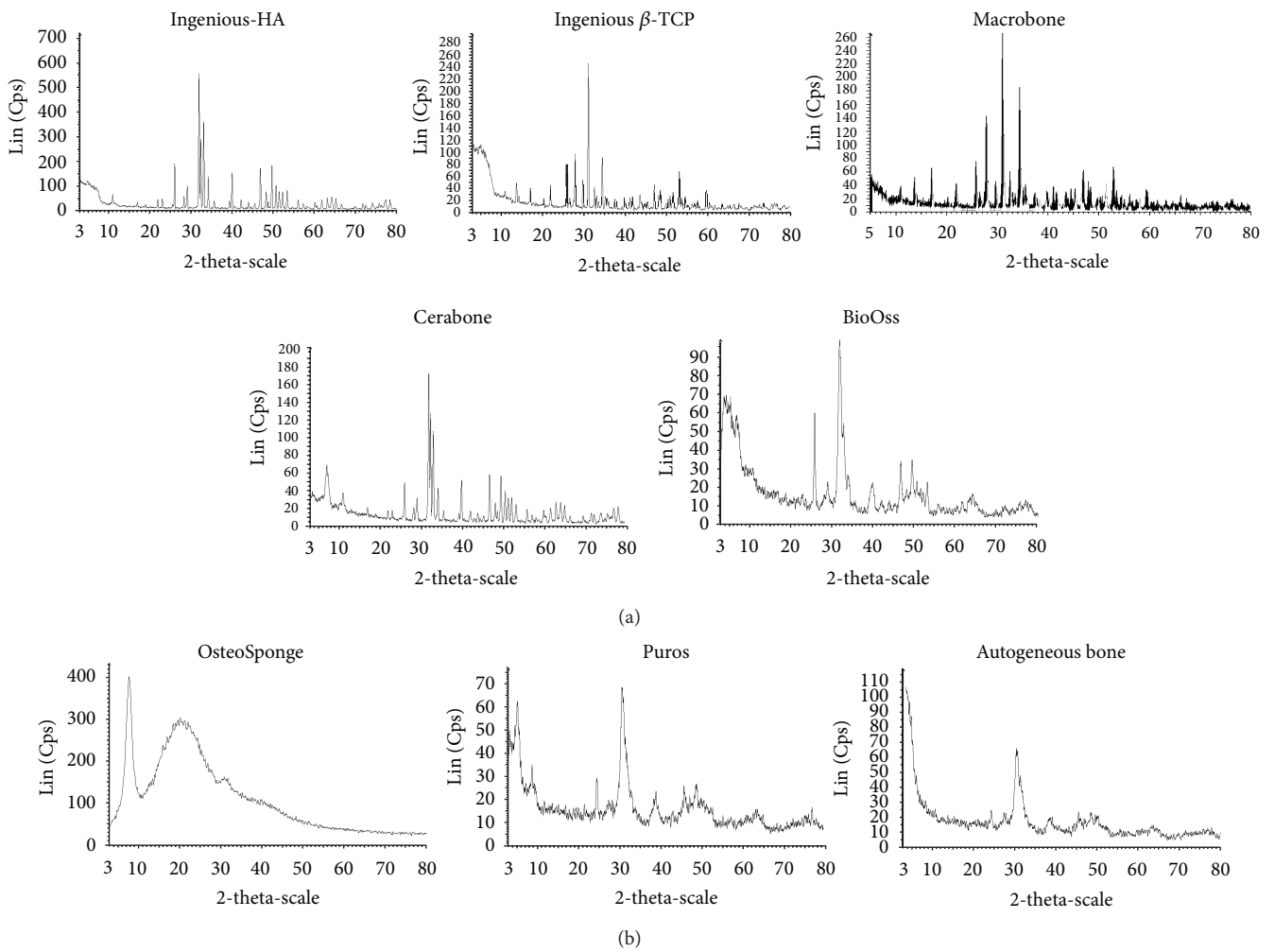


FIGURE 1: X-ray diffraction data for all investigated samples. (a) Ingenios HA, Ingenios β -TCP, Marrowbone, Cerabone, and BioOss have well defined peaks, which reflects their well-crystallized components. (b) OsteoSponge, Puros, and autogenous bone have noisy diffractograms revealing less crystallinity.

The a/c or b/c ratios (9.42/6.89) indicated a flat structure parallel to A_6 axis. Such geometry may enhance the settlement properties of these particles. For Ingenios β -TCP and Macrobone, a and b crystal dimensions in the rhombohedra system were relatively too close to a and b dimensions of the

other bones crystallized in hexagonal system. Nevertheless, c length (373 Å) in Ingenios β -TCP and Macrobone was 5.4 times greater than c (6.89 Å) length in the other bones. Hence, settlement may be oriented preferably orthogonal to A_3 axis. In Ingenios β -TCP and Macrobone, crystal size was

TABLE 3: Chemical compositions and shapes of samples, except for Dyna Blast due to its putylike form, as derived from X-ray diffraction.

Product	Compound name	Formula	System	a (Å)	b (Å)	c (Å)	Alpha (°)	Beta (°)	Gamma (°)
Bio-Oss	Calcium phosphate silicate hydroxide	$\text{Ca}_5(\text{PO}_4)_{2.85}(\text{SiO}_4)_{0.15}(\text{OH})$	Hexagonal	9.42	9.42	6.89	90	90	120
Cerabone	Calcium gadolinium oxide phosphate	$\text{Ca}_8\text{Gd}_2(\text{PO}_4)_6\text{O}_2$	Hexagonal	9.39	9.39	6.89	90	90	120
Macrobone	Calcium phosphate	$\text{Ca}_3(\text{PO}_4)_2$	Rhomboid	10.4	10.4	37.4	90	90	120
Ingenios B-TCP	Sodium calcium iron phosphate	$\text{Na}_2\text{Ca}_{19}\text{Fe}_{0.667}(\text{PO}_4)_{14}$	Rhomboid	10.4	10.4	37.3	90	90	120
Ingenios HA	Calcium phosphate silicate hydroxide	$\text{Ca}_5(\text{PO}_4)_{2.85}(\text{SiO}_4)_{0.15}(\text{OH})$	Hexagonal	9.42	9.42	6.89	90	90	120
Puros	Calcium phosphate silicate hydroxide	$\text{Ca}_5(\text{PO}_4)_{2.85}(\text{SiO}_4)_{0.15}(\text{OH})$	Hexagonal	9.42	9.42	6.89	90	90	120
OsteoSponge	Calcium phosphate silicate hydroxide	$\text{Ca}_5(\text{PO}_4)_{2.85}(\text{SiO}_4)_{0.15}(\text{OH})$	Triclinic	6.25	11.9	5.6	97	114	93
Dyna Blast									
Autogenous Bone	Calcium phosphate silicate hydroxide	$\text{Ca}_5(\text{PO}_4)_{2.85}(\text{SiO}_4)_{0.15}(\text{OH})$	Hexagonal	9.42	9.42	6.89	90	90	120

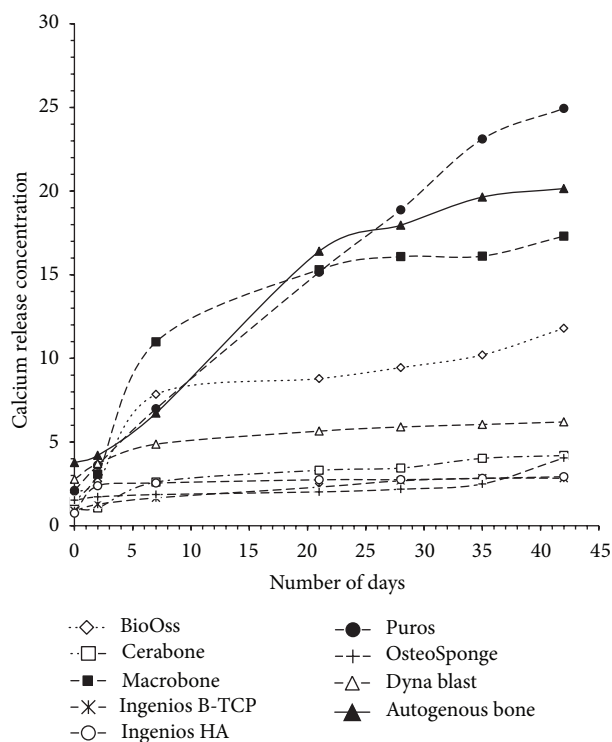


FIGURE 2: AAS results from calcium concentration over the observation period of all tested bone substitutes. Y-axes represent calcium release in mg/g and X axes represent day's number.

greater than that of the other bones. OsteoSponge was the only sample crystallized in the triclinic system.

4. Discussion

The higher the calcium concentration in a biomaterial, the more prone it will be to degradation [3, 42, 43]. The acidic buffer, to some extent, mimics the acidic environment during osteoclastic activity or bone resorption [3, 42, 43]. In our study, different biomaterials had different calcium releasing characteristics. This could be explained by the fact that the speed of BS biodegradability *in vivo* or *in vitro* depends on the material's composition, particle size, crystallinity, porosity, and preparation [3, 38, 42, 43, 48].

From the particle size data, it can be concluded that, in general, size ranges measured for tested materials were different from those reported by manufacturers who do not specify the technique used in the crystalline material's characterization and could explain the noticed differences [49–54]. However, it should be kept in mind that the granules under analysis differed not only in their size but also in their physicochemical properties.

The influence of properties and characteristics of BS on biological response cannot be easily predicted as the published studies involve different types of BS in different particle size ranges. Regarding the ranges of particle size that were tested in the present investigation, there was no relation

between the sizes of particles and calcium concentration with the time (Figure 2).

X-ray diffractograms give a clear idea about the crystallinity of the analyzed materials and their crystal phases. HA, Ingenios β -TCP, Macrobone, Cerabone, and BioOss have well-defined peaks which reflects their well-crystallized components; OsteoSponge, Puros, and autogenous bone have noisy diffractograms revealing the presence of amorphous structure or at least noncrystallized faces of the materials.

All bone substitutes show a typical and most intense diffraction at 2θ of 32° since phosphate is the common component in all used materials. Crystal phases were identified using the powder diffraction files, provided by the Interactive Center for Diffraction Data.

XRD diffractograms of various materials, including human bone, were quite similar to common crystal phase calcium phosphate silicate hydroxide ($\text{Ca}_5(\text{PO}_4)_{2.85} \cdot (\text{SiO}_4)_{0.15}(\text{OH})$) except for Cerabone, which showed the presence of gadolinium in its composition, and Ingenios β -TCP, which showed the presence of iron. However, silicates, when they are present, are not major components of the crystal phases, since their stoichiometry compared to phosphate (2.85) were considerably negligible (0.15). Iron and sodium are also negligible compared to calcium in Ingenios β -TCP. Along with calcium, they help to compensate the negative charges of phosphate. It must be highlighted that, in bone and all bone substitutes, Ca to P ratios fluctuated between 1.75 and 1.33. This could mean that calcium was the major element that compensated phosphate charges.

It is not clear why gadolinium was present in the crystal phase of Cerabone. One possible explanation could be the iron oxidized at high temperature since the product was subjected to high-temperature calcination $\pm 1200^\circ\text{C}$ [55]. Another explanation could be that it was used for its property to enhance the resistance of alloys against oxidation. It should be noted that natural gadolinium occurs in monazite mineral (rare earth phosphate) and gadolinium salt has an exceptionally high absorption of neutrons and therefore is used for shielding in radiography as a contrast agent [56].

Nevertheless, we could not assert if gadolinium in those studied samples naturally occurred or was purposely added.

XRD diffractograms showed that all samples, including natural bone, proved to have the same anisotropic crystal size (9.42 Å in *a*- and *b*-directions and 6.89 Å in *c*-direction with alpha and beta 90° and gamma 120°); Ingenios β -TCP and Macrobone showed different anisotropic size 10.4 Å in *a*- and *b*-directions and 37.3 Å in *c*-direction with alpha and beta 90° and gamma 120° , 6.25 Å in *a*-direction, 11.9 Å in *b*-direction, and 5.6 Å in *c*-direction with alpha 97° and beta 114° and gamma 93° , respectively. These results demonstrated that crystal shapes of the BS and autogenous bone had a similar, hexagonal shape; only Ingenios β -TCP and Macrobone showed a rhomboid design and OsteoSponge a triclinic shape. This structure is the poorest system in the symmetric properties [57].

Eight different bone-grafting materials were herein investigated, and the results were compared to autogenous bone. Even when similar chemical characteristics were found,

significant differences were detected in terms of calcium concentrations, particle sizes, and crystallinity. Although these morphological differences greatly influence *in vivo* behavior of the biomaterial, they are often not taken into consideration when the samples' biological performance is evaluated. It is believed that results provided for biomaterials investigated will be most useful to fully understand their clinical behavior and response. Since the bone substitute of choice depends largely on the possible clinical application and its associated biological and mechanical needs, it is important not to assume that all bone substitutes will show the same pattern of performance and that the validation of a bone substitute in one clinical site may not necessarily predict its identical performance in another anatomical location. Hopefully in the future, hybrid or complex combination products that include cells, growth factors, and/or gene therapy in combination will be likely to provide oral surgeons more effective tools for bone defects reparation. In this regard, it is obvious that further studies are warranted and a new international standard for characterization, classification, and identification of implantable materials is needed.

5. Conclusion

Commercial bone substitutes significantly differ in terms of calcium concentration, particle size, and crystallinity from autogenous bone, which may affect their clinical applications and performance.

Conflict of Interests

The authors do not have any financial interests in the products or information listed in this paper. The authors declare that they have no conflict of interests.

Acknowledgments

The authors would like to thank Manal Houhou, Sarah Hadda, Sahar Rihan, and Hussein Bassal for their excellent technical assistance. This project was supported by a grant from the Ecole Doctorale, Lebanese University.

References

- [1] M. I. Kay, R. A. Young, and A. S. Posner, "Crystal structure of hydroxyapatite," *Nature*, vol. 204, no. 4963, pp. 1050–1052, 1964.
- [2] U. Ripamonti and R. M. Klar, "Regenerative frontiers in craniofacial reconstruction: Grand challenges and opportunities for the mammalian transforming growth factor- β proteins," *Frontiers in Physiology*, vol. 1, no. 1, article 143, 2010.
- [3] R. Z. LeGeros, "Calcium phosphate-based osteoinductive materials," *Chemical Reviews*, vol. 108, no. 11, pp. 4742–4753, 2008.
- [4] H. Orimo, "The mechanism of mineralization and the role of alkaline phosphatase in health and disease," *Journal of Nippon Medical School*, vol. 77, no. 1, pp. 4–12, 2010.
- [5] R. A. Kenley, K. Yim, J. Abrams et al., "Biotechnology and bone graft substitutes," *Pharmaceutical Research*, vol. 10, no. 10, pp. 1393–1401, 1993.
- [6] M. S. Block and J. N. Kent, "Sinus augmentation for dental implants: the use of autogenous bone," *Journal of Oral and Maxillofacial Surgery*, vol. 55, no. 11, pp. 1281–1286, 1997.
- [7] S. L. Wheeler, "Sinus augmentation for dental implants: the use of alloplastic materials," *Journal of Oral and Maxillofacial Surgery*, vol. 55, no. 11, pp. 1287–1293, 1997.
- [8] A. S. Greenwald, S. D. Boden, V. M. Goldberg, Y. Khan, C. T. Laurencin, and R. N. Rosier, "Bone-graft substitutes: facts, fictions, and applications," *Journal of Bone and Joint Surgery A*, vol. 83, no. 2, pp. 98–103, 2001.
- [9] S. N. Parikh, "Bone graft substitutes: past, present, future," *Journal of Postgraduate Medicine*, vol. 48, no. 2, pp. 142–148, 2002.
- [10] C. G. Finkemeier, "Bone-grafting and bone-graft substitutes," *Journal of Bone and Joint Surgery A*, vol. 84, no. 3, pp. 454–464, 2002.
- [11] G. K. B. Sandor, T. C. Lindholm, and C. M. L. Clokie, "Bone regeneration of the cranio-maxillofacial and dento-alveolar skeletons in the framework of tissue engineering," in *Topics in Tissue Engineering*, N. Ashammakhi and P. Ferretti, Eds., chapter 7, pp. 1–46, 2003.
- [12] B. Ben-Nissan, "Natural bioceramics: from coral to bone and beyond," *Current Opinion in Solid State and Materials Science*, vol. 7, no. 4–5, pp. 283–288, 2003.
- [13] D. A. di Stefano, L. Artese, G. Iezzi et al., "Alveolar ridge regeneration with equine spongy bone: a clinical, histological, and immunohistochemical case series," *Clinical Implant Dentistry and Related Research*, vol. 11, no. 2, pp. 90–100, 2009.
- [14] M. Vallet-Regí and J. M. González-Calbet, "Calcium phosphates as substitution of bone tissues," *Progress in Solid State Chemistry*, vol. 32, no. 1–2, pp. 1–31, 2004.
- [15] K. A. Hing, L. F. Wilson, and T. Buckland, "Comparative performance of three ceramic bone graft substitutes," *The Spine Journal*, vol. 7, no. 4, pp. 475–490, 2007.
- [16] D. M. Dohan Ehrenfest, B. S. Kang, G. Sammartino et al., "Guidelines for the publication of articles related to implant surfaces and design from the POSEIDO: a standard for surface characterization," *POSEIDO*, vol. 1, no. 1, p. 15, 2013.
- [17] J. P. Davidas, "Looking for a new international standard for characterization, classification and identification of surfaces in implantable materials: the long march for the evaluation of dental implant surfaces has just began," *POSEIDO*, vol. 2, no. 1, pp. 1–5, 2014.
- [18] J. M. Rueger, W. Linhart, and D. Sommerfeldt, "Biological reaction to calcium-phosphate ceramic implants. Results of animal experiments," *Orthopade*, vol. 27, no. 2, pp. 89–95, 1998.
- [19] M. Bohner, "Calcium orthophosphates in medicine: from ceramics to calcium phosphate cements," *Injury*, vol. 31, no. 4, pp. D37–D47, 2000.
- [20] M. Bohner, "Physical and chemical aspects of calcium phosphates used in spinal surgery," *European Spine Journal*, vol. 10, no. 2, pp. S114–S121, 2001.
- [21] I. Bouchlariotou, J. P. Bernard, J. P. Carrel, and L. Vazquez, "Long-term stability of osseointegrated implants in bone regenerated with a collagen membrane in combination with a deproteinized bovine bone graft: 5-year follow-up of 20 implants," *POSEIDO*, vol. 1, no. 1, pp. 45–53, 2013.
- [22] R. Toeroek and D. M. Dohan Ehrenfest, "The concept of Screw-Guided Bone Regeneration (S-GBR). Part 3: Fast Screw-Guided Bone Regeneration (FS-GBR) in the severely resorbed preimplant posterior mandible using allograft and Leukocyte- and

- Platelet-Rich Fibrin (L-PRF): a 4-year follow-up," *POSEIDO*, vol. 2, no. 2, pp. 93–100, 2013.
- [23] R. Toeroek R and D. M. D. Ehrenfest, "The concept of screw-guided bone regeneration (S-GBR). Part 2: S-GBR in the severely resorbed preimplant posterior mandible using bone xenograft and leukocyte- and platelet-rich fibrin (L-PRF): a 5-year follow-up," *POSEIDO*, vol. 2, no. 2, pp. 85–92, 2013.
- [24] H. Sung, C. Meredith, C. Johnson, and Z. S. Galis, "The effect of scaffold degradation rate on three-dimensional cell growth and angiogenesis," *Biomaterials*, vol. 25, no. 26, pp. 5735–5742, 2004.
- [25] J. Glowacki, "A review of osteoinductive testing methods and sterilization processes for demineralized bone," *Cell and Tissue Banking*, vol. 6, no. 1, pp. 3–12, 2005.
- [26] S. T. Moore, J. M. Katz, R. M. Zhukauskas et al., "Osteoconductivity and osteoinductivity of Puros (R) DBM putty," *Journal of Biomaterials Applications*, vol. 26, no. 2, pp. 151–171, 2011.
- [27] T. Traini, A. Piatelli, S. Caputi et al., "Regeneration of human bone using different bone substitute biomaterials," *Clinical Implant Dentistry and Related Research*, 2013.
- [28] C. Schöpf, W. Daiber, and D. Tadic, "Tutoplast processed allografts and xenografts," in *3D Block Technique in from Image Diagnostics to Block Graft Bone Regeneration*, M. Jacotti and P. Antonelli, Eds., chapter 5, pp. 54–75, RC Libri, Milano, Italy, 2005.
- [29] C. P. Klein, A. A. Driessen, K. de Groot, and A. van den Hooff, "Biodegradation behavior of various calcium phosphate materials in bone tissue," *Journal of Biomedical Materials Research*, vol. 17, no. 5, pp. 769–784, 1983.
- [30] S. Platzer, A. Wildburger, M. Lorenzoni et al., "Human cadaver study evaluating a new measurement technique for graft volumes after sinus floor elevation," *Clinical Implant Dentistry and Related Research*, vol. 16, no. 2, pp. 212–222, 2012.
- [31] C. Dellavia, S. Speroni, G. Pellegrini, A. Gatto, and C. Maiorana, "A new method to evaluate volumetric changes in sinus augmentation procedure," *Clinical Implant Dentistry and Related Research*, vol. 19, 2013.
- [32] Z. Schwartz and B. D. Boyan, "Underlying mechanisms at the bone-biomaterial interface," *Journal of Cellular Biochemistry*, vol. 56, no. 3, pp. 340–347, 1994.
- [33] X. Li, C. A. van Blitterswijk, Q. Feng, F. Cui, and F. Watari, "The effect of calcium phosphate microstructure on bone-related cells in vitro," *Biomaterials*, vol. 29, no. 23, pp. 3306–3316, 2008.
- [34] A. C. C. da Cruz, M. T. Pochapski, J. B. Daher, J. C. Z. da Silva, G. L. Pilatti, and F. A. Santos, "Physico-chemical characterization and biocompatibility evaluation of hydroxyapatites," *Journal of Oral Science*, vol. 48, no. 4, pp. 219–226, 2006.
- [35] A. L. Carvalho, P. E. P. Faria, M. F. M. Grisi et al., "Effects of granule size on the osteoconductivity of bovine and synthetic hydroxyapatite: a histologic and histometric study in dogs," *The Journal of Oral Implantology*, vol. 33, no. 5, pp. 267–276, 2007.
- [36] T. Irinakis, "Efficacy of injectable demineralized bone matrix as graft material during sinus elevation surgery with simultaneous implant placement in the posterior maxilla: clinical evaluation of 49 sinuses," *Journal of Oral and Maxillofacial Surgery*, vol. 69, no. 1, pp. 134–141, 2011.
- [37] C. M. Schmitt, H. Doering, T. Schmidt, R. Lutz R, F. W. Neukam, and K. A. Schlegel, "Histological results after maxillary sinus augmentation with Straumann, BoneCeramic, Bio-Oss, Puros, and autologous bone. A randomized controlled clinical trial," *Clinical Oral Implants Research*, vol. 24, no. 5, pp. 576–585, 2013.
- [38] D. Tadic and M. Epple, "A thorough physicochemical characterisation of 14 calcium phosphate-based bone substitution materials in comparison to natural bone," *Biomaterials*, vol. 25, no. 6, pp. 987–994, 2004.
- [39] D. Chappard, B. Guillaume, R. Mallet, F. Pascaretti-Grizon, M. F. Baslé, and H. Libouban, "Sinus lift augmentation and β -TCP: a microCT and histologic analysis on human bone biopsies," *Micron*, vol. 41, no. 4, pp. 321–326, 2010.
- [40] A. M. Pietak, J. W. Reid, M. J. Stott, and M. Sayer, "Silicon substitution in the calcium phosphate bioceramics," *Biomaterials*, vol. 28, no. 28, pp. 4023–4032, 2007.
- [41] M.-J. Lee, S.-K. Sohn, K.-T. Kim et al., "Effect of hydroxyapatite on bone integration in a rabbit tibial defect model," *Clinics in Orthopedic Surgery*, vol. 2, no. 1, pp. 90–97, 2010.
- [42] F. Peters, K. Schwarz, and M. Epple, "The structure of bone studied with synchrotron X-ray diffraction, X-ray absorption spectroscopy and thermal analysis," *Thermochimica Acta*, vol. 361, no. 1-2, pp. 131–138, 2000.
- [43] M. Figueiredo, J. Henriques, G. Martins, F. Guerra, F. Judas, and H. Figueiredo, "Physicochemical characterization of biomaterials commonly used in dentistry as bone substitutes—comparison with human bone," *Journal of Biomedical Materials Research B*, vol. 92, no. 2, pp. 409–419, 2010.
- [44] R. García and A. P. Báez, "Atomic Absorption Spectrometry (AAS)," in *Atomic Absorption Spectroscopy*, M. A. Farrukh, Ed., chapter 1, pp. 1–13, InTech, 2012.
- [45] T. Wriedt, "Mie theory: a review," in *The Mie Theory*, W. Hergert and T. Wriedt, Eds., vol. 169 of *Springer Series in Optical Sciences*, pp. 53–71, Springer, Berlin, Germany, 2012.
- [46] S. Marković, L. Veselinović, M. J. Lukić et al., "Synthetical bone-like and biological hydroxyapatites: a comparative study of crystal structure and morphology," *Biomedical Materials*, vol. 6, no. 1, pp. 45–50, 2011.
- [47] P. K. Harold and E. L. Alexander, *X-Ray Diffraction Procedures: For Polycrystalline and Amorphous Materials*, Wiley- Interscience, New York, NY, USA, 2nd edition, 1974.
- [48] G. Hannink and J. J. C. Arts, "Bioresorbability, porosity and mechanical strength of bone substitutes: what is optimal for bone regeneration?" *Injury*, vol. 42, no. 2, pp. S22–S25, 2011.
- [49] Geistlich Biomaterials Inc., "Product information on BioOss," <http://www.geistlich.ch/index.cfm?dom=2&rub=42&id=100064>.
- [50] Bacterin, product information on Osteosponge, 2014, <http://bacterin.com/products/osteosponge/>.
- [51] Zimmer dental, products, regenerative, bone grafts, information on Puros, HA, β -TCP, 2014, http://www.zimmerdental.com/products/regenerative/rg_overview.aspx.
- [52] Botiss Biomaterials, *Product Information on Cerabone*, 2014, <https://www.botiss.com/en/content/cerabone%C2%AE>.
- [53] KeyStone Dental Inc. product information on DynaBlast, 2014, <http://www.keystonedental.com/products/dynablast/>.
- [54] Euroteknika, "Product information on MacroBone," 2014, http://www.euroteknika-implants.com/EN/IMG/pdf/FP_Macrobone_EN.pdf.
- [55] A. Gschneidner Jr., V. K. Pecharsky, and A. O. Tsokol, "Recent developments in magnetocaloric materials," *Reports on Progress in Physics*, vol. 68, no. 6, pp. 1479–1539, 2005.
- [56] I. E. Chesnick, C. B. Fowler, J. T. Mason, and K. Potter, "Novel mineral contrast agent for magnetic resonance studies of bone implants grown on a chick chorioallantoic membrane," *Magnetic Resonance Imaging*, vol. 29, no. 9, pp. 1244–1254, 2011.
- [57] H. D. Flack, "Chiral and achiral crystal structures," *Helvetica Chimica Acta*, vol. 86, no. 4, pp. 905–921, 2003.

Clinical Study

Biological Width around One- and Two-Piece Implants Retrieved from Human Jaws

Ricardo Judgar,¹ Gabriela Giro,¹ Elton Zenobio,^{1,2} Paulo G. Coelho,³ Magda Feres,¹ Jose A. Rodrigues,¹ Carlo Mangano,⁴ Giovanna Iezzi,⁴ Adriano Piattelli,⁴ and Jamil Awad Shibli¹

¹ Department of Periodontology and Oral Implantology, Dental Research Division, University of Guarulhos, Praca Tereza Cristina 229, 07023-070 Guarulhos, SP, Brazil

² Department of Oral Implantology, Pucminas, Belo Horizonte, MG, Brazil

³ Department of Biomaterials and Biomimetics, New York University, 45 E 24th Street, New York, NY 10010, USA

⁴ Department of Stomatology and Biotechnologies, University of Chieti-Pescara, Via dei Vestini 31, 66100 Chieti, Italy

Correspondence should be addressed to Jamil Awad Shibli; jashibli@yahoo.com

Received 15 May 2014; Accepted 2 June 2014; Published 23 June 2014

Academic Editor: David M. Dohan Ehrenfest

Copyright © 2014 Ricardo Judgar et al. This is an open access article distributed under the Creative Commons Attribution License, which permits unrestricted use, distribution, and reproduction in any medium, provided the original work is properly cited.

Several histologic studies regarding peri-implant soft tissues and biological width around dental implants have been done in animals. However, these findings in human peri-implant soft tissues are very scarce. Therefore, the aim of this case series was to compare the biological width around unloaded one- and two-piece implants retrieved from human jaws. Eight partially edentulous patients received 2 test implants in the posterior mandible: one-piece (solid implants that comprise implant and abutment in one piece) and two-piece (external hexagon with a healing abutment) implants. After 4 months of healing, the implants and surrounding tissue were removed for histologic analysis. The retrieved implants showed healthy peri-implant bone and exhibited early stages of maturation. Marginal bone loss, gaps, and fibrous tissue were not present around retrieved specimens. The biologic width dimension ranged between 2.55 ± 0.16 and 3.26 ± 0.15 to one- and two-piece implants, respectively ($P < 0.05$). This difference was influenced by the connective tissue attachment, while sulcus depth and epithelial junction presented the same dimension for both groups ($P > 0.05$). Within the limits of this study, it could be shown that two-piece implants resulted in the thickening of the connective tissue attachment, resulting in the increase of the biological width, when compared to one-piece implants.

1. Introduction

Biologic width (BW) is a physiologically formed and stable vertical dimension of the dentogingival junction that comprised the sulcus depth (SD), junctional epithelium (JE), and connective tissue attachment (CTA) [1]. In a similar manner to the teeth, dental implants have also a similar peri-implant soft tissue structure [2–4]. On the dental implants, the biologic width is influenced by several factors, and among them, the macrostructure, that is, one- or two-piece implants, seems to be most relevant [4]. The two-piece implants present a microgap placed at the crestal bone level, while one-piece implants have no gap at this region [5].

Early studies have shown [6–8] that the mucosal barrier around dental implants is composed by sulcular epithelium

ranged between 1.5 and 2 mm and connective tissue between 1 and 2 mm. The oral epithelium presents an extension with a thin junctional epithelium facing the implant surface and extending about 1.64–2.35 mm from the mucosal margin. The dimension from the marginal portion of the peri-implant mucosa to the marginal level of bone-to-implant contact has been found to be about 3 mm.

Although the precise mechanism responsible for the crestal bone remodeling in 2-piece implants is currently under research, factors such as microbial colonization of the microgap, micromovements of the abutment, or an interruption of the blood supply when implants and abutments are placed transmucosally and have been also hypothesized [9–12]. Complementary to these factors, several studies have demonstrated a second discrete inflammatory cell infiltrate,

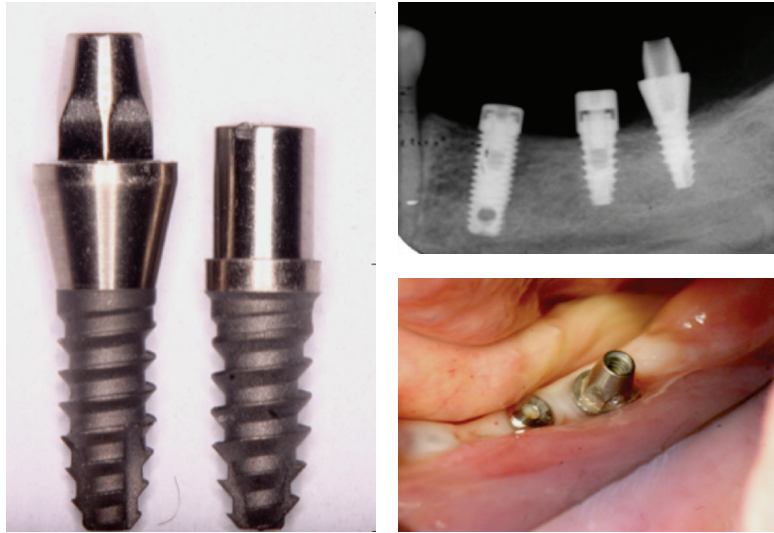


FIGURE 1: Clinical and radiographic view of the implants evaluated in the study.

additionally to the connective tissue lateral to the abutment fixture junction [5, 12, 13]. This infiltrated connective tissue (abutment ICT) was consistently separated from the plaque-associated infiltrate by a zone of normal, noninflamed tissue [5, 12–14].

As these data were obtained mainly from animal studies [5, 6, 8, 10, 12, 13] and only few studies have investigated human peri-implant soft tissues [2, 4, 14], the aim of this case series was to evaluate the biological width around one- and two-piece implants retrieved from human jaws.

2. Material and Methods

2.1. Patient Population. Eight partially edentulous subjects (5 women; 3 men) with a mean age of 56.40 ± 4.7 years, referred for oral rehabilitation of the posterior mandible with dental implants at the Oral Implantology Facility at the University of Guarulhos, were included in this study. Patients presenting mandibular bone height lower than 11 mm, smoking habit, pregnancy, nursing, or any systemic condition that could affect bone healing were excluded from this study. The Ethics Committee for Human Clinical Trials at University of Guarulhos approved the study protocol (CEP# 201/03) following the World Medical Association Declaration of Helsinki requirements. The protocol of the study was explained to each subject that signed the informed consent.

2.2. Experimental Implants. Sixteen screw-shaped implants with sandblasted acid-etched surface, 3.3 mm diameter, and 8 mm length were used in this study. The implants were divided in 2 groups ($n = 8$): the one-piece implant group (solid implants that comprise implant and abutment in one piece) and the two-piece implant group (external hexagon with a healing abutment) (Figure 1).

All patients received an implant of each group (two implants were installed per patient). The implants were placed under the protocol previously reported [15–17]. Briefly,

after crestal incision, mucoperiosteal flap was raised and conventional implant was placed in accordance with the surgical/prosthetic plan prepared for each patient. Afterwards, the experimental implants were placed in suitable areas, mostly in the second and third molar region, that is, posterior to the most distal conventional implant. The experimental implant recipient sites were prepared with a 2.8 mm diameter twist drill. All drilling and implant placement procedures were completed under profuse irrigation with sterile saline. If the experimental implant showed low primary stability, a backup surgical site was prepared. The experimental implants (one- and two-piece) were placed at the level of the alveolar crest. The flaps were sutured to allow nonsubmerged healing (Figure 1).

Amoxicillin was administered every 8 hours for 7 days, in order to avoid postsurgical infection. The sutures were removed 10 days post-operatively. Also, 0.12% chlorhexidine rinses were prescribed twice daily for 14 day in order to enable the postoperative dental biofilm control. Following the healing period of 4 months, the test implants and the surrounding tissues were retrieved with a trephine bur, and the specimens were fixed by immediate immersion in neutral formalin at 4%.

2.3. Specimen Processing and Histometric Analyses. The biopsies were processed to obtain thin ground sections as previously described (Precise 1 Automated System, Assing, Rome, Italy) [18]. The specimens were dehydrated in an ascending series of alcohol rinses and embedded in glycol methacrylate resin (Technovit 7200 VLC, Kulzer, Wehrheim, Germany). After polymerization, the specimens were sectioned lengthwise along the longer axis of the implant, using a high-precision diamond saw, to about $150 \mu\text{m}$, and ground down to approximately $30 \mu\text{m}$. Two slides were obtained from each implant and then averaged for each group. The slides were stained with basic fuchsin and toluidine blue.

The peri-implant tissue width was measured as follows:

- (i) sulcus depth (SD): the distance between the mucosal margin (MM) and the most coronal point of junctional epithelium (CJE);
- (ii) junctional epithelium (JE): the distance between the most coronal point of JE and the most apical point of the JE;
- (iii) connective tissue attachment (CTA): distance between the most apical point of JE and the first bone-to-implant contact.

Therefore, the biological width (BW) was obtained after the sum of SD + MM + CTA.

Bone-to-implant contact (BIC%), defined as the amount of mineralized bone in direct contact with the implant surface, was also evaluated.

These measurements were performed using a light microscope connected to a high-resolution video camera and interfaced to a monitor and personal computer. This optical system was associated with a digitizing pad and a histometry software package with image-capture functionalities (Image-Pro Plus 4.5, Media Cybernetics Inc., Immagini & Computer Snc, Milan, Italy). A single trained examiner performed all histometric parameters.

The mean and standard deviation of histometric variables were calculated for each group. Nonparametric mixed models [19] were applied to evaluate the data clustered within the subject. The significance test was 2-tailed and conducted at a 0.05 level of significance.

3. Results

All 16 implants presented no mobility or clinical signs of infection after healing period. Bone density on the site of implant placement was almost D2 [20]. The retrieved implants showed healthy peri-implant bone. Osteocytes were present in their lacunae, although areas of woven bone could be distinguished. The newly formed peri-implant bone exhibited early stages of maturation. No gaps, marginal bone loss, or fibrous tissue were found surrounding retrieved implants.

The sulcular epithelium was composed of about 4–6 layers of parakeratinized epithelial cells. The junctional epithelium (JE) was composed of about 5–10 layers of epithelial cells. The middle and apical portion of the JE consisted of 3–5 layers of epithelial cells. No acute or chronic inflammatory cell infiltrate was present. Epithelial downgrowth was not depicted in any ground section (Figures 2 and 3).

In the abutment area of both groups, the connective tissue contained few blood vessels, and dense collagen fibers, oriented parallel to the longitudinal axis of the abutment, were present. Collagen fibers oriented in a perpendicular way and inserting directly contacting on the abutment surface were not observed in any of the specimens.

The mean dimensions of SD, JE, and CT for the 16 implants were reported in Table 1. An increase of the biological width's (BW's) dimension was observed, with mean values of 2.55 ± 0.16 and 3.26 ± 0.15 to the one- and two-piece

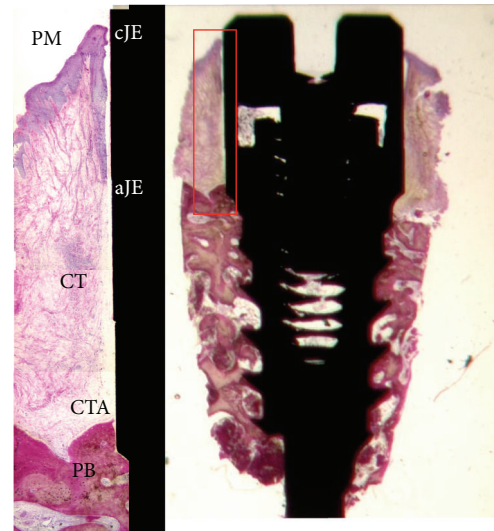


FIGURE 2: Photomicrograph of the ground section of the two-piece implant group (20x) and the high magnification of the biological width (100x).

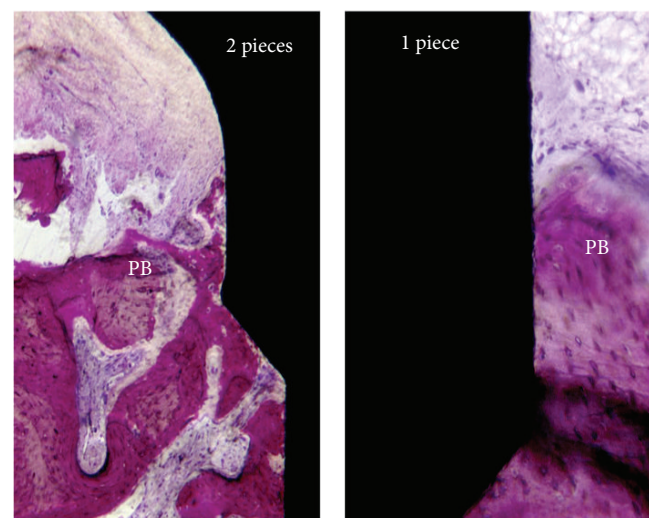


FIGURE 3: Photomicrographs of the one- and two-piece implant group (200x) near the first bone-to-implant contact. Note the disorganization around the peri-implant bone close to the microgap on the two-piece implant group.

implants group, respectively ($P = 0.001$). This difference was influenced by the CTA, since one-piece implants showed a CTA length average of 1.24 mm while two-piece implants presented 1.87 mm ($P < 0.05$). Sulcus depth (SD) and epithelial junction (EJ) presented no statistical significant difference between the groups. ($P > 0.05$). Moreover, BIC% showed no statistical difference between the groups as well.

4. Discussion

The current histological case series evaluated the influence of implant macrostructure (one- or two-piece implants) on human peri-implant soft tissues. Specifically, the biological

TABLE 1: Mean \pm standard deviation for the histometric variables of both groups. Wilcoxon rank test (* $P < 0.05$) ($n = 8$ subjects).

Histometric variables	1-piece	2-piece	P value
SD (mm)	0.33 \pm 0.07	0.36 \pm 0.12	0.98
JE (mm)	1.03 \pm 0.06	1.05 \pm 0.04	0.89
CTA (mm)	1.24 \pm 0.23	1.87 \pm 0.20	0.02*
BW (mm)	2.55 \pm 0.16	3.26 \pm 0.15	0.001*
BIC (%)	67.56 \pm 4.56	66.45 \pm 5.01	0.92

SD: sulcus depth; JE: junctional epithelium; CTA: connective tissue attachment; BW: biologic width; BIC: bone-to-implant contact.

width dimension was examined in implants retrieved from human jaws. The biologic width dimension ranged between 2.5 to 3.2 mm for one- and two-piece implants, respectively ($P < 0.001$). This difference was influenced by the connective tissue attachment, while sulcus depth and epithelial junction presented the same dimension for both groups ($P > 0.05$).

There is a lack of information regarding the histological features of supracrestal peri-implant soft tissue, since the present knowledge is basically constituted by animal studies data, using dogs and nonhuman primates [11] and some patient reports [3, 14, 21]. Although these data presents such important role in this field, sometimes the animal studies results cannot be faithfully transposed to the per-implant tissue behavior in humans [22]. A classical report using human teeth [1] showed that BW is a physiologically formed and stable dimension whose level is dependent upon the location of the alveolar bone crest. Around dental implants, BW determines the minimum dimensions to ensure adequate JE and CT to obtain an optimal seal and to provide protection from mechanical and external biological agents [23]. An external agent invading the BW would induce a response from the epithelium that migrates beyond this agent trying to isolate it [2, 3, 23]. The resulting bone resorption produces a reestablishment of the BW dimension. Regarding dental implants, the dimension of the BW was reported to be dependent on the presence/absence of a microgap and on the location of the microgap in relation to the bone crest [5–10].

Studies have reported the dimension of JE around implants, in animal studies, comprised between 1.16 mm and 1.90 mm [6, 8, 10, 11, 13], while JE around retrieved implants from human jaws ranged between 1.8 and 3.4 mm [4, 14], differing from the findings of this study that showed values similar to those reported in animal studies (~1.05 mm).

Connective attachment dimension, in animal models, ranged between 1.01 mm and 2.01 mm [10, 11, 13]. Loading conditions have also been reported to influence not only the dimension of JE but also the dimension of the CT. Previous canine model study [10] has shown that the CT dimension was significantly higher on unloaded implants when compared to different load conditions. The results of the present study could confirm a tendency for a larger size of the CT around unloaded implants. In fact, in human unloaded specimens, CT has been comprised between 1.8 mm and 3.4 mm [4, 14].

The supracrestal CT was, in animal studies, characterized by a 3D network of collagen fibers running in different directions [6, 8, 10]. In addition, several animal studies

have reported a tight adaptation of the connective tissue to the abutment presenting a thin avascular and collagen fiber-rich, as a scar-like tissue characteristics [13, 23]. In the present specimens, the CT distant from the implant was composed by abundant collagen fibers, running in several directions and appearing to be functionally organized in a 3-dimensional network. Similar results have been reported in human studies [2–4, 14]. This differentiated network of fibers may have clinical relevance as a mechanical protection of the underlying bone [4]. These human histologic data are extremely valuable to validate and confirm those obtained from studies performed on animal models [8, 10, 11].

5. Conclusions

Therefore, within the limits of this histologic report, it could be suggested that the two-piece implant leads to a thicker biological width. These data must be carefully analyzed, and further prospective longitudinal studies are required to clarify the clinical relevance of these findings.

Conflict of Interests

The authors declare that there is no conflict of interests related to this study.

Authors' Contribution

Jamil Awad Shibli was in charge of the elaboration of the study proposal and the financial support of the study, and he participated in the elaboration of the paper and the treatment planning of each case. Carlo Mangano and Paulo G. Coelho were in charge of the statistical analysis, the implant surface characterization, and the financial support for the study. Ricardo Judgar, Gabriela Giro, Elton Zenobio, and Jose A. Rodrigues were in charge of the treatment planning of each case and the implant placement surgery and they participated to the elaboration of the paper. Magda Feres, Elton Zenobio, and Gabriela Giro were in charge of the patients' monitoring after surgery, the biopsies collection, and the oral rehabilitation and they participated in the elaboration of the paper. Giovanna Iezzi and Adriano Piattelli were in charge of the laboratory processing of the samples and the histology and participated in the data analyses and elaboration of the paper. Adriano Piattelli also participated in the elaboration of the study proposal.

References

- [1] A. W. Gargiulo, F. M. Wentz, and B. Orban, "Dimensions of the dentogingival junction in humans," *Journal of Periodontology*, vol. 32, pp. 261–267, 1961.
- [2] M. Degidi, A. Piattelli, A. Scarano, J. A. Shibli, and G. Iezzi, "Peri-implant collagen fibers around human cone Morse connection implants under polarized light: a report of three cases," *The International Journal of Periodontics & Restorative Dentistry*, vol. 32, no. 3, pp. 323–328, 2012.
- [3] M. Degidi, V. Perrotti, J. A. Shibli, A. B. Novaes, A. Piattelli, and G. Iezzi, "Equicrestal and subcrestal dental implants: a histologic and histomorphometric evaluation of nine retrieved human implants," *Journal of Periodontology*, vol. 82, no. 5, pp. 708–715, 2011.
- [4] R. Glauser, P. Schüpbach, J. Gottlow, and C. H. F. Hämmerle, "Peri-implant soft tissue barrier at experimental one-piece mini-implants with different surface topography in humans: a light-microscopic overview and histometric analysis," *Clinical Implant Dentistry and Related Research*, vol. 7, supplement 1, pp. S44–S51, 2005.
- [5] N. Broggini, L. M. McManus, J. S. Hermann et al., "Peri-implant inflammation defined by the implant-abutment interface," *Journal of Dental Research*, vol. 85, no. 5, pp. 473–478, 2006.
- [6] J. S. Hermann, D. Buser, R. K. Schenk, F. L. Higginbottom, and D. L. Cochran, "Biologic width around titanium implants. A physiologically formed and stable dimension over time," *Clinical Oral Implants Research*, vol. 11, no. 1, pp. 1–11, 2000.
- [7] G. Schierano, G. Ramieri, M. Cortese, M. Aimetti, and G. Preti, "Organization of the connective tissue barrier around long-term loaded implant abutments in man," *Clinical Oral Implants Research*, vol. 13, no. 5, pp. 460–464, 2002.
- [8] A. Quaranta, A. Piattelli, A. Scarano, M. Quaranta, G. Pompa, and G. Iezzi, "Light-microscopic evaluation of the dimensions of peri-implant mucosa around immediately loaded and submerged titanium implants in monkeys," *Journal of Periodontology*, vol. 79, no. 9, pp. 1697–1703, 2008.
- [9] X. Vela-Nebot, X. Rodríguez-Ciurana, C. Rodado-Alonso, and M. Segalá-Torres, "Benefits of an implant platform modification technique to reduce crestal bone resorption," *Implant Dentistry*, vol. 15, no. 3, pp. 313–320, 2006.
- [10] J. S. Hermann, D. Buser, R. K. Schenk, and D. L. Cochran, "Crestal bone changes around titanium implants. A histometric evaluation of unloaded non-submerged and submerged implants in the canine mandible," *Journal of Periodontology*, vol. 71, no. 9, pp. 1412–1424, 2000.
- [11] C. H. Siar, C. G. Toh, G. Romanos et al., "Peri-implant soft tissue integration of immediately loaded implants in the posterior macaque mandible: a histomorphometric study," *Journal of Periodontology*, vol. 74, no. 5, pp. 571–578, 2003.
- [12] J. S. Hermann, D. L. Cochran, P. V. Nummikoski, and D. Buser, "Crestal bone changes around titanium implants: a radiographic evaluation of unloaded nonsubmerged and submerged implants in the canine mandible," *Journal of Periodontology*, vol. 68, no. 11, pp. 1117–1130, 1997.
- [13] J. S. Hermann, J. D. Schoolfield, R. K. Schenk, D. Buser, and D. L. Cochran, "Influence of the size of the microgap on crestal bone changes around titanium implants. A histometric evaluation of unloaded non-submerged implants in the canine mandible," *Journal of Periodontology*, vol. 72, no. 10, pp. 1372–1383, 2001.
- [14] A. Piattelli, A. Scarano, M. Piattelli, R. Bertolai, and E. Panzoni, "Histological aspects of the bone and soft tissues surrounding three titanium non-submerged plasma-sprayed implants retrieved at autopsy. A case report," *Journal of Periodontology*, vol. 68, no. 7, pp. 694–700, 1997.
- [15] J. A. Shibli, C. Mangano, S. D'Avila et al., "Influence of direct laser fabrication implant topography on type IV bone: a histomorphometric study in humans," *Journal of Biomedical Materials Research A*, vol. 93, no. 2, pp. 607–614, 2010.
- [16] J. A. Shibli, S. Grassi, A. Piattelli et al., "Histomorphometric evaluation of bioceramic molecular impregnated and dual acid-etched implant surfaces in the human posterior maxilla," *Clinical Implant Dentistry and Related Research*, vol. 12, no. 4, pp. 281–288, 2010.
- [17] J. A. Shibli, C. Mangano, F. Mangano et al., "Histomorphometric evaluation of Direct Laser Metal Forming (DLMF) implant surface in the type IV bone: a controlled study in human jaw," *Poseido*, vol. 1, no. 3, pp. 149–156, 2013.
- [18] A. Piattelli, A. Scarano, and M. Quaranta, "High-precision, cost-effective cutting system for producing thin sections of oral tissues containing dental implants," *Biomaterials*, vol. 18, no. 7, pp. 577–579, 1997.
- [19] E. Brunner and F. Langer, "Nonparametric analysis of ordered categorical data in designs with longitudinal observations and small sample sizes," *Biometrical Journal*, vol. 42, no. 6, pp. 663–675, 2000.
- [20] C. E. Misch, "Divisions of available bone in implant dentistry," *The International Journal of Oral Implantology: Implantologist*, vol. 7, no. 1, pp. 9–17, 1990.
- [21] M. Degidi, A. Piattelli, A. Scarano, V. Perrotti, and G. Iezzi, "Soft tissues around an acid-etched healing abutment: a histological and histomorphometrical analysis," *Poseido*, vol. 1, no. 3, pp. 157–163, 2013.
- [22] M. Degidi, A. Piattelli, J. A. Shibli et al., "Bone formation around a dental implant with a platform switching and another with a TissueCare connection: a histologic and histomorphometric evaluation in man," *Titanium*, vol. 1, pp. 8–15, 2009.
- [23] I. Abrahamsson, T. Berglundh, J. Wennström, and J. Lindhe, "The peri-implant hard and soft tissues at different implant systems: a comparative study in the dog," *Clinical Oral Implants Research*, vol. 7, no. 3, pp. 212–219, 1996.

Research Article

Effect of Low-Level Laser on Bone Defects Treated with Bovine or Autogenous Bone Grafts: *In Vivo* Study in Rat Calvaria

Mércia J. S. Cunha,^{1,2,3} Luis A. Esper,^{2,3} Michyele C. Sbrana,^{2,3} Paula G. F. P. de Oliveira,^{1,3} Accácio L. do Valle,^{3,4} and Ana Lúcia P. F. de Almeida^{3,4}

¹ Hospital for Rehabilitation of Craniofacial Anomalies, University of São Paulo, Brazil

² Bauru School of Dentistry, USP, Brazil

³ Faculdade de Odontologia de Bauru (FOB), Universidade de São Paulo (USP), Alameda Dr. Octávio Pinheiro Brisolla 9-75, Vila Universitária, 17012 901 Bauru, SP, Brazil

⁴ Department of Prosthodontics, Bauru School of Dentistry, USP, Brazil

Correspondence should be addressed to Ana Lúcia P. F. de Almeida; analmeida@usp.br

Received 28 February 2014; Revised 17 April 2014; Accepted 12 May 2014; Published 28 May 2014

Academic Editor: David M. Dohan Ehrenfest

Copyright © 2014 Mércia J. S. Cunha et al. This is an open access article distributed under the Creative Commons Attribution License, which permits unrestricted use, distribution, and reproduction in any medium, provided the original work is properly cited.

Objective. The purpose of this study was to histologically evaluate the effect of low-level laser (LLL) on the healing of critical size defects (CSD) in rat calvaria, filled with autogenous or inorganic bovine bone grafts. **Methods.** Sixty rats were divided into 6 groups ($n = 10$): C (control—filled with blood clot), LLL (low-level laser—GaAlAs, λ 780 nm, 100 mW, 210 J/cm², Φ 0.05 cm²; 6 J/point), AB (autogenous bone), ABL (autogenous bone + low-level laser), OB (inorganic bovine bone), and OBL (inorganic bovine bone + LLL). **Material and Methods.** The animals were killed after 30 days. Histological and histometric analyses were performed by light microscopy. **Results.** The groups irradiated with laser, LLL ($47.67\% \pm 8.66\%$), ABL ($39.15\% \pm 16.72\%$), and OBL ($48.57\% \pm 28.22\%$), presented greater area of new bone formation than groups C ($9.96\% \pm 4.50\%$), AB ($30.98\% \pm 16.59\%$), and OB ($11.36\% \pm 7.89\%$), which were not irradiated. Moreover, they were significantly better than group C (Kruskal-Wallis test followed by Dunn test, $P < 0.05$). **Conclusion.** The laser accelerated the healing of bone defects and the resorption of particles of the graft material.

1. Introduction

Currently, bone grafting has been widely used. It is estimated that approximately 2.2 million bone graft procedures are performed worldwide [1, 2] to repair defects in orthopedics, neurosurgery, and dentistry [2].

Among the graft materials used for bone regeneration, autogenous bone has been considered the ideal material [1, 3, 4]. Even though it is the “gold standard” for reconstructions [1, 3, 5], its collection is associated with 8.5 to 20% of complications, including hematoma [2], damage to anatomic structures [6], infections [2, 6], pain at the donor site [7, 8], and unpredictable graft resorption [3, 5].

For these reasons, several bone substitutes from different sources are available, with the advantages of unlimited supply and no need for a donor site. The inorganic bovine bone is the most researched graft material and is widely used in dentistry

due to its similarity to human bone [3]. Promising results have been demonstrated by its use in clinical and animal studies [9, 10]. Despite its excellent osteoconduction [8, 10], it lacks osteoinductive properties, which has encouraged researchers to find ways to further improve its behavior *in vivo* [9]. In addition, the use of low-level laser (LLL) has been studied as an alternative to speed healing in larger bone defects [10, 11].

The effects related to LLL include increased vascularity, increased osteoblastic activity [12], organization of collagen fibers, and changes in mitochondrial and intracellular levels of adenosine triphosphate [12, 13]. It is a noninvasive method to stimulate osteogenesis [13, 14] and accelerate the healing of bone defects [12–14].

Positive [11, 13, 15] and negative [16, 17] results have been reported in both *in vivo* and *in vitro* studies [11, 15] regarding the repair of soft or mineralized tissue [18, 19], but few

studies have evaluated the role of LLL associated with bone substitutes [20, 21].

Therefore, the purpose of this study was to histologically evaluate the effect of low-level laser on the healing of critical size defects (CSD) in rat calvaria, filled with autogenous or inorganic bovine bone grafts.

2. Material and Methods

2.1. Experimental Design. The experimental protocol was approved by the Institutional Review Board on Animal Studies of Bauru School of Dentistry, University of São Paulo.

A total of 60 male rats (*Rattus norvegicus*, albinus, Wistar) weighing between 250 and 300 g were utilized. The animals were maintained in an environment with 12-hour cycle of light per day and temperature between 22 and 24°C. Throughout the experiment, the animals received selected solid diet and water *ad libitum*. The animals were randomly assigned to the following experimental groups ($n = 10$): (1) group C—control defect filled with blood clot; (2) group LLL—LLL (Theralase DMC, São Carlos, Brazil); (3) group AB—autogenous bone; (4) group ABL—autogenous bone + LLL; (5) group OB—inorganic bovine bone/0.25–1 mm (Bio-Oss—Geistlich Pharma AG, Wolhusen, Switzerland); (6) group OBL—inorganic bovine bone + LLL.

2.2. Surgical Procedure. The animals were anesthetized by an intramuscular injection of xylazine (0.02 mL/kg) and ketamine hydrochloride (0.4 mL/kg). After trichotomy and antisepsis of the dorsal part of the skull of each animal, a semilunar incision was made in the calvaria and a full-thickness flap was raised in posterior direction. A 5 mm diameter CSD was created with a trephine at low speed under thorough irrigation with sterile saline. The defect included a portion of the sagittal suture. The dura mater and the brain were preserved during craniotomy. The full thickness of parietal bone was gently removed [13, 22].

With the aid of a previously made surgical guide, two L-shaped marks were made, one being at 2 mm anteriorly and the other one being at 2 mm posteriorly to the margins of the surgical defect, with a FG-700 truncated carbide cone bur under continuous irrigation with sterile saline and then filled with amalgam [13, 22].

The major axis of each “L” was located on a craniocaudal longitudinal imaginary line that divided the surgical defect into half. These markings were useful to identify the middle of the original surgical defect during laboratory processing and also to locate the original bone margins during histometric analysis [13, 22].

After fabrication of the L-shaped mark, the defect was filled according to each group. In group C, it was only filled with blood clot. Group LLL was filled with blood clot and was submitted to LLL application. In group OB, the defects were filled with 0.02 g of inorganic bovine bone, and group OBL was filled with the same amount of inorganic bovine bone followed by LLL application. In group AB, the calvaria defect was filled with autogenous bone obtained from ground calvaria bone harvested with the trephine; the same was

performed for group ABL, which was thereafter submitted to LLL application.

To standardize the amount of OB used in each defect, the AB was removed from the ground calvaria using a syringe with millimeter markings and weighed on a precision scale. The same weight (0.02 g) and volume (1 mm³) were used for the OB.

The flap was then repositioned and sutured with 4–0 silk suture. Each animal received an intramuscular injection of 24,000 units of penicillin G-benzathine.

All surgical procedures were performed by a single operator, previously trained in a previous study [13].

2.3. Protocol of Low-Level Laser Therapy. The laser used was Theralase DMC (GaAlAs, $\lambda = 780$ nm, 100 mW, $\Phi 0.05$ cm², 210 J/cm² of energy density, 60 s/point, 6 J/point, continuous mode). The applications were made at four points on the surgical wound surface following a clockwise direction (12 h, 3 h, 6 h, and 9 h positions) and a central point [13]. In the LLL group, application was performed after filling with blood clot, while in the other groups application was performed after insertion of the respective graft material (AB and OB).

2.4. Tissue Processing. The animals were killed at 30 days postoperatively with 5 mg/mL of the association of ketamine and xylazine. The original surgical defect area and surrounding tissues were removed en bloc. The specimens were fixed in 10% formalin solution, rinsed in water, and decalcified in an 18% ethylene diamine tetraacetic acid solution.

After decalcification, each specimen was longitudinally divided into two blocks, exactly over the center of the original surgical defect, using the main axes of each amalgam marking as reference. In addition, cross-sections were performed tangentially to the lowest axis on both “L” markings, so that the end of each specimen measured 9 mm in length. This allowed accurate determination of the boundaries of the original surgical defect during histometric analysis [13, 22].

The specimens were then processed and embedded in paraffin. Longitudinal serial sections with 6 μ m thickness were obtained starting from the center of the original surgical defect. The sections were stained with hematoxylin and eosin (HE) for light microscopy analysis.

2.5. Histomorphometric Analysis. The histological and histometric analyses were performed by a previously calibrated examiner blinded to the experimental groups. Four histological sections were selected, representing the central area of the original surgical defect. Images of the histological sections were captured by a digital camera SPOT RT3-2540 Color Slider 2.0 MP connected to the Olympus BX50 microscope at 2x magnification and saved on a computer. For each animal, new bone formation (NBF) values were calculated by the arithmetic mean of three most central histological sections of the calvaria, and another section was used for histological analysis. The histometric analysis was performed on the ImageLab 2000 software (Bio Diracon Informática Ltd., Vargem Grande do Sul, SP, Brazil) [13, 22].

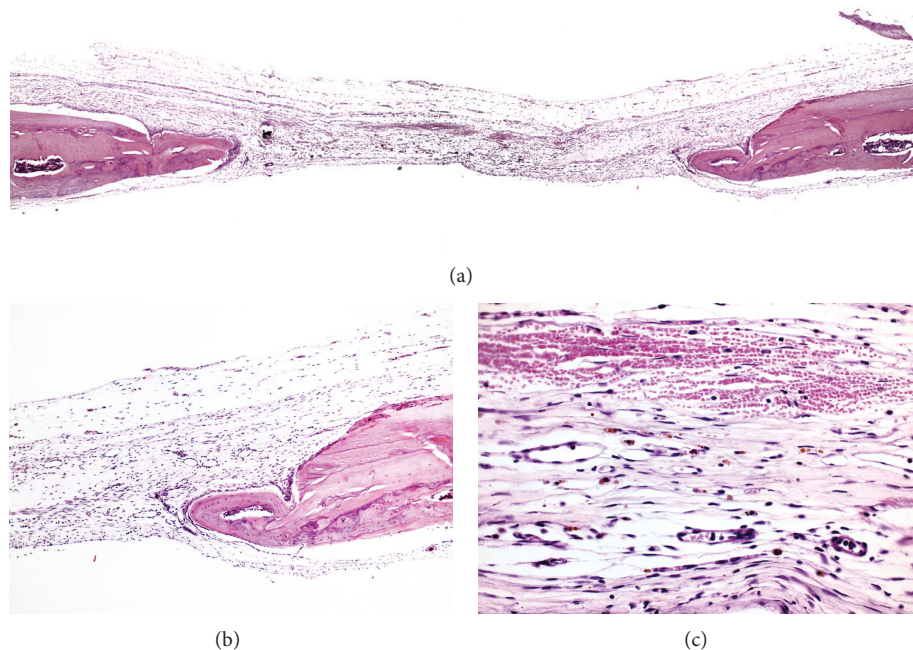


FIGURE 1: Photomicrographs of group C. (a) Panoramic view of the defect (4x); (b) defect filled with bundles of collagen fibers (40x); (c) small amount of newly formed bone (asterisk) along the margins of the surgical defect (10x). Hematoxylin and eosin.

The following criteria, based on the methodology proposed by Furlaneto et al. [22], were followed to standardize the histometric analysis.

- (1) The total area (TA) to be analyzed corresponded to the total area of the original surgical defect. This area was determined by identifying the external and internal surfaces of the original calvaria and the left and right margins of the surgical defect. These surfaces were connected with lines drawn following their respective curvatures. Considering the total length of the histological specimen (9 mm), 2 mm was measured from the left and right ends of the specimen toward the center in order to determine the boundaries of the original surgical defect.
- (2) The area of new bone formation (NBF) and the remaining particle areas (RPA) of the implanted materials were delineated within the boundaries of the TA.
- (3) The TA was measured in mm^2 and 100% of the area being analyzed was considered. The NBF and RPA were also measured in mm^2 and calculated as percentages of TA in accordance with the following formula: $\text{NBF} (\text{mm}^2) / \text{TA} (\text{mm}^2) \times 100$.

2.6. Statistical Analysis. For each animal, the values of NBF and RPA were represented by the arithmetic mean of the four most central histological sections of the calvaria. The values found did not pass the normality test (Shapiro-Wilk). Thus, they were subjected to the nonparametric Kruskal-Wallis test followed by the Dunn test. Analysis of the statistical

test power was verified with a minimum power of 0.86. The differences were considered statistically significant when $P < 0.05$, at a confidence level of 95%.

3. Results

During the laboratory processing, 1 specimen from group C, 3 specimens from group LLL, 1 specimen from group AB, and 2 specimens from group ABL were lost.

3.1. Qualitative Histological Analysis. In all groups absence of inflammatory infiltrate was observed.

In group C, virtually the entire length of the surgical wound was filled by connective tissue with collagen fibers orientated parallel to the wound surface. A small amount of new bone formation was observed along the margins of the surgical defect (Figure 1). Complete regenerated bone repair of the defect did not occur in any specimen.

New bone formation surrounded by an osteoid matrix was observed in some specimens in group LLL. The tissues presented parallel oriented bundles of collagen fibers and absence of inflammatory infiltrate. New bone formation extending linearly toward the center of the original defect was observed in two specimens. Areas of remodeled bone were also observed at the region of old bone, which was preserved (Figure 2).

In group AB, the connective tissue was well organized within the surgical defect, with formation of osteoid matrix, presence of fibroblasts, and absence of inflammatory infiltrate. The new bone formation was present in variable extensions at the margins of the defect and around the grafted

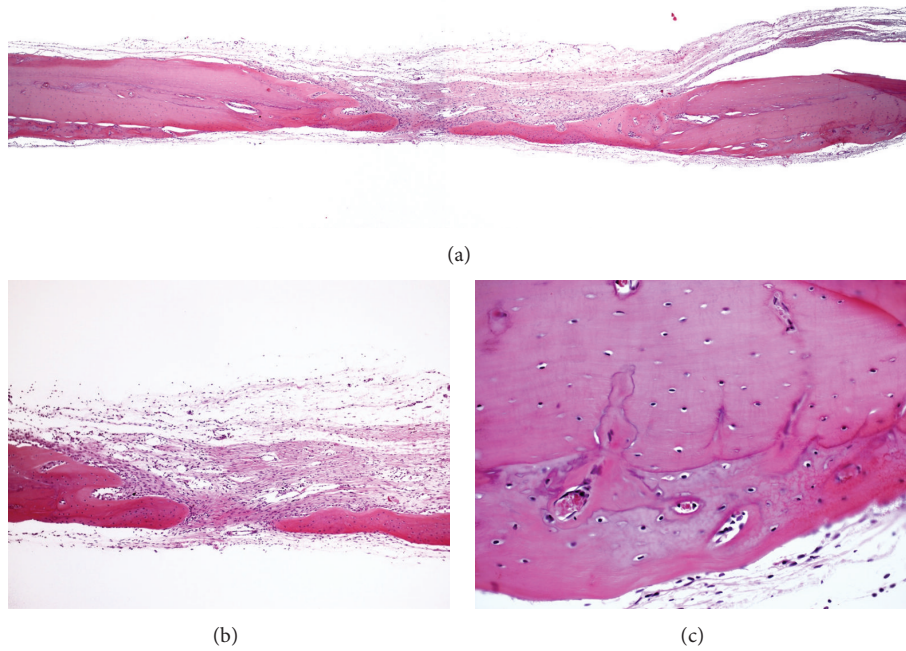


FIGURE 2: Photomicrographs of group LLL. (a) Panoramic view of the surgical defect (4x); (b) bone formation extending toward the center of the original surgical defect (10x); (c) bone remodeling in the region of old bone that was preserved (40x). Hematoxylin and eosin.

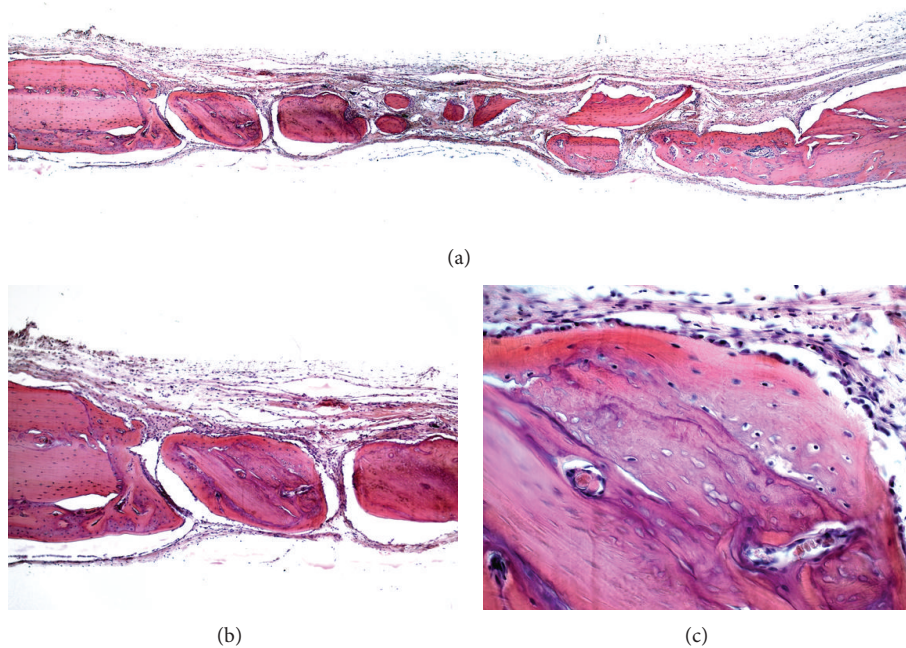


FIGURE 3: Photomicrographs of group AB. (a) Panoramic view of the surgical defect (4x); (b) newly formed bone tissue along the margins of the surgical defect and bone graft particles (10x); (c) autogenous bone particle surrounded by new bone formation (40x).

bone particles (Figure 3). In only one specimen, bone graft particles were not observed.

The osteoid matrix was observed in all specimens in group ABL. New bone formation was present in variable

extensions. Three specimens (37.5%) showed new bone formation toward the center of the surgical defect. Grafted bone particles were also observed, most of which had new bone tissue at the periphery (Figure 4).

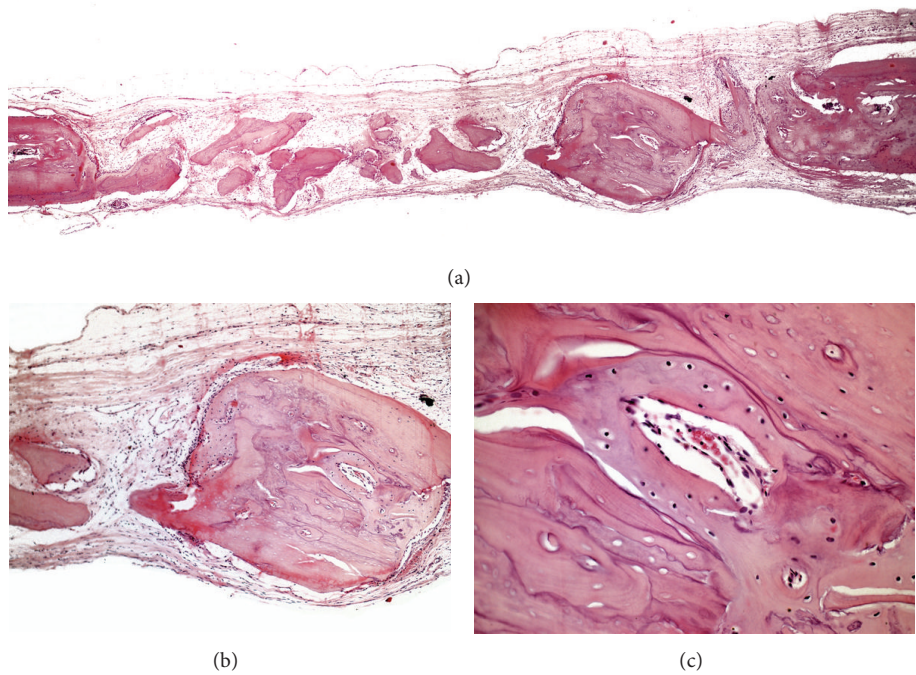


FIGURE 4: Photomicrographs of group ABL. (a) Panoramic view of the surgical defect (4x); (b) autogenous bone particles with new bone formation at the periphery (10x); (c) area of new formation and remodeling of the autogenous bone particle (40x).

TABLE 1: Means and standard deviations of the amount of newly formed bone.

Groups	N	Mean	Standard deviation (sd)	Q25	Median	Q75
C ^a	9	9.96	4.50	8.58	9.52	13.33
L ^b	7	4.67	8.66	43.96	44.58	55.41
AB ^{a,b}	9	30.98	16.59	20.96	25.10	36.24
ABL ^b	8	39.15	16.72	26.89	40.41	53.32
BO ^a	10	11.36	7.89	6.30	9.49	11.57
BOL ^b	10	48.57	28.22	35.76	42.22	74.66

Same letters represent no statistical difference (significance level of 5%).

In OB group, parallel oriented collagen fibers were observed. Inorganic bovine bone particles were present, many with osteoclasts in their periphery. In most specimens there was a slight bone formation at the margins of the defect (Figure 5).

Two specimens in group OB presented new bone formation extending toward the center of the defect, maintaining the original thickness of the calvaria. New bone tissue and osteoclasts were observed at the periphery of the remaining inorganic bovine bone particles. Inflammatory infiltrate was not observed (Figure 6).

3.2. *Histomorphometric and Statistical Analysis.* The groups irradiated with LLL showed higher NBF averages. Correlations were statistically significant ($P < 0.05$) between groups OB \times OBL; LLL \times OB; OB \times ABL; OBL \times C; C \times LLL; C \times ABL (Table 1, Figure 7).

The groups irradiated with LLL had lower RPA averages. There was statistically significant difference ($P < 0.05$) between OB \times OBL and OB \times ABL groups (Table 2, Figure 8).

4. Discussion

The improvement of vascularization after LLL in this study is one of the possible mechanisms for the clinical efficacy of that treatment [12, 13, 23–25]. It has also been reported that LLL increases the osteoblast and osteoclast activity [26] and stimulates production of the bone matrix and the formation of bone callus [25, 27] but also accelerates the dynamics of the bone matrix by modifying the expression of the extracellular matrix components and increasing the area of new bone formation, which reduces the time necessary for bone healing [28].

TABLE 2: Means and standard deviations of the remaining particle.

Groups	N	Mean	Standard deviation (sd)	Q25	Median	Q75
AB ^{a,b}	9	9.16	7.10	4.35	7.04	13.46
ABL ^b	8	3.66	2.79	1.08	4.04	5.84
BO ^a	10	38.73	6.95	35.72	37.71	42.78
BOL ^b	10	16.74	15.25	0.00	22.42	28.23

Same letters represent no statistical difference (significance level of 5%).

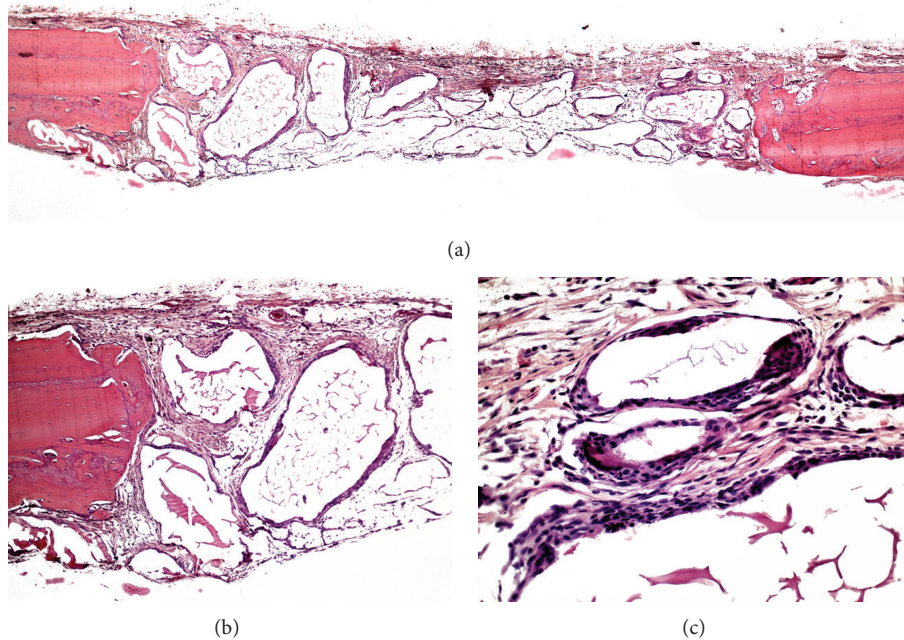


FIGURE 5: Photomicrographs of group OB. (a) Panoramic view of the surgical defect (4x); (b) bone formation along the margins of the defect (10x); (c) osteoclasts in the vicinity of bovine bone graft particles (40x).

Another explanation for the accelerated bone healing observed for groups irradiated with LLL is that the undifferentiated mesenchymal cells can be positively biomodulated to become osteoblasts and evolve to osteocytes faster. It is known that the osteogenic potential of the mesenchymal cells depends, in addition to genetic factors, on induced local and systemic factors. LLL could act as such an inductor factor [24, 29, 30].

It has been reported that the biomodulation of the LLL depends on the wavelength used, since tissue components can influence the dispersion of light [12, 23, 29]. In the infrared spectrum the laser can provide increased osteoblast proliferation, collagen deposition, and bone formation [12, 29]. In this study, there was greater bone formation in the group irradiated with laser (group LLL) compared to the nonirradiated group (group C).

There are no universally accepted parameters for using the LLL. Different irradiation protocols are found with different activation materials, wavelengths, and even dose and number of applications, precluding the comparison of results and choice of treatment parameters [31]. Similar to previous

studies [13, 15], this work intended to establish guidelines for a transoperative protocol immediately involving a single laser application in direct contact with the wound area and confirmed the beneficial effects of a single session irradiation for bone healing of the defect, demonstrating that this type of treatment may be feasible, easy, and fast.

When evaluating the area of new bone formation in this study, the results for groups irradiated with LLL were similar to the AB and ABL groups. This would suggest that only the application of laser would already be beneficial in bone regeneration with this application protocol. Moreover, the association of AB and LLL showed superior results when compared to the treatment with AB alone. The lack of statistically significant difference between the AB and ABL groups can be assigned to the fact that autogenous bone alone can already be considered a very good grafting material. Starting from a high level of excellence, the laser would not be able to add benefits to the point that it would be statistically different.

Although no statistically significant difference was observed in the NBF and RPA between groups AB and

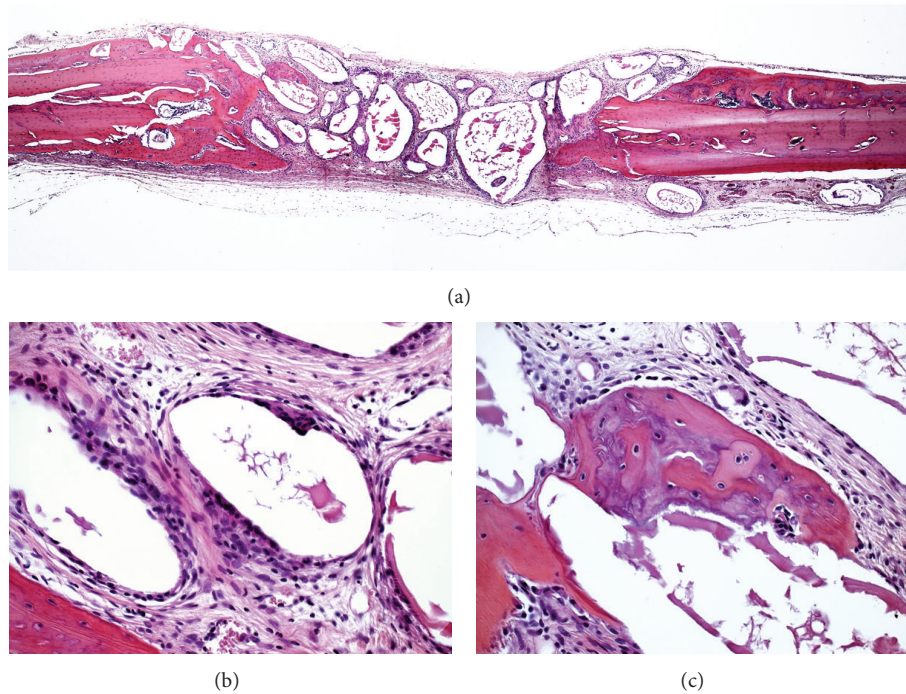


FIGURE 6: Photomicrographs of group OB. (a) Panoramic view of the surgical defect (4x); (b) bone formation along the margins of the defect (10x); (c) osteoclasts in the vicinity of bovine bone graft particles (40x).

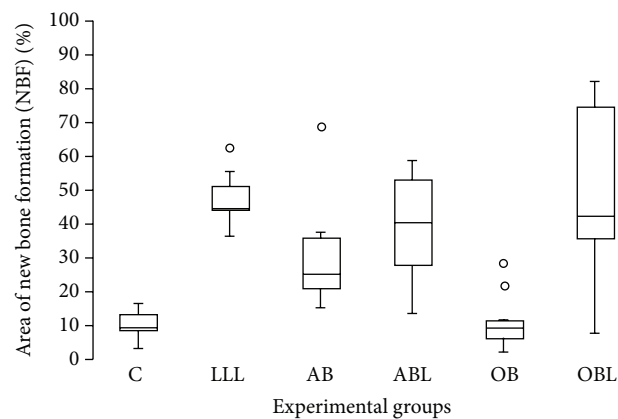


FIGURE 7: Distribution of new bone formation area for all experimental groups.

ABL, it is believed that the laser has also been able to speed up the process of bone remodeling when the allograft was used, since the histological analysis revealed that, in the irradiated group, there were specimens with new bone formation toward the center of the surgical defect, and most graft particles showed new bone formation at the periphery. Thus, the association of LLL and AB could be suggested as advantageous to accelerate cell proliferation and increase the new bone volume, thus aiding the integration of the graft into the recipient area, corroborating the findings of other studies [13, 14, 23]. This is recommended as an additional treatment modality in the regeneration of bone defects, since it is a noninvasive method to stimulate osteogenesis [14] and accelerate the healing of bone defects [12–14].

The resorption of inorganic bovine bone particles is still a conflicting issue in the literature. There are reports that particles in the interior of bone defects fail to resorb and remain like a motionless body surrounded by the host bone [31, 32]. Moreover, after months of healing, osteoblastic activity is observed in the particles and it is believed that, with time, these particles remodel themselves and meanwhile the new bone is formed; however, it appears to be a slow process [33]. It is believed that the laser has accelerated the process of bone formation and resorption of such particles, since the OBL group showed a statistically significant difference in the NBF and RPA when compared to the OB. This may be due to the fact that the laser improves vascularization [12, 23–25], increases the osteoclastic [26] and osteoblastic activity [12],

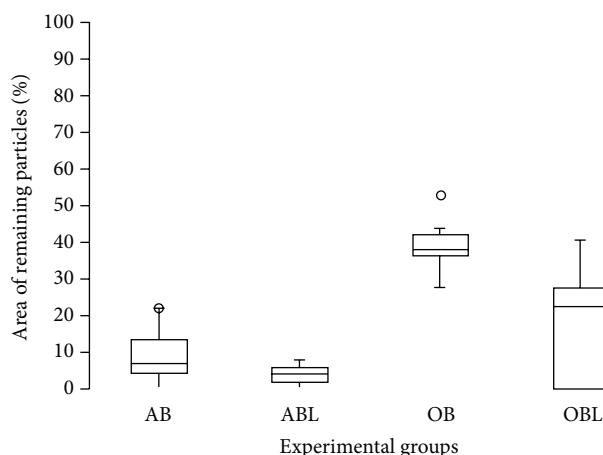


FIGURE 8: Distribution of area of the remaining particle for groups receiving graft material.

stimulates the production of the bone matrix [34], and can act as an osteoinductive factor [24, 29].

In the present study, the fact that all groups irradiated with LLL presented superior results to group C and groups receiving only grafts suggests that this type of therapy may be effective in the healing of bone defects, especially when associated with a filling material.

5. Conclusion

The LLL accelerated the healing of bone defects and the resorption of the graft material particles.

Conflict of Interests

The authors declare that there is no conflict of interests regarding the publication of this paper.

Acknowledgment

The authors would like to thank São Paulo Research Foundation (FAPESP) for the Master's Scholarship (2010/13170-3) and for the Research Grant (2010/10538-0).

References

- [1] K.-U. Lewandrowski, J. D. Gresser, D. L. Wise, and D. J. Trantolo, "Bioresorbable bone graft substitutes of different osteoconductivities: a histologic evaluation of osteointegration of poly(propylene glycol-co-fumaric acid)-based cement implants in rats," *Biomaterials*, vol. 21, no. 8, pp. 757–764, 2000.
- [2] P. V. Giannoudis, H. Dinopoulos, and E. Tsiridis, "Bone substitutes: an update," *Injury*, vol. 36, no. 3, pp. S20–S27, 2005.
- [3] M. Hallman and A. Thor, "Bone substitutes and growth factors as an alternative/complement to autogenous bone for grafting in implant dentistry," *Periodontology 2000*, vol. 47, no. 1, pp. 172–192, 2008.
- [4] C. M. Schmitt, H. Doering, T. Schmidt, R. Lutz, F. W. Neukam, and K. A. Schlegel, "Histological results after maxillary sinus augmentation with Straumann BoneCeramic, Bio-Oss, Puros, and autologous bone. A randomized controlled clinical trial," *Clinical Oral Implants Research*, vol. 24, no. 5, pp. 576–585, 2013.
- [5] G. F. Rogers and A. K. Greene, "Autogenous bone graft: basic science and clinical implications," *Journal of Craniofacial Surgery*, vol. 23, no. 1, pp. 323–327, 2012.
- [6] A. S. Herford and J. S. Dean, "Complications in bone grafting," *Oral and Maxillofacial Surgery Clinics of North America*, vol. 23, no. 3, pp. 433–442, 2011.
- [7] P. Amerio, G. Vianale, M. Reale, R. Muraro, A. Tulli, and A. Piatelli, "The effect of deproteinized bovine bone on osteoblast growth factors and proinflammatory cytokine production," *Clinical Oral Implants Research*, vol. 21, no. 6, pp. 650–655, 2010.
- [8] L. Ohayon, "Ridge enlargement using deproteinized bovine bone and a bioresorbable collagen membrane: a tomodesitometric, histologic, and histomorphometric analysis," *The International Journal of Periodontics & Restorative Dentistry*, vol. 31, no. 3, pp. 237–245, 2011.
- [9] J. Torres, F. M. Tamimi, I. F. Tresguerres et al., "Effect of solely applied platelet-rich plasma on osseous regeneration compared to Bio-Oss: a morphometric and densitometric study on rabbit calvaria," *Clinical Implant Dentistry and Related Research*, vol. 10, no. 2, pp. 106–112, 2008.
- [10] E. Fávoro-Pípi, D. A. Ribeiro, J. U. Ribeiro et al., "Low-level laser therapy induces differential expression of osteogenic genes during bone repair in rats," *Photomedicine and Laser Surgery*, vol. 29, no. 5, pp. 311–317, 2011.
- [11] A. N. S. Júnior, A. L. Pinheiro, M. G. Oliveira, R. Weismann, L. M. Ramalho, and R. A. Nicolau, "Computerized morphometric assessment of the effect of low-level laser therapy on bone repair: an experimental animal study," *Journal of Clinical Laser Medicine & Surgery*, vol. 20, no. 2, pp. 83–87, 2002.
- [12] D. Barbosa, R. A. de Souza, M. Xavier, F. F. da Silva, E. Â. Arisawa, and A. G. J. B. Villaverde, "Effects of low-level laser therapy (LLL) on bone repair in rats: optical densitometry analysis," *Lasers in Medical Science*, vol. 28, no. 2, pp. 651–656, 2013.
- [13] A. L. P. F. de Almeida, I. L. Medeiros, M. J. S. Cunha, M. C. Sbrana, P. G. F. de Oliveira, and L. A. Esper, "The effect of low-level laser on bone healing in critical size defects treated with or without autogenous bone graft: an experimental study in rat calvaria," *Clinical Oral Implants Research*, 2013.

- [14] R. V. da Silva and J. A. Camilli, "Repair of bone defects treated with autogenous bone graft and low-power laser," *Journal of Craniofacial Surgery*, vol. 17, no. 2, pp. 297–301, 2006.
- [15] H. Pretel, R. F. Z. Lizarelli, and L. T. O. Ramalho, "Effect of low-level laser therapy on bone repair: histological study in rats," *Lasers in Surgery and Medicine*, vol. 39, no. 10, pp. 788–796, 2007.
- [16] E. J. Luger, S. Rochkind, Y. Wollman, G. Kogan, and S. Dekel, "Effect of low-power laser irradiation on the mechanical properties of bone fracture healing in rats," *Lasers in Surgery and Medicine*, vol. 22, no. 2, pp. 97–102, 1998.
- [17] G. Anneroth, G. Hall, H. Rydén, and L. Zetterqvist, "The effect of low-energy infra-red laser radiation on wound healing in rats," *British Journal of Oral and Maxillofacial Surgery*, vol. 26, no. 1, pp. 12–17, 1988.
- [18] A. Stein, D. Benayahu, L. Maltz, and U. Oron, "Low-level laser irradiation promotes proliferation and differentiation of human osteoblasts in vitro," *Photomedicine and Laser Surgery*, vol. 23, no. 2, pp. 161–166, 2005.
- [19] A. Leonida, A. Paiusco, G. Rossi, F. Carini, M. Baldoni, and G. Caccianiga, "Effects of low-level laser irradiation on proliferation and osteoblastic differentiation of human mesenchymal stem cells seeded on a three-dimensional biomatrix: in vitro pilot study," *Lasers in Medical Science*, vol. 28, no. 1, pp. 125–132, 2013.
- [20] A. L. B. Pinheiro, F. D. A. L. Limeira Júnior, M. E. M. Gerbi, L. M. P. Ramalho, C. Marzola, and E. A. C. Ponzi, "Effect of low level laser therapy on the repair of bone defects grafted with inorganic bovine bone," *Brazilian Dental Journal*, vol. 14, no. 3, pp. 177–181, 2003.
- [21] A. L. B. Pinheiro, L. G. P. Soares, A. F. S. Barbosa, L. M. P. Ramalho, and J. N. dos Santos, "Does LED phototherapy influence the repair of bone defects grafted with MTA, bone morphogenetic proteins, and guided bone regeneration? A description of the repair process on rodents," *Lasers in Medical Science*, vol. 27, no. 5, pp. 1013–1024, 2012.
- [22] F. A. C. Furlaneto, M. J. H. Nagata, S. E. Fucini, T. M. Deliberador, T. Okamoto, and M. R. Messoria, "Bone healing in critical-size defects treated with bioactive glass/calcium sulfate: a histologic and histometric study in rat calvaria," *Clinical Oral Implants Research*, vol. 18, no. 3, pp. 311–318, 2007.
- [23] J. B. B. Weber, A. L. B. Pinheiro, M. G. de Oliveira, F. A. M. Oliveira, and L. M. P. Ramalho, "Laser therapy improves healing of bone defects submitted to autologous bone graft," *Photomedicine and Laser Surgery*, vol. 24, no. 1, pp. 38–44, 2006.
- [24] N. S. Aboelsaad, M. Soory, L. M. A. Gadalla et al., "Effect of soft laser and bioactive glass on bone regeneration in the treatment of infra-bony defects (a clinical study)," *Lasers in Medical Science*, vol. 24, no. 3, pp. 387–395, 2009.
- [25] Y. Ozawa, N. Shimizu, G. Kariya, and Y. Abiko, "Low-energy laser irradiation stimulates bone nodule formation at early stages of cell culture in rat calvarial cells," *Bone*, vol. 22, no. 4, pp. 347–354, 1998.
- [26] R. A. Nicolau, V. Jorgetti, J. Rigau, M. T. T. Pacheco, L. M. dos Reis, and R. A. Zangaro, "Effect of low-power GaAlAs laser (660 nm) on bone structure and cell activity: an experimental animal study," *Lasers in Medical Science*, vol. 18, no. 2, pp. 89–94, 2003.
- [27] S. K. Shakouri, J. Soleimanpour, Y. Salekzamani, and M. R. Oskuie, "Effect of low-level laser therapy on the fracture healing process," *Lasers in Medical Science*, vol. 25, no. 1, pp. 73–77, 2010.
- [28] L. A. D. S. Merli, V. P. de Medeiros, L. Toma et al., "The low level laser therapy effect on the remodeling of bone extracellular matrix," *Photochemistry and Photobiology*, vol. 88, no. 5, pp. 1293–1301, 2012.
- [29] A. L. B. Pinheiro and M. E. M. M. Gerbi, "Photoengineering of bone repair processes," *Photomedicine and Laser Surgery*, vol. 24, no. 2, pp. 169–178, 2006.
- [30] L. Abramovitch-Gottlieb, T. Gross, D. Naveh et al., "Low level laser irradiation stimulates osteogenic phenotype of mesenchymal stem cells seeded on a three-dimensional biomatrix," *Lasers in Medical Science*, vol. 20, no. 3–4, pp. 138–146, 2005.
- [31] J. P. da Silva, M. A. da Silva, A. P. F. Almeida, I. Lombardi Junior, and A. P. Matos, "Laser therapy in the tissue repair process: a literature review," *Photomedicine and Laser Surgery*, vol. 28, no. 1, pp. 17–21, 2010.
- [32] R. Ewers, W. Goriwoda, C. Schopper, D. Moser, and E. Spassova, "Histologic findings at augmented bone areas supplied with two different bone substitute materials combined with sinus floor lifting," *Clinical Oral Implants Research*, vol. 15, no. 1, pp. 96–100, 2004.
- [33] T. Berglundh and J. Lindhe, "Healing around implants placed in bone defects treated with Bio-Oss: an experimental study in the dog," *Clinical Oral Implants Research*, vol. 8, no. 2, pp. 117–124, 1997.
- [34] K. M. AlGhamdi, A. Kumar, and N. A. Moussa, "Low-level laser therapy: a useful technique for enhancing the proliferation of various cultured cells," *Lasers in Medical Science*, vol. 27, no. 1, pp. 237–249, 2012.

Research Article

Osteoconductive Potential of Barrier NanoSiO₂ PLGA Membranes Functionalized by Plasma Enhanced Chemical Vapour Deposition

**Antonia Terriza,¹ Jose I. Vilches-Pérez,² Emilio de la Orden,²
Francisco Yubero,¹ Juan L. Gonzalez-Caballero,² Agustin R. González-Elípe,¹
José Vilches,² and Mercedes Salido²**

¹ Nanotechnology on Surfaces Laboratory, Instituto de Ciencia de Materiales de Sevilla (CSIC), Universidad de Sevilla, Avenida Américo Vespucio 49, 41092 Seville, Spain

² Facultad de Medicina, Servicios Centrales de Investigación en Ciencias de la Salud, University of Cadiz, Dr. Marañón 3, 11002 Cadiz, Spain

Correspondence should be addressed to Mercedes Salido; mercedes.salido@uca.es

Received 26 February 2014; Accepted 1 April 2014; Published 4 May 2014

Academic Editor: David M. Dohan Ehrenfest

Copyright © 2014 Antonia Terriza et al. This is an open access article distributed under the Creative Commons Attribution License, which permits unrestricted use, distribution, and reproduction in any medium, provided the original work is properly cited.

The possibility of tailoring membrane surfaces with osteoconductive potential, in particular in biodegradable devices, to create modified biomaterials that stimulate osteoblast response should make them more suitable for clinical use, hopefully enhancing bone regeneration. Bioactive inorganic materials, such as silica, have been suggested to improve the bioactivity of synthetic biopolymers. An *in vitro* study on HOB human osteoblasts was performed to assess biocompatibility and bioactivity of SiO₂ functionalized poly(lactide-co-glycolide) (PLGA) membranes, prior to clinical use. A 15 nm SiO₂ layer was deposited by plasma enhanced chemical vapour deposition (PECVD), onto a resorbable PLGA membrane. Samples were characterized by X-ray photoelectron spectroscopy, atomic force microscopy, scanning electron microscopy, and infrared spectroscopy (FT-IR). HOB cells were seeded on sterilized test surfaces where cell morphology, spreading, actin cytoskeletal organization, and focal adhesion expression were assessed. As proved by the FT-IR analysis of samples, the deposition by PECVD of the SiO₂ onto the PLGA membrane did not alter the composition and other characteristics of the organic membrane. A temporal and spatial reorganization of cytoskeleton and focal adhesions and morphological changes in response to SiO₂ nanolayer were identified in our model. The novel SiO₂ deposition method is compatible with the standard sterilization protocols and reveals as a valuable tool to increase bioactivity of resorbable PLGA membranes.

1. Introduction

Cell-biomaterial interaction is a major challenge for tissue engineering, since not only the physico-mechanical-chemical features of the natural extracellular matrix must be mimicked, but also a successful cell to biomaterial adhesion should be achieved in the shortest time. Cell adhesion is critical in the first stages of the tissue engineering methodology where adhesion is the basis and the key process that allows other important cell activities such as migration and growth. In the fields of tissue engineering and guided bone regeneration (GBR), an appropriate cell culture scaffold is required to enhance cell attachment, proliferation, and differentiation

in vitro, as cells interact with native or topographically and chemically tailored structures in many ways [1–5].

The GBR therapeutic approach is based on the concept that regeneration of osseous defects is attainable via the application of occlusive membranes, resorbable or nonresorbable, which mechanically exclude nonosteogenic cell populations from the surrounding soft tissues. Nowadays GBR is subject of growing interest due to the increasing needs for permanent, temporary, or biodegradable orthopaedic devices designed for bone repair and regeneration [6–11].

A variety of polymeric bioresorbable GBR membranes that permit single-step procedures, thus reducing patient discomfort and costs, and potential surgical complications

are currently available. Polymeric coatings for biomedical devices are especially interesting due to the diversity of their chemical and physical properties and natural biopolymers appear promising as biomimetic coatings, as a result of their similarity to human tissues. Although these membranes are biocompatible, nontoxic, or immunogenic and permit mechanical support during bone formation, they do not actually possess bioactive properties to induce osteogenesis [6, 9, 12–14].

Poly(lactide-co-glycolide) (PLGA) is among the few synthetic polymers approved for human clinical use due to its biocompatibility, controllable degradability, and relatively good processability and has been used in the design of scaffolds for bone tissue engineering and for drug delivery purposes [15, 16]. However, the polymer itself is quite bioinert and does not elicit a significant biological response in bone cells [8, 16].

The physicochemical properties of the material at the cell-material interface are decisive for the cell-material interaction, due to its interfacial role between the material and the host tissue, and are able to trigger a wide variety of processes, from the initial inflammatory reaction to ultimate tissue remodelling [13, 17]. Although the bulk properties of materials are important for the overall properties, especially for mechanical strength, a topographical modification of the cell-substrate interface is of utmost importance. Thus, the possibility of tailoring membrane surfaces, in particular in biodegradable devices with bioactive properties, to create modified biomaterials that mimic natural bone extracellular matrix (ECM) and stimulate osteoblast response should make them more suitable for clinical use, hopefully enhancing bone regeneration in the near future [1, 2, 18].

Bioactive inorganic materials, such as silica granules, have been suggested to improve the bioactivity of synthetic biopolymers in promoting the osteogenic performance of osteoblast-like cells. It has been strongly suggested that silicon/silica is functionally active during bone formation with a close relationship between silicate and calcium deposition. Silica is a low cost and biocompatible inorganic material having excellent chemical stability with great commercial value and ideal for tailoring surface topographies [19–24].

We have designed an *in vitro* model in order to assess normal human osteoblasts, HOB, response to a series of SiO₂ functionalized PLGA membranes intended to be used as barrier membranes for bone guided regeneration.

For the synthesis of the PLGA foils we have followed classical synthesis procedures based on the solution/evaporation method [25–27]. A problem encountered by the surface functionalization of these membranes by classical sol-gel or similar wet chemical routes is the degradation of the PLGA when it is exposed to liquid media or treated at relatively high temperatures [28–34]. To avoid these problems, we have followed a new approach consisting of the deposition at room temperature by plasma enhanced chemical vapour deposition (PECVD) of a very thin layer of SiO₂ on the surface of the PLGA membranes (SiO₂/PLGA) [35], in order to achieve a strict control of the deposition conditions without inducing any damage in the PLGA that could efficiently promote the development of bone regenerating cells.

2. Material and Methods

2.1. Cell Culture. HOB human osteoblasts were incubated in Osteoblast Growing Medium with 10% foetal calf serum at 37° and 5% CO₂ until the experiments were started. HOB cells did not exceed ten population doublings. Test surfaces were sterilized under ultraviolet (u.v.) light for 20 min each side, in a laminar flow chamber prior to cell seeding. HOB osteoblasts were seeded at a density of 5000 cells/cm² on test surfaces, that is, bare PLGA or SiO₂/PLGA membranes, and immunolabelled after 24, 48, and 72 hours. HOB osteoblasts, media, and sera were obtained from Promocell (Heidelberg, Germany).

2.2. PLGA Membranes. The PLGA membranes used as substrates were prepared from a 1.5 wt% PLGA dichloromethane solution by evaporation of the solvent on a teflon plate. The size of the membranes was 15 × 15 mm². The thickness of the membranes was of the order of 50 microns.

2.3. Deposition and Characterization of SiO₂ Thin Film Layers. SiO₂ was deposited onto the PLGA membranes by PECVD in a plasma reactor with a remote configuration. The deposition system consisted of a quartz tube with a funnel shape termination attached to a stainless-steel chamber where the samples were placed. The plasma source is a surfatron (Sairem) launcher that was supplied with a microwave power of 60 W. These conditions provide a typical plasma electron density of about $1 \cdot 10^{11} \text{ cm}^{-3}$. Distance from substrate to the quartz tube was 5 cm. The plasma gas and the precursor used were pure Ar (7.5 sccm) and hexamethyldisiloxane (HDMSO, 5 sccm), respectively. Synthesis of the films was carried out at room temperature, working at a pressure of 0.3 Torr. The gas flow was controlled by mass flow controllers (MKS). Both the stainless steel receptacle which contained the precursor and the dosing line were heated at 323 K to prevent any condensation in the tube walls. Before depositing SiO₂, the polymeric substrate was exposed to plasma of pure argon for 2 min, a pretreatment that favours the adhesion of the oxide layer onto the polymer surface. A thin layer of SiO₂ of 15 nm, determined by measuring with an adjacent quartz crystal monitor, was deposited on the polymeric substrate. These measurements were calibrated with the data obtained for thicker layer of SiO₂ deposited on a silicon substrate that were cleaved and examined by scanning electron microscopy. Before the treatments, Ar or the mixture Ar + HDMSO was kept flowing for at least 30 min to ensure the purity of the plasma gas in the reactor [36]. The nonfunctionalized and SiO₂ functionalized membranes will be designated as PLGA and SiO₂/PLGA, respectively. The samples were characterized by X-ray photoelectron spectroscopy (XPS) to determine their surface chemical state and composition, atomic force microscopy (AFM) to ascertain their roughness, scanning electron microscopy (SEM) to assess the film microstructure, infrared spectroscopy (FT-IR) to determine the bonding structure, and water contact angle measurements to check the wetting characteristics of their surfaces. XPS spectra were recorded with a SPECS PHOIBOS-100 spectrometer working in the constant pass energy mode fixed at a value of 20 eV.

The Mg K_{α} radiation was used as excitation source. For calibration of the binding energy scale, a value of 284.6 eV was considered for the Cls component attributed to C–H and C–C bonds. Surface composition was estimated by calculating the area behind the C_{1s} , Si_{2p} , and O_{1s} peaks and by correcting the obtained values with the sensitivity factors of these elements. AFM images were taken with a Cervantes AFM microscope driven with a Dulcinea control system (Nanotec, Madrid, Spain) working in tapping mode and using high frequency cantilevers. The images were processed with Nanotec WSxM software. SEM images were acquired in a Hitachi S4800 microscope. FT-IR spectra were collected in attenuated total reflectance (ATR) mode in a JASCO FT/IR6200 spectrometer, performing 64 scans with a resolution of 0.96 cm^{-1} and a spot size of 1 cm of diameter. Static contact angles of water were determined by the Young method in a SCA20 instrument (Data Physic Instruments, GmbH), with an estimated error of 3%.

2.4. Cell Morphology and Spreading. HOB osteoblasts seeded on test surfaces were daily examined with a DM ILLED Leica phase contrast microscope in order to evaluate cell morphology and spreading, cell alignment, and initial adhesion phase to surfaces, prior to fluorescence and CLSM examination.

2.5. Immunolabelling for Actin Cytoskeletal Organization and Focal Adhesion Expression. At the designed experimental time, cells in each group were washed with pre-warmed phosphate buffered saline (PBS) and fixed with 3.7% paraformaldehyde at room temperature, permeabilized with 0.1% Triton x-100, preincubated in 1% bovine serum albumin in PBS, and then immunolabelled for actin cytoskeleton with rhodamine-phalloidin and for focal adhesion identification with monoclonal antivinculin FITC conjugate. After 20 min samples were twice PBS rinsed prior to mounting with Vectashield (Vector, CA). All chemicals were obtained from Sigma-Aldrich (St. Louis, Mo) unless noted.

2.6. Immunolabelled Cells Examination. Samples were visualized in a Leica TCS-SL confocal microscope. At least five samples were analysed for each experimental group to assess surface influence on cytoskeletal organization, focal adhesion number and development, and cell morphology. Samples were exposed to the lowest laser power that was able to produce a fluorescent signal, with a pinhole of 1 airy. Images were acquired at a resolution of 512×512 , mean voxel size of 209.20 nm.

2.7. Image Analysis. To analyze the differences in focal adhesion number between different sample groups, images were collected and processed. Area, perimeter, roundness, circularity, solidity, and axial ratio were analysed as shape variables. Sample images were collected as frames obtained at 40x magnification and processed using Leica imaging software and Image J software (NIH, <http://rsb.info.nih.gov/ij/>).

2.8. Statistical Analysis. For the variable number of contacts, we used first the nonparametric contrast Kruskal-Wallis and

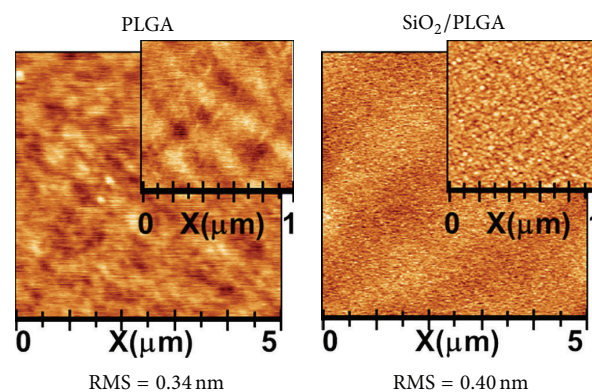


FIGURE 1: AFM images of PLGA (left) and SiO_2 /PLGA (right).

later a two-way ANOVA contrast with the ranges of this variable [37]. Post hoc contrasts were carried out to detect the differences among the experimental groups. For shape variables, a factor analysis was performed in order to reduce the dimension and a two-way ANOVA with the resulting factors to analyze the influence of the experimental conditions. All the analysis was performed with SPSS program.

3. Results

3.1. PLGA Membranes: Deposition and Characterization of SiO_2 Thin Film Layers. The SiO_2 thin films prepared by PECVD presented a homogeneous microstructure and a conformal growth on the PLGA membrane. The 15 nm film surface was rather flat as shown in AFM images (Figure 1) of PLGA and SiO_2 -PLGA samples. In the latter, the deposition of the SiO_2 film only increased the RMS roughness from 0.32 to 0.43 nm, while surface topology slightly changed with the formation of finer grains. Even if the SiO_2 thickness was rather thin (15 nm), the PLGA surface was totally covered by SiO_2 , as can be directly retrieved from the XPS spectra (Figure 2).

The Cls spectrum of the PLGA depicts three components at 284.6, 286.4, and 288.6 eV, attributed to C–C/C–H, C–O, and $>C=O/COOH$ species [22, 23]. This complex spectrum transformed when the PLGA membrane was covered by SiO_2 , where only a Cls component at 284.6 eV, attributed to spurious carbon due to contamination, can be identified. An equivalent modification appears in the O1s spectra, with clearly different widths of PLGA and SiO_2 spectra. The Si_{2p} spectra confirms that the PLGA membrane was free from this element, while the SiO_2 /PLGA samples depict a well-defined Si 2p peak at 103.9 eV, attributed to Si^{4+} ions in SiO_2 [38, 39]. It must be stressed that the deposition by PECVD of the SiO_2 onto the PLGA membrane did not alter the composition and other characteristics of the organic membrane as proved by the FT-IR analysis of samples. The spectral regions reported (Figure 3) for the PLGA and SiO_2 -PLGA samples were very similar and are characterized by the typical shape of the spectra of this polymer. The small increase in the height of the peak at 1050 cm^{-1} observed for the SiO_2 /PLGA sample can be attributed to the contribution at this wavenumbers of

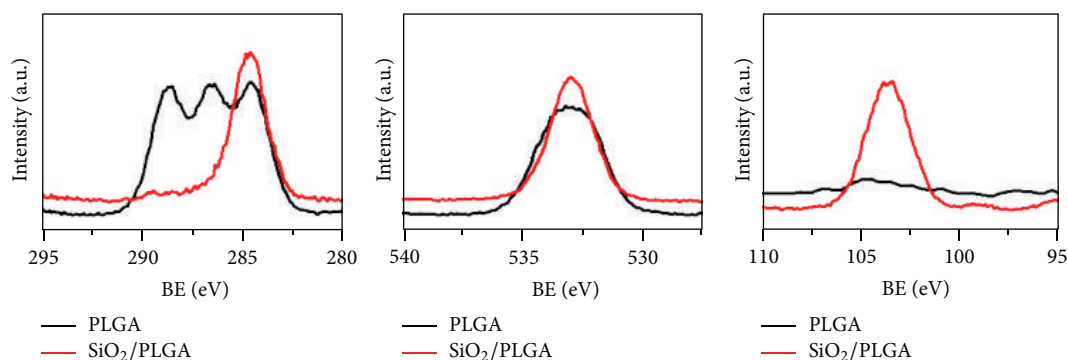


FIGURE 2: From left to right, Cls, O1s, and Si2p photoelectron spectra of PLGA and SiO₂/PLGA as indicated.

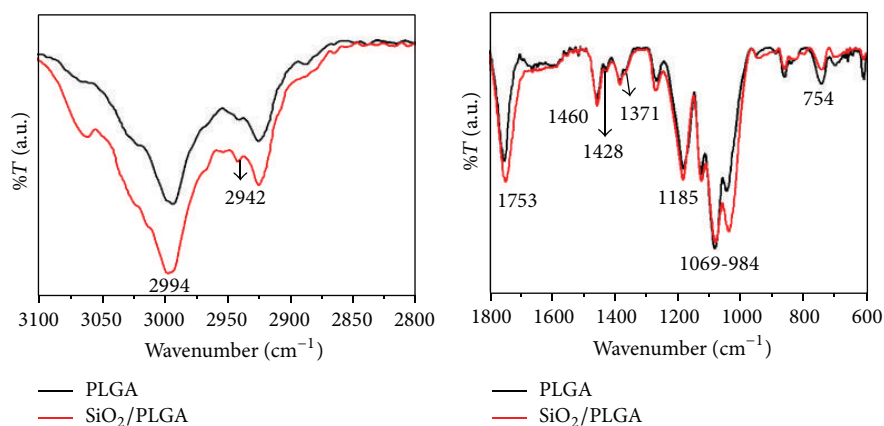


FIGURE 3: FT-IR spectra of the PLGA and SiO₂/PLGA films measured in ATR mode.

the Si–O–Si stretching vibration of the silica network in the SiO₂ film [36]. The other features in the spectra correspond to well-documented vibrations of PLGA polymers: 2994, 2946, 2840 (CH bend), 1753 (C=O ester), 1460, 1428, 1371 (CH₃), 1185, 1080–980 (C–O stretch), and 754 (CH-bend) cm⁻¹ [40]. No significant spectral changes are expected due to the different thickness of the PLGA membrane (50 μm) and the SiO₂ films (15 nm) and the typical thickness proved by ATR analysis (a few tens of microns).

Since wetting behavior and surface tension are important parameters for cell development of cells on bioactive materials [41, 42] the water contact angle was measured for both the PLGA and SiO₂/PLGA membranes and the values obtained were 99.3° and 93.8°, respectively, indicating no significant differences in wetting between these two surfaces.

During the experimental time, no clear signs of degradation were observed in the membranes. During the experimental time, no clear signs of degradation were observed in the membranes. FT-IR, AFM, and XPS analysis of the surface of the PLGA and SiO₂/PLGA membranes extracted from the PBS and gently dried in air did not reveal significant changes suggesting any significant degradation. membrane degradation (loss of physical integrity, changes in color, etc.) could only be observed after 20 weeks of immersion in liquid media, although clear signs of degradation (loss of physical integrity, changes in color, etc.) could be observed after 20

weeks of immersion in liquid media. The exposure of PLGA and SiO₂/PLGA membranes to u.v. irradiation under similar conditions to those used in the sterilization protocol prior to cell seeding did not produce any detectable change.

3.2. Living Cell Examination: Cell Morphology and Spreading.

Living HOB cells examination revealed a successful cell spreading on silica treated membranes, with cell elongation and marked filopodial emission, and the establishment of clear cell contacts and attachment to the functionalized surface in the first 24 hours. Cells clustered and elongated during the next hours, and after 48 hours in culture, cell spreading evolved to a clear cell packaging, with osteoblasts well adhered to the silica treated surface and to the neighboring cells (Figures 4(b) and 4(d)). Cells grown on bare PLGA membranes spread evenly although clearly adhered to surfaces, showing some lamellipodia in the first 24 hours but without clear cell clustering after 48 hours in culture (Figures 4(a) and 4(c)).

3.3. Actin Cytoskeletal Organization and Vinculin Immunolabelling of Focal Adhesion Sites.

Osteoblasts grown on the SiO₂ functionalized PLGA membranes showed defined stress fibers formation, with a clear polarization of actin cytoskeleton towards strongly evident vinculin positive sites. Cell

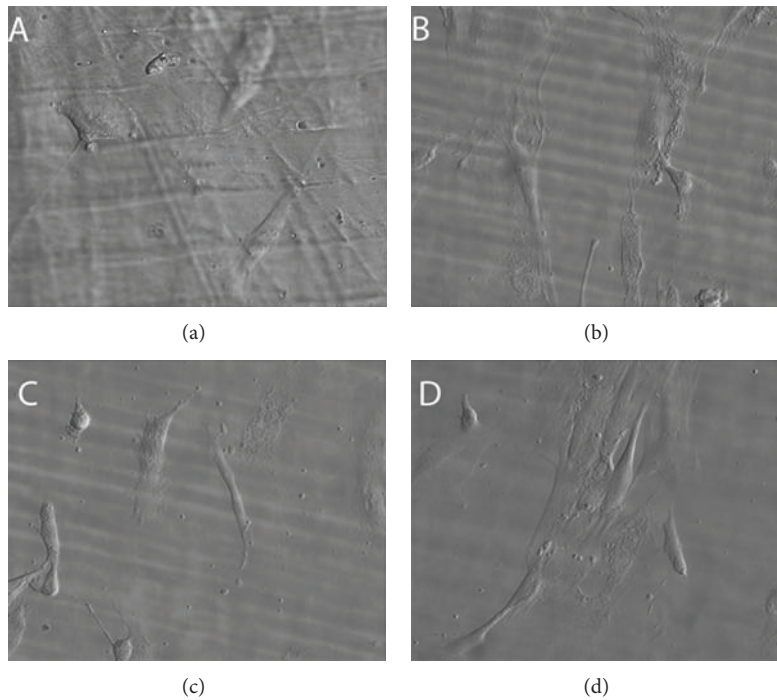


FIGURE 4: HOB cells distribution and spreading after 24 (a, b) and 48 (c, d) hours in culture. Both (b) and (d) represent osteoblasts grown on silica treated PLGA membranes and (a) and (c) represent osteoblasts grown on bare PLGA. All images were obtained in the phase contrast microscope, magnification 40x.

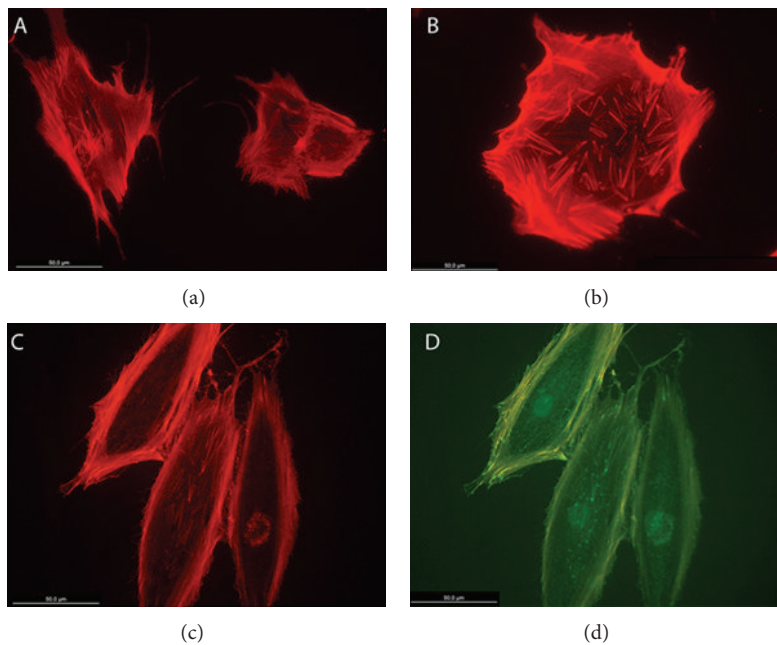


FIGURE 5: HOB cells grown on bare PLGA and immunolabelled, 48 hours (a, b) and 72 hours (c, d) after seeding, with rhodamine-phalloidin for actin cytoskeleton (red) and antivinculin antibody (green) for focal adhesion sites.

polarization was clearly determined by SiO_2 functionalized surfaces, with osteoblasts showing extensive lamellipodial emission reinforced with vinculin positive focal adhesion in the leading edge and supported by a highly defined actin network. Focal adhesions appeared to be significantly

more numerous and well developed in those cells grown on the SiO_2 functionalized membranes HOB grown on bare PLGA randomly orientated and showed a reduced stress fibers and focal adhesion development at the same experimental time. Although some evenly distributed filopodia

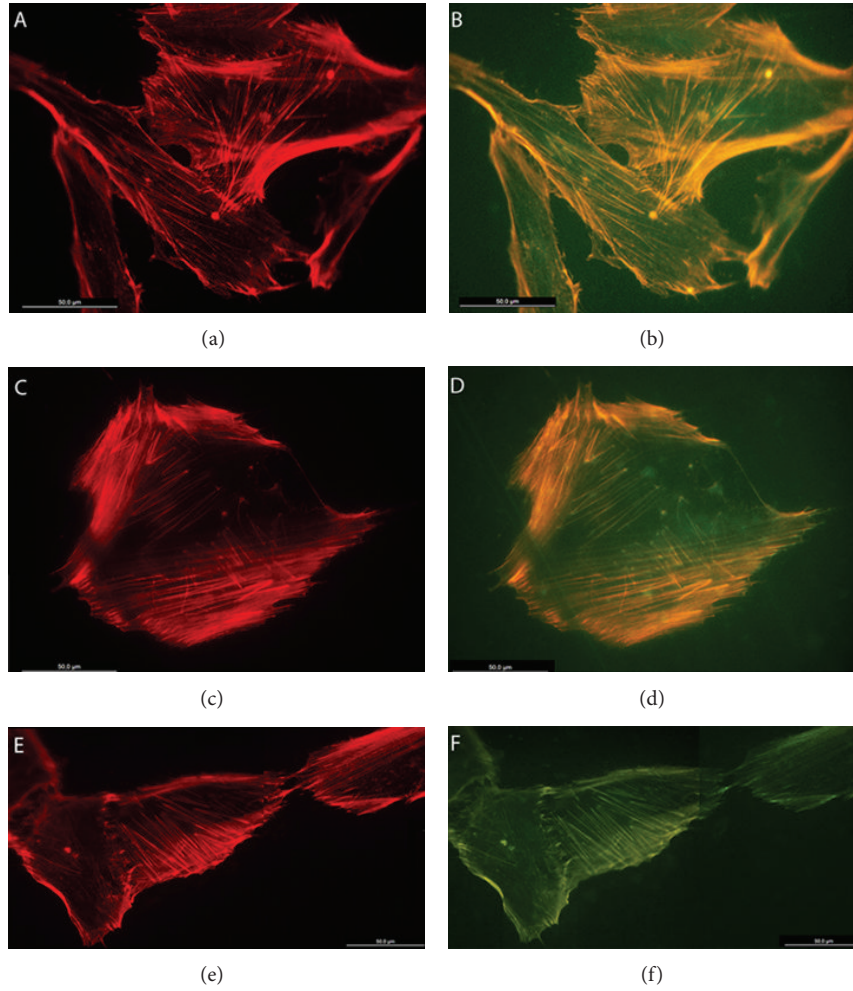


FIGURE 6: HOB cells grown on SiO_2 functionalized membranes, immunolabelled with rhodamine-phalloidin for actin cytoskeleton (red) and antivinculin antibody (green) for focal adhesion sites, 48 hours after seeding. Representative images of cytoskeletal features and focal adhesions, showing in detail (a, b) stress fibers development, (c, d) cell clustering, and (e, f) lamellipodial and (g, h) filopodial emissions.

TABLE 1: Variable number of contacts. Descriptive parameters.

	Groups	<i>N</i>	Minimum	Maximum	Median	Mean	St. dev.
1	PLGA CLEAN 48 H	11	96	274	143	154.27	49.601
2	PLGA SILICON 48 H	11	159	311	229	230.73	46.866
3	PLGA CLEAN 72 H	9	63	198	145	128.89	51.163
4	PLGA SILICON 72 H	10	194	340	241.5	250.50	46.049

were observed, cells did not show a well-organized actin network or polarization, and vinculin positive sites appeared randomly distributed in the cell periphery (Figures 5, 6, and 7).

3.4. Image Analysis: Statistical Analysis of Focal Adhesion Behaviour. The high significance obtained after the quantitative analysis of focal adhesion number by Kruskal-Wallis nonparametric contrast for the 4 groups obtained with the combination of the factors *silicon* and *time* ($H = 23.506$, $P = 0.000$, $df = 3$) indicates that silicon, time, or both influence focal adhesion number. Using the two-way ANOVA,

the analysis of the effects of each factor and their interaction with the ranks of the variable [38], our results indicate that the model is able to explain 58.8% and that *silicon* is a significant factor ($P = 0.000$), while *time* factor is not ($P = 0.929$). Furthermore, silicon treated groups (post hoc contrast of Scheffé, $P = 0.819$) and untreated groups ($P = 0.873$) can be considered homogeneous at any time, and both groups are different from each other ($P = 0.05$) (Figure 8, Table 1).

3.5. Image Analysis: Statistical Analysis of the Shape Variables. The descriptive analysis of the shape variables in the osteoblasts grown in the four experimental groups did

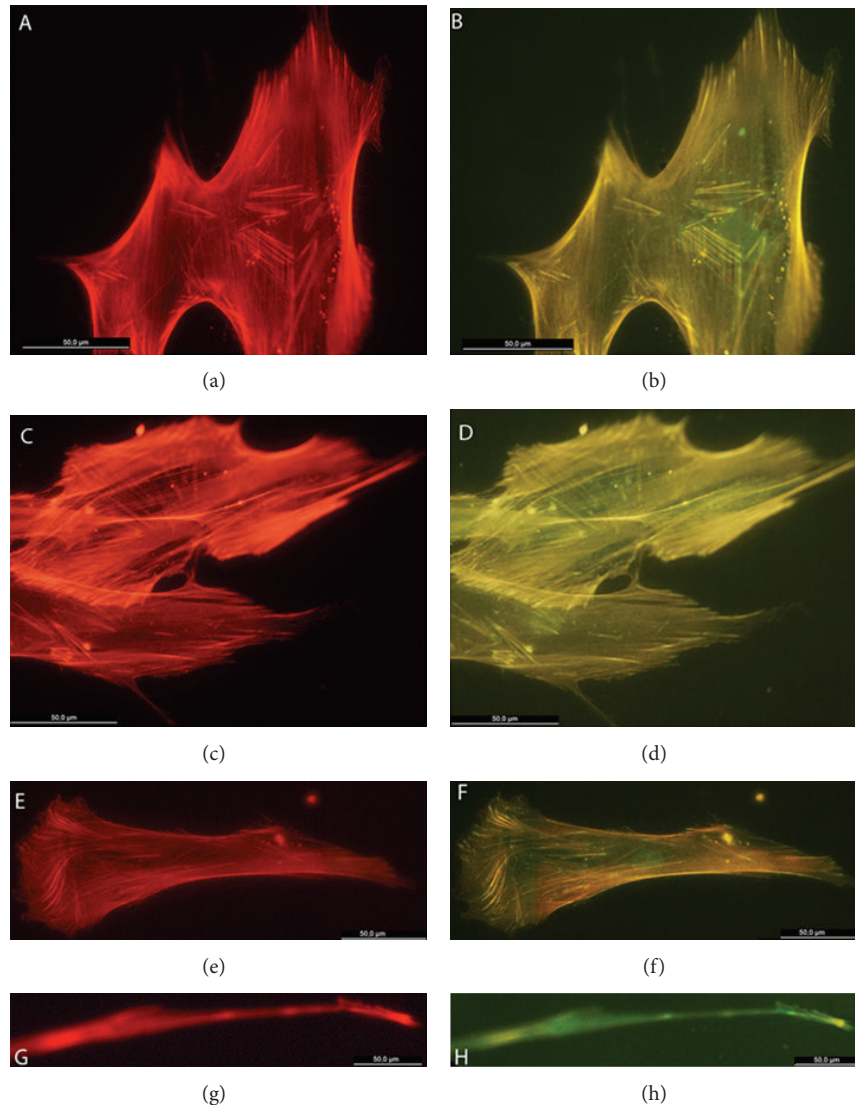


FIGURE 7: HOB cells grown on SiO_2 functionalized membranes, immunolabelled with rhodamine-phalloidin for actin cytoskeleton (red) and antivinculin antibody (green) for focal adhesion sites, 72 hours after seeding. Representative images for (a, b, e, f) cell clustering, (c, d) stress fibers distribution, and (e, f) lamellipodial emissions.

not establish a clear relationship with the factors *silicon* or *time*. Then, an exploratory factor analysis was performed, in the attempt to reduce the number of morphometric indexes (latent factors). The correlation matrix and the factor loadings matrix were obtained first by the method of principal components and later by varimax rotation, which quantify the relationship between the original variables and the indexes achieved. The first index positively related to *circularity* and *solidity* and negatively related to *perimeter*. This first index represents the property of *solid roundness* (SR) showing higher values in those cells that are circular, without voids, and with a medium perimeter. The second index contrasts *roundness* and AR, thus representing *stretch* (ST) or *lengthening*, with the highest values for the more elongated cells, with high AR, and negative values more circular cells, with AR close to 1. The third index relates to

area and *perimeter* and can, therefore, be interpreted as the cell size, with higher values for larger cells.

Growing cells were scored for the morphometric indices according to the values obtained in each one by each individual cell. The two-way ANOVA contrast performed for these indices showed that the experimental factor *silicon* significantly increased ($P = 0.000$) the mean score for SR index, estimating this increase by $\text{CI}_{95\%} = (0.94, 1.71)$, and also caused a decrease in ST index ($P = 0.016$), estimated by $\text{CI}_{95\%} = (-1.03, -0.11)$. Moreover, the factor *time* caused a decrease in the average score for the ST index ($P = 0.012$), estimated by $\text{CI}_{95\%} = (-1.06, -0.14)$, while a significant interaction ($P = 0.029$) was obtained for the index *size*, as cell size decreases in cells grown on bare PLGA surfaces, $\text{CI}_{95\%} = (-1.28, 0.65)$, and increases in silicon treated ones, $\text{CI}_{95\%} = (0.32, 1.30)$. These results indicate that silica treatment,

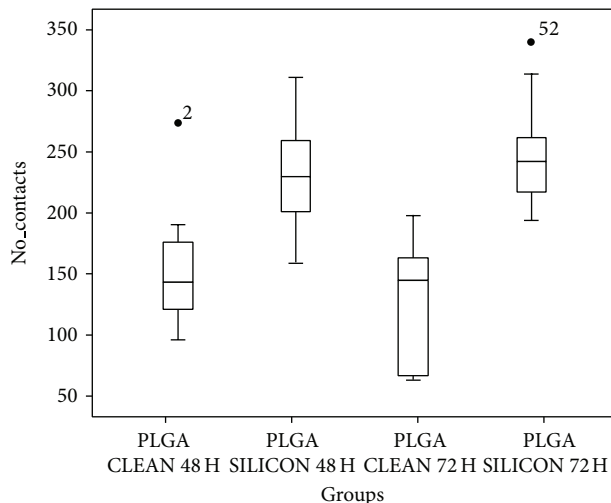


FIGURE 8: Box-Whisker graphics reporting the variable number of contacts among cells on each sample.

independently of time, favors the presence of cells that were *circular* and *solid* (without voids). On the other hand, and independently of silica treatment, the experimental factor *time* favors a lower ST, or *roundness*, and increases the *size* in cells grown on silica treated membranes.

4. Discussion

There are several ways to modify the surface of a material in order to enhance its attractiveness for cell colonization and osteogenic cell differentiation. For biological applications, there is an additional need for versatile deposition methods in the case of devices with potential clinical applications, which should also stand, without alterations, the sterilization processes [13, 16, 18]. We have successfully demonstrated that PECVD TiO₂ functionalization methodology employed by our group enhances HOB cells response to nonresorbable PET devices and stands for standard u.v. sterilization [43]. We now herein present a novel design of barrier membrane for GBR purposes, in which HOB cells response to PECVD SiO₂ functionalized PLGA membranes has been assessed.

Trace amounts of silicon have been described to substantially contribute to strengthening of bones with promotion of bone formation especially during ageing. Well-dispersed nanosized inorganic particles have been described to enhance the mechanical properties of organic materials [10]. A recent study on biosilica influence on the OPG-RANKL ratio in SaOS-2 cells in vitro suggests both osteoinductive and osteogenic potential of biosilica since it combines an upregulation of the genes required for the differentiation with the potential to increase proliferation of the osteogenic cells [18, 24].

Our PLGA membranes were fabricated by using a conventional resorbable PLGA polymer as substrate and then functionalized by depositing a very thin layer of SiO₂, as active layer, by PECVD. A key feature of this method is that it preserved the integrity of the substrate, which remained

practically unaltered after the SiO₂ as revealed by FT-IR analysis (Figure 3). In comparison with wet chemical routes, which may affect the integrity of this sensitivity substrate, PECVD has been demonstrated to be a quite controllable and friendly procedure for the surface functionalization of resorbable polymers. The absence of a significant damage has been proved here by the AFM analysis of the SiO₂/PLGA substrate showing that the surface roughness is not significantly altered after the deposition of SiO₂. Stability of these membranes after 72 hours of immersion in a PBS liquid and after UV irradiation sustains that the in vitro cell growth analysis basically refers to the “as prepared” samples without any significant alteration during its manipulation or during their immersion in the culture medium.

Cell adhesion onto a biomaterial surface is a major contributing factor of its cytocompatibility and the host response when implanted, ultimately determining device biocompatibility. Without adhesion, osteoblasts cannot spread or differentiate. A *princeps* issue in cell adhesion is the development of focal adhesions which, furthermore, are established sites for signal transduction, acting as conveyors of mechanical forces directly to the nucleus via the cytoskeletal network by the complex process of mechanotransduction, where vinculin is required for a strong network formation [1, 4, 44]. Based on the fact that the size and shape of cell spreading area, as well as the number and distribution of focal adhesion plaques, are decisive for migratory, proliferative, and differentiation behaviour of anchorage-dependent cells, we performed an image-based quantitative feature extraction design in which focal adhesion quantification has been used as marker to assess the osteoconductive potential of the substrata, together with actin cytoskeleton arrangement [2, 17, 20, 45].

The relation between focal adhesion number, functionality, cell movement, and growth of skeletal cells has been described, by our group and others [46], and the formation of super-mature adhesions has also been related to osteogenesis support [47]. Actin polymerization and cytoskeleton rearrangement induced by topographical and chemical cues present in the growing surface are known to serve as driving forces for directional migration and morphological alterations. Of particular interest is the temporal and spatial reorganization of cytoskeleton and the focal adhesion formation in response to SiO₂ layer identified in our model, parameters that have been established as important mediators of the mechanotransductive processes, parameters that have been established as important mediators of the mechanotransductive processes [17, 47, 48].

Adherent cells require extracellular matrix anchorage to proliferate and undergo differential function. As shown by our data, HOB cells grown on SiO₂ functionalized PLGA membranes actively probe the physical properties of the ECM, with their contractile machinery clearly facilitating the formation of polarized lamellipodia and evenly distributed filopodia, which gather spatial, topographical, and chemical information from the surface. Initial cell tethering and filopodia exploration are followed by lamellipodia ruffling membrane activity and cellular spreading. The results, obtained after a carefully designed in vitro study, are reinforced with

a powerful statistical treatment and reveal that in vitro HOB cell morphologies are significantly different and vary greatly depending on the substrata and are consistent with an increased cytoskeletal tension related to focal adhesion increase in SiO₂ treated membranes.

5. Conclusions

The methodology described provides a biocompatible and durable functionalization on our PLGA barrier membranes that elicits a significant osteoblast response. Both the morphological changes and the focal adhesion development identified in our model significantly related to SiO₂ treated PLGA both the morphological changes and the focal adhesion development identified in our model are significantly related to SiO₂ treated PLGA. The novel SiO₂ deposition method reveals as a valuable tool to increase bioactivity of PLGA membranes by combining cell nanotopography cues with the incorporation of bioactive factors, that in addition, stands the standard sterilization protocols.

Conflict of Interests

The authors declare that there is no conflict of interests regarding the publication of this paper.

Acknowledgments

The authors thank the Junta de Andalucía (Projects P09-CTS-5189, TEP5283, and FQM-6900) and the Spanish Ministry of Economy and Competitiveness (Projects CONSOLIDER CSD 2008-00023, MAT2010-21228, and MAT2010-18447) and Instituto de Salud Carlos III (FIS PI 09/00508) for financial support (patent P201232018 (Resorbable membrane for guided bone regeneration) PCT pending).

References

- [1] M. J. Biggs and M. J. Dalby, "Focal adhesions in osteoneogenesis," *Proceedings of the Institution of Mechanical Engineers H*, vol. 224, no. 12, pp. 1441–1453, 2010.
- [2] M. J. P. Biggs, R. G. Richards, and M. J. Dalby, "Nanotopographical modification: a regulator of cellular function through focal adhesions," *Nanomedicine: Nanotechnology, Biology, and Medicine*, vol. 6, no. 5, pp. 619–633, 2010.
- [3] E.-J. Lee, S.-H. Teng, T.-S. Jang et al., "Nanostructured poly(ϵ -caprolactone)-silica xerogel fibrous membrane for guided bone regeneration," *Acta Biomaterialia*, vol. 6, no. 9, pp. 3557–3565, 2010.
- [4] T. Orita, M. Tomita, and K. Kato, "Regulation of cellular responses to macroporous inorganic films prepared by the inverse-opal method," *Colloids and Surfaces B: Biointerfaces*, vol. 84, no. 1, pp. 187–197, 2011.
- [5] J. A. Sanz-Herrera and E. Reina-Romo, "Cell-biomaterial mechanical interaction in the framework of tissue engineering: insights, computational modeling and perspectives," *International Journal of Molecular Sciences*, vol. 12, no. 11, pp. 8217–8244, 2011.
- [6] P. Gentile, V. Chiono, C. Tonda-Turo, A. M. Ferreira, and G. Ciardelli, "Polymeric membranes for guided bone regeneration," *Biotechnology Journal*, vol. 6, no. 10, pp. 1187–1197, 2011.
- [7] T.-S. Jang, E.-J. Lee, J.-H. Jo et al., "Fibrous membrane of nano-hybrid poly-L-lactic acid/silica xerogel for guided bone regeneration," *Journal of Biomedical Materials Research B: Applied Biomaterials*, vol. 100, no. 2, pp. 321–330, 2012.
- [8] E. Pamula, E. Filová, L. Bačáková, V. Lisá, and D. Adamczyk, "Resorbable polymeric scaffolds for bone tissue engineering: the influence of their microstructure on the growth of human osteoblast-like MG 63 cells," *Journal of Biomedical Materials Research A*, vol. 89, no. 2, pp. 432–443, 2009.
- [9] M. Retzepi and N. Donos, "Guided bone regeneration: biological principle and therapeutic applications," *Clinical Oral Implants Research*, vol. 21, no. 6, pp. 567–576, 2010.
- [10] J.-H. Song, H.-E. Kim, and H.-W. Kim, "Collagen-apatite nanocomposite membranes for guided bone regeneration," *Journal of Biomedical Materials Research B: Applied Biomaterials*, vol. 83, no. 1, pp. 248–257, 2007.
- [11] S.-H. Teng, E.-J. Lee, P. Wang, D.-S. Shin, and H.-E. Kim, "Three-layered membranes of collagen/hydroxyapatite and chitosan for guided bone regeneration," *Journal of Biomedical Materials Research B: Applied Biomaterials*, vol. 87, no. 1, pp. 132–138, 2008.
- [12] R. Dimitriou, G. I. Mataliotakis, G. M. Calori, and P. V. Giannoudis, "The role of barrier membranes for guided bone regeneration and restoration of large bone defects: current experimental and clinical evidence," *BMC Medicine*, vol. 10, article 81, 2012.
- [13] V. Gribova, R. Auzely-Velty, and C. Picart, "Polyelectrolyte multilayer assemblies on materials surfaces: from cell adhesion to tissue engineering," *Chemistry of Materials*, vol. 24, no. 5, pp. 854–869, 2012.
- [14] T. Tirri, J. Rich, J. Wolke, J. Seppälä, A. Yli-Urpo, and T. O. Närhi, "Bioactive glass induced in vitro apatite formation on composite GBR membranes," *Journal of Materials Science: Materials in Medicine*, vol. 19, no. 8, pp. 2919–2923, 2008.
- [15] Y. Amano, M. Ota, K. Sekiguchi, Y. Shibukawa, and S. Yamada, "Evaluation of a poly-L-lactic acid membrane and membrane fixing pin for guided tissue regeneration on bone defects in dogs," *Oral Surgery, Oral Medicine, Oral Pathology, Oral Radiology, and Endodontics*, vol. 97, no. 2, pp. 155–163, 2004.
- [16] M. Vandrovcová and L. Bačáková, "Adhesion, growth and differentiation of osteoblasts on surface-modified materials developed for bone implants," *Physiological Research*, vol. 60, no. 3, pp. 403–417, 2011.
- [17] C. J. Bettinger, R. Langer, and J. T. Borenstein, "Engineering substrate topography at the Micro- and nanoscale to control cell function," *Angewandte Chemie (International Edition)*, vol. 48, no. 30, pp. 5406–5415, 2009.
- [18] N. Takeuchi, M. Machigashira, D. Yamashita et al., "Cellular compatibility of a gamma-irradiated modified siloxane-poly(lactic acid)-calcium carbonate hybrid membrane for guided bone regeneration," *Dental Materials Journal*, vol. 30, no. 5, pp. 730–738, 2011.
- [19] C. K. Choi, M. T. Breckenridge, and C. S. Chen, "Engineered materials and the cellular microenvironment: a strengthening interface between cell biology and bioengineering," *Trends in Cell Biology*, vol. 20, no. 12, pp. 705–714, 2010.
- [20] F. Intranuovo, P. Favia, E. Sardella et al., "Osteoblast-like cell behavior on plasma deposited micro/nanopatterned coatings," *Biomacromolecules*, vol. 12, no. 2, pp. 380–387, 2011.

- [21] V. Puddu and C. C. Perry, "Peptide adsorption on silica nanoparticles: evidence of hydrophobic interactions," *ACS Nano*, vol. 6, pp. 6356–6363, 2012.
- [22] Y. Tang, Y. Zhao, X. Wang, and T. Lin, "Layer-by-layer assembly of silica nanoparticles on 3D fibrous scaffolds: enhancement of osteoblast cell adhesion, proliferation, and differentiation," *Journal of Biomedical Materials Research*, 2013.
- [23] M. Vallet-Regí, M. Colilla, and B. González, "Medical applications of organic-inorganic hybrid materials within the field of silica-based bioceramics," *Chemical Society Reviews*, vol. 40, no. 2, pp. 596–607, 2011.
- [24] X. Wang, H. C. Schröder, M. Wiens, H. Ushijima, and W. E. G. Müller, "Bio-silica and bio-polyphosphate: applications in biomedicine (bone formation)," *Current Opinion in Biotechnology*, vol. 23, pp. 570–578, 2012.
- [25] H. Shen, X. Hu, J. Bei, and S. Wang, "The immobilization of basic fibroblast growth factor on plasma-treated poly(lactide-co-glycolide)," *Biomaterials*, vol. 29, no. 15, pp. 2388–2399, 2008.
- [26] Y. Wan, X. Qu, J. Lu et al., "Characterization of surface property of poly(lactide-co-glycolide) after oxygen plasma treatment," *Biomaterials*, vol. 25, no. 19, pp. 4777–4783, 2004.
- [27] C. Witt and T. Kissel, "Morphological characterization of microspheres, films and implants prepared from poly(lactide-co-glycolide) and ABA triblock copolymers: is the erosion controlled by degradation, swelling or diffusion?" *European Journal of Pharmaceutics and Biopharmaceutics*, vol. 51, no. 3, pp. 171–181, 2001.
- [28] J. Gao, L. Niklason, and R. Langer, "Surface hydrolysis of poly(glycolic acid) meshes increases the seeding density of vascular smooth muscle cells," *Journal of Biomedical Materials Research*, vol. 42, pp. 417–424, 1998.
- [29] A. C. R. Grayson, M. J. Cima, and R. Langer, "Size and temperature effects on poly(lactic-co-glycolic acid) degradation and microreservoir device performance," *Biomaterials*, vol. 26, no. 14, pp. 2137–2145, 2005.
- [30] C. E. Holy, S. M. Dang, J. E. Davies, and M. S. Shoichet, "In vitro degradation of a novel poly(lactide-co-glycolide) 75/25 foam," *Biomaterials*, vol. 20, no. 13, pp. 1177–1185, 1999.
- [31] H. Kranz, N. Ubrich, P. Maincent, and R. Bodmeier, "Physico-mechanical properties of biodegradable poly(D, L-lactide) and poly(D, L-lactide-co-glycolide) films in the dry and wet states," *Journal of Pharmaceutical Sciences*, vol. 89, pp. 1558–1566, 2000.
- [32] M. Källrot, U. Edlund, and A.-C. Albertsson, "Surface functionalization of degradable polymers by covalent grafting," *Biomaterials*, vol. 27, no. 9, pp. 1788–1796, 2006.
- [33] J. S. C. Loo, C. P. Ooi, and F. Y. C. Boey, "Degradation of poly(lactide-co-glycolide) (PLGA) and poly(L-lactide) (PLLA) by electron beam radiation," *Biomaterials*, vol. 26, no. 12, pp. 1359–1367, 2005.
- [34] H. Tsuji, Y. Tezuka, and K. Yamada, "Alkaline and enzymatic degradation of L-lactide copolymers. II. crystallized films of poly(L-lactide-co-D-lactide) and poly(L-lactide) with similar crystallinities," *Journal of Polymer Science B: Polymer Physics*, vol. 43, no. 9, pp. 1064–1075, 2005.
- [35] A. Barranco, J. Cotrino, F. Yubero et al., "Synthesis of SiO₂ and SiO_xCyHz thin films by microwave plasma CVD," *Thin Solid Films*, vol. 401, no. 1-2, pp. 150–158, 2001.
- [36] A. Barranco, F. Yubero, J. Cotrino et al., "Low temperature synthesis of dense SiO₂ thin films by ion beam induced chemical vapor deposition," *Thin Solid Films*, vol. 396, no. 1-2, pp. 9–15, 2001.
- [37] D. A. Shah and L. V. Madden, "Nonparametric analysis of ordinal data in designed factorial experiments," *Phytopathology*, vol. 94, no. 1, pp. 33–43, 2004.
- [38] T. L. Barr, "An XPS study of Si as it occurs in adsorbents, catalysts, and thin films," *Applications of Surface Science*, vol. 15, no. 1-4, pp. 1–35, 1983.
- [39] J. Finster, D. Schulze, F. Bechstedt, and A. Meisel, "Interpretation of XPS core level shifts and structure of thin silicon oxide layers," *Surface Science*, vol. 152-153, no. 2, pp. 1063–1070, 1985.
- [40] M. M. Stevanovic, B. Jordovic, and D. P. Uskokovic, "Preparation and characterization of poly(D, L-lactide-co-glycolide) nanoparticles containing ascorbic acid," *Journal of Biomedicine and Biotechnology*, vol. 2007, Article ID 84965, 8 pages, 2007.
- [41] H. Aita, N. Hori, M. Takeuchi et al., "The effect of ultraviolet functionalization of titanium on integration with bone," *Biomaterials*, vol. 30, no. 6, pp. 1015–1025, 2009.
- [42] W. Att, N. Hori, F. Iwasa, M. Yamada, T. Ueno, and T. Ogawa, "The effect of UV-photofunctionalization on the time-related bioactivity of titanium and chromium-cobalt alloys," *Biomaterials*, vol. 30, no. 26, pp. 4268–4276, 2009.
- [43] A. Terriza, A. Diaz-Cuenca, F. Yubero et al., "Light induced hydrophilicity and osteoblast adhesion promotion on amorphous TiO₂," *Journal of Biomedical Materials Research A*, vol. 101, pp. 1026–1035, 2013.
- [44] M. J. P. Biggs, R. G. Richards, N. Gadegaard et al., "Interactions with nanoscale topography: adhesion quantification and signal transduction in cells of osteogenic and multipotent lineage," *Journal of Biomedical Materials Research A*, vol. 91, no. 1, pp. 195–208, 2009.
- [45] L. Bacakova, E. Filova, F. Rypacek, V. Svorcik, and V. Stary, "Cell adhesion on artificial materials for tissue engineering," *Physiological Research*, vol. 53, supplement 1, pp. S35–S45, 2004.
- [46] M. Salido, J. I. Vilches-Perez, J. L. Gonzalez, and J. Vilches, "Mitochondrial bioenergetics and distribution in living human osteoblasts grown on implant surfaces," *Histology and Histopathology*, vol. 24, no. 10, pp. 1275–1286, 2009.
- [47] L. E. McNamara, T. Sjöström, K. E. V. Burgess et al., "Skeletal stem cell physiology on functionally distinct titania nanotopographies," *Biomaterials*, vol. 32, no. 30, pp. 7403–7410, 2011.
- [48] M. J. Dalby, "Topographically induced direct cell mechanotransduction," *Medical Engineering and Physics*, vol. 27, no. 9, pp. 730–742, 2005.

Clinical Study

Vertical Ridge Augmentation of the Atrophic Posterior Mandible with Sandwich Technique: Bone Block from the Chin Area versus Corticocancellous Bone Block Allograft—Clinical and Histological Prospective Randomized Controlled Study

Luigi Laino,¹ Giovanna Iezzi,² Adriano Piattelli,² Lorenzo Lo Muzio,¹ and Marco Cicciù³

¹ Department of Clinical and Experimental Medicine, University of Foggia, FO, Italy

² Department of Stomatology and Oral Science, University of Chieti, Italy

³ Human Pathology Department, School of Dentistry, University of Messina, Via Consolare Valeria, 98100 Messina, Italy

Correspondence should be addressed to Marco Cicciù; acromarco@yahoo.it

Received 29 March 2014; Accepted 15 April 2014; Published 29 April 2014

Academic Editor: David M. Dohan Ehrenfest

Copyright © 2014 Luigi Laino et al. This is an open access article distributed under the Creative Commons Attribution License, which permits unrestricted use, distribution, and reproduction in any medium, provided the original work is properly cited.

The aim of the present study is to compare the histological aspects of bone formation in atrophic posterior mandibles augmented by autologous bone block from chin area with corticocancellous bone block allograft used as inlays with the sandwich technique. *Materials and Methods.* Sixteen patients with bilateral partial edentulism in the posterior mandible were selected. The residual bone height, preliminarily measured by computed tomography scans, ranged between 5 and 7 mm from the inferior alveolar nerve. All patients required regeneration procedure with autologous bone block from chin area (control group) versus bone block allograft Puros (Zimmer Dental, 1900 Aston Avenue, Carlsbad, CA, USA) (test group). Histological and histomorphometric samples were collected at the time of implant positioning in order to analyze the percentage of newly formed bone, the residual graft material, and marrow spaces/soft tissue. *Results.* No statistically significant differences between the two groups were found regarding the percentage of newly formed bone. The percentage of residual grafted material was significantly higher in the test group, whilst the percentage of marrow spaces was higher in control group. *Conclusions.* In conclusion, both procedures supported good results, although the use of bone blocks allograft was less invasive and preferable than harvesting bone from the mental symphysis.

1. Introduction

The rehabilitation of posterior mandible with dental implants represents today a hard challenge for clinicians due to the lack of supporting bone. The alveolar nerve presence and lifting and the gradual vertical and horizontal resorption of the mandibular bone crest in both partially and totally edentulous patients can be treated by several prosthetic and surgical options [1–5]. Patients can be rehabilitated with conventional partial removable dentures, but often this treatment does not meet the expectations of the patients. Regarding implant supported treatment options, vertical ridge augmentation, surgical displacement of the inferior alveolar nerve, and, finally, the placement of short implants (8 mm or less) could be necessary for the correction of the atrophic posterior

mandible. The use of short implants represents a simpler and faster alternative to the augmentation procedure, even if in some “critical cases” the residual bone crest above the inferior alveolar nerve is only 5–7 mm in height, and therefore the surgical augmentation treatment is mandatory. Indeed, the displacement of the alveolar nerve is technically tough, and this procedure may be associated with certain degree of permanent loss of nerve sensitivity [1, 6–9]. Different surgical techniques are currently being used to augment the posterior mandible: guided bone regeneration (GBR) and alveolar distraction osteogenesis onlay bone grafting; however, only few of these have been tested in randomized clinical trial (RCT) [10, 11]. Several surgical bone augmentation techniques are related to an unpredictable resorption of the grafted material. Vascularity seems to be the main factor

in determining whether such a graft can be maintained in situ. Traditional distraction osteogenesis aims to maintain the majority of the vascularity to the transported bone segment. The drawbacks of distraction osteogenesis include patient cooperation, technique sensitivity, and the possibility of a second surgery to remove the device [1, 3, 7].

Another possible approach is to use an interpositional bone graft [1, 4, 8, 11]. The rationale of the interpositional techniques is based on the theory that biomaterial placed between 2 pieces of pedicled bone with internal cancellous bone will undergo rapid and complete healing and graft incorporation with a lower percentage of resorption. The sandwich osteotomy allows for the positioning of the graft in a well-delimited area as well as offering adequate blood supply to maintain new bone growth. This procedure enables the simultaneous correction of the sagittal intermaxillary relationship and the vertical dimension. This technique has been used in a variety of maxillary areas including both the anterior and posterior mandible and maxilla. When performing the sandwich osteotomy in the posterior mandible, great surgical precision is required to avoid damage to the inferior alveolar nerve. For these reasons and for the few results available in the literature, it is necessary to carry out further research to validate the predictability of this regenerative technique [1, 3, 8–11].

The aim of the present study is to compare the histological aspects of bone formation in atrophic posterior mandibles augmented by autologous bone block from chin area (control group) to Puros bone block allograft (test group) used as inlays with the sandwich technique.

2. Materials and Methods

Between November and April 2010, nineteen patients with bilateral partial edentulism in the posterior mandible were selected for the present study. They all showed a residual bone height ranging between 5 and 7 mm from the inferior alveolar nerve, which was firstly measured by computed tomography scans. All patients required the placement of at least 3 implants. The protocol of the study was approved by the Ethical Committee of the Second University of Naples, Naples, Italy, and all the patients signed a written informed consent form. All patients were treated in the Department of Oral and Maxillofacial Surgery, Second University of Naples, Naples, Italy. Exclusion criteria were (1) general contraindications to implant surgery, (2) irradiation, chemotherapy, or immunosuppressive therapy over the past 5 years, (3) poor oral hygiene and motivation, (4) active periodontitis, (5) uncontrolled diabetes, (6) pregnancy or lactation, (7) substance abusers, (8) smoking more than 10 cigarettes per day, (9) psychiatric problems or unrealistic expectations, (10) acute infection in the area intended for implant placement, (11) positive to HIV and hepatitis B and C, (12) autoimmune diseases such as rheumatoid arthritis, systemic lupus erythematosus, scleroderma, Sjogren's syndrome, and dermatomyositis/polymyositis, (13) treated or under treatment with intravenous aminobisphosphonates, (14) previously subjected to reconstructive procedures of the

posterior mandible, and (15) under chronic treatment with steroids or nonsteroidal anti-inflammatory drugs. Twelve patients were considered eligible and were enrolled in the trial (mean age was 57 years, 9 females and 3 males).

2.1. Augmentation Procedure. Two weeks before bone augmentation and implant placement, all patients underwent oral hygiene instructions and professional debridement, when necessary. On the day of the augmentation procedure, the envelopes containing the randomized codes were opened. All patients received antibiotics prior to the surgery. Antimicrobial prophylaxis was obtained with the use of 1 gr of amoxicillin + clavulanic acid (Augmentin, Glaxo-SmithKline, Brentford, Middlesex, UK) (or erythromycin 500 mg if allergic to penicillin), starting one day before surgery and for the following 4 days. All patients were treated under local anesthesia with intravenous sedation. A paracrestal incision was made through the buccal mucosa respecting the emergence of the mental nerve, and, as the full thickness flap was retracted, tension on the mental nerve was carefully avoided. The horizontal osteotomy was made at 4 mm from the mandibular canal using conventional surgical micromotor. Two oblique cuts were made in the coronal third of the mandibular bone with the mesial cut at least 2 mm distal to the last tooth in the arch Figures 1(a), 1(b), and 1(c). The osteotomies were completed with the use of bone chisels. The height of the osteotomized segment was at least 3 mm to allow the insertion of a stabilizing screw without risking the fracture of the distracted bone segment. The segment was elevated preserving the lingual periosteum, and according to the outcome of the randomization, the graft materials were modelled to the desired height and shape to fill the site and interposed between the raised fragment and the mandibular basal bone. Titanium miniplates and miniscrews (Gebrüder Martin GmbH & Co., KG, Tuttlingen, Germany) were used to fix the osteotomized crestal bone to the basal bone. The grafted area was covered with a resorbable barrier of pericardium (Copios Pericardium Membrane Zimmer Dental, Switzerland) Figures 2(a), 2(b), and 2(c). Periosteal incisions were made to release the flaps coronally as needed and were sutured with Vicryl 5.0 sutures until the incisions were perfectly sealed. Patients were instructed to use Corsodyl gel 1% twice a day for 2 weeks and then 0.2 chlorhexidine mouthwashes twice a day for up to the second month, to avoid brushing and trauma on the surgical sites. Removable prostheses were not allowed. Patients were seen after 10 days for follow-up examinations and sutures removal. Patients were recalled for additional postoperative check-ups 1, 2, and 4 months after the augmentation procedure. Four months after augmentation, a CT scan was taken to plan implant placement.

2.2. Implant Placement. Six months after the augmentation procedure, at the moment of dental implant surgery, miniplates were removed and the bone core biopsies were retrieved by using 2.9 mm diameter trephine bur (Komet 227b, Italy), and 72 implants (Splint Zimmer Dental, Switzerland) were inserted in situ, as shown in Figure 3. Drills with

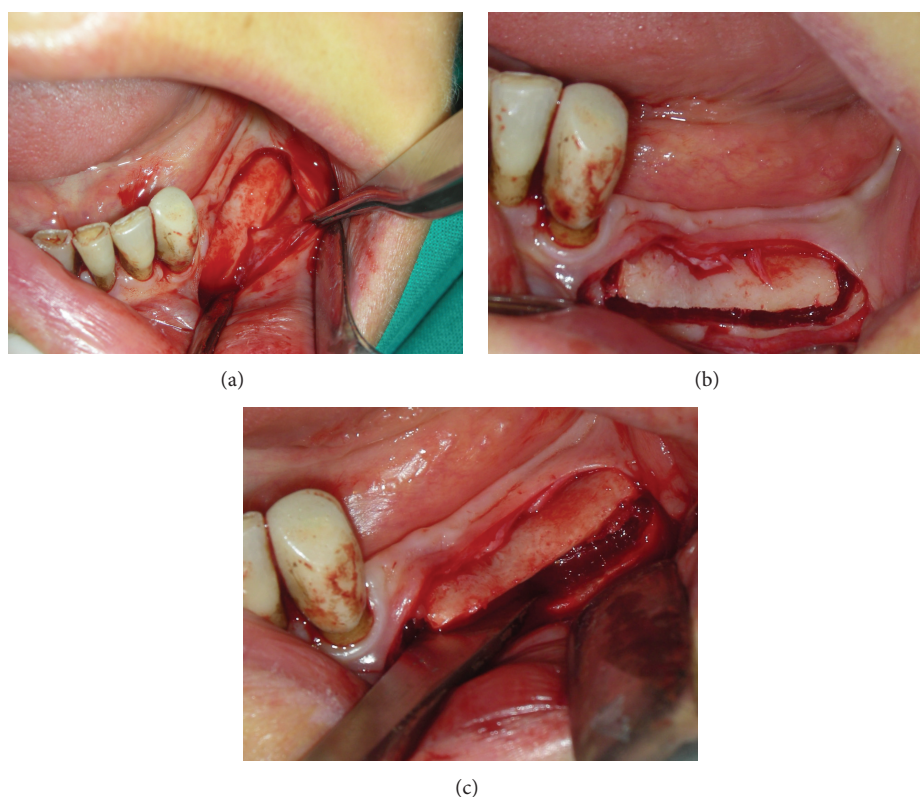


FIGURE 1: Sample of the two oblique cuts performed in the coronal third portion of the mandibular bone with the mesial cut at least 2 mm distal to the last tooth in the arch (a, b, c).

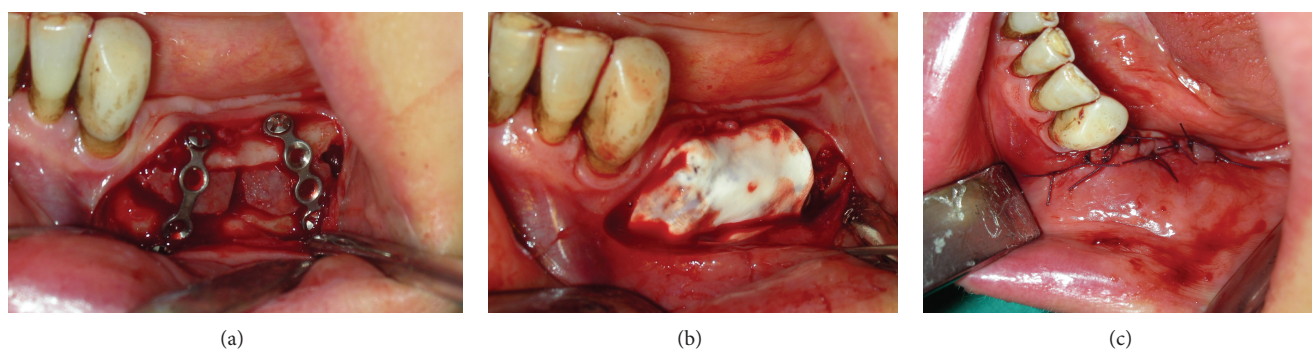


FIGURE 2: Sample of the grafted area covered with a resorbable barrier of pericardium (a, b, c).

increasing diameters were used to prepare the implant sites. The surgical unit was settled with a torque of 25 Ncm. After the dental implant placement, the cover screws were placed and the flap closure was obtained with Vicryl 4.0. Patients were instructed to use 0.2% chlorhexidine mouthwash for 1 min twice a day for 2 weeks, to have a soft diet for 1 week, and to avoid brushing and trauma on the surgical sites. No removable prosthesis was allowed. Sutures were removed after 10 days.

2.3. Histological Procedure. Bone cores were retrieved, immediately stored in 10% buffered formalin, and processed to obtain thin ground sections using the Precise 1 Automated

System (Assing, Rome, Italy). The specimens were dehydrated in a graded series of ethanol rinses and embedded in a glycol methacrylate resin (Technovit 7200 VLC, Kulzer, Wehrheim, Germany). After polymerization, the specimens were sectioned, along their longitudinal axis, with a high-precision diamond disc at about 150 μ m and ground down to about 30 μ m with a specially designed grinding machine. The slides were stained with acid fuchsin and toluidine blue and examined in normal transmitted light under a Leitz Laborlux microscope (Laborlux S, Leitz, Wetzlar, Germany). Histomorphometry of the percentages of newly formed bone, residual grafted material, and marrow spaces was carried out using a light microscope (Laborlux S, Leitz, Wetzlar, Germany) connected to a high resolution video camera

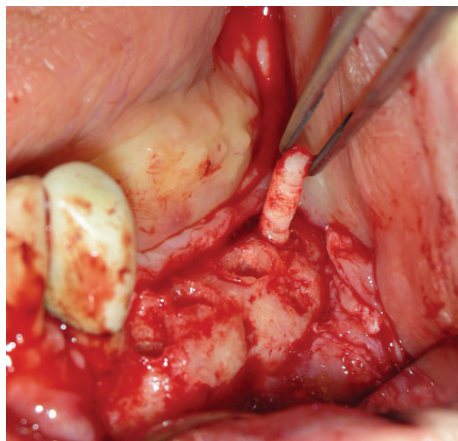


FIGURE 3: Sample of the bone core biopsies that were retrieved by using 2.9 mm diameter trephine bur.

(3CCD, JVC KY-F55B, JVC, Yokohama, Japan) and interfaced to a monitor and PC. This optical system was associated with a digitizing pad (Matrix Vision GmbH, Oppenweiler, Germany) and a histometry software package with image capturing capabilities (Image-Pro Plus 4.5, Media Cybernetics Inc., Immagini & Computer Snc, Milan, Italy). The same investigator made all the measurements.

2.4. Statistical Analysis. Data were evaluated by the Shapiro-Wilk test. All the data are presented as mean \pm standard deviations (SD); statistically significant differences were accepted as $P < 0.05$.

3. Results

The failures and complications that occurred during the entire study period were limited. In one patient treated with the Puros bone block, exposure of a titanium plate 2 months after surgery occurred; it was treated by removing the plaque, and then a satisfactory healing was achieved. In two patients treated with autologous bone from mental symphysis, a temporary paresthesia of the anterior region of the mandible was appreciated and treated by drug solution, Dobetin 5000 mcg 1 time per day for 1 week and 3 doses in the second week.

3.1. Histological Results

3.1.1. Control Group. In the control group, a significant amount of grafted bone, almost completely surrounded by newly formed bone, was observed (Figure 4). The autologous grafted bone showed irregularly shaped margins, probably due to the remodeling process. The demarcation line (cementing line) between grafted bone and newly formed bone was evident (Figure 5). In some areas, bone remodeling was conceivable with a rim of osteoblasts depositing osteoid matrix (Figure 6). Osteons in the vicinity of grafted bone could be observed (Figure 7). No signs of inflammatory infiltrate were present.

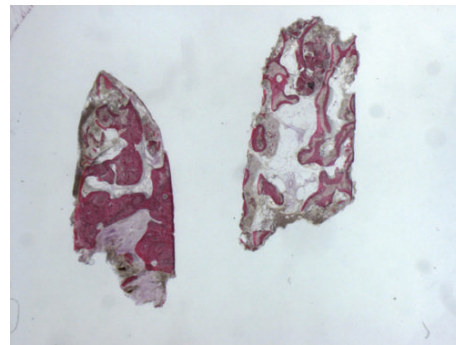


FIGURE 4: Grafted bone, almost completely surrounded by newly formed bone can be observed. Acid fuchsin-toluidine blue; original magnification 60x.

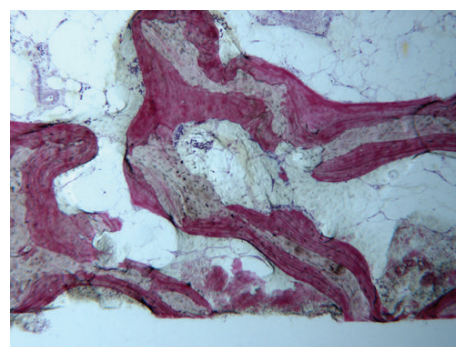


FIGURE 5: The autogenous bone block presents marked staining differences from the host trabecular bone and specifically, it shows a lower affinity for the stains. The block is surrounded by newly formed bone. Acid fuchsin-toluidine blue; original magnification 40x.

3.1.2. Test Group. In all the analyzed samples, a good amount of newly formed bone could be observed (Figure 8). A tight contact between the grafted material and the regenerated bone, without any interposition of fibrous tissue, was found (Figure 9). The newly formed bone had a high affinity for dyes and was acid fuchsin positive; therefore, a highly stained line was observed at the grafting material-new bone interface. In many fields, it was possible to observe the presence of large osteocyte lacunae in contact with the grafted material (Figure 10). Some trabeculae of grafted material were bridged by newly formed bone, which was observed both in the inner and outer portions of some biomaterial particles (Figure 11). Marrow stromal cells and blood vessels were found inside the marrow spaces. In some fields, there was a modest amount of inflammatory infiltrate. No osteoclasts were observed around the graft particles.

The histomorphometric results are summarized in Tables 1, 2, and 3.

There was no statistically significant difference between the two groups in terms of amount of new bone, 31.47 ± 2.2 versus $30.6 \pm 3.7\%$ ($P = 0.5362$ has been recorded, while there was a statistically significant difference in the percentage of residual grafted material higher in test group (Table 2).

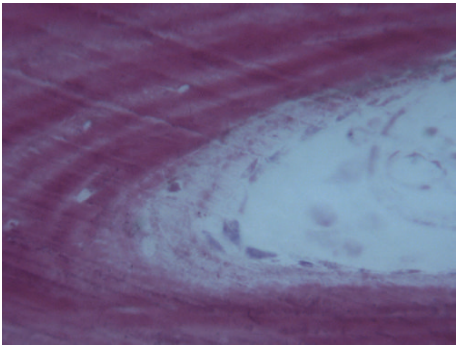


FIGURE 6: A rim of osteoblasts depositing osteoid matrix is evident. Acid fuchsin-toluidine blue; original magnification 200x.

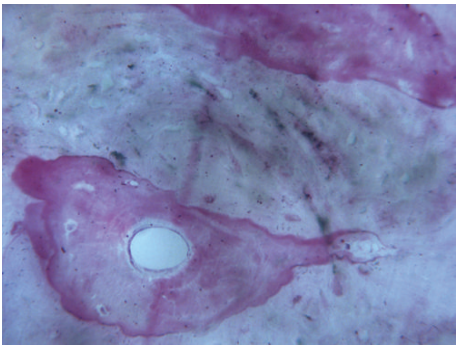


FIGURE 7: An osteon in the vicinity of grafted bone can be seen. Acid fuchsin-toluidine blue; original magnification 200x.

TABLE 1

Group	Obs.	Mean	Std. error	Std. deviation	95% conf. I.
Group Ctrl	12	31.47	7155495	2.262.766	29.85131 33.08868
Group test	12	30.6	117.936	3.729.462	27.9321 33.2679

Newly formed bone, *t* value = 0.6307, and *P* value = 0.5362. There is no statistically significant difference.

TABLE 2

Group	Obs.	Mean	Std. error	Std. deviation	95% conf. I.
Group Ctrl	12	19.56	1.320.959	417.724	16.57178 22.54822
Group test	12	28.9	1.600.069	5.059.864	25.28039 32.51961

Residual graft material, *t* value = -4.5015, and *P* value = 0.0003. There is statistically significant difference.

4. Discussion

This study is designed to evaluate how a bone substitute material may offer some advantages in the place of auto-genous bone grafts harvested from the mental symphysis in the treatment of atrophic posterior mandibles. Moreover, the authors proposed a novel technique for localized vertical bone augmentation using an interpositional bone block

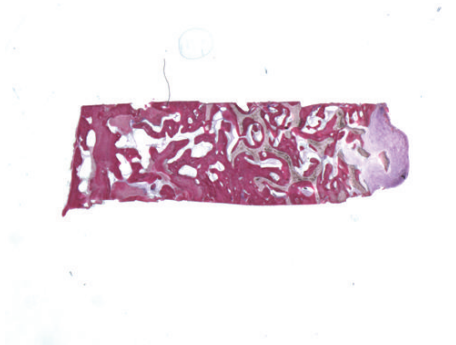


FIGURE 8: A good amount of newly formed bone can be observed. Acid fuchsin-toluidine blue; original magnification 6x.

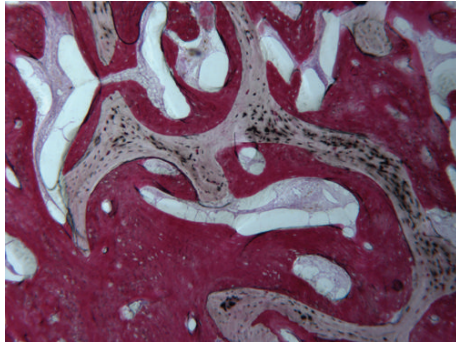


FIGURE 9: The bovine bone block is surrounded by newly formed bone. A tight contact between the grafted material and the regenerated bone without any interposition of fibrous tissue can be observed. Acid fuchsin-toluidine blue; original magnification 40x.

TABLE 3

Group	Obs	Mean	Std. error	Std. deviation	95% conf. I.
Group Ctrl	12	48.97	1.878.241	5.939.519	44.72112 53.21888
Group test	12	41.28	1.888.491	5.971.934	41.84335 48.40665

Marrow space, *t* value = 2.8872, and *P* value = 0.0098. There is statistically significant difference.

representing a valuable and predictable surgical alternative technique for posterior mandible atrophic ridge.

In 2006, Jensen retrospectively evaluated the crestal stability of alveolar augmentation using an interpositional bone graft for dental implant restorations and found a good stability after 4-year follow-up. In 2008, Felice et al. produced a series of clinical investigations for analyzing the effectiveness of this technique in relation to the use of biomaterial, and also in this case the results appeared satisfactory [12–15].

Another main aspect is the choice of the graft material to be used. In 2009, Felice et al. performed a randomized controlled clinical trial to evaluate two different kinds of graft materials: bone from iliac crest and bovine anorganic bone. There were ten selected partially edentulous patients having 5–7 mm of residual crystal height above the mandibular canal. Four months after bone grafting, a bone core was

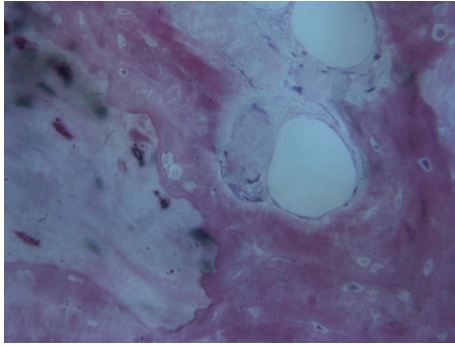


FIGURE 10: Large osteocyte lacunae in contact with the grafted material are present. Acid fuchsin-toluidine blue; original magnification 200x.

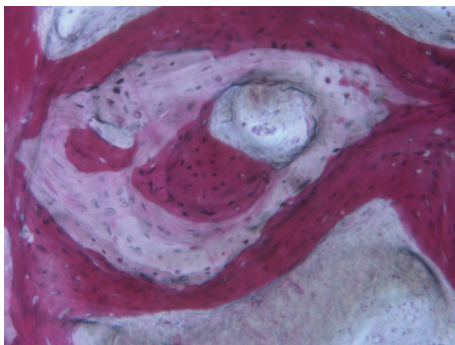


FIGURE 11: New bone can be seen in the inner and outer portions of a residual grafted particle. Acid fuchsin-toluidine blue; original magnification 100x.

retrieved from each side using a 3 mm external diameter trephine for the histological evaluation. The histomorphometric data showed the only statistically significant difference in the mean percentage of residual graft (between 10% and 13%, P values between 0.008 and 0.009) that was greater in the Bio-Oss group, while there were no statistically significant differences in the percentage of newly formed bone and in the marrow space between the two groups. Also the clinical outcomes present in the literature are very interesting [6, 12, 14–18]. In 2006, Jensen published a retrospective study to evaluate the crystal stability of alveolar augmentation using an interpositional bone graft for dental implant restorations. Eight patients with 10 graft sites were followed from 1 to 4 years with panoramic evaluation to determine if dimension changes of the alveolar graft sites had occurred. The author described a little loss of crystal height and 20 of the 22 implants confirmed high stability at the follow up evaluation. These results were later confirmed by various studies conducted by the group of Felice et al. (2008, 2009) and the results of this study confirmed the possibility of considered this surgical technique like predictable one [2, 4, 7, 12, 16, 18].

The sandwich osteotomy can be considered an alternative to other bone augmentation techniques presented in the recent literature. Although one study determined that interpositional bone grafting and alveolar distraction yielded statistically similar results in regard to buccolingual width,

it later stated that bone grafting may form wider bone. No mention was made of the advantage gained with the copious blood supply by the sandwich osteotomy technique [14–19].

Other studies have shown that fewer cases of dehiscence were observed with the sandwich osteotomy than with techniques using only graft or titanium mesh. Laviv et al. recently reported that in 10 patients treated with a similar technique, vertical gain ranged from 3 to 6 mm over a 4-year period [16]. Authors stated that efforts to displace the segment greater than 5 mm “may not only risk the potential for vascular embarrassment by detaching periosteal blood supply, but also can excessively rotate the segment palatally, compromising aesthetic gingival projection.” In the anterior maxilla, it has been shown that one of the disadvantages could be the reduced extensibility of the palatal mucoperiosteum that does not allow a vertical increase of more than 10 mm to be done [6, 18–20]. In a letter to the editor, Robiony et al. suggest that the vertical movement could be extended more than the 10 mm proposed by Jensen, but only in the canine and premolar zones. They described their experience with 25 patients and demonstrated that the technique can be successful without compromising vascular supply and esthetics [20–24]. All those studies clearly demonstrated, even with some limitations, how the use of this technique, by expert surgeons, might be safe and predictable giving less discomfort for the patients [14, 22, 25].

In the present study, in order to offer our patients a less invasive surgery, a biomaterial has been compared to autologous bone and the difference in newly formed bone percentages was not statistically significant. During the histomorphometric evaluation, the percentage of newly formed bone was found to be lower in the test group (28.9/19.5); this meant a slower integration of the grafted material, which is not clinically appreciable; therefore, the use of autologous bone blocks does not seem to provide particular advantages.

5. Conclusion

The results of the present investigation encourage further studies on the present topic. However, other clinical trials are needed, with a greater number of patients. The results reported in the literature and this preliminary study underline how the interposition technique seems to be a valid therapeutic option in the treatment of vertical atrophy of the posterior mandible. Both graft materials gave good results in relation to this type of surgical technique; the use of Puros bone block allograft represents a less invasive alternative for the patients. In the future, it would be interesting to compare this technique with short implants and to record those results over the long term.

Conflict of Interests

As the corresponding author, Marco Cicciù declares that all the authors have no conflict of interests regarding the devices used for this study and that the current research is not influenced by any secondary interests, such as financial gain.

References

- [1] F. D. Das Neves, D. Fones, S. R. Bernardes, C. J. do Prado, and A. J. F. Neto, "Short implants—an analysis of longitudinal studies," *The International Journal of Oral & Maxillofacial Implants*, vol. 21, no. 1, pp. 86–93, 2006.
- [2] H. Li, C. R. Zhou, M. Y. Zhu, J. H. Tian, and J. H. Rong, "Preparation and characterization of homogeneous hydroxyapatite/chitosan composite scaffolds via in-situ hydration," *Journal of Biomaterial and Nanobiotechnology*, vol. 1, pp. 42–49, 2010.
- [3] K. A. Zimmermann, J. M. Leblanc, K. T. Sheets, R. W. Fox, and P. Gatenholm, "Biomimetic design of a bacterial cellulose/hydroxyapatite nanocomposite for bone healing applications," *Materials Science and Engineering C*, vol. 31, no. 1, pp. 43–49, 2011.
- [4] B. Rosenquist, "Implant placement in combination with nerve transpositioning: experiences with the first 100 cases," *The International Journal of Oral & Maxillofacial Implants*, vol. 9, pp. 522–531, 1994.
- [5] A. S. Herford, R. Tandon, T. W. Stevens, E. Stoffella, and M. Cicciù, "Immediate distraction osteogenesis: the sandwich technique in combination with rhBMP-2 for anterior maxillary and mandibular defects," *Journal of Craniofacial Surgery*, vol. 24, no. 4, pp. 1383–1387, 2013.
- [6] M. Chiapasco, M. Zaniboni, and L. Rimondini, "Autogenous onlay bone grafts vs. alveolar distraction osteogenesis for the correction of vertically deficient edentulous ridges: a 2–4-year prospective study on humans," *Clinical Oral Implants Research*, vol. 18, no. 4, pp. 432–440, 2007.
- [7] A. S. Herford, M. Lu, L. Akin, and M. Cicciù, "Evaluation of a porcine matrix with and without platelet-derived growth factor for bone graft coverage in pigs," *The International Journal of Oral & Maxillofacial Implants*, vol. 27, no. 6, pp. 1351–1358, 2012.
- [8] M. Merli, F. Bernardelli, and M. Esposito, "Horizontal and vertical ridge augmentation: a novel approach using osteosynthesis microplates, bone grafts, and resorbable barriers," *International Journal of Periodontics and Restorative Dentistry*, vol. 26, no. 6, pp. 581–587, 2006.
- [9] M. Simion, S. A. Jovanovic, C. Tinti, and S. P. Benfenati, "Long-term evaluation of osseointegrated implants inserted at the time or after vertical ridge augmentation: a retrospective study on 123 implants with 1–5 year follow-up," *Clinical Oral Implants Research*, vol. 12, no. 1, pp. 35–45, 2001.
- [10] J. H. Fu, T. J. Oh, E. Benavides, I. Rudek, and H. L. Wang, "A randomized clinical trial evaluating the efficacy of the sandwich bone augmentation technique in increasing buccal bone thickness during implant placement surgery: I. Clinical and radiographic parameters," *Clinical Oral Implants Research*, vol. 25, no. 4, pp. 458–467.
- [11] S.-H. Park, K.-W. Lee, T.-J. Oh, C. E. Misch, J. Shotwell, and H.-L. Wang, "Effect of absorbable membranes on sandwich bone augmentation," *Clinical Oral Implants Research*, vol. 19, no. 1, pp. 32–41, 2008.
- [12] O. T. Jensen, "Alveolar segmental "sandwich" osteotomies for posterior edentulous mandibular sites for dental implants," *Journal of Oral and Maxillofacial Surgery*, vol. 64, no. 3, pp. 471–475, 2006.
- [13] C. Marchetti, S. Trasarti, G. Corinaldesi, and P. Felice, "Interpositional bone grafts in the posterior mandibular region: a report on six patients," *The International Journal of Periodontics and Restorative Dentistry*, vol. 27, no. 6, pp. 547–555, 2007.
- [14] A. Bianchi, P. Felice, G. Lizio, and C. Marchetti, "Alveolar distraction osteogenesis versus inlay bone grafting in posterior mandibular atrophy: a prospective study," *Oral Surgery, Oral Medicine, Oral Pathology, Oral Radiology and Endodontology*, vol. 105, no. 3, pp. 282–292, 2008.
- [15] P. Felice, G. Cannizzaro, V. Checchi et al., "Vertical bone augmentation versus 7-mm-long implants in posterior atrophic mandibles. Results of a randomised controlled clinical trial of up to 4 months after loading," *European journal of oral implantology*, vol. 2, no. 1, pp. 7–20, 2009.
- [16] A. Laviv, O. T. Jensen, E. Tarazi, and N. Casap, "Alveolar sandwich osteotomy in resorbed alveolar ridge for dental implants: a 4 year prospective study," *Journal of Oral and Maxillofacial Surgery*, vol. 72, pp. 292–303, 2014.
- [17] M. S. Tonetti and C. H. F. Hämmerle, "Advances in bone augmentation to enable dental implant placement: consensus report of the sixth european workshop on periodontology," *Journal of Clinical Periodontology*, vol. 35, no. 8, pp. 168–172, 2008.
- [18] P. Felice, C. Marchetti, A. Piattelli et al., "Vertical ridge augmentation of the atrophic posterior mandible with interpositional block grafts: bone from the iliac crest versus bovine anorganic bone," *European Journal of Oral Implantology*, vol. 1, no. 3, pp. 183–198, 2008.
- [19] B. Fang, Y.-Z. Wan, T.-T. Tang, C. Gao, and K.-R. Dai, "Proliferation and osteoblastic differentiation of human bone marrow stromal cells on hydroxyapatite/bacterial cellulose nanocomposite scaffolds," *Tissue Engineering A*, vol. 15, no. 5, pp. 1091–1098, 2009.
- [20] Y. Zhang and M. Zhang, "Synthesis and characterization of macroporous chitosan/calcium phosphate composite scaffolds for tissue engineering," *Journal Biomedical Material Research*, vol. 55, pp. 304–312, 2001.
- [21] H. M. Hashemi and B. Javidi, "Comparison between interpositional bone grafting and osteogenic alveolar distraction in alveolar bone reconstruction," *Journal of Oral and Maxillofacial Surgery*, vol. 68, no. 8, pp. 1853–1858, 2010.
- [22] M. Politi and M. Robiony, "Localized alveolar sandwich osteotomy for vertical augmentation of the anterior maxilla," *Journal of Oral and Maxillofacial Surgery*, vol. 57, no. 11, pp. 1380–1382, 1999.
- [23] O. T. Jensen, L. Kuhlke, J.-F. Bedard, and D. White, "Alveolar segmental sandwich osteotomy for anterior maxillary vertical augmentation prior to implant placement," *Journal of Oral and Maxillofacial Surgery*, vol. 64, no. 2, pp. 290–296, 2006.
- [24] K.-H. Bormann, M. M. Suarez-Cunqueiro, C. von See et al., "Forty sandwich osteotomies in atrophic mandibles: a retrospective study," *Journal of Oral and Maxillofacial Surgery*, vol. 69, no. 6, pp. 1562–1570, 2011.
- [25] J. A. Elo, A. S. Herford, and P. J. Boyne, "Implant success in distracted bone versus autogenous bone-grafted sites," *The Journal of Oral Implantology*, vol. 35, no. 4, pp. 181–184, 2009.

Research Article

Surface Characteristics and Bioactivity of a Novel Natural HA/Zircon Nanocomposite Coated on Dental Implants

Ebrahim Karamian,¹ Amirsalar Khandan,²
Mahmood Reza Kalantar Motamedi,³ and Hesam Mirmohammadi^{4,5}

¹ Department of Materials Engineering, Najafabad Branch, Islamic Azad University, Isfahan, Iran

² Young Researchers and Elite Club, Khomeinishahr Branch, Islamic Azad University, Isfahan, Iran

³ Dental Students Research Center, School of Dentistry, Isfahan University of Medical Sciences, Isfahan, Iran

⁴ Dental Materials Research Center, Department of Restorative Dentistry, Isfahan University of Medical Sciences, Isfahan, Iran

⁵ Department of Cariology Endodontology Pedodontology, Academic Centre for Dentistry Amsterdam (ACTA), Universiteit van Amsterdam and Vrije Universiteit, Amsterdam 1081 JD, The Netherlands

Correspondence should be addressed to Hesam Mirmohammadi; hmirmoha@acta.nl

Received 5 February 2014; Accepted 1 April 2014; Published 16 April 2014

Academic Editor: David M. Dohan Ehrenfest

Copyright © 2014 Ebrahim Karamian et al. This is an open access article distributed under the Creative Commons Attribution License, which permits unrestricted use, distribution, and reproduction in any medium, provided the original work is properly cited.

The surface characteristics of implant which influence the speed and strength of osseointegration include surface chemistry, crystal structure and crystallinity, roughness, strain hardening, and presence of impurities. The aim of this study was to evaluate the bioactivity and roughness of a novel natural hydroxyapatite/zircon (NHA/zircon) nanobiocomposite, coated on 316L stainless steel (SS) soaked in simulated body fluid (SBF). NHA/zircon nanobiocomposite was fabricated with 0 wt.%, 5 wt.%, 10 wt.%, and 15 wt.% of zircon in NHA using ball mill for 20 minutes. The composite mixture was coated on 316L SS using plasma spray method. The results are estimated using the scanning electron microscopy (SEM) observation to evaluate surface morphology, X-ray diffraction (XRD) to analyze phase composition, and transmission electron microscopy (TEM) technique to evaluate the shape and size of prepared NHA. Surfaces roughness tester was performed to characterize the coated nanocomposite samples. The maximum average R_a (14.54 μm) was found in the NHA 10 wt.% of zircon coating. In addition, crystallinity (X_c) was measured by XRD data, which indicated the minimum value ($X_c = 41.1\%$) for the sample containing 10 wt.% of zircon. Maximum bioactivity occurred in the sample containing 10 wt.% of zircon, which was due to two reasons: first, the maximum roughness and, second, the minimum crystallinity of nanobiocomposite coating.

1. Introduction

Dental implants are well-accepted and predictable treatment modalities for rehabilitation of patients with partial and complete edentulism. Dental implantation has become an established treatment method since its appearance for over 40 years. The future would probably see bioactive surfaces and additives that stimulate the bone growth. According to Albrektsson et al. several factors can affect the osseointegration, including implant material, implant design, implant surface characteristics, status of the bone, surgical technique, and implant loading conditions [1]. Nowadays, there is an effort to speed up the osseointegration by improving the implant-to-bone interface chemically (by incorporating inorganic phases

on or into the titanium oxide layer) or physically (by increasing the level of roughness) [2]. There are some advantages regarding surface modified implants, including (a) providing a better stability between bone and implant during healing process, established by a greater contact area, (b) providing a surface configuration that may retain the blood clot, and (c) stimulating the bone formation and healing process [3]. There are several methods to improve the quality of implant surface; one of them is adding bioactive materials to the surface of the dental implant to induce osteoconductivity.

Hydroxyapatite (HA), $[\text{Ca}_{10}(\text{PO}_4)_6(\text{OH})_2]$, is a calcium phosphate bioceramic material, with osteoconductivity and excellent biocompatibility. However, apatite layers coating

the surface of the implant substrates improve the bone response. For this reason, it has been used successfully in dentistry for many years. HA products are well known as implantable ceramics for hard tissue reconstitution. An example of such application is a coating applied onto dental implants, providing enhanced fixation of the implant for the human bone [4]. HA-coated implants have often been used in load-bearing applications, because HA directly bonds to the bone and promotes the new bone formation, necessary for the implant osseointegration [5–8]. Despite advantages of HA coatings, it has some disadvantages. Enhanced susceptibility to bacterial plaque colonization and HA coating integrity are two major concerns related to HA-coated implants [9]. Such bacterial accumulation can start a chain reaction leading to lesions, and then other risk factors may combine to worsen the condition [10]. An exposed rough surface can lead to increased bacterial plaque accumulation and eventually peri-implantitis [11]. Therefore, the susceptibility of peri-implantitis should be taken into account when using HA-coated implants. It is known that the HA surface degrades and in some instances separates; hence, it has been a trend to substitute the coatings with roughened surface dental implants, which also incidentally presents better and faster integration. Although HA can be a good choice to be applied on the surface of the dental implants as a bioactive and biocompatible material, its mechanical properties (mainly the strength, roughness, and fracture toughness) need to be improved for application in load-bearing parts, since they have limited its usage to nonload-bearing parts due to their poorness [12–16]. This goal can be achievable by adding some materials to the HA coating, which has already been done to improve its final coating characteristics. These additives aim to enhance various properties of the coating, including bioactivity [17], thermal stability, and its mechanical properties.

Zircon is a tetragonal mineral, consisting of a silicate of zirconium. The group of silicate biomaterials has the ability to release silicate ions at a definite concentration which helps the osteoblasts to grow and differentiate [18], leading to bone formation. Therefore, this characteristic of zircon could be beneficial for the surface usage of dental implants. Considering several studies evaluating the additives in the dental implant coatings (such as zirconia (ZrO_2), ZrO_2 - Al_2O_3 , etc.), we sought to find a new additive with better mechanical and biological characteristics. Therefore, the bioactivity and roughness of zircon (ZrSiO_4) added to the HA coating in simulated body fluid (SBF) were evaluated in this study. SBF is an inorganic solution with a similar composition to human blood plasma without organic components. Several studies performed on nanobioceramic coatings include monitoring the behavior of a material when submersed in the saline solution [19] or SBF [20].

Plasma spraying technique is the most commonly used method for the HA coatings application. This is a thermal spraying process in which powder particles are melted in a high temperature plasma flame and propelled towards a substrate material to form a coating. The advantages of this process include high coating adhesion strength and also high deposition rate, which allow rapid formation of the coatings [21]. Surface roughness can be described using a number of

TABLE 1: Chemical composition of NHA (XRF results).

Compound	Concentration (w/w %)
Ca	75.91
P	20.09
Na	1.25
F	1.20
Mg	0.708
Sr	0.151
Cl	0.200
Si	0.150
S	0.073
Al	0.061
Cu	0.056
Zn	0.053
Fe	0.052
K	0.038
Zr	0.008
LOI*	0.376
Total	100

* Loss on ignition (1000°C, 2 h).

different parameters, while R_a (absolute value) is by far the most common. Other common parameters include R_z and R_{\max} .

The aim of this study was to evaluate the bioactivity and roughness of novel natural HA/zircon (NHA/zircon) nanobiocomposite coating, soaked in the SBF solution.

2. Materials and Methods

2.1. NHA Extraction. The present research was an experimental study. Bovine bones were boiled for 12 h to remove the attached flesh and fat. Afterwards, bones were dried at 110°C for 2 h to shed the moisture. To prevent blackening with soot during heating, bones were cut into small pieces with 10 mm thickness and heated at 500°C (bone ash) for 2 h in air to allow evaporation of organic substances. The resulting black bone ash was heated for 3 h at 850°C. This synthesis is called thermal decomposition of bone resource to create NHA. The elemental chemical analysis of NHA using X-ray fluorescence (XRF) (Philips PW1606) is shown in Table 1.

2.2. Fabrication of NHA on the Implant Cores. In this work, 316L stainless steel (SS) was used as substrate. The elemental analysis and the elemental composition (wt.%) of SS were C 0.03, Si 0.8, Mn 1.3, Cr 17.55, Ni 13, Mo 3.1, $P \leq 0.04$, $S \leq 0.03$, and Fe as the balance. Specimens with dimensions 20×10 mm (diameter \times thickness) were cut with CNC Wire Cut EDM Machine (DK7732F-china suppliers). The test was performed on cylindrical porous and all the specimens were immersed in Analar grade H_2SO_4 (specific gravity = 1.84) for 1 h in different volume concentrations varying from 5% to 25% at ambient temperatures. The samples were polished with 100–1200 grit silicon carbide (SiC) paper. In order to produce a scratch-free, mirror-finish surface, final polishing

was performed using 4,000 grit silicon carbide papers. The polished specimens were investigated by the optical microscope to ensure the absence of pits or scratches on the surface. Specimens were cleaned with acetone and thoroughly washed with distilled water. Afterward, specimens were surface treated by grit blasting in order to obtain a desired roughness of surface for better adhesion of coating to the substrate. After the surface treatment process, the specimens were cleaned with distilled water and ultrasonic device as a cleaner technique. NHA/zircon nanobiocomposite was fabricated with 0 (control), 5, 10, and 15 wt.% of zircon in NHA and coated on the surface of the 316L SS cores using plasma spray technique.

2.3. Phase and Composition Analysis. Phase structure analysis was performed by X-ray diffraction (XRD) (Philips X'Pert-MPD diffractometer with Cu K α radiation ($\lambda_1 = 0.15418$ nm) over the 2θ range of 20–80). The obtained experimental patterns were compared to the standards compiled by the Joint Committee on Powder Diffraction and Standards (JCDPS) which involved card number 09-432 for HA. The crystallite size of prepared powders was determined using XRD patterns and modified Scherrer equation. Scanning electron microscopy (SEM) analysis evaluations were performed using a Philips XL30 (Eindhoven, The Netherlands) to investigate the morphology. The Ca/P ratio was determined using energy-dispersive X-ray spectroscopy (EDX) microanalysis (FEI Quanta 200 ESEM equipped with an EDX EDS device). Samples were coated with Au using spraying, high vacuum, and 25 kV accelerating voltage. Ca and P ions contents were measured from four spots (Figure 3), and consequently the average was calculated. Transmission electron microscopy (TEM) technique (Philips CM 200 FEG: Eindhoven, The Netherlands) was utilized to evaluate the shape and size of prepared HA.

2.4. Surface Roughness Evaluation. The roughness (i.e., R_a) of each sample was measured in three directions. Four measurements were taken for each sample and then their average was determined.

2.5. In Vitro Bioactivity Evaluation. *In vitro* bioactivity was investigated by soaking the samples in SBF solution. The SBF solution was prepared according to the procedure described by Kokubo and Takadama [20]. Ion concentrations of SBF are similar to those in human blood plasma. Coated samples were soaked in the cell SBF solution (pH 7.4) at 37°C for 1, 7, and 14 days at a solid/liquid ratio of 1 mg/mL, without refreshing the soaking medium. Element analysis of SBF and physiological saline are shown in Table 2. After the predicted soaking time finished, the disc samples were rinsed with deionized water and dried in an oven at 110°C for 1 h. Samples weight loss was calculated by the following equation:

$$\text{Weight Loss percentage (WL.\%)} = \frac{W - W_0}{W_0} \times 100, \quad (1)$$

where W and W_0 are primary and secondary weights, respectively.

TABLE 2: Nominal ion concentrations of SBF in comparison with those in human blood plasma.

Ion	Ion concentrations (m mol)	
	SBF	Human blood plasma
Na ⁺	142.0	142.0
K ⁺	5.0	5.0
Mg ²⁺	1.5	1.5
Ca ²⁺	2.5	2.5
Cl ⁻	147.8	103.0
HCO ₃ ⁻	4.2	27.0
HPO ₄ ²⁻	1.0	1.0
SO ₄ ²⁻	0.5	0.5
pH	7.4	7.2–7.4

3. Results

3.1. Phase and Composition Analysis of the XRD Results. Figure 1 shows the XRD patterns and SEM images of the NHA 0% and 10% zircon coatings. Figure 1(a) indicates that the only existing phase is for HA (all the peaks belong to HA). However, the peaks observed in the XRD pattern of NHA 10% zircon had a decrease in intensity and an increase in width compared to NHA 0% zircon (Figures 1(a) and 1(c)). In addition, the XRD peaks corresponding to NHA 10% zircon shifted slightly in comparison with NHA 0% zircon (Figures 1(a) and 1(c)). The crystallite sizes of the prepared NHA samples with different degrees of zircon content calculated using XRD data are shown in Table 5. The crystallite size of the obtained nanopowders is in the range of 25.5–32 nm. Determination of crystallite sizes from XRD peak widths makes assumptions on crystallite shape and crystallite size.

3.2. Scherrer Equation. The modified Scherrer equation is advantageous for decreasing the sum of absolute values of errors, $\sum (\pm \Delta \ln \beta)^2$, and producing a single line through the points to give a single value of intercept $\ln(k\lambda/L)$ [22]. At this sample, shown in Figure 2, the linear regression plot is obtained as $y = 0.9267x - 5.225$. This is equivalent to $\ln \beta = \ln(1/\cos \theta) + \ln(k\lambda/L)$. From this line, the intercept is -5.225 , $e^{-5.225} = k\lambda/L$, and $L = 25.5$ nm. Thus, HA crystallite size was 25.5 nm.

3.3. SEM, EDX, and TEM Microstructures. Figure 3 shows the SEM micrographs of NHA powder. In all samples, we found nanoparticles of HA crystals, agglomerated with different dimensions. Morphology of particles is sphere and semisphere. Microchemical composition of the NHA sample was determined using EDX (Figure 3).

TEM technique was utilized to evaluate the shape and size of prepared NHA (Figure 4). The TEM image reveals that the powders are formed by agglomerates of irregular particles in 200 nm, consistent with values calculated from XRD data.

As shown in Figure 1, NHA crystal sizes are in micron size, some particles are spherical, and the others are in sharp shape. The agglomerated particles are composed of very fine particles.

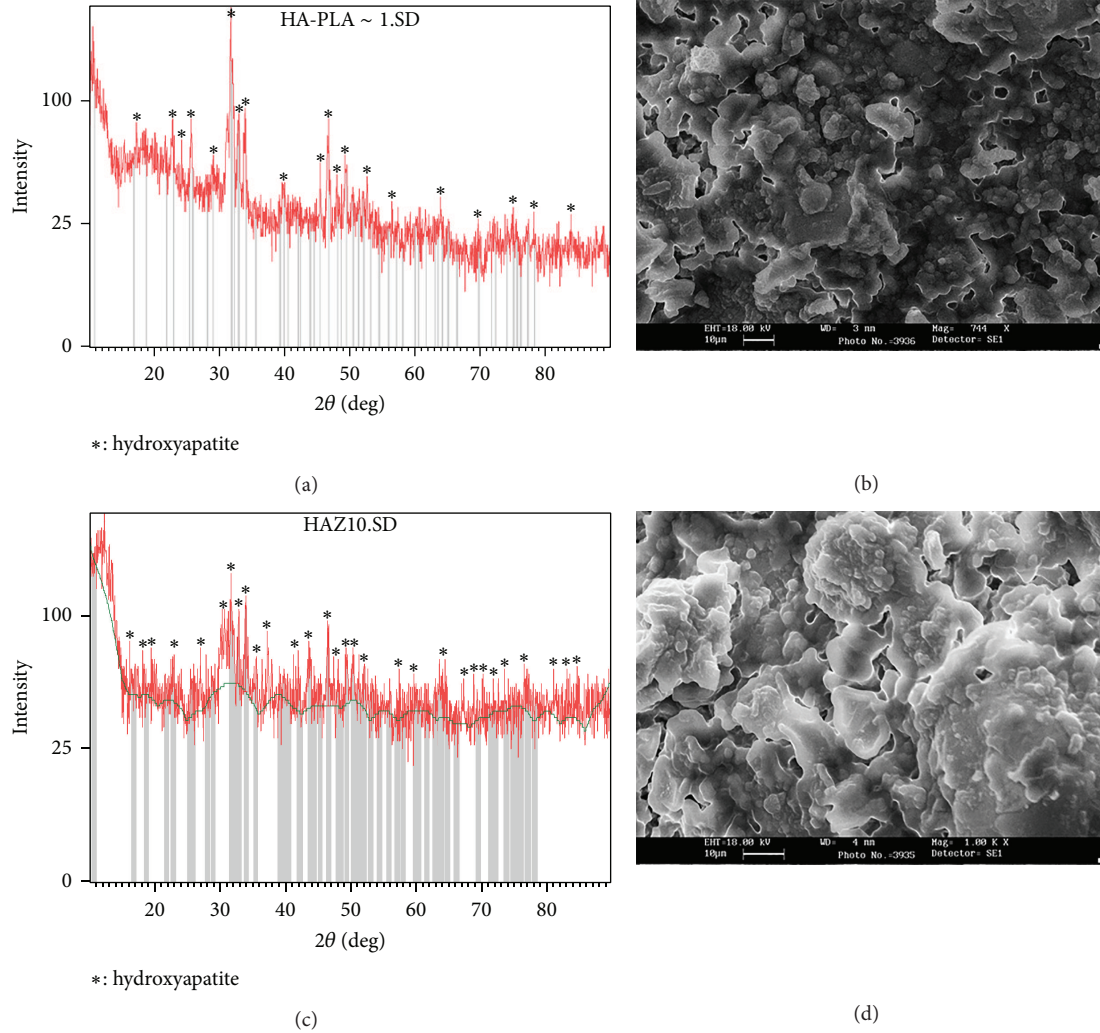


FIGURE 1: (a) XRD pattern and (b) SEM micrograph of the NHA 0% coated by plasma spraying. (c) XRD pattern and (d) SEM micrograph of the NHA 10% zircon coated by plasma spraying.

3.4. Surfaces Roughness Results. The results are given in Table 3. Each sample was measured in three directions. Four measurements were taken for each sample and then their average was determined. R_a was found to vary between 12.63 and 14.85 μm . Coatings with four degrees of average roughness (R_a : 12.63, 14.30, 14.54, and 12.85 μm for NHA 0%, 5%, 10%, and 15% of zircon, resp.) were created. The maximum average R_a was found in the NHA 10% zircon sample.

3.5. In Vitro Bioactivity Evaluation. NHA/ZrSiO₄ nanobio-composite powder with different ZrSiO₄ contents was prepared and coated by plasma spray method. *In vitro* bioactivity of nanopowders was investigated by soaking the powders in the SBF solution. SEM observations of the NHA 0% and 10% zircon coatings soaked in SBF for 1 and 2 weeks are illustrated in Figure 5. Results indicated that during 1, 7, and 14 days of soaking, shown in Table 4, calcium ions were released in the solution. As shown in Figure 6(a), there was a clear increase

TABLE 3: Surfaces roughness results.

Experimental name	Composite (zircon %)	R_a (μm)	Average R_a (μm)
N1	0	12.92	12.63
N2	0	13.97	
N3	0	11	
N4	5	13.59	14.30
N5	5	15.93	
N6	5	13.39	
N7	10	15.55	14.54
N8	10	13.77	
N9	10	14.30	
N10	15	11.86	12.85
N11	15	13.44	
N12	15	13.24	

TABLE 4: The HA biodegradation properties of all the samples in the SBF.

Samples	Ca ²⁺ release in SBF after 1 week (ppm)	Ca ²⁺ release in SBF after 2 weeks (ppm)	WL. % of samples in SBF after 1 week (mg)	WL. % of samples in SBF after 2 weeks (mg)
NHA 0% zircon	36	78	1.13	0.28
NHA 5% zircon	40	90	2.40	2.80
NHA 10% zircon	62	115	3.31	4.02
NHA 15% zircon	48	96	0.25	1.11

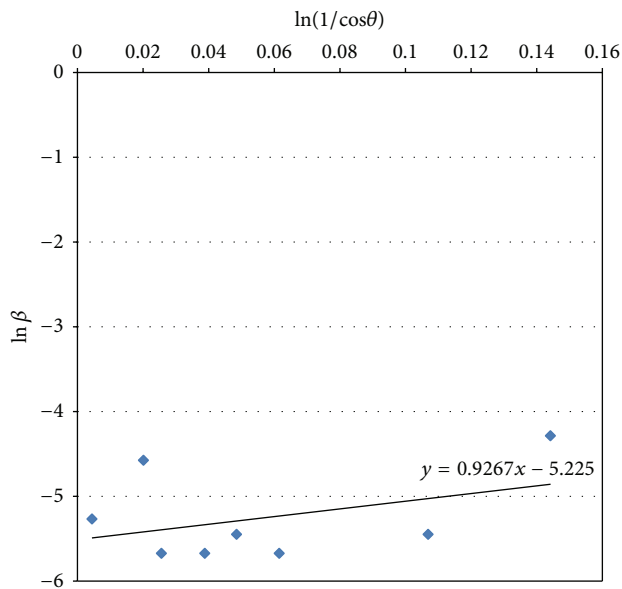
FIGURE 2: Plot of $\ln\beta$ versus $\ln(1/\cos\theta)$ of the HA sample heated at 850°C for 3 h.

TABLE 5: Crystallographic Parameters of the HA Phase of all the Samples.

Samples	Crystallinity (X_c %)	Crystallite Size ± 1 (nm)
NHA 0% Zircon	44.8	25.5
NHA 5% Zircon	43.2	28
NHA 10% Zircon	41.1	32
NHA 15% Zircon	42.9	28.2

in calcium releasing in the sample containing 10% zircon. It depends on two reasons: (1) increase of the roughness (Figure 6(b)) and (2) decrease of the crystallinity of sample containing 10% wt. ZrSiO_4 ($X_c = 41.1\%$) (Table 5).

4. Discussion

In the present study, bioactivity of NHA/zircon coatings with various amounts of zircon (0 wt.%, 5 wt.%, 10 wt.%, and 15 wt.%) within SBF solution was evaluated using XRD and SEM interpretations. The maximum average R_a ($14.54 \mu\text{m}$) was found in the NHA 10 wt.% of zircon coating. In addition, crystallinity (X_c) was measured by XRD data, which indicated the minimum value ($X_c = 41.1\%$) for the sample

containing 10 wt.% of zircon. Maximum bioactivity occurred in the sample containing 10 wt.% of zircon.

According to Kokubo et al. [23–25], *in vitro* immersion of bioactive materials in SBF is thought to make *in vivo* surface structure changes in materials such as bioactive glass/ceramic. Therefore, to evaluate this, we soaked NHA/zircon samples in SBF solution. The grown layer is sometimes called a bone-like apatite because of the XRD pattern similar to that of bone apatite with broad peaks at 2θ angles of HA, which indicates a superfine grain of apatite crystallite [26]. Overall conclusion is that zircon is a very complex material. It is totally different from titanium, a metal used in dentistry in its pure (or commercially pure) form. We reached interesting findings from the present work that NHA/zircon (a) proved to be bioactive and (b) had high roughness and interesting microstructural properties.

There is a consensus regarding HA to be osteoconductive [27, 28] and biocompatible [29, 30]. The biocompatibility [31, 32], osteoconductivity, and osseointegration characteristics of zirconia are reported in several studies [33]. In addition, zirconia has a high flexural strength and fracture toughness. Accordingly, the combination of these characteristics could be found in the prepared coating, the novel NHA/zircon. In fact, this coating due to its bioactivity might speed up the osseointegration. However, this claim should be proved by future cell culturing and animal studies.

It is reported that topography and surface roughness positively affect healing process [34–36]. Dohan Ehrenfest et al. reported that possible physical improvement of the interface between bone and implant by increasing the level of roughness, leading to speed up osseointegration and its quality [2]. Human and animal studies have shown significantly greater bone and implant contact at rough surface implants compared to machined surface implants [37]. In 2009, a consensus report reached a conclusion that “moderately rough and rough surfaces provided enhanced bone integration compared with smooth and minimally rough surfaces” [38]. In this regard, as zircon increased the roughness of HA coating, the positive role of NHA/zircon coating for a fast and better healing might be supported. On the other hand, classic HA-coated implants were reported to have a higher occurrence of complications [39]. In fact, the surface roughness may have a significant impact on the contamination [2], amount and quality of plaque formation [40]. Especially in patients with poor oral hygiene, an exposed rough surface can lead to increased bacterial plaque accumulation and eventually peri-implantitis [11]. However, evidence for the influence of the implant surface characteristics as a risk

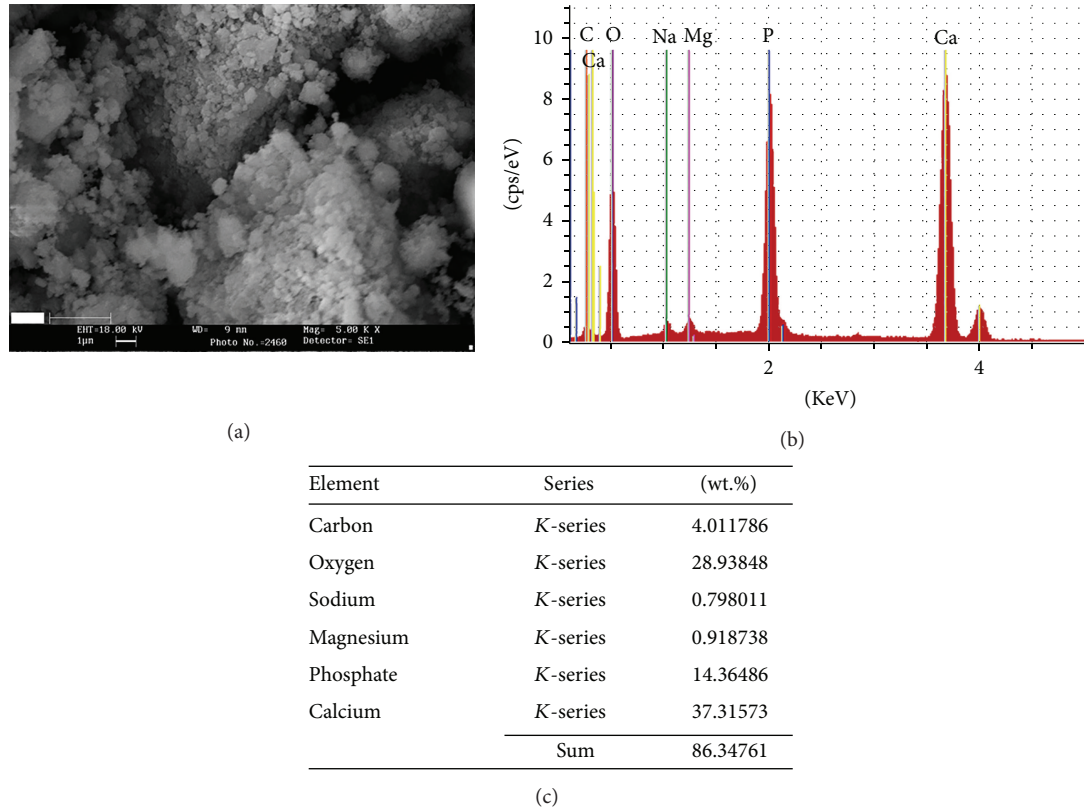


FIGURE 3: (a) SEM micrographs of the NHA powder, (b) EDX spectrum of the NHA powder, and (c) microchemical composition of the NHA powder determined by EDX.

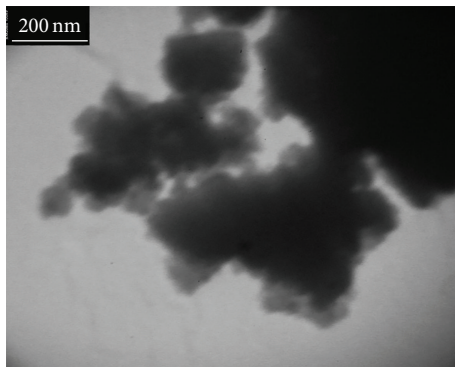


FIGURE 4: TEM micrograph of prepared NHA at 850°C for 3 h.

indicator for peri-implantitis is very limited [41, 42]. In overall, there is controversy in the literature regarding the effect of surface characteristics and peri-implantitis. Based on two systematic reviews in 2008 and 2011, due to limited data available in the literature, there is no evidence that implant surface characteristics can have a significant influence on the initiation of peri-implantitis [41, 42]. Moreover, Persson et al. investigated the effect of surface roughness on the healing following peri-implantitis treatment in the beagle dog [43]. They found further amount of reosseointegration in implants with a rough surface, likely because the rough surface can

facilitate the stability of the blood clot during the early phase of healing.

The advantages of rough-surfaced dental implants could be described by provided support for the coagulum development and facilitating greater bone healing and better qualified osseointegration. Perhaps hybrid implants should be considered in individuals that are highly predisposed to periodontitis [42]. In such cases, inflammation due to a rough or badly designed superstructure causes bone loss and exposed smooth threads. If in such patients the smooth threads become exposed in the oral cavity, the threads may be less plaque retentive, increasing the possibility of arresting the progression of peri-implantitis.

In the current study, crystallinity was measured according to the procedure described by Karamian et al. [44]. As observed in the X_c results, NHA 10% zircon has less crystallinity and more amorphous structure. The dissolution and precipitation behaviour of apatites are the principle factors governing their bioactivity [45]. The obtained SEM micrographs (Figure 5) show the formation and growth of apatite crystals on the surfaces of the NHA 10% zircon coating after soaking in the SBF solution during several periods of time. SEM observations showed amorphous and glassy surface structure, leading to more biodegradation of NHA 10% zircon coating compared to classic HA-coated implants. Dissolution of NHA/zircon coating may have significant advantages, such as an increase in calcium and phosphate.

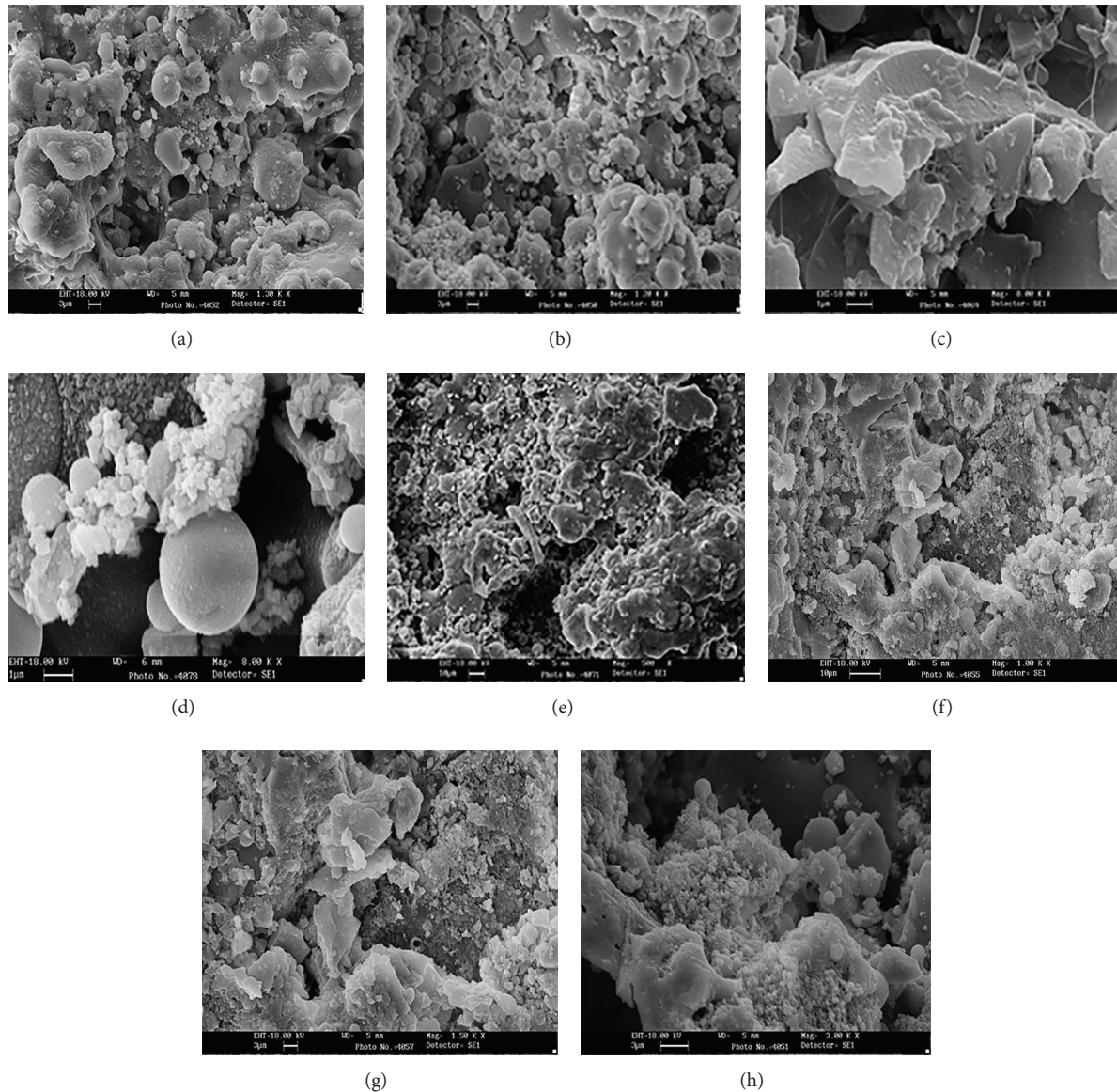


FIGURE 5: SEM observations of the coatings soaked in SBF for (a), (b) 1 week, NHA 10% zircon, (c), (d) 2 weeks, NHA 10% zircon, (e), (f) 1 week, NHA 0% zircon, and (g), (h) 2 weeks, NHA 0% zircon.

The presence of calcium is considered to regulate initiation of messenger ribonucleic acid (mRNA) transcription and protein synthesis and therefore lead to cellular differentiation [46]. It was reported that more soluble phases on the coatings might be more favourable for a stable interface with the biological environment [47]. It might be due to the release of calcium ions necessary for bone formation. As shown, the amount of calcium release in the NHA 10% zircon was three times more than that in classic HA coating (Figure 6(a)). On the other hand, delamination or biodegradation of the coatings might be partly responsible for the failure in the implant-coating interface [48, 49]. These contradictions need to be evaluated by further future studies.

Clinical data recommend that HA-coated implants may be valuable treatment indications when placing implants in

type IV bone, in fresh extraction sites, and in grafted maxillary or nasal sinuses, or when using shorter implants (less than or equal to 10 mm) [9]. Thus, prepared NHA/zircon coating compared to classic HA coating could be more useful in the aforementioned situations due to the higher bioactivity and roughness.

Zircon is a nonresorbable metal which provides good mechanical properties, superior to other ceramic materials, such as high bioactivity and roughness. Zircon seems to be suitable for dental application due to its good chemical and material stability, high strength, and proper roughness. However, considering all the limitations of current work, more studies are needed about the novel NHA/zircon coating. Besides, NHA/zircon as a new material needs extensive *in vivo* and long-term controlled studies.

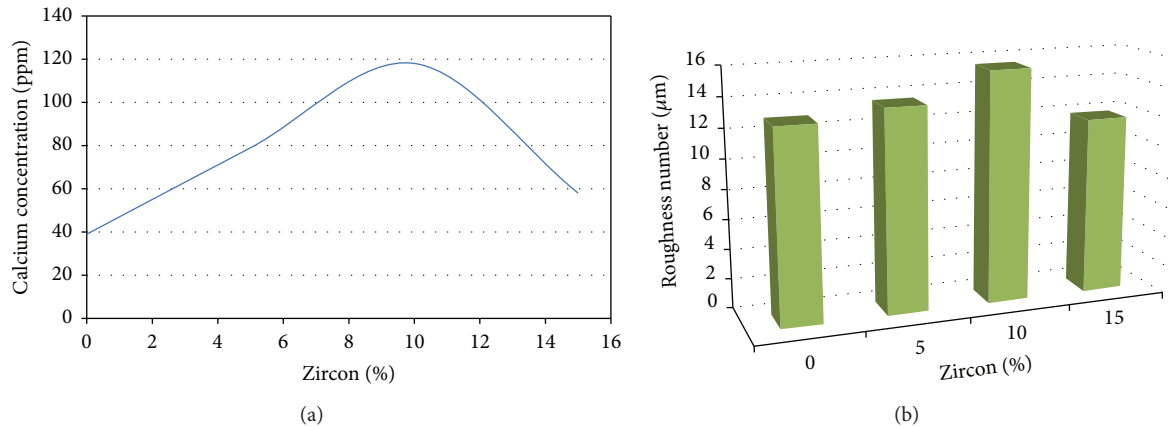


FIGURE 6: (a) Calcium concentration (Ca^{2+} released) after 2 weeks, coatings in SBF solution. (b) Average amount of roughness of the samples.

5. Conclusion

The maximum R_a ($14.54 \mu\text{m}$) was found in the sample containing 10% wt. ZrSiO_4 . In addition, the maximum calcium released (115 ppm) was found in this sample, which depends on two reasons: (a) increase of roughness and (b) decrease of crystallinity (to 41.1%). NHA/zircon nanocomposite coating possessed a good bioactivity and roughness and could be suitable for hard tissue formation in the field of biomedical implants. Further studies are needed to validate the results of this survey.

Conflict of Interests

The authors declare that there is no conflict of interests regarding the publication of this paper.

Acknowledgment

The authors would like to extend their gratitude for the support provided by Najafabad Branch, Islamic Azad University, Isfahan, Iran.

References

- [1] T. Albrektsson, P. I. Branemark, H. A. Hansson, and J. Lindstrom, "Osseointegrated titanium implants. Requirements for ensuring a long-lasting, direct bone-to-implant anchorage in man," *Acta Orthopaedica Scandinavica*, vol. 52, no. 2, pp. 155–170, 1981.
- [2] D. M. Dohan Ehrenfest, P. G. Coelho, B. S. Kang, Y. T. Sul, and T. Albrektsson, "Classification of osseointegrated implant surfaces: materials, chemistry and topography," *Trends in Biotechnology*, vol. 28, no. 4, pp. 198–206, 2010.
- [3] A. Wennerberg and T. Albrektsson, "Effects of titanium surface topography on bone integration: a systematic review," *Clinical Oral Implants Research*, vol. 20, no. 4, pp. 172–184, 2009.
- [4] C. V. M. Rodrigues, P. Serricella, A. B. R. Linhares et al., "Characterization of a bovine collagen-hydroxyapatite composite scaffold for bone tissue engineering," *Biomaterials*, vol. 24, no. 27, pp. 4987–4997, 2003.
- [5] R. Garcia and R. H. Doremus, "Electron microscopy of the bone-hydroxylapatite interface from a human dental implant," *Journal of Materials Science: Materials in Medicine*, vol. 3, no. 2, pp. 154–156, 1992.
- [6] Y. Harada, "Experimental studies of healing process on compound blocks of hydroxyapatite (HAP) particles and tricalcium phosphate (TCP) powder implantation in rabbit mandible—comparison of HAP/TCP ratios and plastic methods," *Shika Gakuho. Dental Science Reports*, vol. 89, no. 2, pp. 263–297, 1989.
- [7] L. L. Hench, "Bioceramics: from concept to clinic," *The American Ceramic Society Bulletin*, vol. 74, no. 7, pp. 1487–1510, 1991.
- [8] T. J. Webster, C. Ergun, R. H. Doremus, and R. Bizios, "Hydroxylapatite with substituted magnesium, zinc, cadmium, and yttrium. II. Mechanisms of osteoblast adhesion," *Journal of Biomedical Materials Research*, vol. 59, no. 2, pp. 312–317, 2002.
- [9] A. R. Biesbrock and M. Edgerton, "Evaluation of the clinical predictability of hydroxyapatite-coated endosseous dental implants: a review of the literature," *The International journal of oral & maxillofacial implants*, vol. 10, no. 6, pp. 712–720, 1995.
- [10] J. Mouhyi, D. M. Dohan Ehrenfest, and T. Albrektsson, "The peri-implantitis: implant surfaces, microstructure, and physicochemical aspects," *Clinical Implant Dentistry and Related Research*, vol. 14, no. 2, pp. 170–183, 2012.
- [11] L. Zetterqvist, S. Feldman, B. Rotter et al., "A prospective, multicenter, randomized-controlled 5-year study of hybrid and fully etched implants for the incidence of peri-implantitis," *Journal of Periodontology*, vol. 81, no. 4, pp. 493–501, 2010.
- [12] J. W. Choi, Y. M. Kong, H. E. Kim, and I. S. Lee, "Reinforcement of hydroxyapatite bioceramic by addition of Ni_3Al and Al_2O_3 ," *Journal of the American Ceramic Society*, vol. 81, no. 7, pp. 1743–1748, 1998.
- [13] L. L. Hench and J. Wilson, *An Introduction to Bioceramics*, World Scientific, River Edge, NJ, USA, 1993.
- [14] S. Kim, Y. M. Kong, I. S. Lee, and H. E. Kim, "Effect of calcinations of starting powder on mechanical properties of hydroxyapatite-alumina bioceramic composite," *Journal of Materials Science: Materials in Medicine*, vol. 13, no. 3, pp. 307–310, 2002.
- [15] Y. M. Kong, S. Kim, H. E. Kim, and I. S. Lee, "Reinforcement of hydroxyapatite bioceramic by addition of ZrO_2 coated with Al_2O_3 ," *Journal of the American Ceramic Society*, vol. 82, no. 11, pp. 2963–2968, 1999.

- [16] I. S. Lee, C. N. Whang, H. E. Kim, J. C. Park, J. H. Song, and S. R. Kim, "Various Ca/P ratios of thin calcium phosphate films," *Materials Science and Engineering C*, vol. 22, no. 1, pp. 15–20, 2002.
- [17] T. J. Levingstone, *Optimisation of Plasma Sprayed Hydroxyapatite Coatings*, Dublin City University, 2008.
- [18] C. Wu, J. Chang, S. Ni, and J. Wang, "In vitro bioactivity of akermanite ceramics," *Journal of Biomedical Materials Research A*, vol. 76, no. 1, pp. 73–80, 2006.
- [19] T. M. Sridhar, U. Kamachi Mudali, and M. Subbaiyan, "Sintering atmosphere and temperature effects on hydroxyapatite coated type 316L stainless steel," *Corrosion Science*, vol. 45, no. 10, pp. 2337–2359, 2003.
- [20] T. Kokubo and H. Takadama, "How useful is SBF in predicting in vivo bone bioactivity?" *Biomaterials*, vol. 27, no. 15, pp. 2907–2915, 2006.
- [21] S. Jinawath, D. Pongkao, and M. Yoshimura, "Hydrothermal synthesis of hydroxyapatite from natural source," *Journal of Materials Science: Materials in Medicine*, vol. 13, no. 5, pp. 491–494, 2002.
- [22] A. Monshi and S. S. Attar, "A new method to measure nano size crystals by scherrer equation using XRD," *Majlesi Journal of Materials Engineering*, vol. 2, no. 3, 2010.
- [23] T. Kokubo, S. Ito, Z. T. Huang et al., "Ca, P-rich layer formed on high-strength bioactive glass-ceramic A-W," *Journal of Biomedical Materials Research*, vol. 24, no. 3, pp. 331–343, 1990.
- [24] T. Kokubo, H. Kushitani, C. Ohtsuki, S. Sakka, and T. Yamamuro, "Chemical reaction of bioactive glass and glass-ceramics with a simulated body fluid," *Journal of Materials Science: Materials in Medicine*, vol. 3, no. 2, pp. 79–83, 1992.
- [25] P. Li, C. Ohtsuki, T. Kokubo et al., "Effects of ions in aqueous media on hydroxyapatite induction by silica gel and its relevance to bioactivity of bioactive glasses and glass-ceramics," *Journal of Applied Biomaterials*, vol. 4, no. 3, pp. 221–229, 1993.
- [26] A. S. Posner, "The mineral of bone," *Clinical Orthopaedics and Related Research*, vol. 200, pp. 87–99, 1985.
- [27] K. Soballe, H. Brockstedt-Rasmussen, E. S. Hansen, and C. Bunger, "Hydroxyapatite coating modifies implant membrane formation: controlled micromotion studied in dogs," *Acta Orthopaedica Scandinavica*, vol. 63, no. 2, pp. 128–140, 1992.
- [28] K. Soballe, E. S. Hansen, B. H. Rasmussen, P. H. Jorgensen, and C. Bunger, "Tissue ingrowth into titanium and hydroxyapatite-coated implants during stable and unstable mechanical conditions," *Journal of Orthopaedic Research*, vol. 10, no. 2, pp. 285–299, 1992.
- [29] D. P. Rivero, J. Fox, A. K. Skipor, R. M. Urban, and J. O. Galante, "Calcium phosphate-coated porous titanium implants for enhanced skeletal fixation," *Journal of Biomedical Materials Research*, vol. 22, no. 3, pp. 191–201, 1988.
- [30] C. A. van Blitterswijk, S. C. Hesselting, J. J. Grote, H. K. Koerten, and K. de Groot, "The biocompatibility of hydroxyapatite ceramic: a study of retrieved human middle ear implants," *Journal of Biomedical Materials Research*, vol. 24, no. 4, pp. 433–453, 1990.
- [31] Y. Ichikawa, Y. Akagawa, H. Nikai, and H. Tsuru, "Tissue compatibility and stability of a new zirconia ceramic in vivo," *The Journal of Prosthetic Dentistry*, vol. 68, no. 2, pp. 322–326, 1992.
- [32] T. Albrektsson, H. A. Hansson, and B. Ivarsson, "Interface analysis of titanium and zirconium bone implants," *Biomaterials*, vol. 6, no. 2, pp. 97–101, 1985.
- [33] P. Assal, "The osseointegration of zirconia dental implants," *Schweizer Monatsschrift für Zahnmedizin*, vol. 123, no. 7-8, pp. 644–654, 2012.
- [34] G. E. Romanos and C. B. Johansson, "Immediate loading with complete implant-supported restorations in an edentulous heavy smoker: Histologic and histomorphometric analyses," *International Journal of Oral and Maxillofacial Implants*, vol. 20, no. 2, pp. 282–290, 2005.
- [35] R. Crespi, P. Capparé, E. Gherlone, and G. E. Romanos, "Immediate versus delayed loading of dental implants placed in fresh extraction sockets in the maxillary esthetic zone: a clinical comparative study," *International Journal of Oral and Maxillofacial Implants*, vol. 23, no. 4, pp. 753–758, 2008.
- [36] V. Borsari, G. Giavaresi, M. Fini et al., "Physical characterization of different-roughness titanium surfaces, with and without hydroxyapatite coating, and their effect on human osteoblast-like cells," *Journal of Biomedical Materials Research B: Applied Biomaterials*, vol. 75, no. 2, pp. 359–368, 2005.
- [37] R. J. Lazzara, T. Testori, P. Trisi, S. S. Porter, and R. L. Weinstein, "A human histologic analysis of osseointegration and machined surfaces using implants with 2 opposing surfaces," *International Journal of Periodontics and Restorative Dentistry*, vol. 19, no. 2, pp. 117–129, 1999.
- [38] N. P. Lang and S. Jepsen, "Implant surfaces and design (Working Group 4)," *Clinical Oral Implants Research*, vol. 20, supplement 4, pp. 228–231, 2009.
- [39] A. Piattelli, F. Cosci, A. Scarano, and P. Trisi, "Localized chronic suppurative bone infection as a sequel of peri-implantitis in a hydroxyapatite-coated dental implant," *Biomaterials*, vol. 16, no. 12, pp. 917–920, 1995.
- [40] W. Teughels, N. Van Assche, I. Sliepen, and M. Quirynen, "Effect of material characteristics and/or surface topography on biofilm development," *Clinical Oral Implants Research*, vol. 17, supplement 2, pp. 68–81, 2006.
- [41] L. J. A. Heitz-Mayfield, "Peri-implant diseases: diagnosis and risk indicators," *Journal of Clinical Periodontology*, vol. 35, supplement 8, pp. 292–304, 2008.
- [42] S. Renvert, I. Polyzois, and N. Claffey, "How do implant surface characteristics influence periimplant disease?" *Journal of Clinical Periodontology*, vol. 38, supplement 11, pp. 214–222, 2011.
- [43] L. G. Persson, T. Berglundh, L. Sennnerby, and J. Lindhe, "Re-osseointegration after treatment of peri-implantitis at different implant surfaces," *Clinical Oral Implants Research*, vol. 12, no. 6, pp. 595–603, 2001.
- [44] E. Karamian, A. Khandan, M. Eslami, H. Gheisari, and N. Rafiaei, "Investigation of HA nanocrystallite size crystallographic characterizations in NHA, BHA and HA pure powders and their influence on biodegradation of HA," *Advanced Materials Research*, vol. 829, pp. 314–318, 2014.
- [45] Q. Zhang, J. Chen, J. Feng, Y. Cao, C. Deng, and X. Zhang, "Dissolution and mineralization behaviors of HA coatings," *Biomaterials*, vol. 24, no. 26, pp. 4741–4748, 2003.
- [46] M. Gregoire, I. Orly, and J. Menanteau, "The influence of calcium phosphate biomaterials on human bone cell activities. An in vitro approach," *Journal of Biomedical Materials Research*, vol. 24, no. 2, pp. 165–177, 1990.
- [47] C. Van Blitterswijk, H. Leenders, J. van der Brink, Y. Bovell, J. Flach, J. de Bruijn et al., "Degradation and interface reactions of hydroxyapatite coatings: effect of crystallinity," *Transactions of the Society for Biomaterials*, vol. 16, p. 337, 1993.

- [48] Y. L. Chang, D. Lew, J. B. Park, and J. C. Keller, "Biomechanical and morphometric analysis of hydroxyapatite-coated implants with varying crystallinity," *Journal of Oral and Maxillofacial Surgery*, vol. 57, no. 9, pp. 1096–1108, 1999.
- [49] J. J. Lee, L. Rouhfar, and O. R. Beirne, "Survival of hydroxyapatite-coated implants: a meta-analytic review," *Journal of Oral and Maxillofacial Surgery*, vol. 58, no. 12, pp. 1372–1379, 2000.

Research Article

Solubility of Two Resin Composites in Different Mouthrinses

Sezin Ozer,¹ Emine Sen Tunc,¹ Nuray Tuloglu,² and Sule Bayrak²

¹ Faculty of Dentistry, Department of Pediatric Dentistry, Ondokuz Mayıs University, Kurupelit, 55139 Samsun, Turkey

² Department of Pediatric Dentistry, Faculty of Dentistry, Eskisehir Osmangazi University, Eskisehir, Turkey

Correspondence should be addressed to Sezin Ozer; sezinsezgin78@yahoo.com

Received 19 February 2014; Accepted 20 March 2014; Published 7 April 2014

Academic Editor: David M. Dohan Ehrenfest

Copyright © 2014 Sezin Ozer et al. This is an open access article distributed under the Creative Commons Attribution License, which permits unrestricted use, distribution, and reproduction in any medium, provided the original work is properly cited.

Aim. This study aimed to compare the solubility of a universal restorative resin composite (Filtek Z250; FZ250) and a silorane-based resin composite (Filtek Silorane; FS) after immersion in alcohol-containing mouthrinse, alcohol-free mouthrinse, and artificial saliva. **Methods.** 30 discs (10 mm × 1 mm) were prepared from each material and desiccated until a constant mass was obtained. Specimens were immersed in the test solutions for two days and desiccated again. Solubility was calculated based on the change in weight of each specimen before and after immersion. Data was analyzed using two-way ANOVA and Tukey's Post Hoc test ($P < 0.05$). **Results.** Solubility values for both resin composites were the highest in the alcohol-containing mouthrinse. FZ250 showed greater solubility than FS; the difference was only significant in artificial saliva. **Conclusion.** Both resin-composite materials tested exhibited some degree of solubility in each of the test solutions. The use of an alcohol-free mouthrinse may be preferable for patients with extensive composite restorations.

1. Introduction

Dental composites constitute an important group of materials in modern restorative dentistry [1]. Composites—which generally consist of a resin matrix, inorganic filler, and coupling agent—are becoming more and more popular as dental restorative materials because of their strength, rapid polymerization, and esthetic appearance [2]. However, polymerization shrinkage and shrinkage-related stress are two major drawbacks of resin composites that still need to be addressed. In order to overcome these shortcomings, dental siloranes consisting of a new type of organic matrix (i.e., monomers with a ring-opening oxirane) were introduced in 2007 [3].

Upon intraoral application, resin composites face constant exposure to an aqueous environment. Water diffused into the resin matrix may contribute to the relaxation of polymerization shrinkage stress to some extent [4], and, by expanding the polymer matrix and increasing the bulk volume of the resin composite, water sorption may reduce the size of marginal gaps generated by polymerization shrinkage [5]. On the other hand, water sorption may lead to degradation of the resin matrix and debonding of the matrix-filler interface, resulting in a deterioration of mechanical

properties. In addition, leakage of fillers, ions, and organic substances such as residual monomers, methacrylic acid, and formaldehyde from resin composite material can occur as a result of exposure to an aqueous environment. Some of these organic substances are potent irritants and may induce delayed allergic reactions. Both material degradation and leakage have been shown to be dependent upon time and material composition [6].

Effective plaque control is crucial for the maintenance of periodontal health and control of cariogenic activity. For most individuals, toothbrushing with a dentifrice is the most efficient, safe and economical method of removing plaque; however, many individuals find it difficult to achieve a plaque-free dentition with this method alone. While the use of an antiseptic agent such as a mouthrinse as an adjunct to toothbrushing with a dentifrice may be justified, especially in caries-active patients [7, 8], the detrimental effects of mouthrinses on resin composite restorations must be taken into account [9].

The organic matrix of conventional resin composites is generally based on methacrylate chemistry, especially cross-linking dimethacrylates. The solubility of dimethacrylate-based resin composites in various solutions including water

and mouthrinses has been widely studied [2, 10–12]; however, few studies have been carried out on silorane-based resin composites [13–15]. Therefore, this study aimed to measure the solubility of two different resin composites in three different solutions: an alcohol-free mouthrinse, an alcohol-containing mouthrinse, and artificial saliva [16]. The null hypothesis was that solubility values would not differ, regardless of the restorative material or solution tested.

2. Materials and Methods

2.1. Restorative Materials and Solutions. This study employed a randomized factorial design conducted with 10 replications of 2 different restorative materials (FZ250 and FS) and 3 different solutions (artificial saliva, an alcohol-free mouthrinse (Oral-B, Pro-Expert), and an alcohol-containing mouthrinse (Oral-B, Advantage)) (Table 1).

2.2. Preparation of Specimens. For each material, a total of 30 disc-shaped specimens were prepared using a plastic mold ($1 \pm 0.1 \text{ mm} \times 10 \pm 0.1 \text{ mm}$). The mold was filled and pressed by hand between two glass microscope slides to extrude any excess material. Specimens were light-cured on both sides and in different positions for a total of 60 seconds using an LED curing unit (Elipar Free Light II, 3M/ESPE, St. Paul, MN, USA; light intensity: 1000 mW/cm^2). Specimens were removed from the molds, and any excess material was removed by gently grinding on both sides with 600-grit silicon carbide paper (Phoenix Beta, Buehler, Germany). Debris was removed with a dust blower.

2.3. Solubility Measurements. Solubility measurements were conducted in line with ISO 4049 standards [17]. A digital caliper (Digimatic Caliper, Mitutoyo, Tokyo, Japan; accuracy = 0.002 mm) was used to measure diameter and thickness. The diameter of each specimen was measured at two points at right angles to one another, and the mean diameter was calculated. The thickness of each specimen was measured at the center of the specimen and at four equally spaced points on the circumference, and the mean thickness was calculated. The volume (V) of each specimen was calculated in mm^3 using the formula $V = \pi \times r^2 \times h$, where r is the mean sample radius (diameter/2) and h is the mean sample thickness.

For each material, 10 specimens were placed in a glass vial containing 10 mL of artificial saliva, 10 in a glass vial containing 10 mL of alcohol-free mouthrinse (Oral-B, Pro-Expert) and 10 in a glass vial containing 10 mL of alcohol-containing mouthrinse (Oral-B, Advantage). Vials were wrapped in aluminum foil to exclude light and placed in an incubator at 37°C .

Specimens were weighed using an analytical scale accurate up to 0.0001 mg (Precise XB 220A, Switzerland). All specimens were stored in a vacuum desiccator at 37°C until a constant weight (m_0) was obtained. Specimens were then immersed in the solutions for 2 days, removed, and desiccated again until a constant mass was obtained, and the weights were recorded again (m_1). Solubility (SL) was recorded in

$\mu\text{g/mm}^3$ as the change in weight before and after immersion using the formula $\text{SL} = m_0 - m_1 / V$, where V is the volume of the sample in mm^3 .

2.4. Statistical Analysis. Statistical analysis was conducted using the software SPSS 12.0 (SPSS Software, Munich, Germany). Means and standard deviations were calculated, and multiple comparisons were performed using two-way ANOVA and Tukey's Post Hoc test, with a level of $P < 0.05$ considered statistically significant.

3. Results

Means, standard deviations, and significant differences in solubility are presented in Table 2. Solubility values of FS were lower than those of FZ250 in each of the solutions tested; however, these differences were only statistically significant in artificial saliva ($P < 0.05$). Although no statistically significant differences were observed between the solubility values of the same material in different mouthrinses ($P > 0.05$), solubility values for both materials were higher in the alcohol-containing mouthrinse than in the alcohol-free mouthrinse.

4. Discussion

The current study found the solubility of the universal resin composite FZ250 to be higher than that of the silorane resin composite FS; however, the difference between the two was only statistically significant in artificial saliva ($P < 0.05$). Thus, the null hypothesis was accepted, with the exception of solubility performance in artificial saliva.

Excessive solubility of dental restorative materials can lead to surface deformation and marginal discrepancies. Resin composite materials come into extensive contact with oral fluids, food components, and drinks in the oral environment [18], and while the solubility of dimethacrylate-based resin composites in different solutions has been widely studied [2, 10–12], to our knowledge, there is very little information available regarding the solubility of silorane-based resin composites [13–15]. Therefore, the present study aimed to evaluate the solubility of FS and FZ250 in 3 different solutions.

Solubility mean values presented by the composite resins tested varied from 2.3 to $4.2 \mu\text{g/mm}^3$; these values were lower than the maximum value established by the ISO 4049 standard ($<7.5 \mu\text{g/mm}^3$) [17]. Although the direct exploration is not possible, the results of the present study showed that the solubility of all materials in all solutions is acceptable for ISO 4049.

With the exception of artificial saliva, the solubility of FS and FZ250 did not differ significantly ($P > 0.05$); however, the solubility of FZ250 was greater than that of FS. It is likely that the low solubility of FS is related to the distinctive polymerization characteristics of the material. This finding is consistent with a previous study showing silorane-based resin composites to be more hydrophobic than methacrylate-based resin composites [13, 19]. The solubility

TABLE 1: Materials used in the study.

Material	Contents	Lot no	Manufacturer
Filtek Z250 universal restorative	Bisphenol A polyethyleneglycol diether dimethacrylate (bis-EMA) (5–10% by wt), silane treated ceramic (75–85% by wt), urethane dimethacrylate (UDMA) (5–10% by wt), bisphenol-A-glycidyl dimethacrylate (Bis-GMA) (<5% by wt), triethyleneglycol dimethacrylate (TEGDMA) (<5% by wt), and water Filled to 60% by volume with zircon silica filler, average particle size = 0.6 μ m	8FA	3M/ESPE, St. Paul, MN, USA
Filtek Silorane (posterior restorative)	Silorane (3,4-epoxycyclohexylethylcyclo-polymethylsiloxane, bis-3,4-epoxycyclohexylethyl-phenylmethylsilane) Fillers: Quarz (silane layer) radiopaque yttrium fluoride Filler loading 76% (wt %)	N236344	3M/ESPE, St. Paul, MN, USA
Oral-B, Pro-Expert mouthrinse (alcohol-free mouthrinse)	Aqua, Glycerin, polysorbate 20, Aroma, methylparaben, cetylpyridinium chloride, sodium fluoride, sodium saccharin, sodium benzoate, propylparaben, Cl 42051, and Cl 47005	99602155	Procter & Gamble MN GmbH, Straße e 1, 64521 Gross Gerau, Germany
Oral-B, Advantage mouthrinse (alcohol-containing mouthrinse)	Aqua, glycerin, alcohol, aroma, methylparaben, poloxamer 407, cetylpyridinium chloride, sodium fluoride, sodium saccharin, Propylparaben, Cl 42051, and Cl 47005	95587215	Procter & Gamble UK, Weybridge, KT13 0XP
Artificial saliva	NaCl (400 mg/L), KCL (400 mg/L), CaCl ₂ ·2H ₂ O (795 mg/L), NaH ₂ PO ₄ ·H ₂ O (690 mg/L) KSCN (300 mg/L), Na ₂ S·9H ₂ O (5 mg/L), and urea (1000 mg/L)		

TABLE 2: Mean solubility values of materials tested (μ g/mm³).

Solutions	Test materials	
	FZ250 (sd)	FS (sd)
Alcohol-containing mouth rinse (advantage)	4.2 (1,4) ^(A,1)	3.1 (1,7) ^(B,1)
Alcohol-free mouth rinse (Pro-Expert)	3.5 (0,9) ^(A,1)	3.0 (1,1) ^(B,1)
Artificial saliva	3.4 (1,3) ^(A,1)	2.3 (0,6) ^(B,2)

Differences in superscript letters indicate statistically significant differences within columns and differences in superscript numbers indicate significant differences within rows.

of resin composites is related to the dissolution and leaching of various components, particularly unreacted monomers [20]. The organic matrix of conventional resin composites is generally based on methacrylate chemistry, especially cross-linking methacrylates, as in FZ250. The density of the links in methacrylate-based resin composites may vary as a result of the polymerization of free radicals, causing spatial heterogeneity that may facilitate the entrapment of residual monomers in microgels, from where they may be easily leached [21]. When compared to methacrylate-based resin polymerization, the photoactivated cationic polymerization process of silorane resins is relatively insensitive to oxygen. Not only does this reduce polymerization shrinkage, it also increases the degree of conversion [15, 22, 23].

Ethanol, which is found in many mouthrinses, may accelerate the hydrolytic degradation of resin-based materials [24]. In vitro studies have reproduced the subsurface and surface degradation of resin composites by storing them in ethanol [6], and the mechanical properties of composite

resins have been compromised by aging them in alcohol-containing solutions [9]. In the present study, both materials tested exhibited greater solubility in the mouthrinse containing alcohol when compared to the alcohol-free mouthrinse ($P > 0.05$). These findings suggest that it may be preferable for patients with extensive restorations to avoid the use of mouthrinse containing alcohol as part of their daily oral hygiene routine so as to prevent the need for recurrent restorative treatment.

As with all in vitro studies, caution must be used when extrapolating the results of the present study to the oral environment. Clinical studies are needed to examine the in vivo solubility behavior of different resin composites.

5. Conclusion

Within the limitations of this in vitro study, the following conclusions can be drawn:

- (1) the solubility of FS was lower than that of FZ250 in all the solutions tested;
- (2) solubility of both of the restorative materials tested was lower in alcohol-free mouthrinse than in alcohol mouthrinse containing;
- (3) alcohol-free mouthrinse may prefer to alcohol containing mouthrinse in patients with extensive restorations.

Conflict of Interests

The authors declare that there is no conflict of interests.

References

- [1] W. Geurtsen and U. Schoeler, "A 4-year retrospective clinical study of class I and class II composite restorations," *Journal of Dentistry*, vol. 25, no. 3-4, pp. 229-232, 1997.
- [2] Y. Zhang and J. Xu, "Effect of immersion in various media on the sorption, solubility, elution of unreacted monomers, and flexural properties of two model dental composite compositions," *Journal of Materials Science: Materials in Medicine*, vol. 19, no. 6, pp. 2477-2483, 2008.
- [3] W. Weinmann, C. Thalacker, and R. Guggenberger, "Siloranes in dental composites," *Dental Materials*, vol. 21, no. 1, pp. 68-74, 2005.
- [4] A. J. Feilzer, A. J. de Gee, and C. L. Davidson, "Relaxation of polymerization contraction shear stress by hygroscopic expansion," *Journal of Dental Research*, vol. 69, no. 1, pp. 36-39, 1990.
- [5] T. Hirasawa, S. Hirano, S. Hirabayashi, I. Harashima, and M. Aizawa, "Initial dimensional change of composites in dry and wet conditions," *Journal of Dental Research*, vol. 62, no. 1, pp. 28-31, 1983.
- [6] J. L. Ferracane, "Hygroscopic and hydrolytic effects in dental polymer networks," *Dental Materials*, vol. 22, no. 3, pp. 211-222, 2006.
- [7] M. Addy, "Chlorhexidine compared with other locally delivered antimicrobials. A short review," *Journal of Clinical Periodontology*, vol. 13, no. 10, pp. 957-964, 1986.
- [8] M. Addy and J. M. Moran, "Clinical indications for the use of chemical adjuncts to plaque control: chlorhexidine formulations," *Periodontology 2000*, vol. 15, no. 1, pp. 52-54, 1997.
- [9] J. E. McKinney and W. Wu, "Chemical softening and wear of dental composites," *Journal of Dental Research*, vol. 64, no. 11, pp. 1326-1331, 1985.
- [10] K. Asaoka and S. Hirano, "Diffusion coefficient of water through dental composite resin," *Biomaterials*, vol. 24, no. 6, pp. 975-979, 2003.
- [11] L. Musanje and B. W. Darvell, "Aspects of water sorption from the air, water and artificial saliva in resin composite restorative materials," *Dental Materials*, vol. 19, no. 5, pp. 414-422, 2003.
- [12] H. Koizumi, H. Satsukawa, N. Tanoue, T. Ogino, M. Nishiyama, and H. Matsumura, "Effect of metal halide light source on hardness, water sorption and solubility of indirect composite material," *Journal of Oral Science*, vol. 47, no. 4, pp. 165-169, 2005.
- [13] W. M. Palin, G. J. P. Fleming, F. J. T. Burke, P. M. Marquis, and R. C. Randall, "The influence of short and medium-term water immersion on the hydrolytic stability of novel low-shrink dental composites," *Dental Materials*, vol. 21, no. 9, pp. 852-863, 2005.
- [14] J. D. Eick, R. E. Smith, C. S. Pinzino, and E. L. Kostoryz, "Stability of silorane dental monomers in aqueous systems," *Journal of Dentistry*, vol. 34, no. 6, pp. 405-410, 2006.
- [15] N. Ilie and R. Hickel, "Macro-, micro- and nano-mechanical investigations on silorane and methacrylate-based composites," *Dental Materials*, vol. 25, no. 6, pp. 810-819, 2009.
- [16] H. H. Huang, Y. H. Chiu, T. H. Lee et al., "Ion release from NiTi orthodontic wires in artificial saliva with various acidities," *Biomaterials*, vol. 24, no. 20, pp. 3585-3592, 2003.
- [17] EN ISO, 4049, *Dentistry—Polymer-Based Filling, Restorative and Luting Materials*, International Organization for Standardization, Geneva, Switzerland, 1988.
- [18] R. Bagheri, M. F. Burrow, and M. Tyas, "Influence of food-simulating solutions and surface finish on susceptibility to staining of aesthetic restorative materials," *Journal of Dentistry*, vol. 33, no. 5, pp. 389-398, 2005.
- [19] Y. J. Wei, N. Silikas, Z. T. Zhang, and D. C. Watts, "Diffusion and concurrent solubility of self-adhering and new resin-matrix composites during water sorption/desorption cycles," *Dental Materials*, vol. 27, no. 2, pp. 197-205, 2011.
- [20] P. L. Fan, A. Edahl, R. L. Leung, and J. W. Stanford, "Alternative interpretations of water sorption values of composite resins," *Journal of Dental Research*, vol. 64, no. 1, pp. 78-80, 1985.
- [21] J. Malacarne, R. M. Carvalho, M. F. de Goes et al., "Water sorption/solubility of dental adhesive resins," *Dental Materials*, vol. 22, no. 10, pp. 973-980, 2006.
- [22] N. Ilie and R. Hickel, "Silorane-based dental composite: behavior and abilities," *Dental Materials Journal*, vol. 25, no. 3, pp. 445-454, 2006.
- [23] W. Lien and K. S. Vandewalle, "Physical properties of a new silorane-based restorative system," *Dental Materials*, vol. 26, no. 4, pp. 337-344, 2010.
- [24] S. Y. Lee, H. M. Huang, C. Y. Lin, and Y. H. Shih, "Leached components from dental composites in oral simulating fluids and the resultant composite strengths," *Journal of Oral Rehabilitation*, vol. 25, no. 8, pp. 575-588, 1998.